Development of Conductive Nanocomposite Sensors for Anticipated Diagnostic of Diseases

Sananda Nag

THESE / UNIVERSITE DE BRETAGNE-SUD

sous le sceau de l'Université européenne de Bretagne

pour obtenir le titre de
DOCTEUR DE L'UNIVERSITE DE BRETAGNE-SUD
Mention :
Ecole doctorale SICMA

présentée par
Sananda NAG

Préparée à **LIMATB**
Etablissement de rattachement : **UBS**
Nom développé de l'unité : **Laboratoire d'Ingénierie des Matériaux de Bretagne**

Development of Conductive Nanocomposite Sensors for Anticipated Diagnostic of Diseases

Thèse soutenue le 19th September 2014
devant le jury composé de :

Prof. Jean-Francois Feller
Directeur deThèse (UBS, France)

Prof. Veena Choudhary
Co-Directeur deThèse (IIT-Delhi, India)

Dr. Mickaël Castro
Co-Directeur deThèse (UBS, France)

Prof. Philippe Guégan
Rapporteur (UPMC Paris, France)

Dr. Chris Ewels
Rapporteur (Université de Nantes, France)

Prof. Tristan Montier
Examinateur (Université de Bretagne Occidentale, France)

Development of Conductive Nanocomposite Sensors for Anticipated Diagnostic of Diseases

A dissertation submitted in the partial fulfilment of the requirement for the degree of

Doctor of Philosophy

by

Sananda Nag

University of South Brittany (UBS)

Department of Sciences & Engineering Sciences

&

Indian Institute of Technology-Delhi (IIT-D)

Centre for Polymer Science & Engineering

Defended on the 19th of September, 2014, in front of the following commission:

Prof. Jean-Francois Feller	Director of Thesis (UBS, France)
Prof. Veena Choudhary	Co-Director of Thesis (IIT-Delhi, India)
Dr. Mickaël Castro	Co-Director of Thesis (UBS, France)
Prof. Philippe Guégan	Reviewer (UPMC Paris, France)
Dr. Chris Ewels	Reviewer (Université de Nantes, France)
Prof. Tristan Montier	Examiner (Université de Bretagne Occidentale, France)

Dedicated to my Parents

Late Dr. Biplab Nag

&

Mrs. Nupur Nag

Acknowledgements

It gives me immense pleasure and honour to thank my supervisor, Prof. Jean-Francois Feller, Head of the smart plastics group, LIMAT^{B},UBS who helped me in climbing the rocky terrain of research during the past three years. I would like to take this opportunity to express my sincere gratitude to him for allowing me to accomplish research under his guidance and for keeping his confidence in my capabilities. He has been very supportive to me throughout my thesis with his patience and knowledge whilst allowing me the room to work in my own way. I appreciate his encouragement and enthusiasm which helped me to keep myself motivated even during the hardest times. I am deeply indebted to Prof. Jean-Francois Feller for providing me a research oriented environment along with his relentless encouragement and support.

I would like to thank my co-supervisor Prof. Veena Choudhary, Head of Centre for Polymer Science & Engineering IIT Delhi, for her efforts and direction throughout my Ph.D work. Through her wealth of knowledge, direction and leadership I have been able to expand my knowledge in many areas of polymer science, starting from my M.Tech days in IIT-Delhi. She has always been an ideal example of passionate and inspiring mentor to me. Her scientific judgment is impeccable and she helped me to develop a scientific attitude with her sheer patience and motivation. She encouraged me to think independently and develop newer ideas regarding my research work.

I would like to deliver my sincere vote of thanks to Dr. Mickaël Castro for his guidance, co-operation and technical advices in every step to reach the goal of this thesis. His contribution in correcting this thesis is sincerely acknowledged. I would also take the opportunity to acknowledge the contribution of Prof. Philippe Guégan and his research group for successful collaborative work.

I would particularly thank jury members Prof. Philippe Guégan and Dr. Chris Ewels for devoting their valuable time to review this thesis and Prof. Tristan Montier who agreed to take part to this committee.

*Nothing can be accomplished without family support. I would like to extend my special gratitude to my father Late Dr. Biplab Nag, whose memory has always been the source of my motivation even during the hardest times. I have always considered my father as my idol and even no longer with us, he remains the compass of my life**.** The urge to fulfil his dreams is the ultimate source of my motivation. I would like to express my deepest sense of gratitude to my mother, Mrs. Nupur Nag, without her continuous support, encouragement and endless*

sacrifices I never would have been able to achieve my goals. Her infallible love and patience will remain my inspiration and strength throughout my life.

I owe my deepest gratitude towards my husband Suvam for his eternal support and understanding of my goals and aspirations. Without his help, I would not have been able to complete much of what I have done and become who I am. It would be ungrateful on my part if I thank him in these few words. Not only as a husband but also as my best friend and colleague he has always extended his hand of selfless supports, technical and scientific advices.

My heartfelt regards go to my father in law Mr. Sailendra Nag Chowdhury, mother in law Mrs. Gopa Nag Chowdhury and sister in law Payel for their love and moral support.

I would like to acknowledge Dr Isabelle Pillin, Mr. Hervé Bellegou, Mr. Anthony Magueresse, Mr. Antoine Kervoelen, Mme. Francoise Péresse for their technical supports. I also appreciate the contributions of Prof. Yves Grohens, Prof. Christophe Balley, Dr. Bastien Seantier, Dr. Stéphane Bruzaud, Dr. Alain Bourmaud, Dr. Antoine Le-Duigou for their scientific advices.

My thanks also go to my colleagues and friends Dr. Robert, Dr. Tung, Dr. Tripathi, Dr. Vincent, Morgan, Anaelle, Nicolas, Laetitia, Dr. Saulnier, Neethu, Kishore, Aparna, David, Clara, Marine, Clement, Abdelkader and all other labmates for their timely help, and contribution to create a friendly and co-operative atmosphere in laboratory. Also I express my sincere note of thanks to everybody who has extended their helping hands towards the successful accomplishment of this thesis work, as well as expressing my apology not been able to mention all those individual names.

Finally, my greatest regards to the Almighty for bestowing upon me the courage to face the complexities of life and complete this project successfully.

TABLE OF CONTENTS

Chapter I: Structure & content of the thesis

Summary:

This first chapter of the thesis deals with a general introduction of the topic, explanation the problem and context of the thesis. Structure and content of the thesis is also summarized in this introductory chapter. The outline of this manuscript is briefly illustrated highlighting the focus of each chapter.

I.1. General introduction & context of the thesis

Since the survival of cancer patients depends on early detection of tumour cells, developing technologies applicable for rapid detection of carcinoma is a challenge for the researchers. Breath analyzing has emerged as a non-invasive technique for anticipated diagnosis of lung cancer, as the breath extract of lung cancer patients are found to display elevated levels of several volatile organic compounds (VOC). Clearly, the invention of a fast, reliable, economic and portable technique is highly required before breath testing becomes a clinical reality. Nanomaterial based sensor arrays can fulfil all these requirements and can form a solid foundation for the identification of disease related VOC fingerprint in exhaled breath. It has already been proved by researchers of our group that conductive polymer nanocomposites possess far better sensing properties than pristine nanomaterials like carbon nanotube and graphene in terms of sensitivity and selectivity. Starting from the light of this finding, the goal of this thesis is to develop a new generation of conducting nanocomposite or nanohybrid based vapour sensors of high sensitivity and tuneable selectivity towards specific targeted disease VOC biomarkers, and finally to construct an electronic nose with the ability to identify and discriminate a set of specific disease VOC biomarker.

I.2. Outline of the manuscript

The content of the thesis can be summarized briefly.

After a general introduction to present the content of the thesis in this present **chapter I**, the next chapter is focused on the synthesis of bibliographic data. **Chapter II** begins with a background of several kinds of malignancy. An overview of cancer related death worldwide is provided to show how carcinoma has emerged as a major health problem of human race. The shortcomings of current diagnostic methods of malignancy and the importance of breath analysis to be recognized as a noninvasive tool for anticipated diagnosis of cancer is elaborated afterwards. The advantages of biomarker analysis by electronic nose composed of chemoresistive VOC sensors over the other conventional methods of breath analysis are also mentioned. Finally the entire focus is given to different smart carbon nanomaterials which can be used as a basic component for VOC sensors. A detailed description of literature is also provided on the different strategies to structure conductive networks and to functionalize carbon nanomaterials.

Results and discussion of all the experiments for this dissertation is subdivided into the following three chapters. In order to develop set of sensors, selective towards different targeted

VOC, different strategies were developed. Each of the undertaken strategies aiming to develop conductive nanocomposites or nanohybrids was separately focused in these chapters along with their vapour sensing performance. **Chapter III** deals with the development of cyclodextrin based conductive nanocomposites for vapour sensing applications. The synthesis, fabrication and vapour sensing performance of a set of functionalized cyclodextrin wrapped reduced graphene oxide sensors is broadly discussed in this chapter. Tuning of the selectivity of these sensors, by variations of organic functionality on the cyclodextrins is the aim of this strategy.

Chapter IV is devoted to a second strategy of structuring of the conductive architecture, i.e., the development of conductive nanohybrids which are multicomponent systems where two or more nanomaterials are integrated, for the purpose of synthesizing a novel nanomaterial with attractive multifunctionality. In the first part of this chapter, development and vapour sensing applications of polyhedral oligomeric silsesquioxane (POSS) and CNT based hybrid sensors are illustrated. Effect of variation of the organic functionality of POSS, on the selectivity of the sensors was studied in detail. Whereas, the second part of this chapter deals with hybridization of CNT/graphene with spherical Buckminsterfullerene nanoparticles. In this latter part, the effect of grafting Buckminsterfullerenes on the sensitivity of the CNT/graphene based nanosensors was thoroughly studied.

Chapter V is focused on the fabrication and vapour sensing characterization of conductive polymer nanocomposites (CPC). This strategy has already been used in the last years by the researchers of our group. CPC, being the combination of an insulating polymer matrix and conductive nanofillers like carbon nanotubes, have shown to respond selectively towards targeted VOC through the choice of a proper polymer matrix. However in this part, the proper choice of a polymer matrix was combined with variation of the degree of sulfonation of the polymer matrix and the use of hybrid nanofiller as a controlling parameter of the sensitivity of the VOC sensors.

Finally **Chapter VI** deals with construction of novel electronic nose by a judicial combination of high performance sensors in an array. This last chapter ends with conclusive remarks and future aspects of the development of conductive nanocomposite sensors for anticipated diagnosis of diseases.

To facilitate the reading of the document, a detailed description of all the materials, methods, tools and some synthesis procedures are gathered in **appendix** at the end of this manuscript. This appendix also covers the basic carbon nanomaterials used in this work and the stepwise

methods of sensor fabrication along with morphological, thermal, structural characterization methods undertaken.

Chapter II: Bibliographic survey

Summary

The inability of currently available techniques used for cancer detection, to diagnose the malignancy of a tumour cell at its very early stage of development, is mostly responsible for death of approximately 7.6 million people from cancer each year. Therefore, the development of advanced technology, capable of doing rapid and reliable discrimination between healthy and cancer cells is an important challenge for the diagnosis and treatment of tumours. The analysis of specific VOC in exhaled breath (identified as biomarkers of specific disease like cancer) gives an idea of metabolic and physiological activities of an individual and can provide non-invasive and potentially inexpensive anticipated diagnosis of cancer. The potential role of nanotechnology in the development of electronic noses, as a non-invasive complementary technique for the detection of malignancy at the primary stage, is thoroughly reviewed in this chapter.

II.1. Brief note on cancer

Uncontrolled growth and spread of abnormal cells leads to the initiation of a group of diseases, known as cancer. In a healthy adult body, cell division occurs either to replace damaged cells or to repair injuries. There are many kinds of cancer, but they all start because of out-of-control growth of abnormal cells followed by invasion of other tissues. In normal cell, when DNA gets damaged, either the damage gets healed up or the cell dies. In cancer cells, the damaged DNA neither gets repaired, nor dies of. Instead, this cell goes on making new cells having the same damaged DNA. In most cases the cancer cells form a tumour. Cancer cells often travel to other parts of the body, where they begin to grow and form new tumours that replace normal tissue. This process is called metastasis. Metastasis is frequently the terminal process in the progression of tumours. Cancer is caused by both external factors (tobacco, infectious organisms, chemicals, and radiation) and internal factors (inherited mutations, hormones, immune conditions, and mutations that occur from metabolism). These causal factors may act together or in sequence to initiate or to promote the development of cancer. Ten or more years often pass between exposure to external factors and detectable cancer [1].

II.2. Statistics of cancer related deaths

Cancer is a major public health problem all over the world. In 2013, a total of 1,660,290 new cancer cases and 580,350 cancer deaths are estimated to occur in the United States [2]. Another study states that there were 3.45 million new cases of cancer (excluding non-melanoma skin cancer) and 1.75 million deaths from cancer in Europe in 2012. In the European Union, the estimated numbers of new cases of cancer were approximately 1.4 million in males and 1.2 million in females, and around 707,000 men and 555,000 women died from cancer in the same year [3]. The current 5-year survival rate for lung cancer is 15 %, but this rate may rise to 49 % if the cancer could be diagnosed when it is still localized [4]. The most widespread cancers in the developed world, accounting for half of the cancer deaths, are prostate, lung, and colorectal cancers for men, and breast, colorectal, and lung cancers for women. Therefore lung cancer is the leading cause of cancer related deaths common for both men and women and causes 1.4 million deaths per year worldwide. It is the second most common cancer in men and the third in women (22% of all cancer cases). However breast cancer is one of the most common cancer in women. Throughout the world, more than 1 million women are diagnosed with breast cancer every year and in the USA, the National Cancer Institute estimated that more than 182,000 women were diagnosed with breast cancer in 2008, and more than 40,000 died of the disease

[5]. The incidence rate of cancer depends upon geographical location of the world, for instance, the highest rates of the diseases in men are determined in Europe, particularly eastern and central Europe, and northern America as depicted in Figure 1 [6], [7].

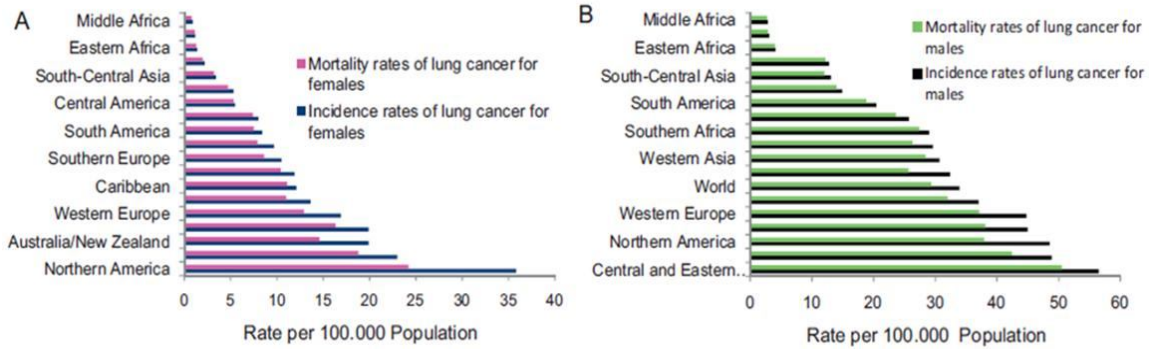

Figure 1 Mortality and incidence rate of lung cancer based on geographical location (A) female (B) male [7]

II.3. Conventional diagnostic tools for cancer

Lung cancer is rapidly becoming one of the greatest health hazards of our day. The problem associated with lung cancer detection is the lack of symptoms in its early stage of development. Unfortunately, the most common methods currently used to diagnose lung cancer can occasionally miss tumours because they depend on tumour size [8]. Also these methods are expensive and unsuitable for widespread screening. Survival of a cancer patient depends on early stage detection and thus developing technologies applicable for sensitive and specific methods to detect cancer at its primary stage, is an inevitable task for cancer researchers.

Detection method	Advantage	Disadvantage
Chest X-ray	Reliable	Use of radiation, false negative response, high cost
Computerized tomography(CT)	Reliable	Use of radiation, false negative scan, high cost
Magnetic resonance imaging (MRI)	Reliable	Use of magnetic field, high cost, not suitable for all patients that have other complications
Positron emission tomography	Reliable	Need for radioactive substance and sophisticated instrument, high cost, not suitable for all patients that have other complications
Sputum cytology	Easy and non-invasive	Degradation of biomarkers due to the enzymes in sputum, false positive results
Biopsy	Fast and easy	Inflammation, painful, invasive

Table 1 Currently available detection methods for lung cancer (extracted from [7])

Existing cancer screening methods include the PAPANICOLAU test for women to detect cervical cancer, mammography to detect breast cancer, prostate-specific antigen (PSA) level detection in blood sample for men to detect prostate cancer, occult blood detection for colon cancer, chest radiography, sputum cytology, bronchoscopy, biopsy, endoscopy, CT scans, X-ray, ultrasound imaging, MRI, computer tomography, nuclear magnetic resonance, positron emission tomography, and single photon emission computed tomography [8] for various cancer detection [9]–[11]. None of these methods are completely free from all short comings as shown in Table 1. In most cases the efficiency of detection is directly proportional to tumour size and fails to detect malignancy at early stage. Some of the techniques are very expensive or painful.

Therefore extensive research is still on progress to help early detection and treatment of cancer. In one direction research is going on for the development of cancer biomarker sensors and biosensors which might help in early level the detection of malignancy [12]. In another direction, the design of targeted anticancer drug delivery nanocarriers has received a great deal of attention, which possess significant potentiality in efficient treatment of malignant cells [13], [14].

II.4. Interest of VOC sensing

Volatile organic compounds (VOC) are a diverse group of carbon-based chemicals that are volatile at ambient temperature. The demand for the development of miniaturized sensors arrays for fast, low-cost, low-power detection and discrimination of VOC has increased dramatically over the years. Breath testing is a recognized diagnostic method which links specific VOC in exhaled breath to medical conditions. Our exhaled breath is a complex matrix with thousands of molecules that constitute a breath print carrying certain information about our state of health. It may provide the metabolic and physiological status of body organs such as liver [15], kidneys [16], [17] breast, colorectum, prostate or even skin [18]–[20]. The detection and identification of VOC in exhaled breath may lead to the development of novel, noninvasive diagnostic methods for a wide range of diseases [21]–[24], including different types of cancer [25], [26], tuberculosis [27], [28] liver failure [29], kidney failure, PARKINSON's disease [30] etc.

The application sphere of VOC sensing beyond medicine [31], [32] are food degradation monitoring [33]–[36], aroma characterization of alcoholized beverages [37], [38], environment monitoring (e.g. indication of hazardous chemical leakage, monitoring of organic solvent

vapour concentration in the air) [39]–[45] space exploration, and homeland security [46], process control of chemical and food production [47], monitoring of quality and alcohol content in automotive fuel [48], [49]. In the fields of workplace safety and environmental monitoring, there is a growing need for monitoring VOC from exogamic sources, mostly from industrial processes, that could be hazardous, even at very low levels, to humans, animals, and plants [50], [51]. Chemical sensors for the rapid detection of explosives are also important for tactical and humanitarian demining, remediation of explosives manufacturing sites, and forensic and criminal investigations [52].

II.5. Exhaled breath VOC biomarkers

In 1971, PAULING reported that normal human breath contained over 200 VOC, which presented a potential source of information concerning both systemic and lung physiology [53], [54]. Only 1% of these VOC can work as biomarker for a certain disease; 75% of them are common to all subjects and can be discriminating in case of altered concentration levels, while 25% of this 1% is unusual volatiles and could be indicated as biomarkers for specific diseases. A biomarker is an indicator of a biological state of disease. It can be used to study cellular processes, and to provide us information on the underlying mechanism of the initiation of a disease, the process of aggravation, and ultimately to provide a method to diagnose and treat the disease with appropriate measures at desired time. VOC present in exhaled breath may be either endogenous or exogenous. First they are produced during different biochemical processes which occur in living organisms and second they can be undertaken with food, inhaled with the air or absorbed by the skin. Endogenous VOC in exhaled gases of human breath provide important information about the metabolic or any pathologic processes in the body [55], [56].

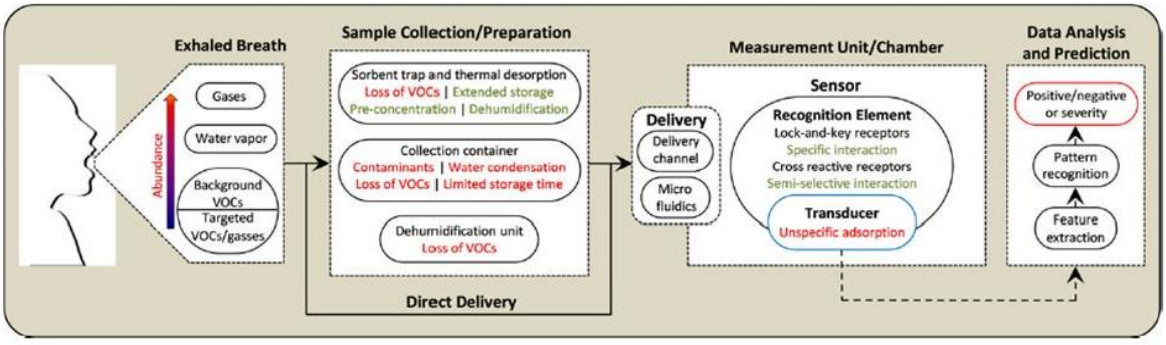

Figure 2 Breath collection and VOC extraction [2] (left) Overview of the processes involved in breath testing (right) [31]

In addition, also VOC are emanated by the skin [57], which are intermediaries in cell metabolism [58], [59]. The method of extracting and testing of breath VOC is schematically shown in Figure 2.

II.6. Biomarker analysis: a non-invasive technique of cancer diagnosis

The development of specific, easily accessible and reliable technology, for painless detection of cancers at preliminary stages, is of utter importance. Therefore, researchers are tapping into this field to develop a non-invasive technique that can diagnose cancer by identifying specific cancer-related VOC [60]. Biomarker analysis is a complementary method and seems to be a relevant screening method for early cancer detection [61], [62]. Early detection while the tumour cells are still localized, is essential to reduce the morbidity and mortality rates associated with cancer [63], [64]. However, using exhaled breath as a diagnostic test method, is an age old concept. The ancient Greek physicians already knew that some diseases could be diagnosed from the characteristic odour of patients'. For example, a fishy smell of breath could indicate liver disease; the sweet acetonic smell of breath is related to uncontrolled diabetes, a urine-like odour to kidney disease, the smell of "freshly baked bread" on the skin of patients with typhoid and the smell of grapes to *Pseudomonas* infections [65]. A compendium of all the volatile organic compounds emanating from the human body are known as 'volatolome' [66] and 1840 VOC have been assigned from breath (872), saliva (359), blood (154), milk (256), skin secretions (532) urine (279), and faeces (381) in apparently healthy individuals [67]. The breath of human, a basic characteristic of life carrying various information [68], [69], is significant to the comprehensive analysis of lung function [70], [71] asthma detection, diabetes mellitus diagnosis etc [72]–[74]. Increased concentrations of VOC in exhaled air correlate with diseases, for example ammonia in relation to hepatitis, dimethyl sulfide in relation to cirrhosis, and dimethyl and trimethylamine in relation to uraemia. Breath analysis [75] is a promising approach to identify inflammatory and oxidative stress markers implicated in the pathogenesis of various respiratory conditions. Although disease diagnosis by breath analysis is very interesting, it has two serious problems like presence of huge quantity of water and very low concentration (parts per billion level) of VOC biomarker (out of detection limit in most cases). Table 2 displays the list of all the cancer biomarker VOC.

II.7. Cancer biomarkers

Biomarkers have opened up a new era of early cancer diagnosis [76], [77]. VOC sensors have found a high potential in the field of cancer detection in recent years, as a number of VOC found in the exhaled breath of human beings are marked as cancer biomarkers. The exhaled breath VOC profile of cancer patients can be discriminated from that of healthy subjects through pattern recognition of VOC [78], [79]. Recent studies using gas chromatography/mass spectroscopy (GC-MS) [80] linked with a pre-concentrator have shown that the compounds of interest are generally to be found at 1-20 parts per billion (ppb) in healthy human breath but can be seen in distinctive mixture compositions and at elevated levels of 10-100 ppb in the breath of lung cancer patients [81], [82]. The VOC biomarkers of cancer and other diseases can be broadly divided into polar and nonpolar compound. The polar VOC are part of categories such as alcohols, carbonyl compounds like aldehydes, ketones. Whereas nonpolar VOC are of two types; aliphatic hydrocarbons and aromatic hydrocarbons. However the concentrations of alkanes and aromatic hydrocarbons in human breath are from 10−12 parts per trillion (ppt) to 10−9 parts per billion (ppb); hence pre-concentration became a very important step before analysis [83], [84].

Cancer type	Chemical nature of VOC	VOC biomarkers
Lung cancer [9], [85]–[90]	Alcohols	methanol, ethanol, isopropanol,1-propanol
	Aliphatic hydrocarbons	heptane, decane, undecane, cyclopentane, 1,3-butadiene, octane, 1-hexene, nonane, methyl heptene, cyclohexane, pentane
	Aromatic hydrocarbons	isoprene, benzene, toluene, ethyl benzene, xylene, styrene, propyl benzene, trichlorofluoro benzene, 1,2,4-trimethyl benzene, 1,4-dimethyl benzene
	Carbonyl compounds	formaldehyde, propanal, butanal, pentanal, hexanal, heptanal, octanal, nonanal, acetone, butanone
Skin cancer [18]	Alcohols	ethyl hexanol, cyclohexanol
	Aliphatic hydrocarbons	cyclohexane, nonane, decane, heptadecane
	Aromatics	benzaldehyde, benzyl alcohol, 1,4-dimethyl benzene, 1,2,4-trimethyl benzene
Breast cancer [91], [92]	Aliphatic hydrocarbons	nonane, 5-methyl tridecane, 3-methyl undecane, 6-methyl pentadecane, 2-methyl propane, 3-methyl nonadecane, 4-methyl dodecane, 2-methyl octane
	Carbonyl compounds	heptanal and hexanal

Table 2 Cancer biomarkers among breath VOC

II.7.1. Alcohols

Alcohols mostly originate from food and alcohol beverages and are absorbed from all parts of the gastrointestinal tract, largely by simple diffusion into the blood. Alcohols are also derived from the metabolism of hydrocarbons. Since alcohol has high affinity for water, it is found in body tissues and fluids and is absorbed rapidly in the blood. *Hakim et al.* in 2012 and *Gordon et al.* in 1985 had stated that 1-propanol was found at increased concentrations in the case of lung cancer, as compared to healthy subjects [85], [86]. Moreover in 2005, *Machado et al.* proved that breath extract of lung cancer patients contain alcohols like methanol, ethanol, and isopropanol [87]. On the other hand ethyl hexanol and cyclohexanol were proved to be skin cancer biomarkers [18].

II.7.2. Carbonyl compounds

Straight chain aldehydes found in breath extract of humans, include all C1−C9 aldehydes. All of them, apart from acetaldehyde, were found in the breath of lung cancer patients. According to *Spanel et al.* formaldehyde is a potential biomarker of bladder and prostate cancer too [93]. Concerning other aldehydes such as heptanal and hexanal they are supposed to be characteristic of patients with breast cancer also [91]. Acetone is one of the most abundant compound in breath and an important lung cancer biomarker as it is formed under metabolic conditions associated with a high oxidation rate of fatty acids in lung cancer [88], [89], [94]. In 1985, *Gordon et al.* identified acetone, and methyl ethyl ketone as lung cancer biomarkers. Acetone is also an indicator of serum glucose level [95]. The level of acetone in the breath extract of healthy person is around 5 ppm while up to 300 ppm acetone could be found in the breath extract of patients suffering from diabetis mellitus [96].

II.7.3. Aliphatic hydrocarbons

In 1985, *Gordon et al.* identified several alkanes and monomethylated alkanes in the exhaled breath of lung cancer patients [86]. In 1999 a combination of VOC like 2,2,4,6,6-pentamethyl heptane, 2-methyl heptane, decane, undecane, cyclopentane, methyl-cyclopropane, 1-methyl-2-pentyl-methane, 1,3-butadiene, 3-methyl-octane, 1-hexene, nonane, 3-methyl-1-heptene, heptane, cyclohexane etc were proved to provide breathprint of lung cancer by *Philips et al.* [90]. A combination of VOC like pentane, 2-methyl pentane, heptane, octane, decane, pentamethyl heptanes are proved to be non small cell lung cancer biomarkers by *Poli et al.* [9]. In 2005 *Machado et al.* proved that breath extract of lung cancer patients contain several VOC like pentane [87]. Malignant pleural mesothelioma (MPM) is a cancer mainly caused by asbestos exposure and cyclohexane is the predominant discriminative compound in the breath

extract of MPM patients. [97]. Breast cancer is accompanied by increased oxidative stress [5] leading to increased concentration of pentane [98]. The breast cancer biomarkers reported by *Phillips et al.* in 2003 are nonane, 5-methyl tridecane, 3-methyl undecane, 6-methyl pentadecane, 2-methyl propane, 3-methyl nonadecane, 4-methyl dodecane, 2-methyl octane [92]. Nonane, decane, heptadecane are found to be skin cancer biomarkers [18].

II.7.4. Aromatic hydrocarbons

A combination of VOC styrene, propyl-benzene, trichlorofluoro benzene, 1,2,4-trimethyl-benzene, 2-methyl isoprene, 1,4-dimethyl benzene, 1-methylethenyl benzene were proved to provide breathprint of lung cancer by *Philips et al.* [90]. A combination of VOC like benzene, toluene, ethyl benzene, isoprene, xylene, styrene, are proved to be non small cell lung cancer biomarkers by *Poli et al.* [9]. In 2005 *Machado et al.* proved that breath extract of lung cancer patients contained several VOC like, isoprene, benzene, toluene [87]. Several aromatic hydrocarbons such as benzaldehyde, benzyl alcohol, 1,4-dimethyl benzene, 1,2,4-trimethyl benzene were identified as skin cancer biomarkers [18].

II.8. Different methods of biomarker analysis

Many research papers have already been published on the breath analysis by gas chromatography- mass spectroscopy (GC-MS) [99]. There are some other methods used for the analysis of breath of a person such as ion flow tube mass spectrometry, proton transfer reaction mass spectroscopy [100], chemo-luminescence sensors, opto-chemical fibres, infrared spectroscopy, and polymer coated surface acoustic wave sensors. So far, the use of these techniques for the analysis of volatile fingerprints has been impeded by the need for expensive equipment, the degree of expertise required for operating such instruments, the long times required for sampling and analysis, the need for pre-concentration, non portability and large response time [101].

II.9. Electronic nose

An electronic nose (e-nose) is an artificial mimic of mammalian olfactory system. The human nose is composed of a number of receptors in nasal epithelium each of which respond to a wide variety of odorants. This response after being transmitted through the primary and secondary neuron reaches the brain as elaborated in Figure 3 [102].

Therefore olfactory receptors respond non-specifically to smelly compounds and the overall response is interpreted by the brain, by providing information about volatile derivatives. In

2004, AXEL and BUCK won the Nobel prize in Physiology or Medicine for their research on "odorant receptors and the organization of the olfactory system" where it is estimated that humans can sense as many as 10000 to 100000 chemicals as having a distinct odor. The olfactory epithelium contains millions of olfactory sensory neurons. Evidence for as many as 1000 different odor receptor genes has been found [103].

Similarly an electronic nose consists of an array of nonspecific sensors which are analogous to the receptors in the nasal epithelium of mammals [104]. A characteristic response pattern is provided by these sensor arrays which, treated by appropriate data analysis techniques, allows us to identify and quantify certain gas compounds [105]–[107].

The electronic nose consists of three functional components that operate serially on an odorant i.e., a sample handler, an array of vapour sensors and a signal-processing system [108]. The odour molecules are drawn into the e-nose using sampling techniques such as headspace sampling, diffusion methods, bubblers or pre-concentrators [109], [110] and induce a reversible physical and/or chemical change in the sensing material, which causes an associated change in electrical properties, such as conductivity [111], [112].

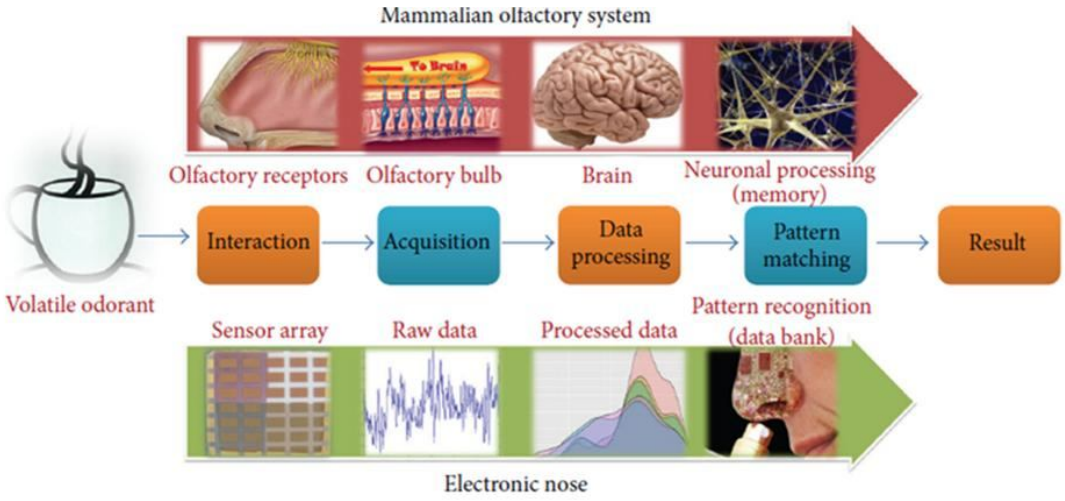

Figure 3 Schematic showing the comparison between mammalian olfactory system and an e-nose [102]

Different VOC have been identified in human exhaled breath. Thus far, only a small proportion of those VOC has been identified as disease-related. Most (respiratory) diseases are not characterized by an increase of a single chemical compound. The challenge therefore is to capture the mixture (profile) of exhaled VOC, which can be seen as a signature related to particular underlying conditions [113].

The electronic nose consists of a matrix of chemical sensing elements having partial selectivity coupled with an appropriate data analysis system enabling the characterization of complex gas

mixtures by recognition of sensor response patterns [114]. The output of e-noses represents a signature of the total expired VOC-profile, which is called a 'smellprint' or 'breathprint'. Individual VOC cannot be identified, but breath prints can be analyzed by modern pattern recognition algorithms in order to discriminate different VOC mixtures and thereby potentially diseases and disease phenotypes. Figure 4 represents a spectrum of exhaled VOC biomarkers, provided by the e-noses in the form of fingerprint of the breath VOC. Several independent studies have recently shown that an electronic nose can distinguish the VOC pattern in exhaled breath of lung/breast/skin cancer patients compared to healthy subjects [115].

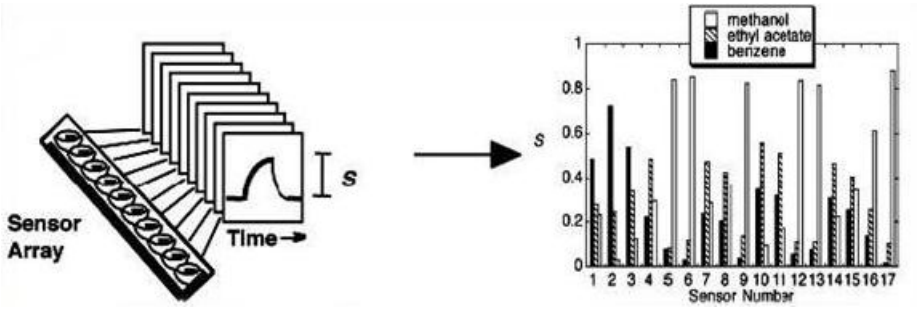

Figure 4 Differentiation between odorants: an array of broadly-cross reactive sensors in which each individual sensor responds to a variety of odors; (left) pattern of differential responses across the array produces a unique pattern for each odorant or odor (right) [116]

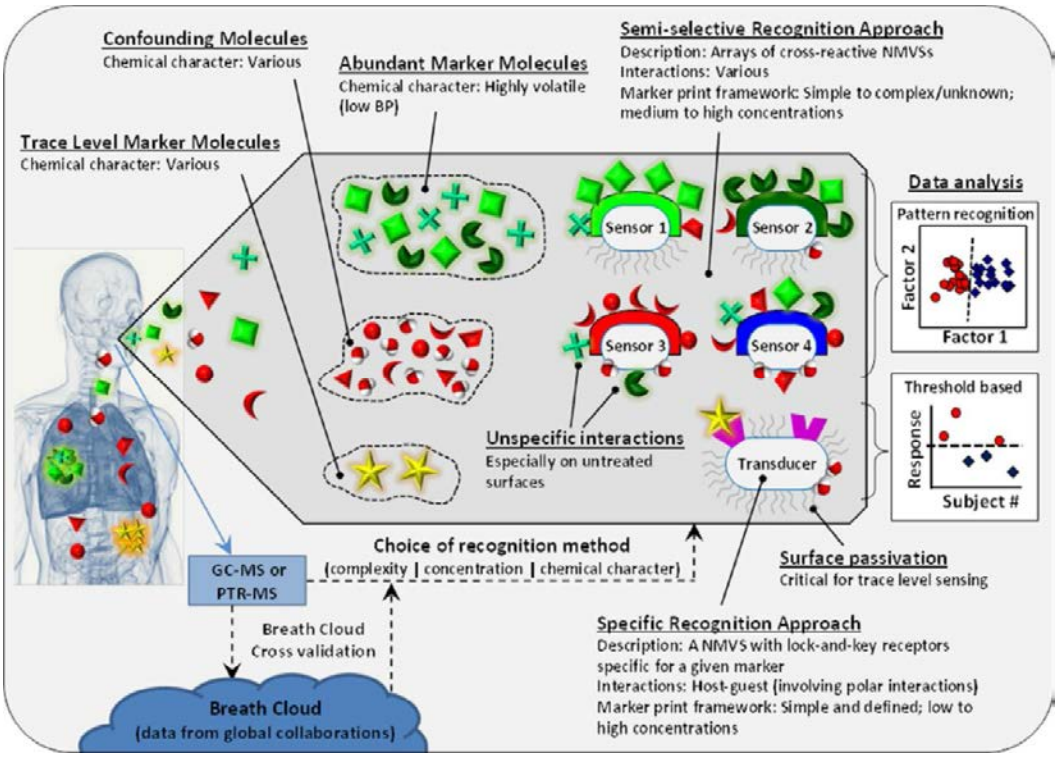

Figure 5 Schematic reviewing the links between the different frameworks of breath marker-prints and the appropriate sensing approach (specific vs cross-reactive approach) [117]

E-noses may serve as a cheap and rapid alternative to chemical analytical methods for anticipated diagnosis of disease by biomarker detection. They have the advantages of portability, continuous real time monitoring at specific sites, cost-effectiveness, easy operation, fast reading, and the potential to produce a chemical fingerprint when an array of chemical sensors coupled with pattern recognition is used.

The sensor arrays are multi-sensor systems, used to enhance the redundancy and diversity of the sensors responses and to provide a reliable and unique profile for analysis using pattern recognition techniques, as shown in Figure 5. Sensors in the array differ from each other in terms of the chemical and physical properties of the mediator molecules, which include hydrophobicity, hydrogen-bonding capacity, chain length or structure etc.

II.10. Chemical sensors in e-nose

According to the definition of gas sensor, given by the International Union of Pure and Applied Chemistry (lUPAC), "a chemical sensor is a device that transforms chemical information, ranging from the concentration of a specific sample component to total composition analysis, into an analytically useful signal. The chemical information, mentioned above, may originate from a chemical reaction of the analyte or from a physical property of the system investigated". Typically, chemical sensors consist of two main parts, a receptor and a transducer. The receptor transforms chemical information into a form of energy, which can be measured by the transducer. The transducer converts this energy into a useful, typically electrical, analytical signal [26].

Chemical sensors are normally designed to operate under well defined conditions for analytes of certain groups. Therefore, it is not always necessary that a sensor responds specifically to a specific analyte. Unspecific but partially selective, satisfactory reproducible sensors can be assembled in an e-nose in series for multicomponent analysis.

A variety of signal transduction mechanisms have now been implemented to construct electronic nose systems, such as acoustic wave (SAW, BAW) sensors [119] or quartz crystal microbalance (QCM) [120]–[125], metal oxide semiconductor, field effect transistors (FETs) [126]–[130], conductive nanocomposites [131]–[133], conducting polymers (CP) [134], optical sensors [135], gas chromatography [136], [137], ion flow tube mass spectroscopy [138], infrared spectroscopy [139], colorimetric sensors, and gold nanoparticles [140]–[144]. Besides there are many examples of amperometric electrochemical sensors to measure target gases [145]. Most of these e-noses have been developed for a broad range of applications [146]–

[148]. The suitability of the instrument for detection of specific disease states depends on the selection of sensors in relation to the gas mixture of interest and the choice of pattern.

II.11. Smart materials

By definition, “Smart” materials are materials that respond to a stimulus on their environment to produce a dynamic and reversible change in critical properties and have enabled progress in many areas, including sensor technologies, drug delivery, and self-healing materials for coating applications [149], [150]. The response of smart materials to various stimuli is shown schematically in Figure 6. Many of the current examples of smart materials are biomimetic. Smart materials are used to construct these smart structures, which can perform both sensing and actuation functions. A smart structure is a system containing multifunctional parts that can perform sensing, control, and actuation; it is a primitive analogue of a biological body.

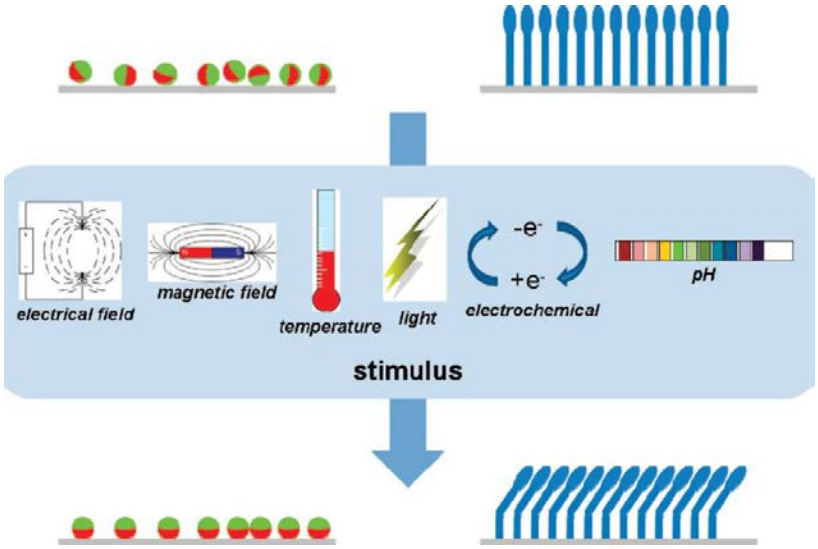

Figure 6 Two potential approaches toward the design of smart materials. The orientation of anisotropic particles as well as the conformation of molecular switches are altered relative to a surface by application of a stimulus [150]

II.12. Definitions of properties related to vapour sensing

Generally, there are several basic criteria for good and efficient vapour sensing systems such as (i) high sensitivity; (ii) good selectivity; (iii) fast response time and recovery time; (iv) high reproducibility; (v) reversibility; (vi) low noise; (vii) low operating temperature; (viii) stability in performances; (ix) long range limit of detection. However it is important to define some of these terms in order to have a proper understanding of sensing performance. In order to characterize sensor performance a set of parameters is used which are listed below.

- ***Sensitivity*** is the ratio between output signal and measured property. A sensor's sensitivity indicates how much the sensor's output changes when the measured quantity changes.
- ***Selectivity*** refers to characteristics that determine whether a sensor can respond selectively to a group of analytes or even specifically to a single analyte. Selectivity is a qualitative value that measures the difference in sensitivities as shown in Figure 7.
- ***Stability*** is the ability of a sensor to provide reproducible results for a certain period of time. This includes retaining the sensitivity, selectivity, response, and recovery time.
- ***Limit of detection*** is the lowest concentration of the analyte that can be detected by the sensor under given conditions, particularly at a given temperature.
- ***Response time*** is the time required for sensor to respond to a step concentration change from zero to a certain concentration value.
- ***Recovery time*** is the time it takes for the sensor signal to return to its initial value after a step concentration change from a certain value to zero [151].

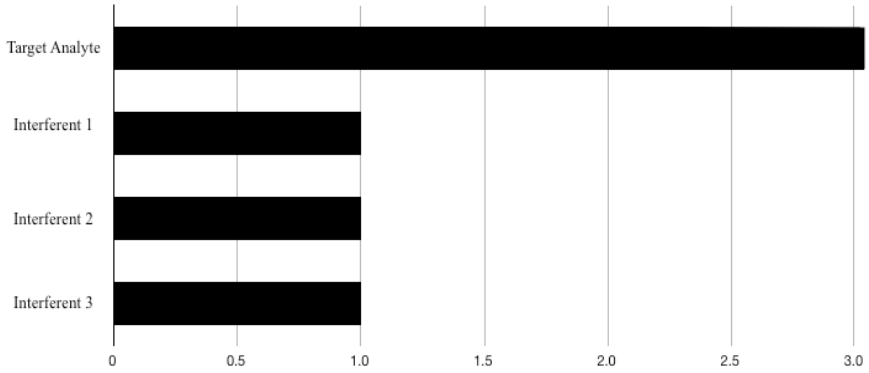

Figure 7 Ideal case for selectivity

II.13. Classification of sensors

Normally the sensors can be been categorized into following general groups on the basis of their operating principal: (1) chromatography and spectrometry; (2) electrochemical sensors; (3) mass sensors; (4) optical sensors and (5) chemoresistive sensors.

II.13.1. Chromatography

Chromatography is a method for the separation and analysis of complex mixtures of volatile organic and inorganic compounds. Chromatography relies on separation of complex mixtures

by percolation through a selectively adsorbing medium, with subsequent detection of compounds of interest. When a mixture of components is injected into a chromatograph equipped with an appropriate column, the components travel down the column at different rates and therefore reach the end of the column at different times. Non-portability, high cost and dependence on handling efficiency are the disadvantages of this technique. Chromatography/spectrometry, includes ion-mobility spectrometry and mass spectrometry which also have excellent discrimination capabilities, but like the gas chromatographs, they are not currently amenable for in-situ applications [152].

II.13.2. Electrochemical sensors

Electro-chemical sensors, include sensors that detect signal changes (e.g. resistance) caused by an electrical current being passed through electrodes that interact with chemicals. Such effects may be stimulated electrically or may result in a spontaneous interaction at the zero-current condition. Electrochemical sensors have been categorized by *Wilson et al.* [153] and *Janata* [154] into three groups: (1) potentiometric (measurement of voltage); (2) amperometric (measurement of current); and (3) conductimetric (measurement of conductivity). However, the amperometric and potentiometric devices are not widely used for detection of VOC. The conductimetric sensors may include polymer-absorption chemiresistors, catalytic bead sensors, and metal oxide semiconductors. These devices are sensitive to VOC exposure, resulting in large changes to resistance in the device but mainly used for liquid medium.

II.13.3. Mass sensitive sensors

Mass sensors rely on disturbances and changes to the mass of the surface of the sensor during interaction with chemicals, due to accumulation of the analyte. The detection can be accomplished through changes in acoustic waves propagated along the surface by QCM as in Figure 8 (a) or SAW devices or by actual bending or a change in shape of the device as mass is accumulated (micro-cantilever devices) [155].

II.13.4. Optical sensors

Optical sensors detect changes in visible light or other electromagnetic waves during interactions with chemicals [156]. These include fibre optical sensors as in Figure 8 (b) [157], colorimetry, and infrared sensors [158]. These sensors rely on changes in electromagnetic radiation (e.g. visible, infrared) to detect and identify the presence of chemicals. The sensitivity

of these sensors to VOC can be good but are also complex and expensive. Within each of these categories, some sensors may exhibit characteristics that overlap with other categories.

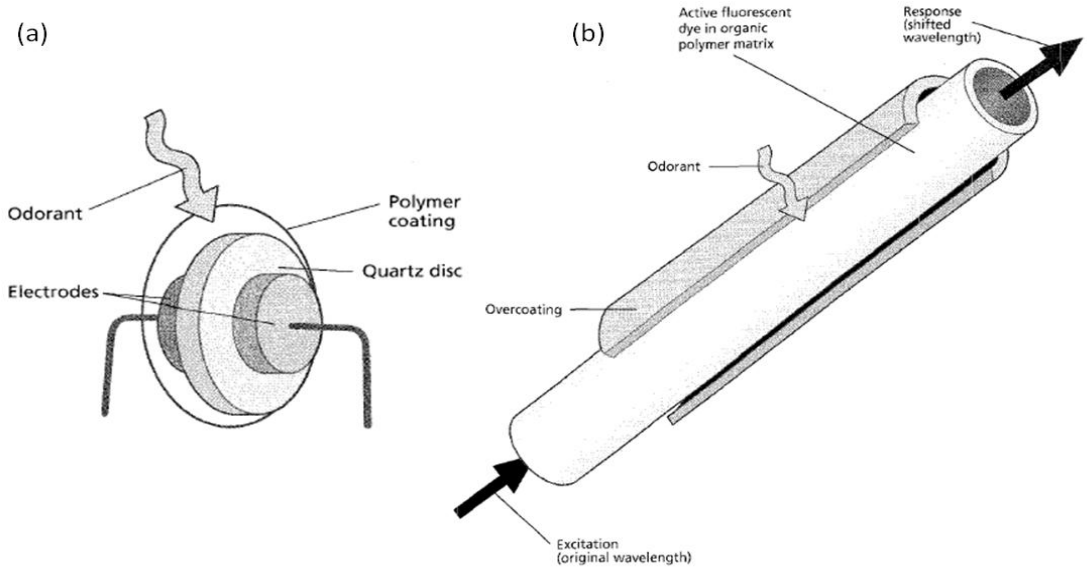

Figure 8 (a) The quartz crystal micro- balance (QCM) sensor made of a polymer-coated resonating disk, a few millimeters in diameter, with metal electrodes on each side connected to lead wire. Gas molecules adsorbed to the surface if the polymer coating increase the mass of the disk, thereby reducing its resonance frequency [108] (b) Odorant optical fibre sensors employ a glass fibre coated on its sides or ends with a thin chemically active materials containing fluorescent dyes immobilized in an organic polymer matrix. A pulse of light from external source propagates along the fibre and interrogates with the active materials with which VOC can interact leading to alteration of polarity of the dyes i.e., shifting of fluorescent spectrum [108]

II.13.5. Chemoresistive sensors

Chemoresistive sensors belong to a class of chemical sensors in which the absorption of chemical molecules leads to a change in electrical resistance [159]. One of the main ideas behind the chemical vapour sensor is based on a change in resistance of the sensitive material in response to the binding of chemical vapours (chemoresistors). The main focus of this review will retain on literature study and general trends of chemoresistive gas/ vapour sensors.

The operating mechanism of conductive nanocomposite based chemoresistive vapour sensors can be explained by a positive vapour coefficient (PVC) effect [160], [161]. The exposure of the sensors to vapour molecules, leads to the swelling at the junctions of the polymeric or non-polymeric matrix by the diffusion of gas or vapour molecules, which increases in turn filler/filler average gap and partially destroys the interconnected conductive networks of the nanocomposites. As shown in Figure 9, resistivity of conductive nanocomposite enhances due to partially disconnection of inter-connected network.

The stabilization of the selectrical signal, characterized by a plateau, is usually observed after exposing it a sufficiently long time to vapours, corresponding to its thermodynamic equilibrium. Relative amplitude (A_r), can be expressed by $R-R_0 / R_0$ where R and R_0 are electrical resistance of the nanocomposite sensor under exposure to the vapour and the initial resistance when exposed to inert gas atmosphere respectively.

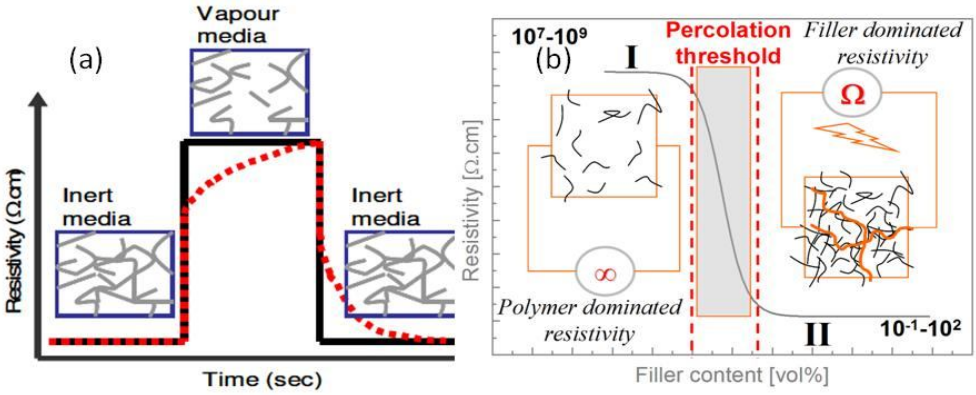

Figure 9 (a) Vapour sensing mechanism of chemoresistive sensors (b) Percolation of the conductive nanocomposites

II.13.5.1. Metal oxides

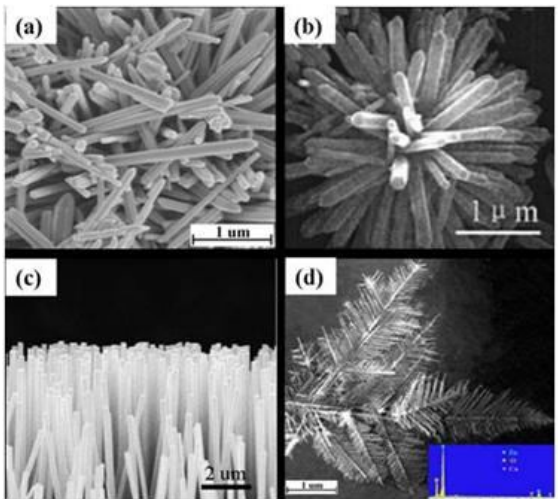

Figure 10 Scanning electron microscopy (SEM) images of (a) SnO_2 nanofibres produced by electrospinning after heating at 600 °C for 2 h (b) SnO_2 nanoribbons synthesized by direct oxidization (c) On-chip fabrication of SnO_2 nanowires grown on Au deposited Pt interdigitated substrate by thermal evaporation (d) SnO_2-ZnO hybrid nanofibre by electrospinning [170]

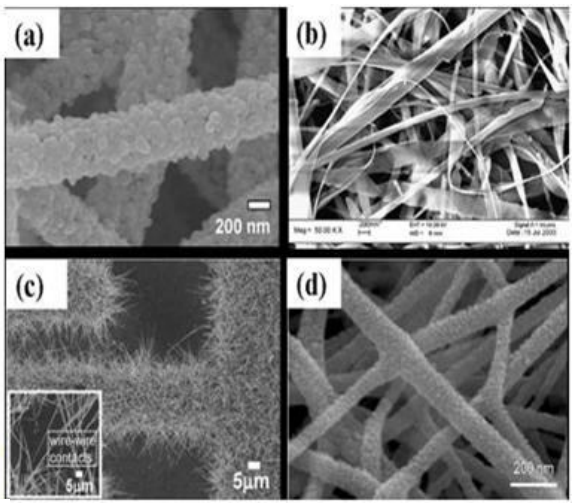

Figure 11 ZnO nanostructures. (a) Randomly distributed nanorods produced by hydrothermal process (b) Flowerlike nanorods produced by hydrothermal process (c) Vertically aligned nanorods produced by chemical vapor deposition process (d) Hierarchical dendrites produced by vapor-phase transport process [170]

Metal oxides are among the most widely used materials for chemical vapor sensors [162]–[165]. The principle operation of metal oxide sensors is based on the change in conductance of the oxide on interaction with a gas and the change is usually proportional to the concentration of the gas.

There are two types of metal oxide sensors; n-type sensors (zinc oxide, tin dioxide, titanium dioxide or iron (III) oxide) which respond to reducing gases and p-type sensors (nickel oxide, cobalt oxide) which respond to oxidizing gases. The SEM micrograph image of various types of nanostructured metal oxide is shown in Figure 10 and Figure 11. Indium tin oxide has been shown to respond to methanol, ethanol, butanol, and acetone by *Vaishanv et al*. as in Figure 12 (a) [166]. *Wang et al*. [167] demonstrated that a metal oxide semiconductor sensor responds to methyl, ethyl, isopropyl and butyl alcohol in Figure 12 (b) [168]. Gas sensing response of TeO_2 nanowires is shown in Figure 12 (c) and (d). Despite their sensitivity, the applications of these materials have been limited by their high power consumption, poor selectivity and high operational temperature from 100 °C to 400 °C in most cases [169], [170].

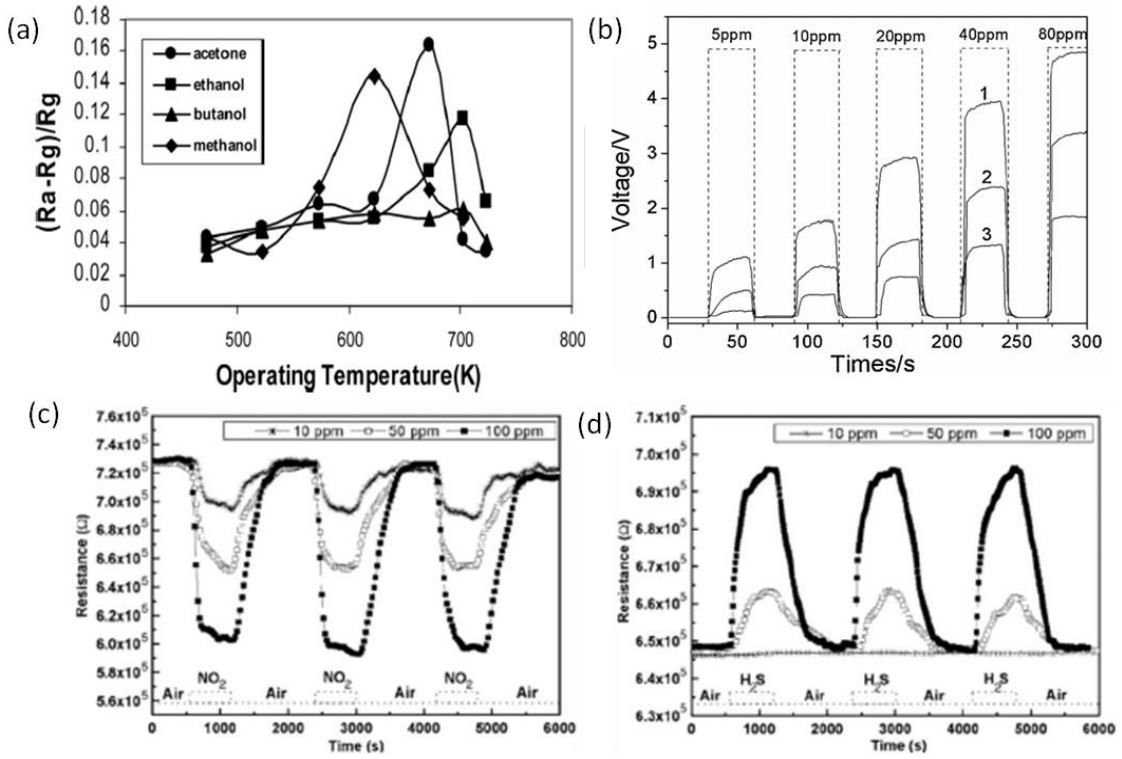

Figure 12 (a) Response of ITO thin fim gas sensor at different VOC [166] (b) Typical response curves of 14-faceted polyhedral (line 1) and octahedral (line 2) $ZnSnO_3$ and $ZnSnO_3$ powder (line 3) gas sensors to ethanol [168] (c) Response of p-type TeO_2 nanowires towards oxidizing NO_2 gas (d) Response of p-type TeO_2 nanowires towards reducing H_2S gas (right) [170]

II.13.5.2. Conjugated polymers

Intrinsically Conducting polymers (ICP) have been widely used as polymer-based chemical gas/vapor sensors in electronic nose systems [171]–[175]. Intrinsically conducting polymers, such as poly (aniline) (Pani) [176], poly (pyrrole) (PPy) [177]–[179], poly (thiophene) (PTh) and their derivatives have been used as the active layer of gas sensors from the 80's and are typically used for e-nose sensing [180]–[182]. As the ICP interacts with gaseous species it can act either as an electron donor or an electron acceptor. If a p-type ICP donates electrons to the gas its whole conductivity increases.

Conversely, when the same ICP acts as an electron acceptor its conductivity decreases. Besides the change in the number of carriers, there can be a change in their bulk mobility due to conformational changes of the polymer backbone [183]. However, the poor environmental stability and sensor drift, due to oxidation of the polymers over time associated with most conjugated polymers, has limited the scope of their use for practical applications [184]. Also one-dimensional conducting polymer nanostructures are promising materials for fabricating polymeric nanodevices such as chemical and bio-sensors [185]. *Hosono et al.* investigated the VOC gas sensing properties of highly conducting poly (pyrrole) thin films prepared by plasma polymerization and doped with 4-ethylbenzenesulfonic acid (EBSA) as shown in Figure 13 (a) [186]. The sensitivity of poly (pyrolle) nanowire to methanol vapour is shown in Figure 13 (b) [187].

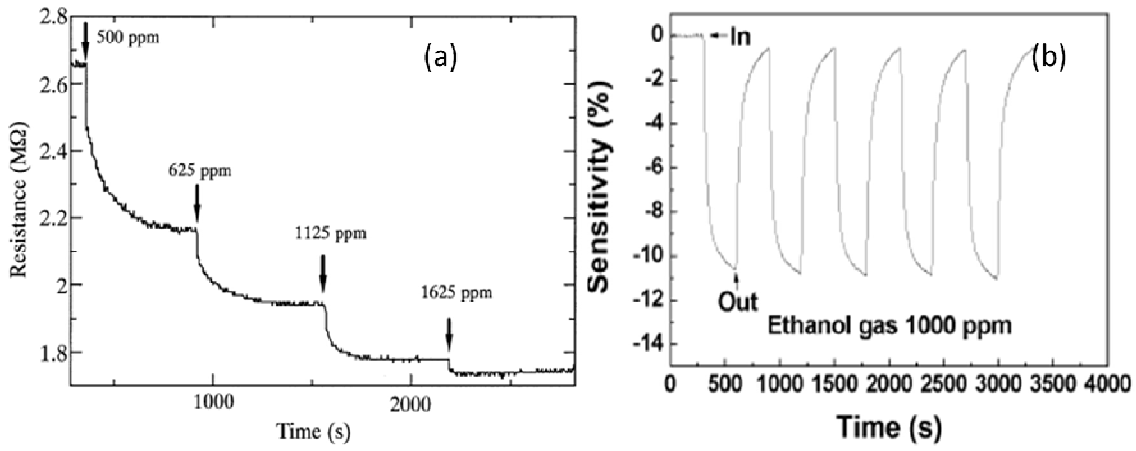

Figure 13 (a) Dynamic response of the PPy/EBSA film maintained at room temperature to increasing acetaldehyde concentration in air [186] (b) Reproducibility of nanowire PPy sensor to ethanol [187]

II.13.5.1. Conductive polymer nanocomposite (CPC) sensors

CPC sensors are polymer composite materials consisting of an insulating polymer matrix and conducting filler. Quantum resistive sensors based on conductive polymer nanocomposites are able to behave as chemoresistive, piezoresistive or thermoresistive, depending upon the nature of external solicitations. External solicitations like chemicals, mechanical strain or temperature lead to interpretable electrical signals, i.e., change in resistivity for chemical sensor, strain sensor [188]–[193] and temperature sensor respectively. These sensors offer some distinct advantages with respect to commercially available sensor technologies such as catalytic sensors, metal oxide sensors, electro-chemical sensors, infrared and optical sensors [194]–[197]. Arrays of detectors, in which each element contains a chemically different polymer, have been demonstrated to allow discrimination between various vapours based on the differences in response patterns produced by the detector array [198].

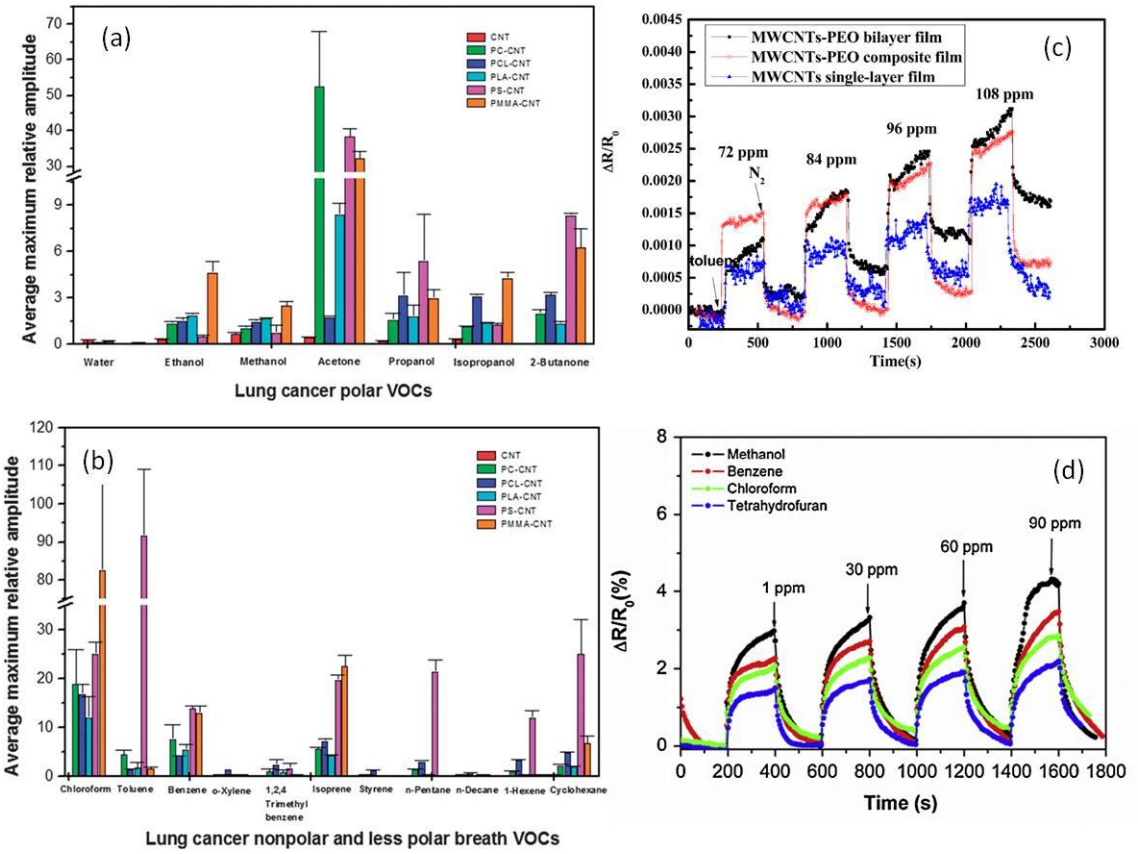

Figure 14 Chemo-electrical response of 6 sensors' array to the saturated (a) 7 polar VOC biomarkers and (b) 11 less and nonpolar VOC biomarkers (chloroform is more a pollutant in breath than a biomarker) [196] (c) Real-time response curves of PEO-MWNT sensors to various toluene vapor concentrations [199](d) Sensing response of RG-O:PIL/PEDOT composite-based chemiresistor sensors upon periodic exposure to different analytes [197]

Polymers are useful materials for chemical vapour sensing for several reasons, such as, their capability to collect and concentrate analytes on sensor surfaces by reversible sorption; their suitability for application on devices as thin adherent films (sensing skins); and the fact that their selective interactions with the vapour is determined by their chemical structure, which can be easily tuned through synthesis. Polymers can yield sensors with rapid, reversible, and reproducible responses. In addition, diverse sets of polymers nanocomposites can be assembled for use in sensor arrays, providing the variable selectivity across the array that is required to obtain useful chemical information for pattern-recognition analysis. For example a room temperature operating electronic nose has been developed by *Chatterjee et al*. by the assembly of conductive polymer nanocomposite (CPC) quantum resistive sensors (QRS) where the selectivity of QRS was varied by changing the chemical nature of the polymer matrix. The e-nose was then successfully used to detect several volatile organic compounds (VOC) selected among lung cancer biomarkers as shown in Figure 14 (a) and (b) [196].

Sensor-array design for detecting organic vapors includes the selection of a set of polymers where each emphasizes a different interaction [200], [201]. For instance, poly(ε-caprolactone) grafted CNT sensors, resulting from the assembly of MWNT functionalized by in-situ ring opening polymerization of caprolactone, were found to be highly sensitive and selective towards organic vapours [202]. Nevertheless, to ensure that functionalization will not degrade nanotube surface, it is possible to use non-covalent bonding, as proposed by *Star et al*. [203] who have adsorbed 1-pyrenesulfonic acid (PSA) on CNT prior to the polymerization of poly(aniline) to form a continuous film on their surface, or *Johnson et al.* [204] who have decorated SWNT with DNA strands. Moreover, *Feller et al.* proposed to control directly CNT/CNT junction gap by either coiling amylose chains around CNT [205] or crosslinking a thin layer of chitosan around CNT [206] which resulted in stable responses with enhanced sensitivity and selectivity. Additional solutions to stabilize the architecture of CNT networks can be found through the use of exclusion volumes with hard [207] or soft spheres [208]. *Zhou et al*. synthesized MWNTs-PEO composite film and bilayer film, fabricated by airbrush spray deposition technology which was sensitive to toluene vapour as depicted in Figure 14 (c) [209]. *Tung et al.* synthesized a thin hybrid film of reduced graphene oxide (RG-O) and poly(3,4-ethylenedioxythiophene) (PEDOT) which was fabricated by means of vapor phase polymerization and explored as active material for chemical sensors for trace level VOC as depicted in Figure 14 (d) [197]. As swelling of the polymer at the nanojunctions is generally assumed to be the key operating mechanism in CPC chemical sensors; *Francia et al*. carried

out a real time investigation of swelling kinetics and electrical response in poly(2-hydroxyethyl methacrylate)/ carbon nanoparticle nanocomposites chemical sensor with respect to ethanol vapours [210].The filler structure and morphology have been found to differently affect the polymer nanocomposite swelling behaviour.

II.14. Smart carbon nanomaterials

Diverse nanostructured materials ranging from nanoparticles (0D) to nanowires and nanotubes (1D) have been explored as active sensing materials because their high surface-to-volume ratio enables electron transport through these materials to be highly sensitive to adsorbed molecules [211]–[213]. Carbon nanomaterials have attracted significant attention from the scientific community for various applications [214] due to their unique electronic, optical, thermal, mechanical, and chemical properties. Carbon nanomaterials, composed entirely of sp^2 bonded graphitic carbon, are found in all reduced dimensionalities including zero-dimensional fullerenes, one-dimensional carbon nanotubes, and two-dimensional graphene [215], [216]. With nanometer-scale dimensions, the properties of carbon nanomaterials are strongly dependent on their atomic structures and interactions with other materials.

II.14.1. Structural aspect of carbon nanomaterials

Carbon is well known to form distinct solid state allotropes with diverse structures and properties ranging from sp^3 hybridized diamond to sp^2 hybridized graphite. Diamond is metastable whereas graphite is the most thermodynamically stable form of carbon at room temperature and consists of a layered two-dimensional structure [217] where each layer possesses a hexagonal honeycomb structure of sp^2 bonded carbon atoms with a C–C bond length of 0.142 nm These single atom thick layers (i.e., graphene layers) interact via noncovalent van der WAALS forces with an interlayer spacing of 0.335 Å. The weak interlayer bonding in graphite implies that single graphene layers can be exfoliated via mechanical or chemical methods. Various carbon allotrops are shown in Figure 15 (a) to (g).
Graphene is often viewed as the two-dimensional building block of other sp^2 hybridized carbon nanomaterials as shown in Figure 15, in that it can be conceptually rolled or distorted to form carbon nanotubes and fullerenes. Graphene, first discovered by Geim and Novoselov in 2004, single layer of carbon packed in a hexagonal lattice, with a carbon-carbon distance of 0.142 nm is the first truly two-dimensional crystalline material, which is stable at room conditions [218]–[220].

The joint award of the 2010 Physics Nobel prize to Andre GEIM and Konstantin NOVOSELOV, as stated by the Royal Swedish Academy (2010), "for groundbreaking experiments regarding the two-dimensional material graphene", highlights the importance of this single atomic layer of carbon. This discovery is considered a breakthrough in the nanotechnology era, bringing the concept of single atomic component closer to reality [221], [222].

Fullerenes are the zero-dimensional form of graphitic carbon that can be visualized as an irregular sheet of graphene being curled up into a sphere by incorporating pentagons in its structure. Fullerenes come in various forms and sizes ranging from 30 to 3,000 carbon atoms.

Carbon nanotube belong to the family of fullerene structures. There are several types of nanotubes including single-walled carbon nanotubes (SWNT), double-walled carbon nanotubes (DWNT), few-walled carbon nanotubes (FWNT) and multiwalled carbon nanotubes (MWNT). The structure of the SWNT can be considered as a one-atom thick layer of graphite rolled up into a seamless cylinder with a diameter of several nanometers, and length on the order of 1–100 microns. MWNT consist of multiple layers of graphite wrapped up together to form a tube shape, sharing the same central axis with a spacing between individual walls of 0.34 nm [223].

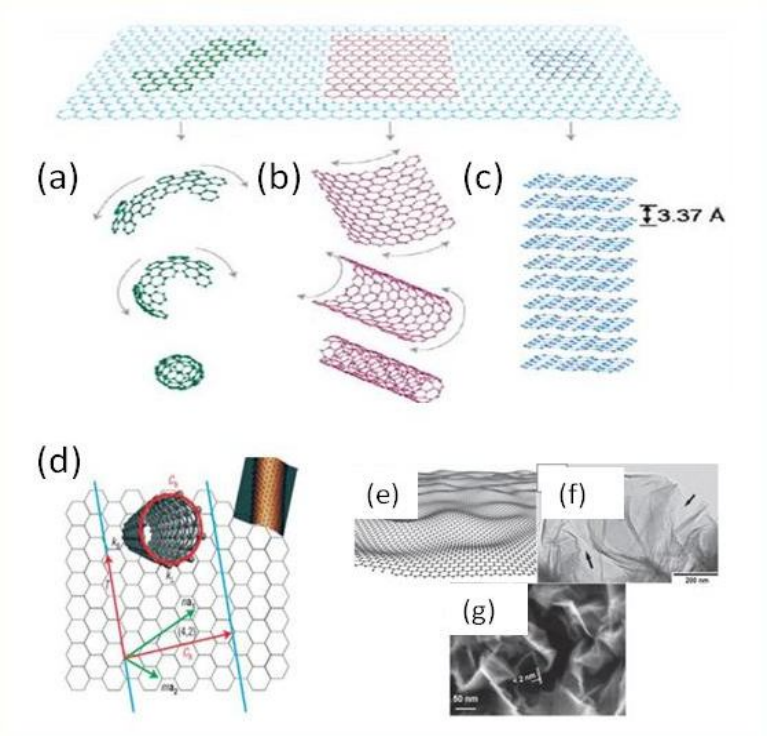

Figure 15 Forms of sp^2-bonded carbon (a) Fullerene (0D), (b) single-walled carbon nanotubes (1D), (c) graphene (2D), graphite [224] (d) schematic of the lattice structure of graphene. Wrapping a rectangular section of graphene along the chiral vector conceptually produces a SWCNT [215] (e) Structural model of pristine graphene, (f) TEM image of graphene, and (g) SEM image of graphene produced from chemical reduction of graphene oxide [225]

II.14.2. Synthesis and growth

The first carbon nanomaterial to be successfully isolated was C_{60} (Buckminsterfullerene) using laser ablation of graphite in a high flow of helium by *Kroto et al.* [226]. Fullerenes have since been synthesized by a large number of groups using a variety of processes which include electric arc discharge, electron beam ablation, and sputtering. Fullerenes have been detected in common combustion flame soot and have also been synthesized using bottom-up chemical methods.

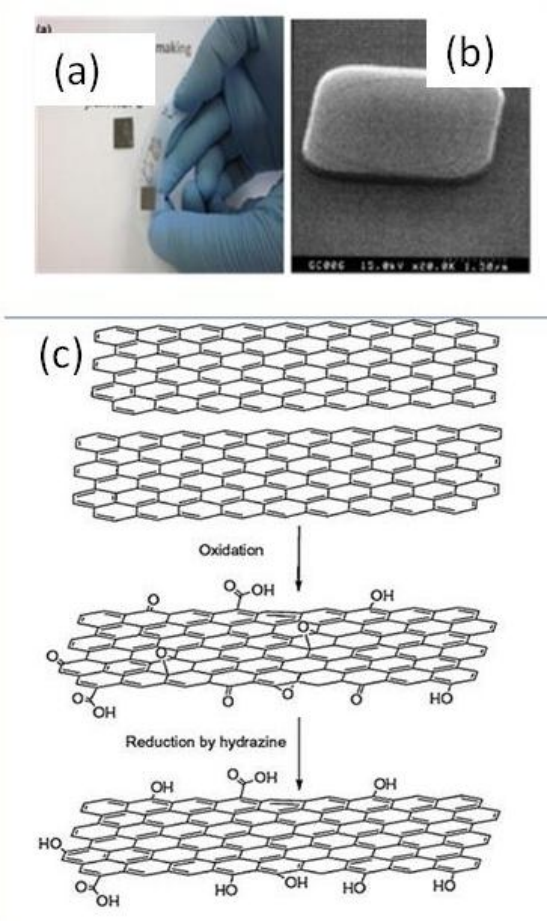

Figure 16 (a) Mechanical exfoliation of graphene using scotch tape (b) SEM image (c) Oxidation of graphite to graphene oxide and reduction to reduced graphene oxide

CNT were firstly observed by *Radushkevich et al.* [227] and then popularized by Iijima [228]. Three main techniques to prepare CNT are: (i) arc-discharge technique; (ii) laser ablation technique; (iii) chemical vapour deposition (CVD) technique. CNT were observed in 1991 in the carbon soot of graphite electrodes during an arc discharge. During this process, the carbon contained in the negative electrode sublimates because of the high discharge temperatures. Of the various means for nanotube synthesis, laser ablation is the most expensive and arc

discharge results in the lowest yield. Therefore, CVD is best for industrial-scale deposition, because of its price/unit ratio, and because CVD is capable of growing CNT directly on a desired substrate, whereas the CNT must be collected in the other growth techniques [229].

Different methods have been reported to fabricate graphene. These methods consist of the mechanical cleaving of graphite, chemical cleaving or exfoliation of graphite, epitaxial growth and chemical vapour deposition [230], [231].

Mechanical exfoliation was the method first used by *Noveselov et al.* to produce high-quality single crystal graphene by repeated stripping of graphite fragment with adhesive tape to eventually obtain isolated single layers [232]. Figure 16 (a) shows such a flake which is a single-layer graphene flake captured on a 300 nm surface. This process is laborious but results in nearly defect-free graphene. Clearly, the micromechanical cleavage method of Nobelists GEIM and NOVOSELOV is not suitable for producing large quantities of graphene from graphite [233].

Chemical exfoliation is a low cost technique for large scale production of multifunctional graphene oxide. Chemical exfoliation of graphite implies employing a strongly acidic solution to introduce oxygen-containing moieties into graphene sheets and create graphene oxide as illustrated in Figure 16 (b).

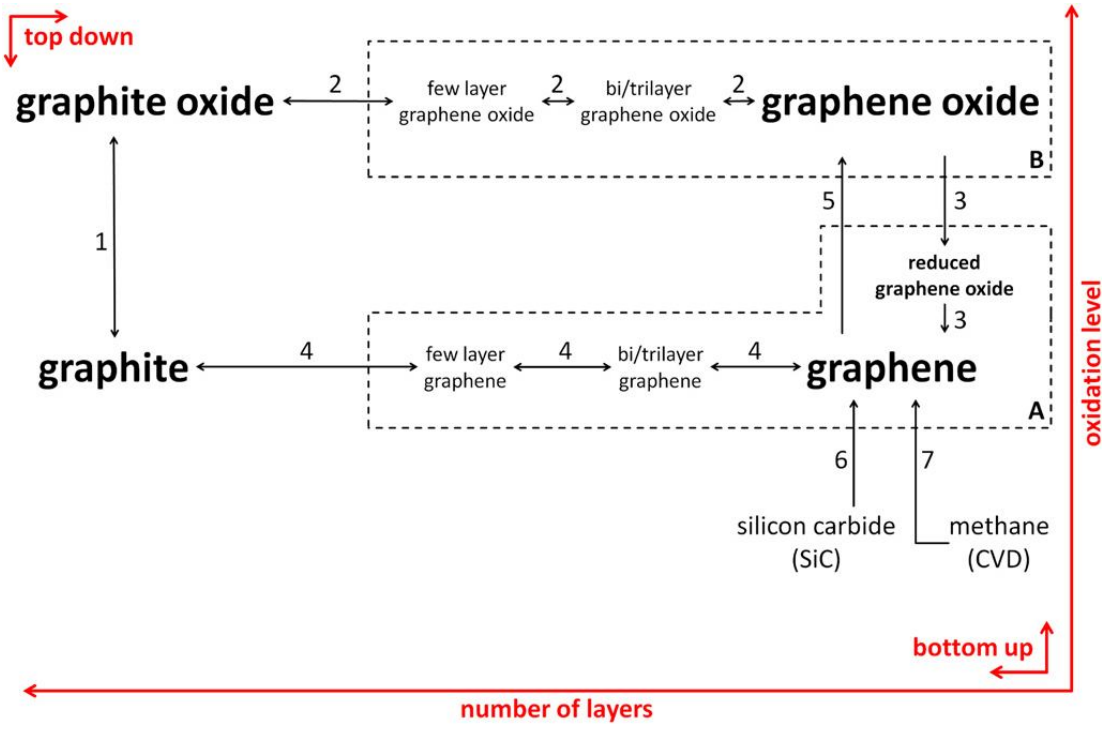

Figure 17 Classification of graphene-related materials Routes: (1) Oxidation of graphite to graphite oxide according to the HUMMERS, STAUDENMEIER or BRODIE method. (2) Step-wise exfoliation of graphite oxide to give graphene oxide in aqueous colloidal suspensions by sonication and stirring. (3) Reduction of graphene oxide

by chemical reactions, thermal annealing, flash reduction, enzymatic reduction or electrodeposition. (4) Mechanical exfoliation of graphite to give graphene (tape method). (5) Oxidation of graphene sheets to graphene oxide. (6) Thermal decomposition of an SiC wafer. (7) Growth of graphene films by chemical-vapour deposition. Group A includes graphene materials primarily used for their electronic properties, group B for their optical properties. [234]

Graphene oxide can be easily exfoliated into individual sheets and dispersed into an aqueous solution due to the strength of interactions between water and the oxygen-containing (epoxide and hydroxyl) functionalities. Graphene oxide is then reduced, either chemically or thermally in an attempt to eliminate as many as possible of these functional groups to restore the original properties of graphene. However the harsh oxidizing conditions irreversibly damage the basal plane of graphene, leading to deterioration of its properties [234].

Epitaxial growth of graphene involves heating hexagonal silicon carbide crystals to temperatures of more than 1200 ºC, which allows evaporation of silicon and then formation of graphene on the basal planes. This technique can produce large areas of continuous graphene layers but electronic properties are disturbed by disorder introduced by the substrate [235], [236].

Chemical vapour deposition (CVD) provides an inexpensive and readily accessible method for producing single-layer and few layer graphene of reasonably high quality. It allows growth of graphene on metal substrates such as copper or nickel from hydrocarbon vapours at temperatures that typically range from 700 ºC to 1000 ºC. CVD-grown graphene is continuous with uniform thickness over large areas, thus making it promising for electronic applications [237]. Classification of the graphene family and the possible routes from one material to another is proposed in Figure 17.

II.14.3. Carbon nanomaterials for vapour sensing applications

The development of nanotechnology has created huge potential to build highly sensitive, low cost, portable sensors with low power consumption. Various nanomaterials such as carbon nanotube [238]–[240], metal oxides nanowires [241], carbon nanoparticles [242] and graphene sheets [243], [244] along with their nanocomposites have been successfully used for the detection of a wide range of gases and vapours. Low-dimensional carbon structures have most of their atoms exposed to the environment and, therefore, offer high specific surface area, which is ideal for adsorption of vapour molecules leading to high sensitivity. Therefore carbon nanomaterials with inherent nanoscale features have the potential for becoming ideal components for the next generation of autonomous sensor technology, since they combine

excellent detection sensitivity with interesting transduction properties in a single layer of material.

The discovery of carbon nanotubes [228] has generated great interest among researchers to explore their unique electrical, physical, mechanical and chemical properties to develop high performance devices. Particularly, the advent of carbon nanotubes has fuelled the inventions of gas/vapour sensors that exploit CNT unique geometry, morphology, and material properties. Upon exposure to certain analytes, the changes in CNT properties can be detected by various methods [245]. The quick change of their intrinsic properties such as conductivity, capacitance and dielectric constant with the adsorption of vapour/gas molecules, makes CNT very attractive candidates for sensors [246]–[248] and biosensors [249], [250]. Although both SWNT [251] and MWNT can be applied for vapour sensing, MWNT exhibit advantages over SWNT, such as ease of mass production, low product cost per unit, and enhanced thermal and chemical stability hence better retention of inherent physical properties on surface functionalization. Because of these advantages of MWNT over SWNT, multiwalled carbon nanotubes (MWNT) were used for vapour sensor construction in this thesis.

Single & multi (few) layer graphene (SLG and FLG, respectively) are shown to have countless scientific and technological breakthrough with novel nanodevice applications [252], [253]. Among this, the most important are chemical [254] and bio sensors [255]–[257] owing to its unprecedented structural, mechanical and electrical properties [258]. The operational principle of graphene based gas or bio electronic sensors is based on the change of graphene's electrical conductivity (σ) due to adsorption of molecules on graphene surface. The ultra sensitive sensor response of graphene with the lowest detection capability approaching even a single molecule for detection of different gases existing in various environments, is due to the following features: (1) potentiality of ultrafast electron transport (highest mobility 200,000 $cm^2.V^{-1}.s^-$) since electrons traveling through the perfect honeycomb lattice of graphene have the smooth sailing [259] (2) every carbon atom in graphene is a surface atom providing the greatest possible surface area per unit volume so that electron transport through graphene is highly sensitive to adsorbed molecular species (3) graphene is transparent, conducting, bendable and yet it is one of the strongest known materials (4) the electrical conductivity of graphene changes drastically upon exposure to and subsequent adsorption of the target chemical species owing to change in free electron concentration (concentration increases/decreases if the target species act as donor/acceptor) [260] (5) Graphene has inherently low electrical noise due to the quality of its crystal lattice and its very high electrical conductivity [261], [262]. The reason

behind the ultra sensitivity of graphene based sensor was nicely explained by Prof. Andre Geim, who said, "*Graphene has the ultimate sensitivity because in principle it cannot be beaten—you cannot get more sensitive than a single molecule*". So, in principle the dynamic range of detection (gas/vapor concentration level) may cover from a single molecule to a very high concentration level, which is impossible with the conventionally used 3D gas sensing materials. The limit of detection (LOD) of graphene sensors are as low as some parts per billion (ppb) level because of low electrical noise of graphene based devices compared to those based on CNT. This is attributed to the two dimensional nature of the material. *Khojin et al.* reported simple chemiresistors with randomly stacked graphene films using surfactant-assisted exfoliation of graphite. They showed superior sensitivity towards target molecules at low filtration volumes compared to previously developed polycrystalline graphene, polycrystalline graphene microribbon, and CNT chemical sensors as depicted in Figure 18 (a) [263]. As shown in Figure 18 (b), *Schedin et al.* fabricated a microscopic sensor made from graphene that is capable of detecting individual gas molecules [264].

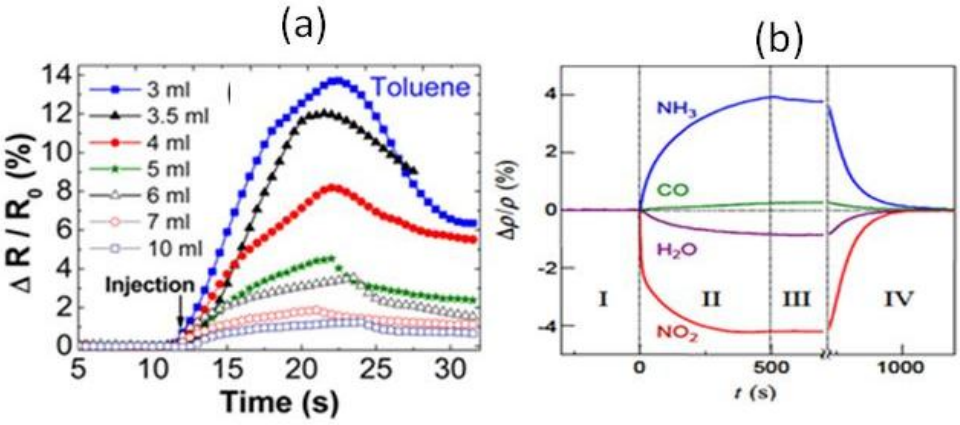

Figure 18 (a) Sensitivity response (%) of randomly stacked graphene sensors with varying filtration volumes to toluene molecules [263] (b) Changes in resistivity, of graphene by exposure to various gases diluted to 1 ppm [264]

In this context it is relevant to remember that computational studies have been useful in elucidating electronic and structural properties of the nanomaterials and demonstrating the gas-sensing mechanisms [265]. Interaction between gas or vapour molecules with different carbon nanomaterials during gas/vapour sensing may be determined via comparison with density functional calculations of gas molecule absorption onto representative defect structures. Density functional theory (DFT) is a computational quantum mechanical modelling method used in physics, chemistry and materials science to investigate the electronic structure of many-body systems, in particular atoms and molecules. Weak covalent interactions, hydrogen

bonding, dipole–dipole and other static binding interactions are included in the density functional calculations although dynamic interactions such as dispersion forces are not considered. *Ewels et al.* had explained through DFT modelling that doping with B or N modifies carbon nanotube morphology and enables the detection of NO_2, CO and C_2H_4 at very low (ppb) concentrations, unlike that of pristine carbon nanotubes [240].

II.14.4. Different strategies for functionalization of carbon nanomaterial based sensing materials: State of the art

The direct use of pristine carbon nanotubes to design vapour transducers is limited by the difficulty to change their selectivity, resulting from their surface chemistry and low sensitivity towards vapour molecules. Moreover although individual graphene sheets are exquisitely sensitive to the chemical environment and offer ultrahigh sensitivity for gas-sensing, the fabrication and operation of devices that use individual graphene sheets for sensing can be complex, expensive, and can suffer from poor reliability due to contamination and large variability from sample-to-sample [262]. As the CNT/graphene network is not protected from pollution by adsorption of non-desirable molecules or structural changes by unexpected deformation, it is likely that their sensing performances will be altered and not durable.

Consequently, functionalization of the sidewalls is mandatory to improve both the solvent dispersion [266] and sensitivity, selectivity of CNT/graphene based vapour sensors. Sensor applications of carbon nanomaterials require chemical modification of the nanotubes by controlled functionalization for the amplification of molecular recognition, selectivity and/or electrocatalytic properties. *Robinson et al*. could show that for chemical sensors, increase in sensitivity and decrease in the level of noise occur by tuning the chemically modified graphene film chemistry [267]. On this account there are two main types of functionalizations: organic and inorganic.

The main focus is on mainly organic functionalization techniques of CNT/graphene, which can be made by two distinct approaches.

1. Covalent attachment via the formation of covalent bonds
2. Non-covalent attachment via electrostatic, van der WAALS, or hydrophobic interactions.

Different functionalization strategies applied on SWNT are schematically shown in Figure 19. While covalent attachment requires complex chemical reactions, the non-covalent attachment

involves dispersing the graphene/ CNT in a solution of functional substances such as surfactants, or protein of polymers.

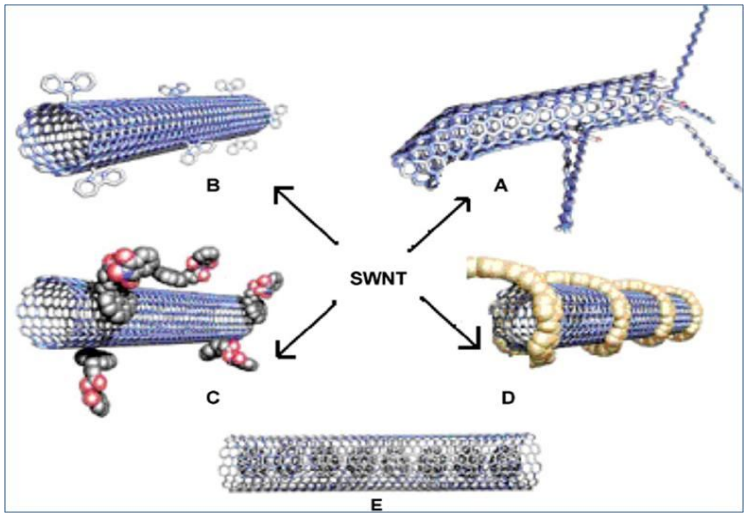

Figure 19 Several functionalization mechanisms for SWNTs [74] (A) Defect-group functionalization; (B) covalent sidewall functionalization; (C) noncovalent exohedral functionalization with surfactants; (D) noncovalent exohedral functionalization with polymers; and (E) endohedral functionalization with C_{60} [268].

II.14.4.1. Noncovalent functionalization

Noncovalent functionalization of CNT or graphene [269] are based on secondary interactions such as π–π stacking, hydrogen bonding, or electrostatic, van der WAALS, or hydrophobic interactions. Non-covalent functionalization of carbon nanomaterials is of particular interest because it does not compromise the physical properties of CNT/graphene, does not interfere in any destruction of aromatic structure [270], [271].

Graphite oxide (GO) is chemist's principal tool to modify graphene. It is obtained from the exhaustive oxidation of graphite, and contains a range of oxygen functional groups with specific chemistry, rendering it a good candidate for further functionalization [272]. GO can also form various multifunctional materials through non-covalent bonds, either of the Van der WAALS or ionic type, as its surface is negatively charged due to the presence of oxygen functional groups. In addition, its graphitic structure with delocalized π orbital allows π-π interaction. Chemical functionalization of graphene enables this material to be processed by solvent- assisted techniques, such as layer-by-layer assembly, spin-coating, and filtration. It also prevents the agglomeration of single layer graphene during reduction and maintains the inherent properties of graphene [273].

Chemical or thermal reduction of graphene oxide platelets can restore the graphitic network in the basal plane of reduced graphene oxide platelets. Consequently, reduced graphene oxides have been frequently modified by non-covalent physisorption of both polymers [274] and

small molecules onto their basal planes via π-π stacking or van der WAALS interactions. Adsorption of pyrene and perylene derivatives and other aromatic species is likely caused by π-π stacking interactions [275]–[277]. It is reported by *Mao et al.* that non-covalent functionalization of graphene with 1-pyrenecarboxylic acid (PCA), enhances the sensitivity of graphene to a large variety of polar molecules, such as acetone, ethanol, ethyl acetate, iso-propanol, methanol etc., as shown in Figure 20 [278].

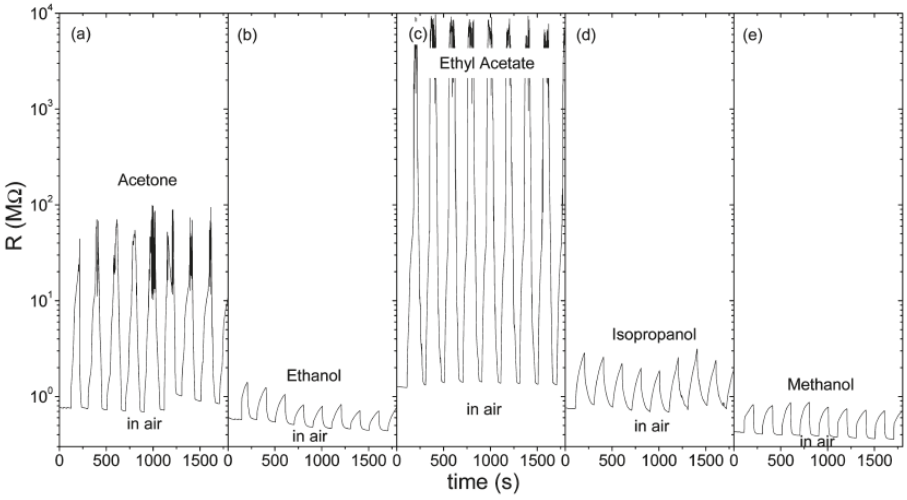

Figure 20 Variations of PCA functionalized graphene sensor resistance in response to periodic exposure to saturated vapors of different organic solvents [278]

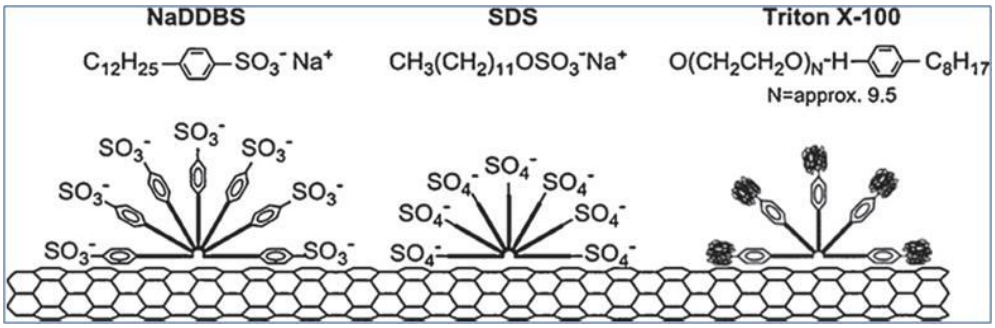

Figure 21 Schematic diagram of surfactants adsorbed nanotube [279]

Noncovalent functionalization of CNT mainly involves surfactants [280]–[282] biomacromolecules or wrapping with polymers, and are based on weak interactions such as hydrogen bonding, π-π stacking, electrostatic forces, van der WAALS forces and hydrophobic interactions [283]. In the search for non-destructive purification methods, nanotubes can be transferred to the aqueous phase in the presence of surfactants. In this case, the nanotubes are surrounded by the hydrophobic components of the corresponding micelles. The electrostatic repulsion provided by adsorbed surfactants stabilizes the nanotubes against the strong van der

WAALS interactions between the nanotubes, hence preventing agglomeration. This repulsive and attractive force balance creates a thermodynamically stable dispersion, which results in separation of CNT from the bundles into individual nanotubes. Anionic surfactants, such as sodium dodecylsulfate (SDS) and sodium dodecylbenzene sulfonate (NaDDBS) shown in Figure 21, are commonly used to disperse CNT aggregation in polar media [284].

The physical interaction of polymers with CNT to make specific formation can be explained by the 'wrapping' mechanism which is π-stacking interactions between the polymer and the nanotube surface.

II.14.4.2. Covalent functionalization

The covalent functionalization of CNT/graphene creates discrete zones of discontinuity on sp^2 hybridized network not allowing the electron conduction, which has significant implications in reducing the conductivity of nanocomposites.

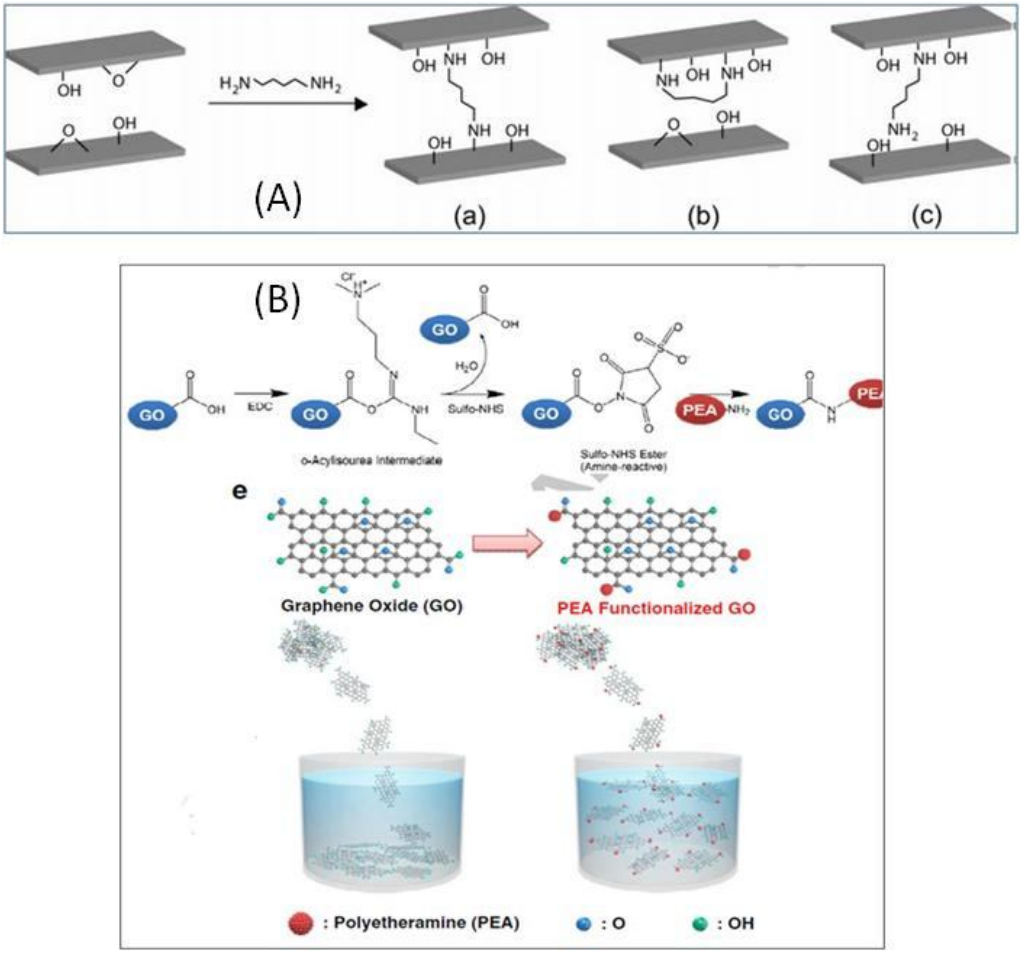

Figure 22 (A) Schematic representation of the intercalation reaction of a diaminoalkane in the interlayer spacing of GO, showing the intercalant in a bridge conformation (a), loop conformation (b), and tail conformation (c) [285] (B) Functionalization of GO with poly ether amine [286]

But this functionalization can improve solubility as well as dispersion in solvents and polymer and can help in the improvement of selectivity and sensitivity of CNT/graphene based sensors by utilizing the interaction between analyte VOC with the organic functionality grafted covalently on the surface of nanofiller. Covalent functionalization can be accomplished by either modification of surface-bound carboxylic acid groups or by direct reagents to the side walls.The covalent modification of graphene can be achieved in four different ways: nucleophilic substitution, electrophilic addition, condensation, and addition [273]. In contrast to reduced graphene oxide, the existence of various types of oxygenated species (carboxyl, epoxy and hydroxyl groups, etc.) facilitates the covalent molecular functionalization of GO as in Figure 22 (A) and (B) [285], [286]. The main reactive sites in the nucleophilic substitution reaction are the epoxy groups of GO. The amine functionality of the organic modifiers bearing a lone pair of electrons attacks the epoxy groups of the GO. In comparison to other methods, nucleophilic substitution occurs very easily, also at room temperature and in an aqueous medium.

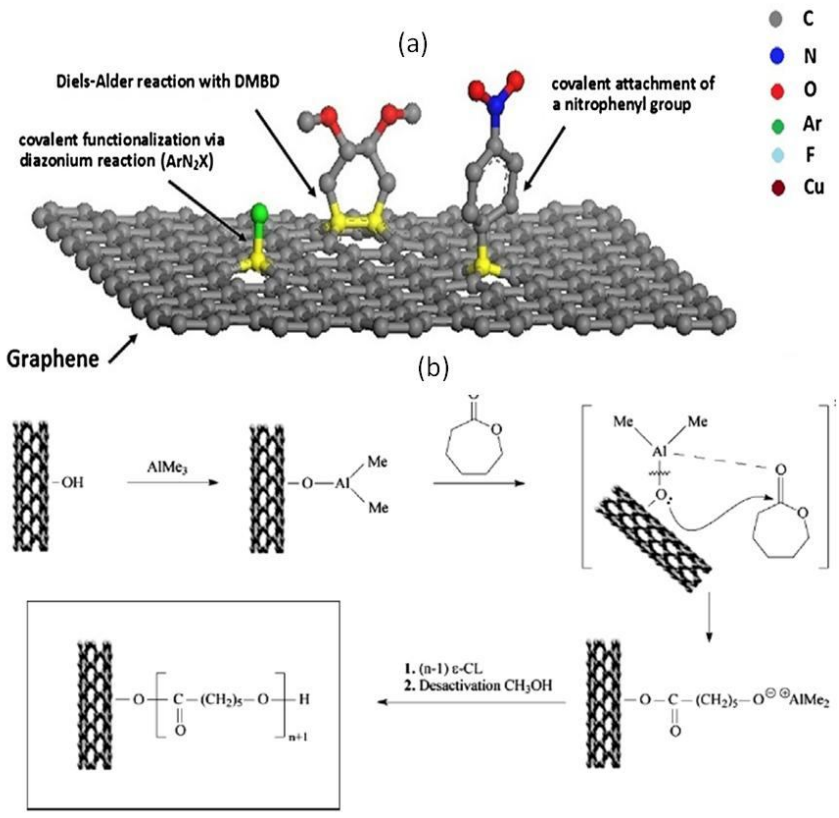

Figure 23 (a) Schematic illustration of covalent functionalization of graphene [287] (b) Schematic representation of different steps leading to PCL-g-CNT CPC [202]

Graphene is chemically unsaturated due to the presence of sp^2 hybridized carbon atoms, thereby its surface functionalization is associated with rehybridization of one or more sp^2 carbon atoms of the carbon network into the sp^3 configuration accompanied by simultaneous loss of electronic conjugation [65], [288] as shown in Figure 23 (a) [287].

Because of the orbitals of the sp^2-hybridized C atoms, CNT are more reactive than flat graphene sheets, and they have an enhanced tendency to covalently attach with chemical species [289]. The chemically functionalized CNT can produce strong interfacial bonds with many polymers, allowing CNT-based nanocomposites to possess high mechanical, functional properties and good sensing performance. For example, *Castro et al.* fabricated vapour sensors by covalent grafting of ε-caprolactone on the surface of CNT by ring opening polymerization as in Figure 23 (b) with high amplitude of response [202].

II.14.4.3. Hybridization

In general, combining two or more different materials via interaction forces leads to novel hybrid materials [290]–[294] which have received substantial interest in both the academic and technological domains due to their exceptional properties and applications [295]–[304]. Although CNT, graphene or fullerenes may constitute a highly functional architecture individually, their different shapes and material properties can also be synergistically hybridized by a co-assembly strategy [305]–[309].

Rapid charge transfer and conduction is normally expected from the 3D multiplexed highly conductive network. The incorporation of CNT into graphene either by CVD or physical mixing can not only improve the surface area of graphene materials, but also act as “spacer” to supply diffusion path, facilitating rapid transport of the electrolyte ions within the electrode material [310], [311].

Jeong et al. presented a flexible room temperature NO_2 gas sensor as shown in Figure 24 (a) consisting of vertical carbon nanotubes CNT/reduced graphene hybrid film supported by a polyimide substrate [312]. *Tung et al.* reported a hybrid of magnetic and silver nanoparticle decorated-reduced graphene oxide sensor with better sensitivity and selectivity when compared to pristine graphene sensor as in Figure 24 (b) [243]. *Zhang et al.* have demonstrated the preparation of 3D CNT-pillared graphene oxide and reduced graphene oxide nanostructures with tuneable length of the CNT as shown in Figure 24 (c) resulting in reduction of the dynamic resistance of ion transport due to the synergetic effect between the 1D CNT and 2D reduced graphene oxide platelets [313].

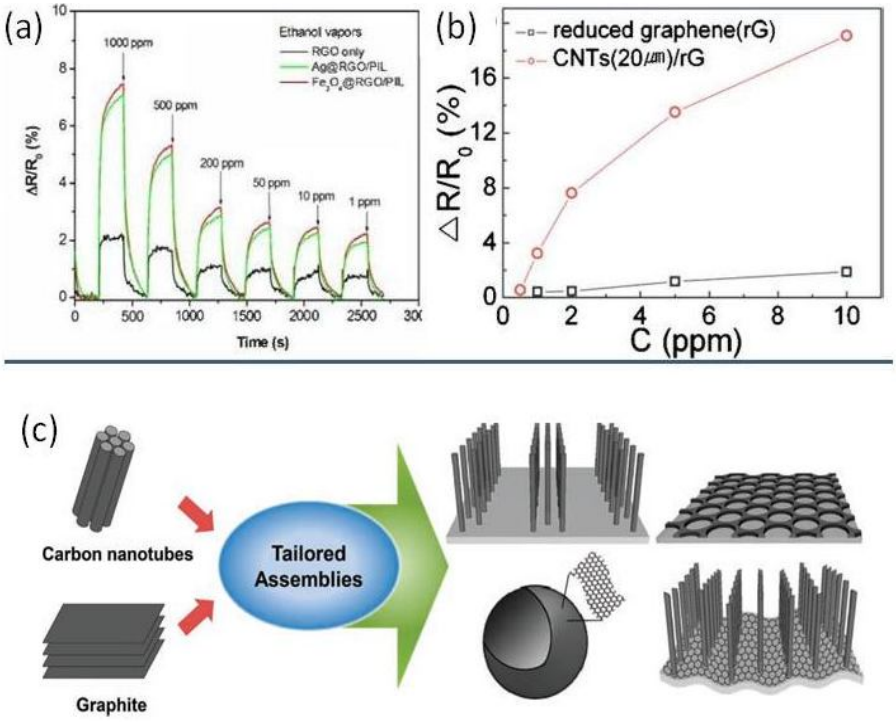

Figure 24 (a) Sensing responses as a function of different ppm concentrations of ethanol vapors [243] (b) Resistance response of reduced graphene and CNT/reduced graphene gas sensors measured after 60 min exposure to NO_2 at various concentrations [312] (c) Schematic illustration of tailored assembly of carbon nanotubes and graphene into hierarchically organized three-dimensional architectures. [310]

II.15. Safety and security: Environmental issue with carbon nanomaterials

Although carbon nanomaterials have gained immense research interest for multidisciplinary applications due to their extraordinary properties, synthesis and application of carbon nanomaterials by many industries increase unintended or intentional human exposure, creating the need to determine its safety profile and potential toxic effects.

II.15.1. Toxicity of carbon nanotubes

Potential toxic effects of MWNT on living organisms are due to the following properties of CNT: 1) being nanoscopic, MWNT may deposit in the deep lung on chronic exposure, leading to damage to the mitochondrial membranes, oxidative stress, and even death [314], [315]. They can also enter the bloodstream leading to cardiovascular diseases or inflammatory response in the lung [316]; 2) MWNT are thin, fibrous with high aspect ratio, which may exert asbestos-like pathogenic effects like mesothelioma on prolonged exposure [317]; and 3) MWNT are resistant to high temperature and acid treatment, so are considered durable. Moreover intratracheal administration of SWNT or MWNT may cause pulmonary inflammation as

shown in Figure 25. MWNT are genotoxic as shown by in vitro studies, hence carcinogenic. Chronic exposure to MWNT may induce DNA damage and increase mutation frequency [318]. However toxic effects of CNT are influenced by various factors such as surface charge, shape, length, diameter, agglomeration, and purity [319].

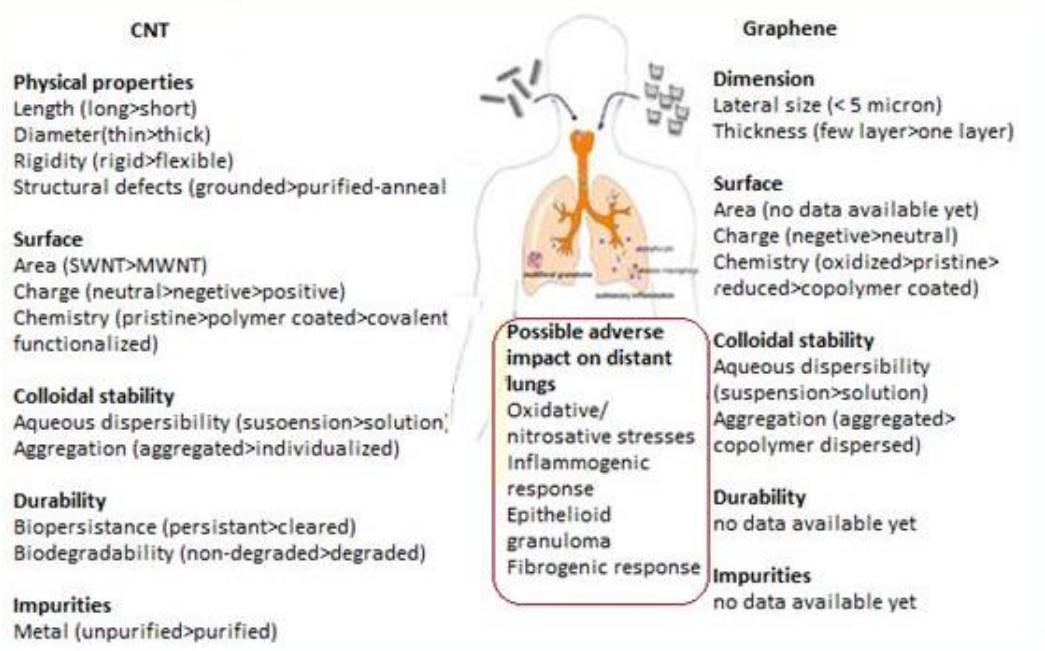

Figure 25 Physicochemical characteristics of CNT and graphene relevant to pulmonary exposure and adverse effects. The first characteristic in brackets induces the most severe biological response [320]

II.15.2. Toxicity of graphene

Although both carbonaceous, carbon nanotube and graphene are structurally very distinct as shown in, Figure 25. Overall, graphene and its derivatives are characterized by a lower aspect ratio, larger surface area, and better dispersibility in most solvents compared to carbon nanotubes. Very importantly, graphene nanostructures are not fibre-shaped. These features theoretically offer significant advantages in terms of safety over inhomogeneous dispersions of fibre-shaped carbon nanotubes.

Three primary rules have been ordered that can be applied in the development of graphene-based biomedical applications to enhance the overall safety from exposure of the material and minimize the risks for adverse responses: (1) use of small, individual graphene sheets that macrophages can efficiently internalize and remove from the site of deposition; (2) use of hydrophilic, stable colloidal dispersions of individual graphene sheets to minimize aggregation in vivo; and (3) use of graphene material that can be excreted or chemically modified graphene that can be degraded effectively [320]–[322].

II.15.3. Occupational exposure limits: safe handling of toxic nanoparticles

In the workplace, inhalation is suspected to be the most potentially harmful human exposure to nanoparticles (NP), followed by dermal exposure and ingestion [323], [324]. Concern about health and environmental effects due to NP was taken into consideration by industries and public agencies, and the first study of workplace-related exposure was performed in 1998 by the International Carbon Black Association [325]. One of the major tools for prevention of occupational disease from exposure to specific agents is the use of occupational exposure limits (OELs) [326]. The nano-reference values (NRV) are also introduced as a voluntary risk-management instrument for airborne nanomaterials in the workplace. NRV are intended to be precautionary warning levels, and, when they are exceeded, exposure-control measures should be taken.

II.16. Conclusion and outlook

This review was initially focused on the limitations of conventional diagnostic tools for detection of cancer at preliminary stage, which has emerged as a serious problem for the cancer researchers. Afterwards, in this context, the immense importance of breath testing as a noninvasive cancer diagnostic technique was elaborately discussed. Although a huge amount of research has taken place on spectroscopic and chromatographic tools of breath VOC biomarker analysis, it is found that until now the commercial applications of this technique has been impeded by the need for expensive equipment, nonportability, large response time and complexity of operational technique. Clearly, the invention of a noninvasive, fast, reliable, economic, portable and easy technique is highly required before breath testing become a clinical reality. Nanomaterial based sensor arrays can most possibly fulfil all these requirements and are therefore very attractive for breath VOC biomarker analysis. Thus arrays of broadly cross reactive nanomaterial based chemoresistive sensors can form a solid foundation for identification of disease related VOC patterns in exhaled breath.

II.17. Experimental strategies undertaken from the light of literature survey

From this literature survey it is well clear that pristine CNT is considered as a suitable candidate for vapour sensing because of its fast change in conductivity, dielectric constant or capacitance with adsorption of gas or vapour molecules [22]. Graphene is also expected to perform well as a chemical vapour sensor, since absorption of individual gas molecules onto graphene-based sensor brings about significant changes in electrical resistance [264]. Moreover

because of the high carrier mobility of graphene [232], [327], a high room temperature sensitivity and high signal to noise ratio [328] are achievable with graphene based quantum resistive sensors. Unfortunately its poor dispersbility in organic solvents, inability to control selectivity (due to surface property), low sensitivity to vapour molecules (due to small junction gap) and hence poor tunnelling effect, are the limitations of using pristine CNT or graphene for vapour sensing [246]. Covalent or noncovalent functionalization of CNT/graphene with various polymeric or non-polymeric organic, inorganic or biological molecules may bring about a solution to the above mentioned problems of pristine carbon nanomaterials.

The development of a set of sensors with enhanced sensitivity and selectivity towards targeted cancer biomarker VOC is our objective so that the set of sensors can be integrated finally into an electronic nose with high efficiency in the discrimination of diverse group of VOC. For this purpose different strategies were undertaken to synthesize conductive nanocomposites, which are mentioned below.

II.17.1. Strategy 1: Conductive oligomeric nanocomposites (COC)

Non-covalent modification of chemically functionalized cyclodextrin with reduced graphene oxide was carried out by using pyrene adamantan as a linker wherever necessary, in order to construct a supra molecular assembly. The chemical functionality on cyclodextrin was varied utilising the principle of selective chemical modification of cyclodextrin.

The final objective of this strategy is to exploit, the combined benefits of host-guest inclusion complex formation ability and tuneable chemical functionality of cyclodextrin, as well as high surface area and electrical conductivity of graphene, for the development of a set of highly selective chemical vapour sensors as elaborated in chapter III.

II.17.2. Strategy 2: Conductive nanohybrids

Hybridization of more than one nanofillers by covalent or non covalent functionalization was adopted in this strategy (as described in chapter IV) to develop a multicomponent system where two or more nanomaterials are integrated, for the purpose of synthesizing a novel nanomaterial with attractive sensing performance [329].

II.17.3. Strategy 3: Conductive polymer nanocomposites (CPC)

Conductive polymer nanocomposites were synthesized using an insulating polymer matrix and conductive nanofillers like CNT as elaborated in chapter V. In this strategy the selectivity of

the sensors towards a targeted VOC is brought about by the appropriate choice of the polymer matrix.

Chapter III:
Vapour sensing properties of cyclodextrin based conductive nanocomposites

Summary

A novel electronic nose system comprising functionalized β-cyclodextrin wrapped reduced graphene oxide (RGO) sensors with distinct ability of discrimination of a set of volatile organic compounds, has been developed. Non-covalent modification of chemically functionalized cyclodextrin with RGO was carried out by using pyrene adamantan as a linker wherever necessary, in order to construct a supra molecular assembly. The chemical functionality on cyclodextrin was varied utilizing the principle of selective chemical modification of cyclodextrin. In the present study, the combined benefits of host-guest inclusion complex formation ability and the tuneable chemical functionality of cyclodextrin, as well as high surface area and electrical conductivity of graphene were utilized for the development of a set of highly selective chemical vapour sensors. Finally the effect of polymerized cyclodextrin on vapour sensing performance of graphene based sensors was studied.

III.1. Introduction

Because of its unique physicochemical properties such as high electrical (7200 $S.m^{-1}$) [330] and thermal conductivity (5000 $W.m^{-1}.K^{-1}$) [331], large surface area (2630 $m^2.g^{-1}$ for single layer) [332], high aspect ratio, mechanical strength (130 GPa) [333], optical transmittance, flexibility [334], high carrier mobility and charge carrier concentration at room temperature (250000 $cm^2.V^{-1}.s^{-1}$) [222], graphene has found many potential applications [335] including sensors [336]. Non-covalent modification of graphene oxide (GO) with different functional molecules followed by reduction not only helps to prevent the restacking of individual graphene sheets, but also may bring about alteration of sensitivity and selectivity of the graphene based quantum resistive sensors to different volatile organic compounds [337], [338].

The β-cyclodextrin (CD) is a cyclic oligosaccharide having a toroidal shape. β-CD is composed of 7 D-glucopyranosidic units containing a hydrophobic internal cavity and a hydrophilic outer side with primary and secondary hydroxyl groups on narrower and wider side respectively. The presence of hydroxyl groups on its outer surface not only makes CD water soluble but also makes it eligible for regio-selective chemical modification [339], while the hydrophobic internal cavity provides an ability to form host guest inclusion complexes with various organic, inorganic, biological guest molecules and polymers showing high molecular selectivity [340]. The main driving forces for the host guest inclusion complex formation are hydrophobic interaction, van der WAALS interaction or hydrogen bonding. Various fields of applications of chemically modified CD include drug delivery [341], catalysis [342], sensing [343], artificial channels [344], and loading and release of hydrophobic molecules [345].

A synergistic effect between RGO (due to high conductivity and high surface area) and native CD (thanks to host-guest recognition and enrichment) has been anticipated in 2010 by *Guo et al.* who found that RGO-CD hybrids simply prepared by dispersing CD in a graphene oxide (GO) solution followed by the reduction of GO, led to interesting electrochemical response towards biomolecules and drugs, unlike unmodified graphene or carbon nanotubes [346]. Additionally, *Kong et al.* have successfully grafted monofunctional-CD derivatives onto SWNT (Single wall carbon nanotube) by in situ diazonium reaction, to synthesize novel SWNT-CD with excellent sensitivity and selectivity towards organic pollutants, thanks to molecular recognition [347]. MWNT (multi walled carbon nanotubes) was also functionalized with monofunctional CD, dangling on the MWNT and thus providing an easy access to the cavity of the CD [348]. *Yang et al.* also reported the adsorption of a protein, bovine serum albumin, on these functionalized MWNT through non-covalent interactions with CD

derivatives functionalized aligned carbon nanotubes for the electrochemical sensing of DNA via host–guest recognition [349]. Their study recalls that the diazonium reaction does not allow the formation of a single layer of cyclodextrin on the carbon nanotubes, which may limit the performances of the detection. Finally, *Guo et al.* modified native CD with a pyrene residue to allow the adsorption of the pyrene labeled cyclodextrin on SWNT to prepare light-switchable SWNT [350]. However, the reported modifications of graphene or CNT for sensing applications are not versatile, and can only be dedicated to one kind of detection. Furthermore, no chemo-resistive sensing application has been investigated with cyclodextrin functionalized conductive nanocomposites so far.

The originality of the present work is to take benefit from the multiscale architecture of quantum chemo-resistive transducers resulting from the supramolecular assembly of graphene and CD-derivate hybrids, in order to get a high sensitivity of the nanoswitching at junctions due to the insertion of CD between graphene foils. A tailorable selectivity to cancer biomarkers can also be obtained due to CD functionalization and geometry. This strategy includes the effectiveness of spray layer by layer to maintain the nanomaterial's properties across the different scales (from nano to micro) and the versatility of non-covalent bonding of functionalized-CD onto graphene via a pyrene spacer (by π-π stacking), which preserves at the same time the integrity of conducting foils and manages to some extent junctions' gap. Moreover, RGO-CD is expected to combine two types of molecular recognitions, non-specific, via van der WAALS interactions, and specific reversible chemical reactions with CD functions, coming for instance, from a free amino group that can react with acetone.

The objective of the present study was to develop chemo-resistive sensors with distinct ability to discriminate a set of VOC lung cancer biomarkers. Efficient detection and clear discrimination of alcohols, ketone bodies like acetone and aliphatic or aromatic hydrocarbons was targeted in the present study. Since breath extract contains huge amount of water with trace amounts of VOC [83], water is also be included into the selected set of VOC. In the present work different varieties of chemically functionalized cyclodextrins were wrapped onto RGO using pyrene adamantan as linker wherever necessary. A nanocomposite of cyclodextrin modified graphene can be considered as a functional hybrid material which can take the advantages of high electrical conductivity and large surface area of graphene and also tuneable molecular selectivity of CD. Hence further, these functionalized CD modified graphene are leading to high performance chemical sensors. The key goal of this present work is, to be able to tune the molecular selectivity of cyclodextrin modified graphene based sensors by altering

the chemical functionalities of CD. The specific functionality of CD would thus act as the key parameter to control the molecular selectivity of the sensors.

III.2. Synthesis of nanocomposites and fabrication of sensors

The consideration of the wide range of polar/non-polar interactions possible with the selected biomarkers is justifying the varieties of transducers used (Table. 3):

- ✓ Reduced graphene oxide (RGO) will exhibit non-polar interactions and low disconnection capability, it is used as a reference,
- ✓ Pyrene adamantan linked RGO (RGO@PYAD) will increase junctions' gap due to PYAD spacer but is not expected to change selectivity,
- ✓ Native cyclodextrin linked RGO (RGO@PYAD-CD) is providing OH polar groups susceptible of interaction with polar analytes,
- ✓ Mannose functionalized cyclodextrin linked RGO (RGO@PYAD–MCD) is providing OH polar groups with a longer spacer capable of easier disconnection,
- ✓ Amino functionalized cyclodextrin linked RGO (RGO@PYAD-NCD) is bringing reversible covalent bonding of its free amino group with acetone for instance,
- ✓ Perbenzylated cyclodextrin linked RGO (RGO@PBCD) is providing a strong non-polar character to the junction due to its numerous aromatic rings.

The variety of CD functionalization is a strong advantage, which makes this molecule an important brick in the sensors' design, allowing tailoring the junction's physico-chemical properties, i.e., the gap and the intermolecular interactions. Moreover, the association of functionalized CD with RGO foils is expected to preserve the accessibility of analytes to functional sites by maintaining a distance between foils that can be varied as a function of substituents' size and conformation.

The fabrication of quantum resistive sensor (QRS) is a key point to ensure a good reproducibility of sensing performances. Firstly, the RGO decorated with different kinds of functionalized cyclodextrins needs to be efficiently dispersed in acetone with the aid of ultra-sonication for 1 h at 50 °C with a BRANSONS 3510 device (100 W, 40 kHz), and secondly this well dispersed solution can be sprayed layer-by-layer (sLbL) onto inter-digitated electrodes

[351]. Both the solutions' content and the number of sprayed layers allow to adjust the initial resistance of all the sensors to comparable values, so that only the chemical functionality of CD and not the transducer's percolation level [352], will have an influence on sensors sensitivity to VOC. After fabrication, all sensors were conditioned in controlled atmosphere for one night before chemo-resistive tests.

III.2.1. Synthesis of pyrene butyric acid adamantine methyl amide (pyrene adamantan/ PYAD)

0.77 g of 1-pyrenebutyric acid N-hydroxy succinimide ester (2 mmole) was dissolved in dried methylene chloride followed by the addition of 2 mmole 1-adamantanemethylamine. The reaction mixture was stirred under nitrogen at room temperature for 91 hours. After evaporation of the solvent, the product was purified by silica flash chromatography. The used eluant was first CH_2Cl_2 then a mixture CH_2Cl_2/methanol (95/5). Pure pyrene butyric acid adamantanemethyl amide was obtained with a yield of 65% as in Figure 26.

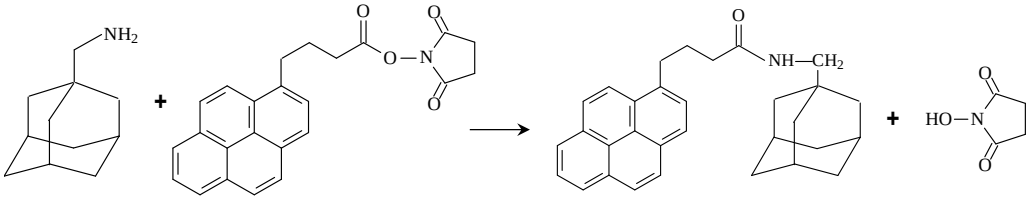

Figure 26 Synthesis of pyrene adamantan

III.2.2. Synthesis of Graphene Oxide (GO)

Graphite oxide (GO) was synthesized from natural graphite powder by a modified Hummers method [353]. Briefly, 5 g of graphite and 3.75 g of $NaNO_3$ were placed in a flask. Then, 375 mL of H_2SO_4 was added while stirring in an ice-water bath, and 25 g of $KMnO_4$ were slowly added for 1 h. Stirring was continued for 2 h in the ice-water bath. The reaction mixture was washed with deionized water, and reacted with a 30 wt. % 150 mL aqueous solution of H_2O_2 to complete oxidation. The ions of oxidant and other inorganic impurity were removed by repeating cycle of centrifugation, removal of the supernatant liquid, and redispersing the solid using 3 wt. % HCl aqueous solution. Finally, the solid was dispersed again in water using ultrasonication for 2 h and centrifuged at 6000 rpm for 30 min to remove the multilayered species followed by reduction with hydrazine hydrate at 100°C under reflux condition for 24 hours.

III.2.3. Synthesis of RGO and pyrene adamantan linked RGO (RGO@PYAD)

For preparation of pyrene adamantan linked RGO, 250 mg pyrene adamantan was dispersed in ethanol and added to aqueous homogeneous dispersion of GO followed by stirring at room temperature for 6 hours. After addition of hydrazine hydrate the in-situ reduction of GO was carried out at 100°C under reflux condition for 24 hours. The stable black dispersion was filtered with a nylon membrane (0.2 µm) to obtain pyrene adamantan linked RGO. Additionally, the preparation of RGO was similar except addition of pyrene adamantan.

III.2.4. Synthesis of functionalized CD wrapped RGO

In the final step of synthesis, three different functionalized oligomeric cyclodextrins (CD) were treated with RGO@PYAD. Synthesis and characterizations of functionalized CD is available in the appendix at the end (page number 148). Globular shaped adamantan of about 0.7 nm diameter [354] fits inside the cage of cyclodextrin as shown in route (a) of Figure 27. Preparation technique was similar for perbenzylated CD modified graphene except the fact that chemical modification of graphene with perbenzylated CD was done directly, taking the advantage of π-π interactions between them, without the use of pyrene adamantan as in route (b) of Figure 27.

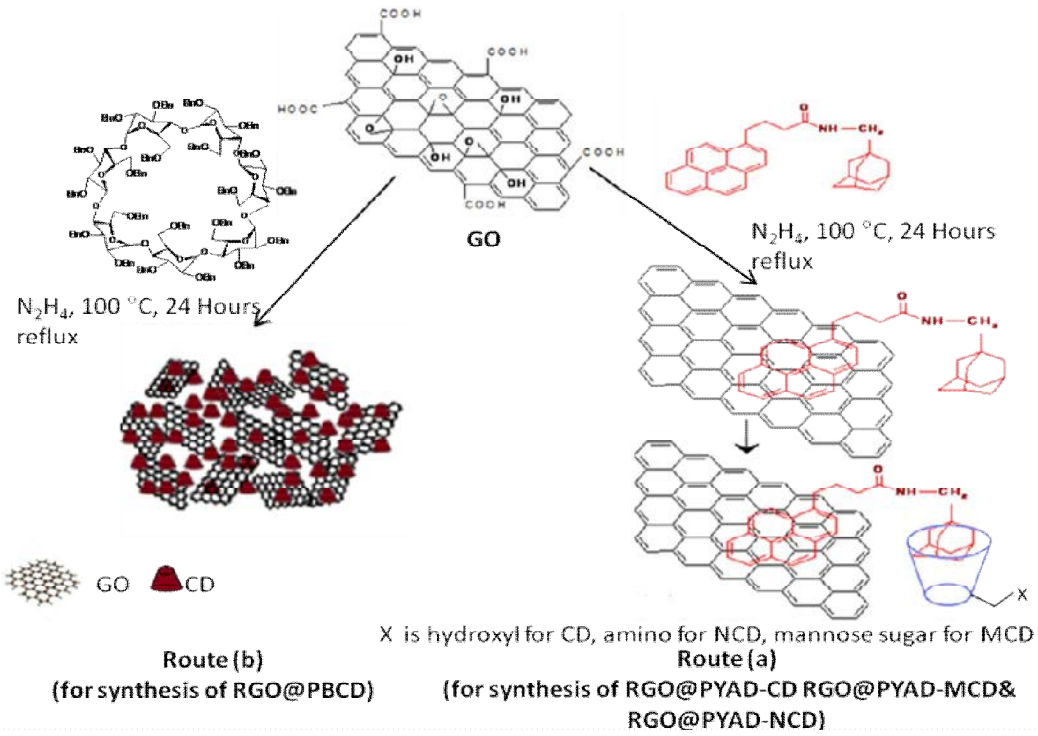

Fig. 27 Synthesis of supramolecular assembly of functionalized cyclodextrin and RGO

The synthesis, characterizations of functionalized cyclodextrins along with the sensor fabrication techniques are available in the appendix (page number 148) at the end of this manuscript. The details of composition and fabrication conditions of each sensor are provided in Table 3.

Description of the sensor	**Designation of sensor**	**Structure of CD attached**	**Number of layers sprayed**	**Initial resistance of the sensor (R_0) KΩ**
Reduced graphene oxide	RGO	N.A	8	120±4
Pyrene adamantan linked RGO	RGO@PYAD	N.A	9	130±6
Native cyclodextrin linked RGO	RGO@PYAD-CD	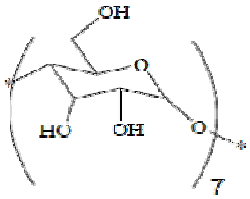	10	150±7
Mannose functionalized cyclodextrin linked RGO	RGO@PYAD–MCD	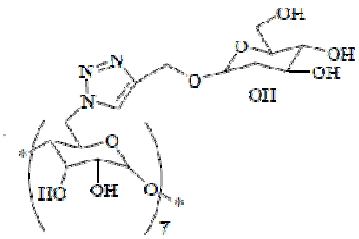	12	150±3
Amino functionalized cyclodextrin linked RGO	RGO@PYAD-NCD	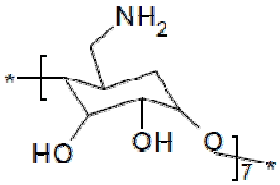	15	155±4
Perbenzylated cyclodextrin linked RGO	RGO@PBCD	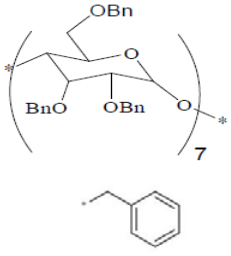 Bn=	10	125±5

Table 3 List of the fabricated sensors

Also star polymer (triazole PEG) functionalized β-CD was wrapped on to reduced graphene oxide in the similar manner using pyrene adamantan as linker (Figure 28).Click chemistry

based synthesis of star polymer (triazole PEG) functionalized β-CD [PEGCD] is available from literature [355].

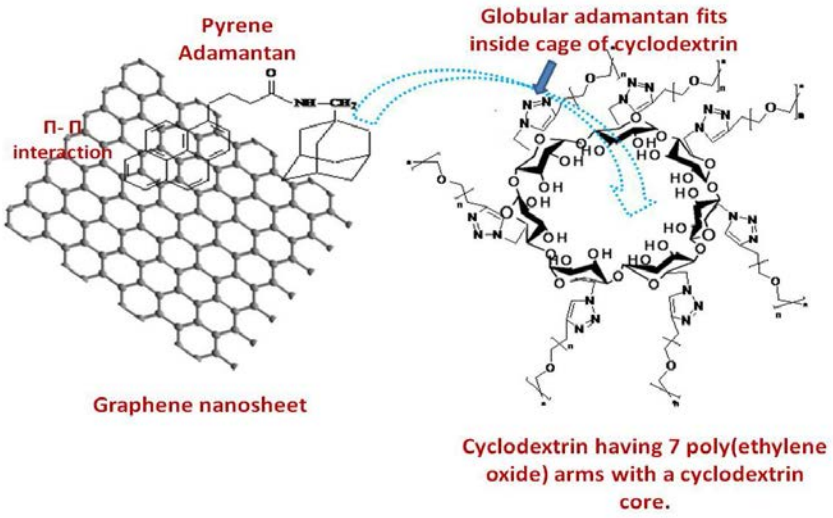

Figure 28 Synthesis of star polymer triazole PEG functionalized CD wrapped RGO@PYAD

III.3. Morphological characterizations of nanocomposites

The technique consisting in the superimposition of layers of several tens of nm up to a final film thickness of some µm showed in Figure 29 (a), has proved to allow the building of hierarchically structured transducers, which presents the advantage of bridging the original nanostructures developed by self assembly of RGO with CD, to the macroscopic parameter to measure (resistance variation). Atomic force microscopy (AFM) can give a good idea of the nano-structure obtained after sLbL in ambient conditions, using light tapping mode (TM-AFM) on a calibre multimode scanning probe microscope from Bruker-Veeco, France. By comparing the images of Figure 29 (b) and Figure 29 (c), one can notice a three times increase of graphene sheets' thickness in RGO@PBCD (around 3 nm) compared to GO (around 1.2 nm), which is comforting the idea that the decoration of RGO with functionalized CD has been effective and useful to prevent the restacking of graphene sheets.

Comparing the SEM images of RGO@PYAD and PEG-CD-RGO@PYAD in Figure 30 (a) and (b) respectively, attests that the presence of PEG-CD on the surface of graphene sheets is effective in PEGCD-RGO@PYAD. Moreover the AFM images of Figure 30 (c) and (d) indicate the presence of PEG-CD on the surface of graphene in PEG-CD-RGO@PYAD.

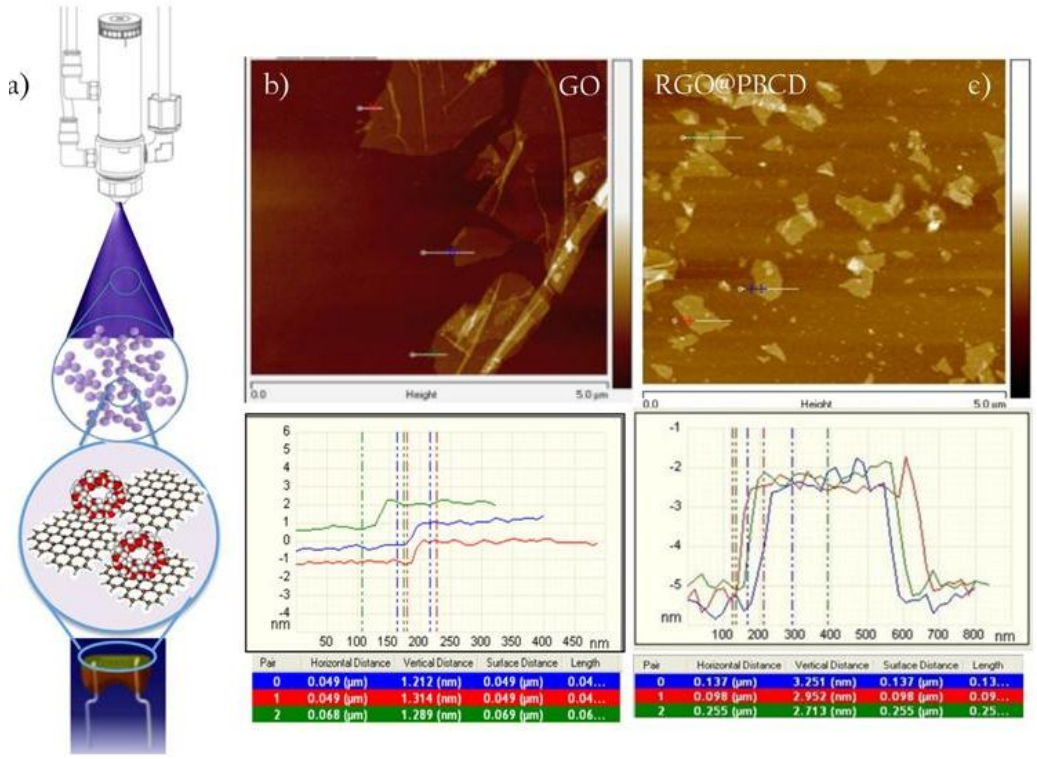

Figure 29 (a) Scheme showing spray LbL deposition and AFM images of (b) GO and (c) RGO@PBCD.

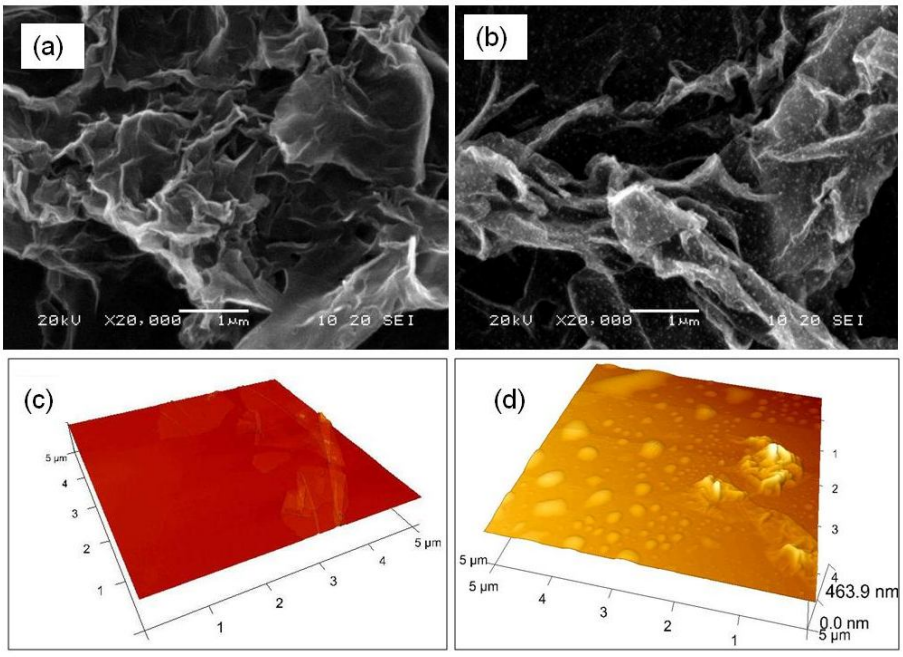

Figure 30 SEM images of (a) RGO@PYAD (b) PEGCD-RGO@PYAD and AFM images of (c) RGO@PYAD (d)PEGCD-RGO@PYAD

III.4. Other characterizations in support of successful synthesis

III.4.1. Compositional analysis by thermo gravimetric Analysis (TGA)

The comparison of thermo gravimetric analysis curves for RGO, RGO@PYAD and pyrene adamantan (PYAD) in Figure 31 (a) confirms that about 60 wt. % of pyrene adamantan has been grafted onto RGO in RGO@PYAD. Hence the ratio of PYAD to RGO in RGO@PYAD is 1.5/1. Thermo Gravimetric Analysis (TGA) was done as a proof of successful non-covalent modification of RGO with perbenzyle β- Cyclodextrin (PBCD) as shown in Figure 31 (b). The experiment proves that about 45 wt. % of PBCD has been wrapped onto RGO in RGO@PBCD. In RGO@PBCD, the ratio of PBCD to RGO is 1/1.22

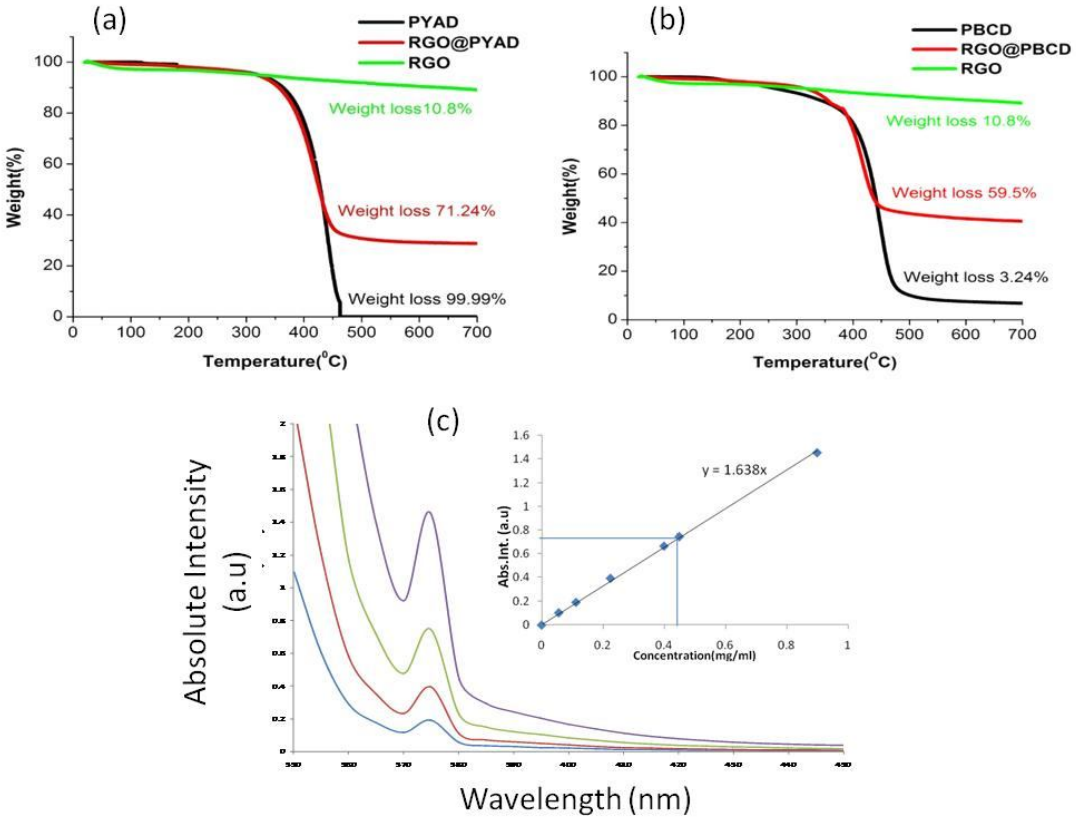

Figure 31 (a) TGA curves of RGO, RGO@PYAD and PYAD and (b) Thermogravimetric analysis of RGO, RGO@PBCD and PBCD (c) UV-vis spectra of pyrene adamantan in ethanol concentrations of 0.9 mg/mL (violet curve), 0.45 mg/mL (green curve), 0.225 mg/mL (red curve), 0.1156 mg/mL (blue curve)and absorbance vs concentration at constant wavelength (286 nm) curve following LAMBERT-BEER's law (inset)

III.4.2. Compositional analysis by UV-Visible spectroscopy

The amount of pyrene adamantan linked to RGO was also confirmed by UV-Vis Spectroscopy as shown in Figure 31 (c). A solution of pyrene adamantan in ethanol was made in four

different concentrations as shown in Figure 31 (c) and they were submitted to UV-visible spectroscopy. The Absorbance was plotted as a function of concentration at constant wavelength to get the calibration curve. Using the calibration curve after doing UV-Vis spectroscopy for the filtrate obtained after reaction of graphene and pyrene adamantan, it was found that the concentration of unreacted pyrene adamantan in the filtrate is 0.43 mg/mL whereas, initial concentration of pyrene adamantan before reaction was 0.67 mg/mL. So amount of pyrene adamantan reacted is 0.24 mg/mL, i.e., 54 mg. The total production of RGO@PYAD obtained was 100 mg. Thus, a weight ratio of pyrene adamantan to graphene of 1.1/1 was found. The good agreement between TGA and UV-Visible spectroscopy is validating our results.

III.5. Vapour sensing performance of functionalized CD wrapped RGO sensors

The chemo-electrical properties of the fabricated sensors were studied by measuring the electrical resistance when exposed alternatively to a 5 minute cycle of dry nitrogen and saturated VOC while the sensors were placed in a 100 mm× 10 mm× 3 mm chamber with 10 slots. The dynamic vapour sensing device is provided with a mass flow controller, solvent bubbler, electrical valves controlled by Labview software program and KEITHLEY 6517 multimeter as depicted in Figure 32 (a). The total flow rate is always kept constant at 100 mL/min. The chemo-resistive responses of conductive CD nanocomposite (CCDC) sensors can be easily expressed by calculating the relative amplitude of electrical signals (A_r) towards solvents using Equation 1:

$$A_r = \frac{R-R_0}{R_0} \quad \text{..... (1)}$$

Where R_0 and R are the initial resistance of the sensor in pure nitrogen and the resistance of the sensor in the presence of solvent vapour, respectively.

However, the same volume of each vapour under saturated condition does not contain the same number of molecules due to differences in saturation vapour pressure of each analyte. Hence, in order to get rid of the influence of the number of molecules, which acts on the response amplitude, each response was normalized by a factor related to the number of analyte molecules, following Equation 2.

$$\boldsymbol{A_{r\ normalized} = \frac{Ar}{[Analyte]_{sat}^{T,p}} * 10^5} \text{..... (2)}$$

Where $[Analyte]_{sat}$ is the concentration of analyte molecules at saturation in ppm, T = 25 °C and p = 0.098 MPa

The vapour sensing performance of sensors under exposure of a ppm-ppb level concentration of VOC was carried out using a combination of LABVIEW software and OVG-4, a versatile chemical vapour generator which consists of two main sections, the oven and the flow control system. The flow control system is comprised of a sample flow and a split flow. The sample flow was kept fixed at 100 mL/min and the split flow was varied to alter the concentration of vapour at a fixed temperature of 25° C.

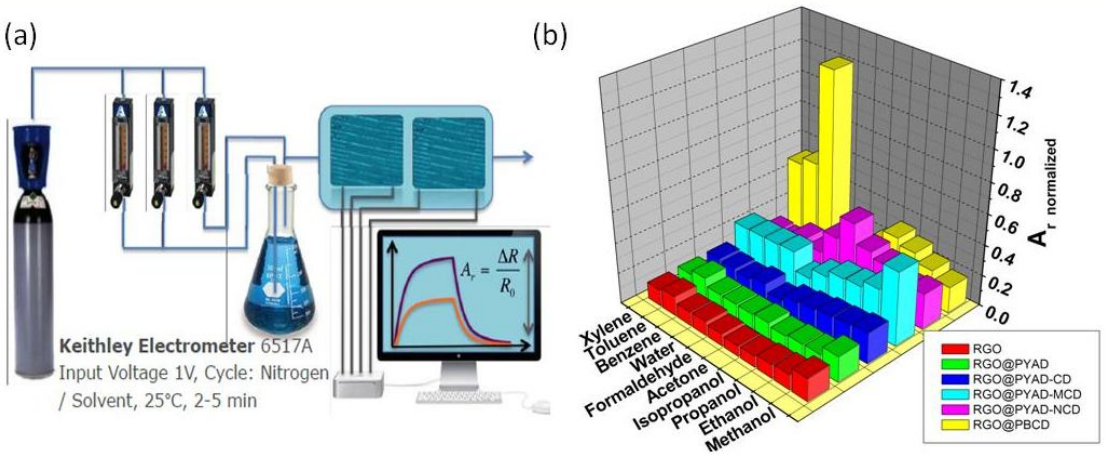

Figure 32 (a) Dynamic mode of vapour sensing (b) Normalized Average maximum relative amplitude of 6 sensors array towards 10 VOC

III.5.1. Sensitivity and selectivity of the functionalized cyclodextrin wrapped graphene based sensors

The normalized average maximum relative amplitude of RGO, RGO@PYAD, RGO@PYAD-CD, RGO@PYAD-MCD, RGO@PYAD-NCD, RGO@PBCD sensors successively exposed to a set of 10 saturated VOC (all of which are known as cancer biomarkers) and dry nitrogen streams have been expressed in three dimension, in Figure 32 (b). The resistance of graphene based sensors quickly increased with starting of a VOC cycle, and went back to the initial value of resistance when purged with dry nitrogen after the end of the VOC cycle as depicted in the chemo-resistive response curves of RGO@PYAD-MCD and RGO@PBCD in Figure 33 (a) and (b) respectively. The chemo-resistive signals obtained during the sensing of VOC by conductive nanocomposite based sensors suggested a reversible and reproducible behaviour of sensors. The CD modified graphene based sensors showed a distinct sensitivity for VOC, and the difference in sensitivity of CCDC based sensors to different VOC indicated a good

selectivity of the sensors for some VOC. Looking at Figure 32 (b) in more details shows the selectivity of the different sensors and also allows noticing their non-specificity (they all respond to all VOC but not with the same segregation ability, as it is the case for the olfactory receptors of mammal nostrils).

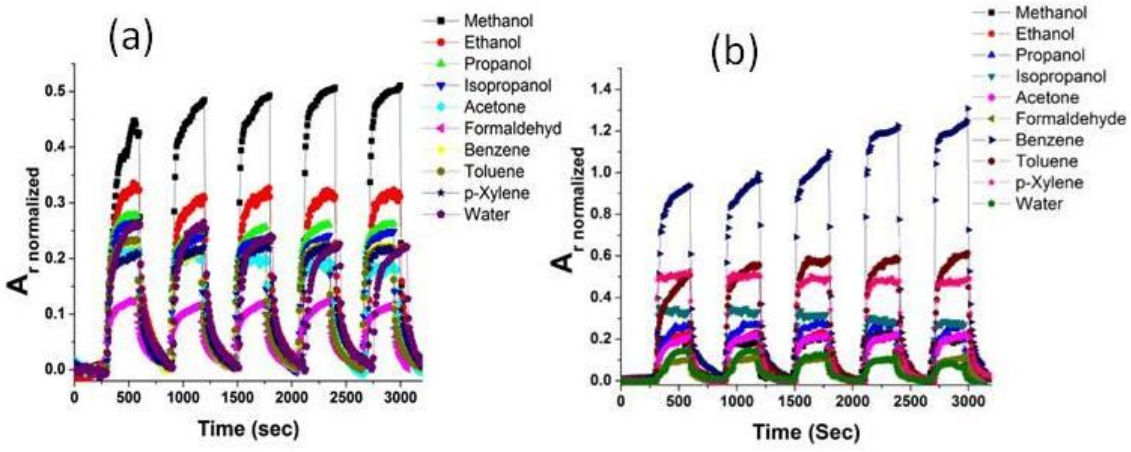

Figure 33 Chemo-resistive response of (a) RGO@PYAD-MCD and (b) RGO@PBCD sensor in a set of 10 VOC

As postulated before, the sensitivity/selectivity of each sensor can be interpreted as a function of the modification of junctions' physico-chemical properties. In this study two main parameters can significantly affect junctions to promote tunnelling to the detriment of ohmic conduction in the CCDC network, the steric hindrance of linkers and their ability to adsorb analytes that will expand the junctions. This last parameter is in turn related to the functionality of the CD. For instance the slightly higher sensitivity of RGO@PYAD than RGO must be due to a better exfoliation of the graphene sheets due to PYAD spacing that is preventing at the same time the restacking of foils. However it can be noticed that PYAD is not changing the selectivity of pristine graphene, meaning that this molecule is not specifically interacting with any of the studied VOC. The best selectivity of RGO@PYAD-CD towards polar VOC (although of low magnitude) can be explained by the presence of several hydroxyl groups on native CD. Moreover the fact that RGO@PYAD-MCD, RGO@PYAD-NCD and RGO@PBCD have different selectivity than RGO@PYAD-CD is a confirmation of the effectiveness of the strategy chosen in this work i.e., to tailor the sensors' selectivity, by changing its van der WAALS interactions with the analytes by CD functionalization. Nevertheless, the strong sensitivity of RGO@PYAD-NCD sensors to acetone vapour is more likely coming from its free amino group in RGO@PYAD-NCD that might have undergone a

reversible imine formation reaction with acetone, and not from specific van der WAALS interactions. The ranking of sensitivity to VOC of RGO@PBCD deduced from Figure 32 (b) [benzene> toluene > p-xylene> isopropanol> propanol> ethanol> acetone> methanol> water> formaldehyde] is consistent with the fact that the perbenzylation of β-CD enhances the affinity of RGO@PBCD for non-polar VOC. Reversely the ranking of sensitivity to VOC of RGO@PYAD-MCD sensors is demonstrating a higher affinity for polar vapours, i.e., methanol > ethanol > propanol > isopropanol > water > benzene > toluene > p-xylene > acetone > formaldehyde. In this case the presence of triazole rings and free hydroxide groups (of the sugar residue) in the MCD can explain the enhancement of affinity of this sensor for polar solvents, especially alcohols, thanks to the possibility of hydrogen bonding. Furthermore, it can be noticed distinctly that RGO@PYAD-MCD sensors are able to discriminate alcohols, depending on their number of carbon atoms. Hence, in this case the analytes' size might also contribute to the selectivity of sensors.

III.5.2. Functionalization of CD as a tool of tailoring selectivity of sensors

As intuited in an early work [356] and confirmed later [357] the van der WAALS interaction between the chemical groups present in the CCDC and in the VOC can be correlated to the normalized amplitude of their chemo-resistive response ($A_{r\,normalized}$), thus explaining the selectivity of CCDC sensors provided that no stronger effect interferes, such as size of analytes or stronger interactions (ionic, or covalent bonding). When these constraints are satisfied, secondary interactions between molecules can be well described by the FLORY-HUGGINS interaction parameter (χ_{12}). χ_{12} is expected to tend to zero in case of strong secondary interactions that correspond also to high values of $A_{r\,normalized}$. Normally for CPC vapour QRS, A_r increases exponentially with the inverse of χ_{12} according to Equation 3, but it is expected to be the same in CCDC in which the polymer phase is replaced by functionalized CD. As CD is oligomeric it is expected to share many of polymers characteristics.

$$A_{r\,normalized} = ae^{b/x_{12}} \quad \text{..... (3)}$$

With χ_{12} the FLORY-HUGGINS intermolecular interaction parameter which can be determined using Equation 4,

$$\chi_{12} = \frac{V_m}{RT}(\delta_{T\,Pol} - \delta_{T\,Sol})^2 \quad \text{..... (4)}$$

where V_m is the molar volume of the solvent, T is temperature in KELVIN, R is the universal gas constant and $\delta_{T\ pol}$ and $\delta_{T\ sol}$ are the polymer and the solvent total solubility parameter respectively

To check that functionalized cyclodextrins, which can be considered as oligomers, satisfy also the FLORY-HUGGINS approach, the global solubility parameter δ_T of four of them, i.e., CD, MCD, PBCD and NCD, have been evaluated by the FEDORS' method of groups contribution [358]. The following values of δ_T were found to be respectively 27.6, 28.3, 20.29 and 25.9 J ^{½}.cm$^{-3/2}$, allowing to calculate the corresponding χ_{12} parameters using Equation 3 and gathered in Table 4.

VOC	V_m ($cm^3.mol^{-1}$)	$\delta_{T\ sol}$ ($J^{½}.cm^{-3/2}$)	$(\chi_{12})_{CD}$	$(\chi_{12})_{MCD}$	$(\chi_{12})_{PBCD}$	$(\chi_{12})_{NCD}$
Methanol	40.7	29.6	0.06	0.02	1.438	0.227
Ethanol	58.5	26.6	0.02	0.06	0.95	0.011
Propanol	74.84	23.8	0.44	0.62	0.37	0.13
Isopropanol	76.4	23.57	0.5	0.69	0.335	0.169
Benzene	89.7	18.5	3.44	3.51	0.117	2
Toluene	106.3	18.16	3.86	4.45	0.196	2.59
p-Xylene	122.8	18.2	4	5.1	0.218	2.968
Water	18.1	47.9	3	2.83	5.62	3.57
Acetone	74	19.7	1.88	2.23	0.01	1.16
Formaldehyde	36.8	24.6	1.195	0.205	0.278	0.025

Table 4 Florry-Huggins interaction parameters of functionalized cyclodextrins

The validity of the model can then be evaluated by plotting the evolution of the normalized relative amplitude A_r of RGO@PBCD, RGO@PYAD-NCD, RGO@PYAD-MCD and RGO@PYAD-CD transducers with $1/\chi_{12}$ using Equation 2**.** The resulting curves plotted in Figure 34 (a), show that three over the four sensors, i.e., RGO@PBCD, RGO@PYAD-MCD and RGO@PYAD-CD are well fitting the exponential law, whereas RGO@PYAD-NCD evolution seems to be better described by a logarithm. Comparing the curves of RGO@PYAD-CD and RGO@PYAD-MCD shows that they can almost be superimposed by translation, which means that they have quite the same discrimination ability due to similar interactions with analytes, RGO@PYAD-MCD being always more sensitive probably because of the larger size of its spacer, making more easy the disconnection of junctions. The larger slope of RGO@PBCD compared to that of RGO@PYAD-MCD demonstrates the superior discrimination ability of the former, which appears to offer a better compromise between

selectivity and sensitivity. The peculiar behaviour of RGO@PYAD-NCD, which is not following the same law as the other sensors, seems to confirm the possibility of a chemo-resistive response based on molecular recognition by the reversible reaction of the amine function of NCD that can form an imine with analytes such as acetone. Thus, this chemo-resistive behaviour must not be mainly based on weaker van der WAALS interactions. Therefore it can be concluded that the decoration of graphene platelets with different types of cyclodextrins is an effective strategy to tailor the sensors' selectivity to VOC, simply by changing the chemical nature of the functions present on CD.

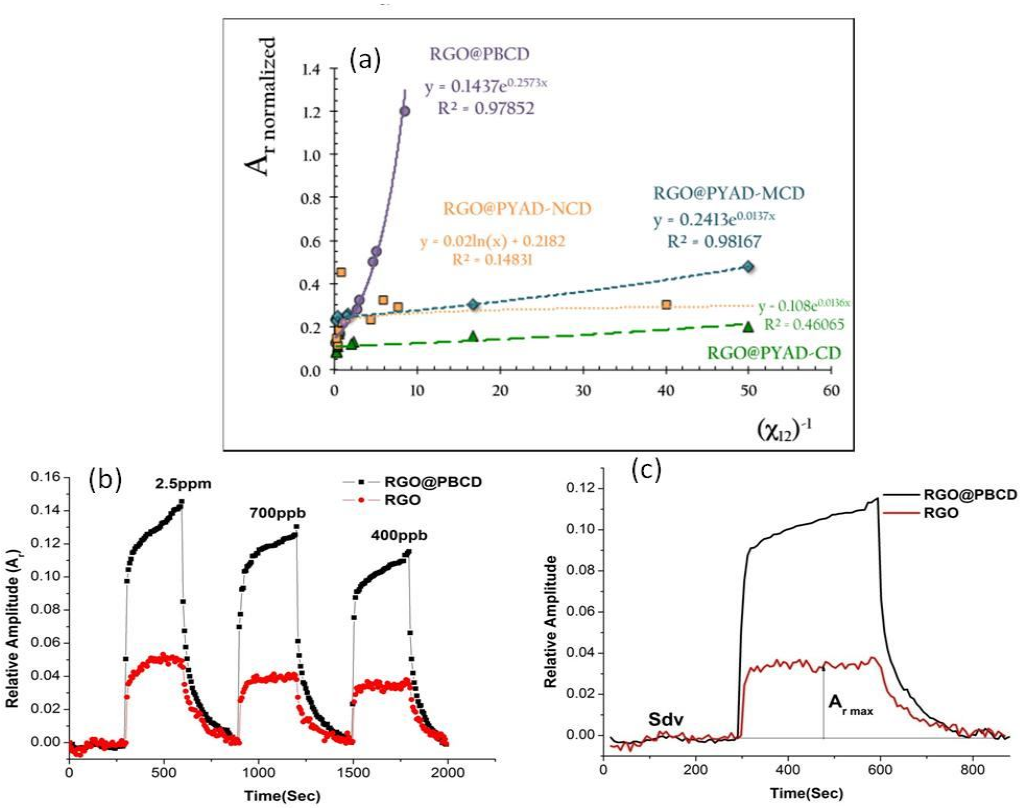

Figure 34 (a) Correlation between χ_{12} parameter and transducer's selectivity for RGO@PBCD, RGO@PYAD-NCD, RGO@PYAD-MCD and RGO@PYAD-CD (b) Response of RGO@PBCD and RGO sensor to benzene vapour in the ppm-ppb concentration range (c) Signal to noise of sensor response at 400 ppb concentration of benzene vapour

III.5.3. Limit of detection

Since all the lung cancer biomarker VOC found in breath extract are usually at ppm-ppb level, it is very relevant to check the limit of detection of at least some selected sensors used in this study. In order to assess the efficiency of the sensors during sensing of trace level of vapour molecules in the surroundings, the signal to noise ratio (*SNR*) for the CPC sensors during

sensing of VOC was introduced [359]. The SNR value of the sensor was determined by the following equation 5

$$SNR = \frac{\Delta R_{max}}{\sigma_{baseline}} \ldots\ldots\ldots\ldots\ldots (5)$$

where ΔR_{max} corresponds to steady-state resistance change upon exposing the sensor to solvent vapour molecules (analyte), i.e., difference between the maximum resistance of a sensor obtained after exposure to solvent and the baseline resistance of a sensor and $\sigma_{baseline}$ is the standard deviation in baseline resistance of the sensor before analyte's delivery, calculated using 10 data points. The concentration of the solvent vapour (analyte) determined by a sensor is considered acceptable if its SNR value is larger or equal to 2.0 (SNR $\geq$ 2.0) at that solvent concentration.

As shown in Figure 34 (b) and (c), a limit of detection down to 400 ppb of benzene vapour has been reached. SNR ratios are found as high as 11 and 88 for RGO and RGO@PBCD respectively, when exposed to 400 ppb of benzene vapour. This demonstrates a strong capacity of the RGO to reduce the noise density and to enhance the sensitivity of the sensor after it has been wrapped by perbenzyle cyclodextrin (PBCD).

III.6. Vapour sensing performance of star polymer (triazole PEG) functionalizaed β-CD wrapped graphene

Description of the sensor	Designation of sensor	Structure of CD attached	Number of layers sprayed	Initial resistance of the sensor (KΩ)
Native cyclodextrin wrapped RGO	RGO@ PYAD - CD	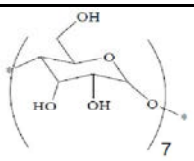	10	150±7
Star polymer (triazole PEG) functionalized cyclodextrin wrapped RGO	**RGO@ PYAD-PEGCD**	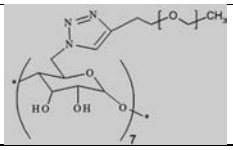	**15**	**205±5**
PEG +RGO@PYAD	RGO@ PYAD –PEG	-	10	200±5

Table 5 Details of the set of sensors to analyze the influence of polymerized CD on vapour sensing

As we could see from the above results, the selectivity of functionalized oligomeric CD wrapped RGO sensors could be intelligently tuned by varying the organic functionality on CD. But is it possible to extend the same concept to polymerized CD based sensors to get an even

larger sensitivity? As it is expected that polymers may bring about enhanced sensitivity, the vapour sensing performance of polymerized CD (star PEG polymer) wrapped RGO sensors were studied in this section. In order to understand the influence of each component of this sensor, a set of sensors were prepared. The details of each sensor in this set are available in Table 5.

RGO@ PYAD -PEGCD is the main sensor to be studied in this set. In order to understand the influence of the star structure and chemical functionality of this polymer on its sensing performances, it's responses have been compared respectively with RGO@PYAD-CD and RGO@PYAD-PEG, RGO@PYAD being kept as a reference.

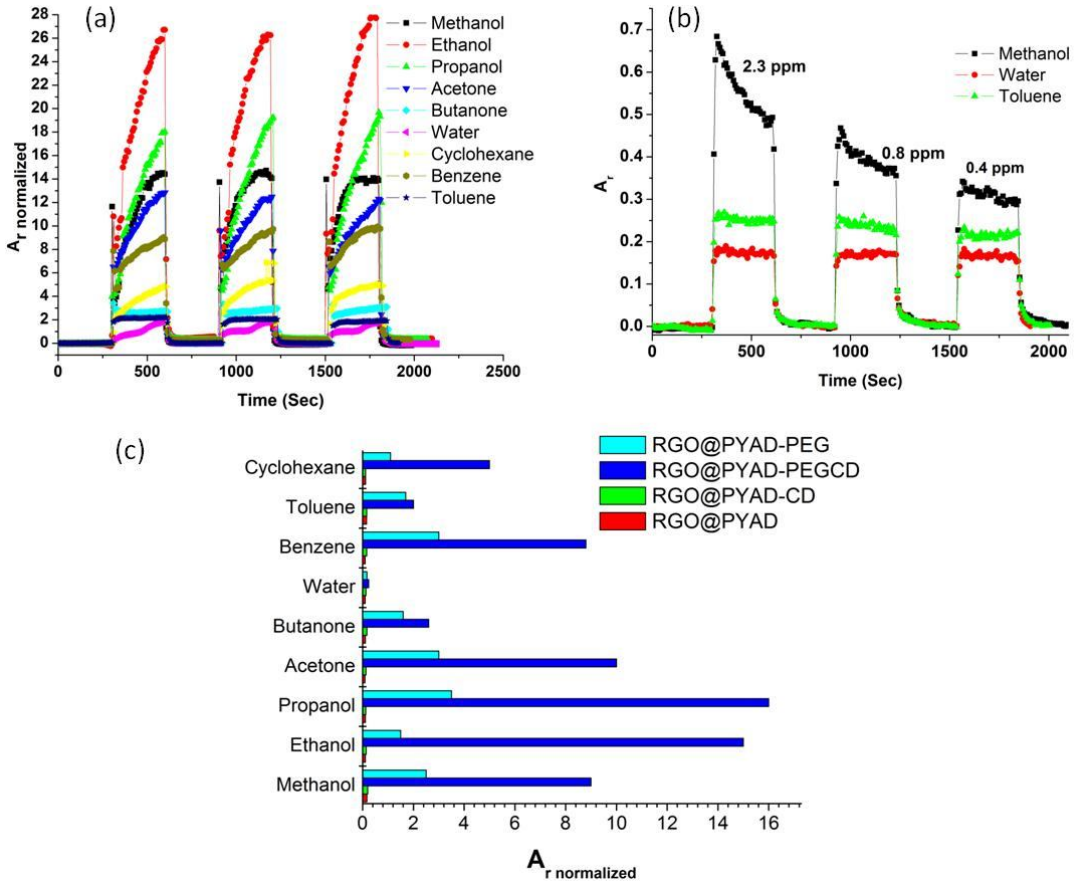

Figure 35 (a) Chemo resistive response of RGO@PYAD-PEGCD sensors to a set of 9 VOC under saturated atmosphere (b) ppm-ppb level sensor response of RGO@PYAD-PEGCD sensors (c) Sensing response of an array of four sensors in nine selected VOC

As evident from Figure 35 (a), the RGO@PYAD-PEGCD sensor is highly sensitive with the following ranking of affinity for VOC [propanol≈ ethanol>acetone≈ methanol> benzene> cyclohexane> butanone> toluene> water]. Figure 35 (b) indicates that this sensor is still operative down to 400 ppb range. From Figure 35 (c), comparing the sensing performance of

RGO@PYAD-CD with RGO@PYAD-PEGCD, it is evident that the presence of a star PEG polymer on the surface of the CD does not only considerably enhance the sensitivity, but also amplifies the selectivity towards propanol and ethanol VOC. This enhanced sensitivity and selectivity to polar VOC is brought about by the PEG polymer matrix which is highly polar. Now in order to understand the influence of CD on the sensing response, RGO@PYAD-PEGCD sensor was also compared with RGO@PYAD-PEG sensor which was prepared by simple solution mixing of PEG polymer into RGO@PYAD. It is clear from Figure 35 (c), that the sensitivity of RGO@PYAD-PEGCD sensor is 5-6 times higher than that of RGO@PYAD-PEG. Its higher sensitivity is certainly also responsible for its better selectivity towards alcoholic VOC. In RGO@PYAD-PEGCD, the adamantan group of RGO@PYAD fits inside the cage of the star polymer functionalized CD unlike RGO@PYAD-PEG where a random distribution of polymer chains within graphene foils has taken place. However, the selectivity for alcohols brought by PEG is the same in both cases, whereas it is different for other vapours. The effect of CD cages used as linkers between the polymer and graphene in the conducting architecture,seems to be limited to the improvement of junctions' disconnection and hence to increase sensitivity. Thus, the effect of CD on sensors selectivity appears negligible compared to PEG. These results fully justify the strategy used to tailor sensors sensitivity and selectivity.

III.7. Conclusion

The sensing performances of an electronic nose composed of 3 types of functionalized oligomeric CD wrapped graphene sensor along with one pristine graphene and one pyrene adamantan linked graphene sensor were analyzed, after being exposed to 10 selected cancer biomarker VOC. One of the sensors was found selective towards aromatic hydrocarbons while the other was more selective to acetone. Another sensor was found to show a higher sensitivity for alcohols and was found able to discriminate different alcoholic VOC. This is an interesting finding as, elevated levels of acetone (several ppm) is found in the breath extract of lung cancer patients because of the higher rate of oxidation of fatty acids under the conditions of oxidative stress. Aromatic hydrocarbons like benzene, toluene are prominent lung cancer biomarker. Alcohols are abundant in the breath extract of both healthy subjects and lung cancer patients but 1-propanol is found in the breath extract of lung cancer patients at higher concentration than healthy subjects [94]. The specific functionality of CD is found to be a predominant influencing parameter to tune the specific molecular selectivity of the sensors.

Our study is opening a novel approach to control the multiscale architecture of quantum chemo-resistive transducers by the supramolecular assembly of graphene and CD-derivate hybrids. This strategy allows to get a high sensitivity of the nanoswitching at junctions due to the insertion of CD between graphene foils and to obtain a tailorable selectivity to cancer biomarkers due to CD functionalization and geometry. The resulting CCDC QRS have demonstrated a high sensitivity, evidenced by SNR up to 88 at a concentration as low as 400 ppb without any pre-concentration of vapours or amplification of electrical signals. These sensors also proved to have good discrimination ability towards the 10 lung cancer VOC biomarkers studied, which could interestingly be predicted by a model based on van der WAALS interactions, excepted in case of a covalent bonding used for molecules' recognition (acetone).

Later, in order to understand the effect of polymerization of CD on the sensing performance, a star polymer functionalized CD wrapped graphene was prepared and from the sensing response, it is clear that in this system, the conductive network is formed by graphene, whereas, both sensitivity and selectivity are enhanced by the influence of the star polymer and also further enhancement of sensitivity is brought about by cyclodextrin cages which acts as a spacer.

Chapter IV:

Vapour sensing properties of conductive nanohybrids

Summary

This chapter is devoted to another strategy of structuring of the conductive architecture, i.e., the development of conductive nanohybrids which are multicomponent systems where two or more nanomaterials are integrated, in order to synthesize a novel nanomaterial with attractive multifunctionality. In the first part of this chapter, the development of hybrid sensors based on polyhedral oligomeric silsesquioxane (POSS) and CNT has been investigated. The organic functionality on the surface of POSS can be tuned to change the selectivity of the sensors. In the second part of this chapter, the hybridization of CNT and graphene is achieved with spherical Buckminsterfullerene nanoparticles. In this strategy, the electronic mobility through the CNT/graphene network is enhanced by the grafting of Buckminsterfullerenes of very high surface to volume ratio at their junctions, which results in a strong enhancement of nanosensors'sensitivity.

IV.1. Influence of polyhedral oligomeric silsesquioxane on the molecular selectivity of CNT based hybrid chemical vapour sensors for disease specific biomarker detection

IV.1.1. Introduction

The hybridization of CNT/graphene by covalent or non covalent functionalization is found to be interesting to develop a multicomponent system where two or more nanomaterials are integrated, for the purpose of synthesizing a novel nanomaterial with attractive multifunctionality [329]. So far metals, metal oxide, graphene, various biological compounds have been used to develop hybrid nanomaterials with carbon nanotubes (CNT) for various applications such as sensors and biosensors [291], [360] solar cells [361], and supercapacitors [362] etc. In addition, nanostructured hybrids derived from polyhedral oligomeric silsesquioxanes (POSS) and carbon nanomaterials like CNT or graphene were found to be quite efficient for optical limiting [363] and EMI shielding [364] applications. POSS is the smallest known silica particle with a rigid, cubic shaped, three-dimensional Si–O cage structure with overall diameter of 1.5-3 nm, where tetravalent silicon atoms are externally surrounded by eight covalently bonded organic groups that may or may not be reactive [365]. The monodispersed, nano-scopic size of POSS as well as the presence of synthetically well controlled organic functionalities on its surface enhance its reactivity and solubility with the organic solvents [366]. The potentiality of POSS to develop nanohybrid materials by further functionalization is of great interest to experiment. In particular, the ability of POSS cage to allow a change of its surface organic functionality makes it a versatile nanoparticle for applications in the field of sensors. *Castaldo et al.* developed polymeric nanocomposite sensors, based on a POSS matrix and nanostructured fillers, that could be used in the sensing of both polar and apolar analytes such as water vapour and hexane respectively, although they did not mention sensing responses towards any other vapour and also the limit of detection of these sensors were not reported [367]. POSS based polymeric nanocomposite, amperometric chemical sensors were also studied by *Massera et al.,* which exhibited very strong, nicely reversible, response to relative humidity varying from 0 to 100 % [368].

In the present study, two kinds of POSS, with open or close cages,were hybridized with multiwalled carbon nanotubes by either non-covalent or covalent bonding,in order to study whether CNT chemo-resistive sensing performances could be enhanced by POSS. In addition,

the influence of the chemical structure of POSS organic functions on the molecular selectivity of CNT based sensors was examined.

IV.1.2. Synthesis of nanohybrids and fabrication of sensors

Dry CNT (Nanocyl™ NC3100) were subjected to acyl chloride functionalization with thionyl chloride followed by an amidization with amino propyl isooctyl POSS in order to obtain isooctyl POSS-g-CNT where POSS is grafted onto CNT via amide linkage [363], [364]. On the other hand trisilanol phenyl POSS was non-covalently modified with carboxylated CNT by π-π stacking between sp^2 hybridized carbon atoms of CNT and phenyl groups of POSS to obtain TSPH-POSS/CNT. Sensors were then fabricated using the technique elaborated in appendix (page number 142). The details of composition of the hybrid sensors are provided in Table 6.

Nomenclature of hybrid sensor	POSS structure 	POSS cage nature	Nature of bonding
IO-POSS-g-CNT 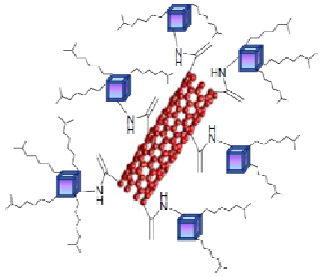	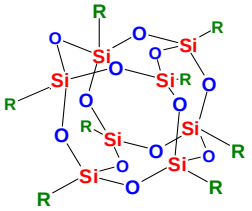 R= iso octyl group	Open cage	Covalent bonding via amide linkage
TSPH-POSS/CNT 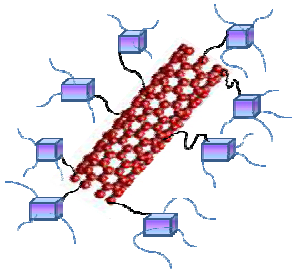	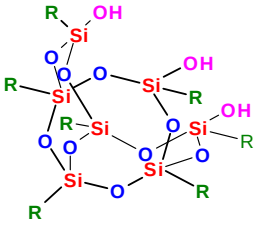 R=phenyl group	Closed cage	Non-covalent bonding via π-π interaction

Table 6 Structural characteristics of hybrid sensor

IV.1.3. Characterization of nanohybrids

IV.1.3.1. Morphological study by atomic force microscopy (AFM)

Figure 36 (a) and (b) present AFM images of carboxylated CNT and IO-POSS-g-CNT respectively. Diameter of carboxylated CNT and IO-POSS-g-CNT were measured to be 12 nm

and 20 nm respectively. Therefore around 1.6 times increase in diameter of carboxylated CNT has been observed after grafting with amino propyl isooctyl POSS. Hence POSS has coated the surface of CNT.

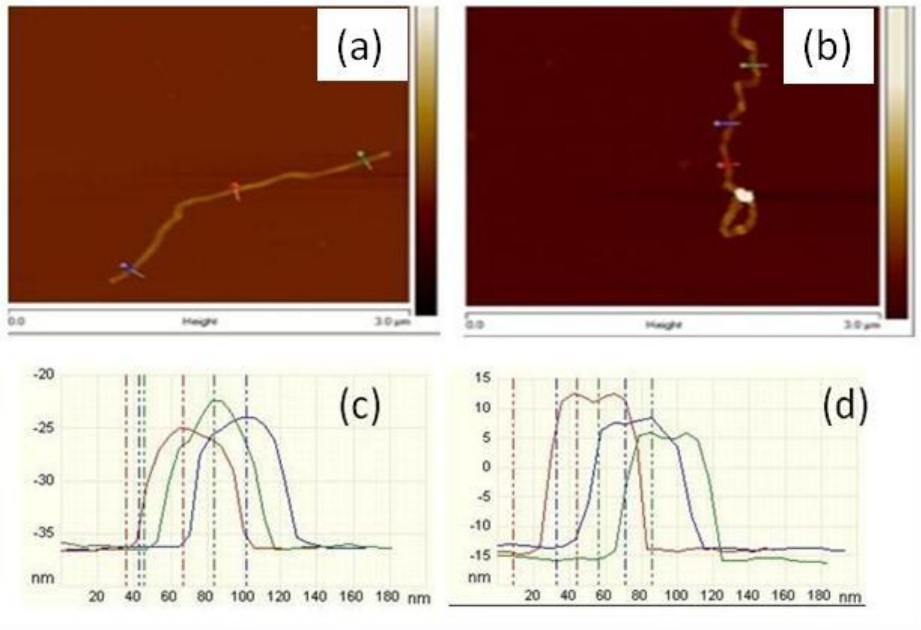

Figure 36 AFM height images and profile measurement for IO-POSS-g-CNT (a, c) and carboxylated CNT (b, d)

IV.1.3.2. Structural characterization by Fourier transform infra red spectroscopy (FTIR)

Figure 37 (a) shows the FTIR spectrum of carboxylated CNT where the peaks at 3442 cm^{-1} and at 1704 cm^{-1} are attributed to acidic carboxyl groups, whereas the prominent peak at 1561 cm^{-1} is assigned to the carboxylate anion stretching mode. FTIR absorption spectrum of amino propyl isooctyl POSS displays characteristic peaks at 2953 cm^{-1} and 2880 cm^{-1},corresponding respectively to $–CH_3$and $-CH_2$ stretching vibrations of iso-octyl group on the POSS molecule, while the strong peak at 1106 cm^{-1} is coming from Si-O-Si stretching. Additionally the peaks at 1666 and 3180 cm^{-1}can be assigned to primary amine functions.

In POSS-g-CNT, the absorption peaks at 1630 $cm^{-1}$and 3442 $cm^{-1}$are assigned to –C=O and to–NH stretching modes respectively. The O-Si stretching at 1100 cm^{-1} supports that POSS molecules have effectively been covalently attached to CNT by the formation of amide bonds. Figure 37 (b) displays the FTIR spectrum of trisilanol phenyl POSS modified CNT, where the strong and sharp peak of Si-O-Si at 1123 cm^{-1} (unlike carboxylated CNT) proves that POSS has been well wrapped onto CNT by π-π interaction between phenyl groups of POSS and that of CNT.

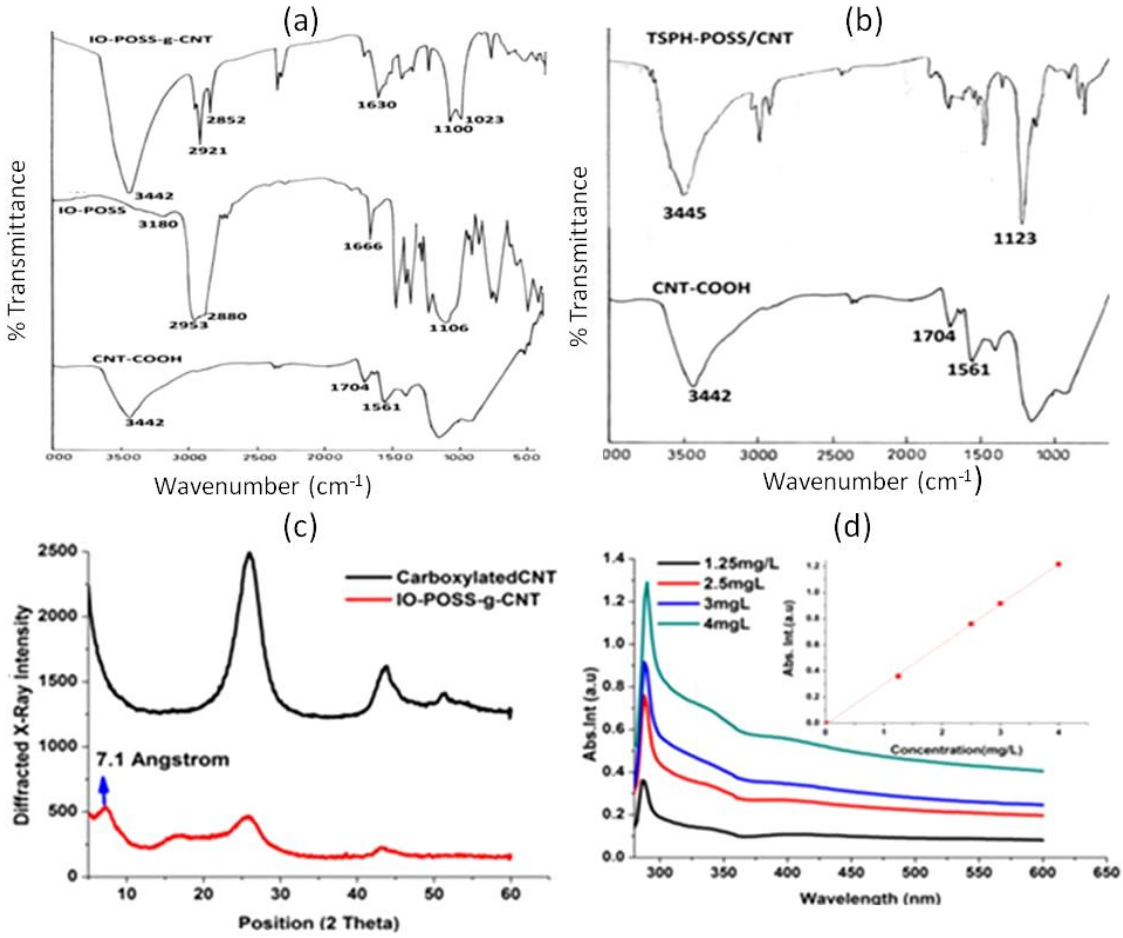

Figure 37 (a) FTIR images of CNT-COOH, Amino propyl iso octyl POSS (IO-POSS) and IO-POSS-g-CNT (b) FTIR images of CNT-COOH and TSPH-POSS/CNT (c) X-Ray diffractogram of IO-POSS-g-CNT and carboxylated CNT (d) UV-vis spectra of IO-POSS-g-CNT in THF in different concentrations (i) 1.25mg/L ,(ii) 2.5mg/L ,(iii) 3mg/L and (iv) 4mg/L and absorbance as a function of concentration at constant wavelength of 294 nm following LAMBERT-BEER'law (inset)

IV.1.3.3. Structural characterization by X-ray diffractogram

The Figure 37 (c) shows the X-ray diffractogram of carboxylated CNT and IO-POSS-g-CNT respectively. In carboxylated CNT some XRD peaks appear at 26° and 43° showing the fingerprint of pure CNT whereas in IO-POSS-g-CNT the characteristic peaks of CNT still exists but are completed by a new peak at 7.1 ° which is the characteristic of POSS. Therefore XRD supports that POSS has been successfully incorporated onto CNT.

IV.1.3.4. Study of dispersion of CNT by UV-Visible spectroscopy

UV–vis spectroscopy was used to monitor the dynamics of the dispersion process of CNT in a particular solvent as shown in Figure 37 (d). Individual CNT are active in the UV/Vis region

and exhibit characteristic bands corresponding to additional absorption. This is evident from the UV/Vis spectra of solutions of IO-POSS-g-CNT in THF, where the absorbance is increasing gradually with the concentration of CNT,following LAMBERT-BEER' Law. Thus it can be concluded that POSS functionalization has led to an enhancementof CNT dispersibility and individualization in THF.

IV.1.3.5. Elemental analysis by energy dispersive X-ray spectroscopy (SEM-EDX)

Figure 38 (a) shows EDX spectra of IO-POSS-g-CNT. The atomic percent and weight percent of Si for the MWNT-POSS nanohybrids were calculated by EDX measurement of the same sample under SEM, as shown in Table 7.

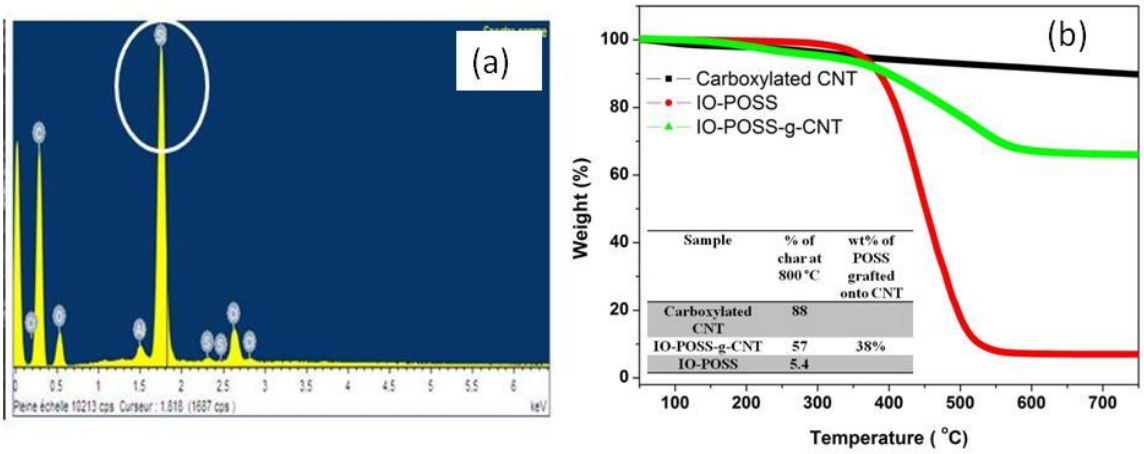

Figure 38 (a) EDX spectra of IO-POSS-g-CNT (b) TGA curve and data of carboxylated CNT, IO-POSS and IO-POSS-g-CNT

Sample	Element	Weight (%)	Atomic (%)
IO-POSS-g-CNT	C	66.14	75.17
	O	18.27	15.46
	Si	11.78	5.7
	N	3.9	3.67
TSPH-POSS/CNT	C	54.86	67.35
	O	22.58	20.81
	Si	22.56	11.85
Carboxylated CNT	C	86.38	89.42
	O	3.62	10.58

Table 7 EDX experimental data

The atomic % of Silicon in IO-POSS-g-CNT and TSPH-POSS/CNT were found to be 5.7% and 11.85% respectively whereas the silicon content in carboxylated CNT is nil. This finding proves that the silicon content in IO-POSS-g-CNT and TSPH-POSS/CNT is due to POSS grafting onto CNT.

IV.1.3.6. Compositional analysis by thermo gravimetric analysis (TGA)

As shown in Figure 38 (b) the TGA analysis provides further evidence of the functionalization of MWNT with POSS. The difference in weight loss between carboxylated CNT and carboxylated CNT-POSS nanohybrid can be attributed to the presence of POSS molecules on the surface of the CNT. The TGA data of POSS show almost 94.6 % mass loss at temperatures over 600°C. By comparing the TGA curves of carboxylated CNT, IO-POSS and IO-POSS-g-CNT and applying the rule of mixture from TGA data, it is confirmed that about 38 wt. % POSS has been grafted onto CNT in IO-POSS-g-CNT.

IV.1.4. Dynamic vapour sensing

The average maximum chemo-resistive response of carboxylic acid functionalized CNT, IO-POSS-g-CNT and TSPH-POSS/CNT sensors, successively exposed to pulses of 9 saturated cancer biomarkers VOC (methanol [87], ethanol[87], propanol [85], [86] acetone[85], [86], butanone[85], water, toluene [85], [87], cyclohexane [97], and pentane) and dry nitrogen streams are presented in Figure 39 (a).Since breath extract contains a huge amount of water with trace amounts of VOC [83], water is also included into the selected set of VOC. The average of responses' maxima were calculated over 3 cycles and then normalized to 1ppm for each vapour using ANTOINE's equation.

The nanoscopic size of POSS as well as the presence of organic functions on the surface of POSS/CNT hybrid makes it soluble in organic solvents. Therefore, sidewall functionalization of CNT with POSS improves their dispersion stability in suitable organic solvents like THF. This in turn increases the specific surface accessible to vapour molecules and finally CNT based sensors' sensitivity.

Figure 39 (a) clearly shows that among the set of VOC the IO-POSS-g-CNT sensor is distinctly more selective to non-polar hydrocarbon solvents like cyclohexane, pentane and toluene than the other polar VOC. In IO-POSS-g-CNT the POSS cage is closed and hence not expected to adsorb vapour molecules that could contributed to the disconnection of the CNT network. In such a case, the sensitivity of the hybrid sensor to organic vapour molecules is only due to the physico-chemical interactions of the targeted VOC with the organic functional

group (R) of POSS. The presence of seven iso octyl groups on the surface of the POSS molecule, covalently bonded to tetravalent silica atoms of the cage, bring a marked hydrophobic character to POSS and hence selectivity for non-polar hydrocarbons. The large amplitude of the responses of these sensors to most saturated vapours is suggesting that they will have also a detectable sensitivity at the ppm level, which will be studied in the following. It is clear that their selectivity is well matching with the polarity of targeted VOC analytes, leading to a higher sensitivity for aliphatic hydrocarbons such as cyclohexane and pentane.

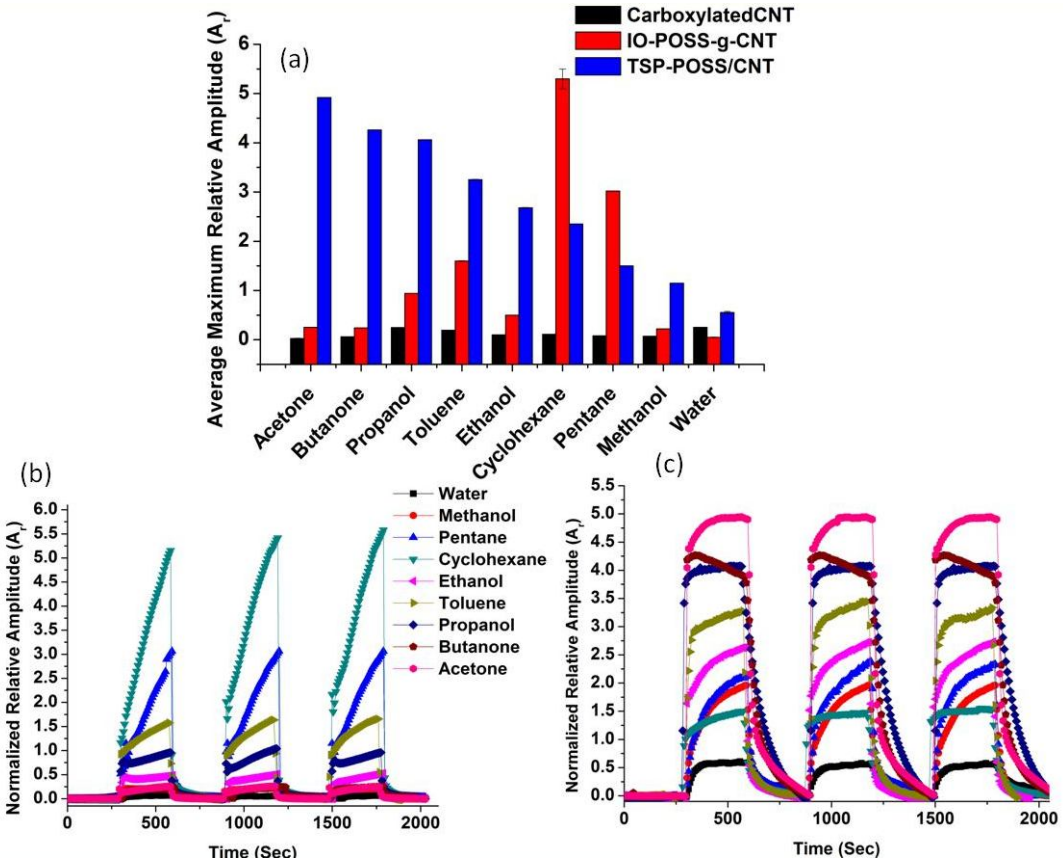

Figure 39 (a) Average maximum relative amplitude of 3 sensors array towards 9 saturated VOC; Chemo resistive signals of (b) IO-POSS-g-CNT sensor and (c) TSPH-POSS/CNT sensor

The TSPH-POSS/CNT sensor is a non-covalently modified hybrid of carboxylated CNT and trisilanol phenyl POSS (with an open cage), which shows the following ranking of sensitivity for various VOC: [acetone> butanone> propanol> toluene> ethanol> cyclohexane> pentane> methanol> water]. As in this case the POSS cage is open, some free hydroxyl groups from inside the cage are now available to interact with analytes, together with the phenyl groups brought by the silane. Most of the phenyl groups are expected to be involved in π-π interaction with CNT, but some hydroxyl groups from the silane may also not have reacted with POSS

and be free to interact with analytes. Since both polar and nonpolar groups are present on POSS, it is difficult to directly deduce the selectivity of these sensors simply from polarity considerations. Thus it is likely that the solubility parameter χ_{12} canbe more helpful to explain the selectivity ranking, what will be discussed in the next section.

Moreover, Figures 39 (b) and (c) are showing that both IO-POSS-g-CNT and TSPH-POSS/CNT transducers are exhibiting fast, reversible and reproducible chemo-resistive signals when exposed to the set of 9 selected VOC.

IV.1.5. Tailoring selectivity

The selectivity of conductive polymer nanocomposites towards organic vapours is generally well described by the solubility parameter δ through the FLORY-HUGGINS intermolecular interaction parameter χ_{12} that can be calculated from equation (4) as described in chapter III.

The solubility parameter approach is expected to fit well also with the POSS based hybrid sensor systems used in the present study, since organo-silicon materials like polyhedral oligomeric silsesquioxane share many similar features with common organic oligomers. Theoretical solubility parameter of POSS is determined by HOY's method. POSS is inherently an organic-inorganic hybrid although, only the organic functional groups in the vertex of its inorganic cage influences the solubility parameter while the inorganic siloxane bonded cage is excluded in the solubility parameter calculation. The lower the difference of polarity between the POSS vertex organic group and the solvent, the higher the swelling of POSS in that solvent hence higher the sensitivity of POSS based sensor to a VOC.

VOC	δ_T $(Jcm^{-3})^{1/2}$	$V_{Molar\ Volume}$ (cm^3mol^{-1})	$\Delta\delta_{(TSPH)}$	χ_{12} (TSPH)	$A_{r\ Normalized}$ (TSPH)	$\Delta\delta_{(IO)}$	χ_{12} (IO)	$A_{r\ Normalized}$ (IO)
Water	47.9	18.1	26.67	5.25	0.5	31.85	7.25	0.05
Pentane	14.4	115.2	6.83	2.19	1.5	1.65	0.127	3.02
Methanol	29.6	40.7	8.37	1.16	1.15	13.55	3	0.22
Cyclohexane	16.8	108.7	4.43	0.87	2.35	0.75	0.02	5.3
Ethanol	26.6	58.5	5.37	0.68	2.68	10.55	2.65	0.5
Toluene	18.6	105.9	2.5	0.4	3.25	2.617	0.29	1.6
Propanol	23.8	74.84	2.57	0.2	4.06	7.75	0.94	0.94
Butanone	19.3	89.57	1.93	0.136	4.26	3.25	0.24	0.24
Acetone	19.7	74	1.53	0.07	4.92	3.65	0.25	0.2

Table 8 Solubility parameters (δ),FLORY-HUGGINS interaction parameters (χ_{12}) and response (A_r) of POSS based hybrid sensors.

The HOY's solubility parameter of trisilanol phenyl POSS and iso octyl POSS are reported to be 21.23$(J.cm^{-3})^{1/2}$ and 16.05 $(J.cm^{-3})^{1/2}$ respectively[369]. Table 8 shows that the sensitivity ranking of TSPH-POSS/CNT hybrid sensor is coherent with its χ_{12} values. Similarly, the sensitivity ranking of IO-POSS-g-CNT hybrid sensor:[water< acetone< methanol< butanone< ethanol< propanol<toluene< pentane< cyclohexane], is coherent with the χ_{12} values excepted for acetone and butanone.

The normalized values of A_r were perfectly fitted with a logarithmic law, when plotted against reciprocal of χ_{12} for all the VOC in case of IO-POSS-g-CNT hybrid and also for TSPH-POSS/CNT hybrid as shown in Figure 40 (a) and (b) respectively.

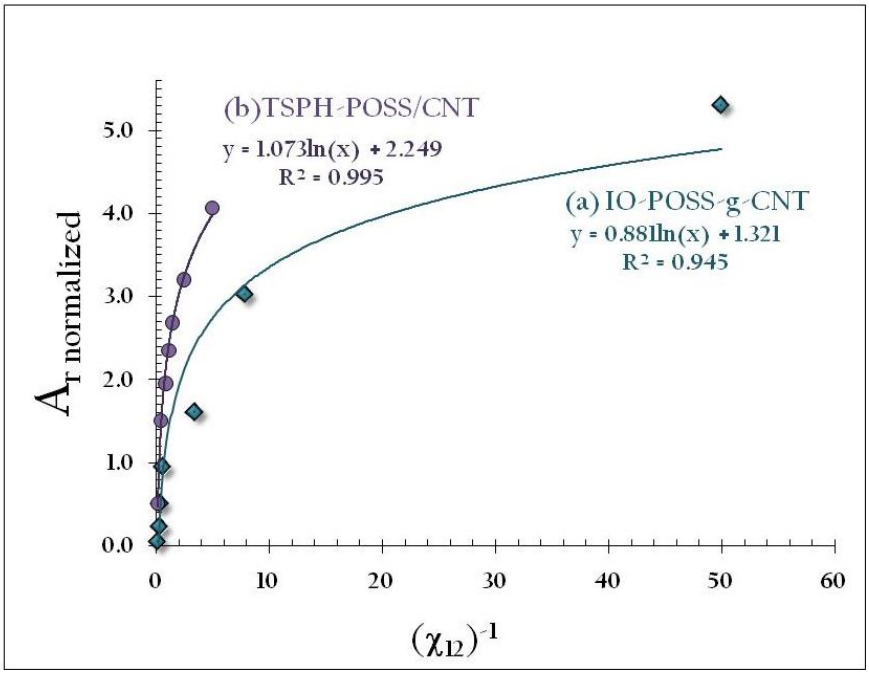

Figure 40 Correlation between normalized Ar and χ_{12} for (a) IO-POSS-g-CNT and (b) TSPH-POSS/CNT

IV.1.6. Limit of detection

As shown in Figure 41 (a) a limit of detection of 6 ppm of acetone vapour and a SNR ratio of 20 for carboxylated CNT and 66 for TSPH-POSS/CNT has been confirmed respectively, when exposed to 6 ppm of acetone vapour. Consequently, the non-covalent modification of carboxylated CNT with TSPH-POSS is found to significantly decrease its noise density and strongly enhance its sensitivity. Additionally the progressive increase of amplitude of TSPH-POSS/CNT sensor's response with increasing concentration of acetone from 6 ppm to 26 ppm is a proof of its efficiency to quantify the concentration of vapour even at the ppm level (top inset image). Similarly, the response of carboxylated CNT and IO-POSS-g-CNT sensors to

cyclohexane vapour at 7, 3 and 1.5 ppm concentrations can be seen in Figure 41 (b). Interestingly, one can see that the SNR of carboxylated CNT at 1.5 ppm of cyclohexane has been enhanced from 29 to 40 after grafting of IO-POSS, which is suggesting that the limit of detection could be still decreased to the ppb level.

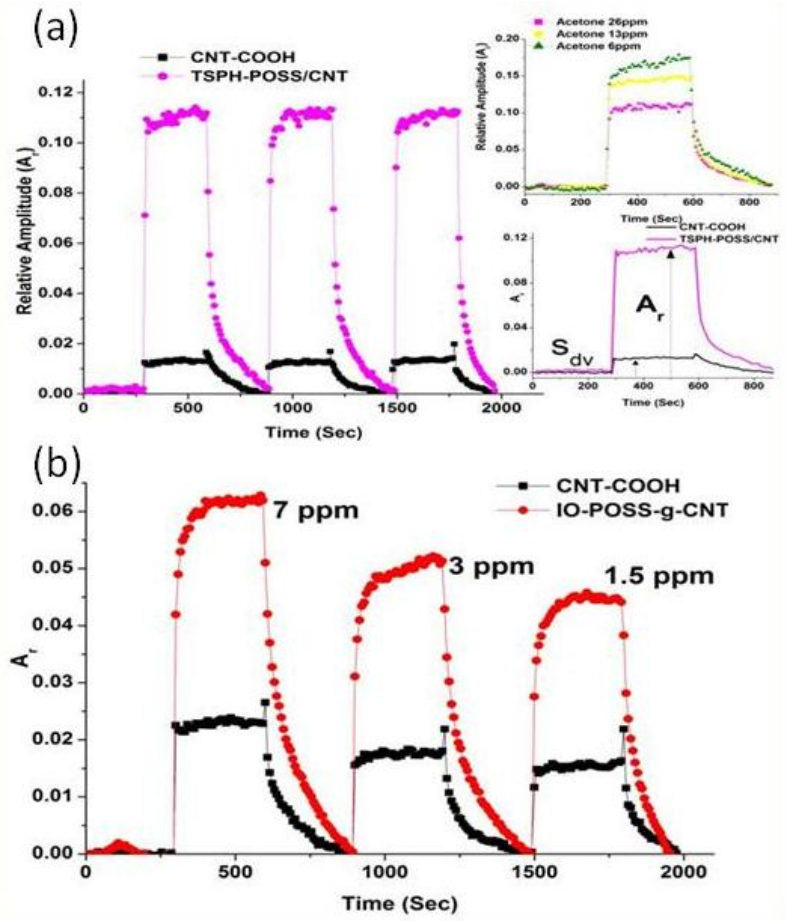

Figure 41 (a) Response of TSPH-POSS/CNT and carboxylated CNT sensors to acetone vapour at 6 ppm (main image), response of TSPH-POSS/CNT and sensor to acetone vapour at 6, 13 and 26 ppm (inset image top), signal to noise ratio of sensor response at 6ppm concentration of acetone vapour (inset image below) (b) Response of IO-POSS/CNT and carboxylated CNT sensor to cyclohexane vapour at ppm level

IV.1.7. Conclusion

The potential of POSS as an effective modifier of CNT to develop hybrid functional nanomaterial with distinct molecular selectivity when applied in the field of chemical vapour sensor, has been investigated. The selectivity of hybrid sensors could be tuned using two different synthesis strategies i.e., covalent and noncovalent modification. The presence of POSS on the surface of CNT not only improves the sensitivity of resulting sensors due to a better dispersion of CNT in organic solvents, but also brings adjustable molecular selectivity.

One of the sensors was found highly selective to cyclohexane and the other one towards acetone which is a very interesting finding since, elevated levels of acetone are found in the breath extract of diabetic [96] and lung cancer patients [370] while cyclohexane is a biomarker of both malignant pleural mesothelioma [97] and lung cancer [90]. Therefore the possibility of variation of pendant organic groups on the surface of POSS cage opens future prospects of POSS based hybrid sensors to develop novel chemical sensor of specific molecular selectivity.

IV.2. Tailoring the selectivity & sensitivity of CNT / graphene based vapour sensors by grafting of fullerene

IV.2.1. Introduction

Fullerenes are fully carbonaceous molecules that can have a planar, hollow spherical or tubular shape. Carbon nanotubes, graphene, Buckminsterfullerenes (C_{60}) each of these three allotropes of carbon belonging to fullerene family, have attracted a tremendous research interest since their discovery, because of their unique physic-chemical properties. C_{60} are zero dimensional with discrete molecular weight while CNT and graphene are one and two dimensional respectively with an anisotropic structure and a broad molecular weight distribution. But each of these carbon allotropes is composed of sp^2 hybridized carbon atoms [371]. However the electrical conductivity of C_{60} (10^{-14}-10^{-8} S/cm) is much lower than that of CNT and graphene ($\approx 10^5$ S.cm^{-1}).

Buckminsterfullerenes (C_{60}) were discovered in 1985 by *Kroto et al.* [226]. But the true research interest of this material has been demonstrated in1990, when *Kratschmer et al.* developed a method of synthesis in macroscopic quantities [372]. C_{60} consists of polyhydral pentagonal-hexagonal carbon rings with each carbon atom bonded to three other neighbours. C_{60} has drawn appreciable research interest since several decades because of its exceptional physical, chemical and electronic properties, such as very high reactivity, an excellent solubility in organic solvents, a very high surface to volume ratio, a high electron mobility (~0.1 cm^{-2} V^{-1} S^{-1}) [373] and the free electron trapping ability [374], [375]. It is considered as a novel electron pool π system [376]. In addition, C_{60} can be reduced readily because of the presence of low energy LUMO which are triply degenerated t_{1u} orbital. Even they can be readily polymerized into directly linked fullerenes nanotubes by application of pressure, temperature or light. A potential application of C_{60} is hydrogen storage since it can bind a number of hydrogen molecules without structure disruption [377]. In addition gas sensing

characteristics of C_{60} were studied by *Sakurai et al.* by observing change of electrical conductivity on exposure to gases such as ammonia, acetaldehyde etc.

The literature survey reveals that the hybridization of C_{60} with polymers, various organic molecules or different nano-materials by covalent or non covalent technique may provide a synergistic combination of properties of both the two components, hence attractive for a number of electronic and optical applications. *Yu et al.* developed covalently bonded C_{60}-Graphene hybrids for bulk heterojunction polymer photovoltaic devices such as solar cells [378]. Immobilized C_{60}-SWNT complexes were synthesized by *Li et al.* via microwave induced functionalization approach for the same application in polymer photovoltaic cells. These devices could exploit the strong electron accepting feature of C_{60} and the high electron transport ability of CNT [379]. *Liu et al.* developed C_{60}-graphene hybrids by covalent techniques to reach superior nonlinear optical properties [380]. C_{60}-graphene hybrids were also prepared by *Zhang et al.* by chemical coupling between graphene oxide and pyrollidine fullerene for potential applications in solar cells or optical limiting [381]. *Song et al.* fabricated fullerene decorated CNT for applications in flame retardant poly (propylene). Flame retardancy could be enhanced by utilizing free electron accepting property of C_{60} with barrier property of CNT [382]. However so far there is no report on vapour sensing applications of C_{60} based nanohybrids.

By the control of geometry and dispersion of the nanofillers, conductive architecture, organic functionality etc, it is possible to achieve a concerted disconnection of entangled percolated network upon chemical solicitation leading to large change in electrical resistance. The sensitivity of CNT or graphene based chemo-resistive sensors can however be tuned by the control of tunnel junctions in the percolated network. In one of our previous studies, unique hierarchical structure of hard PMMA micro beads bridged by CNT was developed to form a segregated network, in which high specific surface could enhance the sensitivity of CNT by 240% keeping the original selectivity of CNT unaltered [206].

In the present study, Buckminterfullerene (C_{60}) have been grafted on to MWNT and reduced graphene oxide in order to construct a conductive architecture of CNT/graphene with nanoscopic C_{60} of large surface to volume ratio, at the junctions. A new generation of hybrid chemical vapour sensors have been synthesized in this study by the combination of two original techniques i.e., hybridization of two nanomaterials and spray layer by layer (sLbL) deposition [195], [243], [383] of the synthesized nanohybrids for a controlled structuring of the 3D conductive architecture. The presence of spherical C_{60} at the junctions of CNT or graphene

sheets is expected to enhance the sensitivity of CNT based chemoresistive vapour sensors appreciably which might be integrated into an electronic nose with distinct ability of discrimination of a set of VOC disease biomarkers. The final objective of this work is to construct a set of new generation chemoresistive hybrid nanosensors whose sensing performance would be better than each of the two component nanomaterials in terms of both sensitivity and selectivity.

IV.2.2. Synthesis of hybrid nanomaterials

In the first step of synthesis, lithiated CNT was produced by the dropwise addition of n-butyl lithium (in hexane) into a dispersion of CNT in toluene under the condition of continuous stirring and nitrogen protection. In the next step the lithiated CNT is reacted with a large excess of Buckminsterfullerene by a nucleophilic addition reaction, resulting in C_{60}-g-CNT as in Figure 42. C_{60}-g-RGO was then produced [378] following the similar procedure as C_{60}-g-CNT. The details of composition of the hybrid sensors are provided in Table 9.

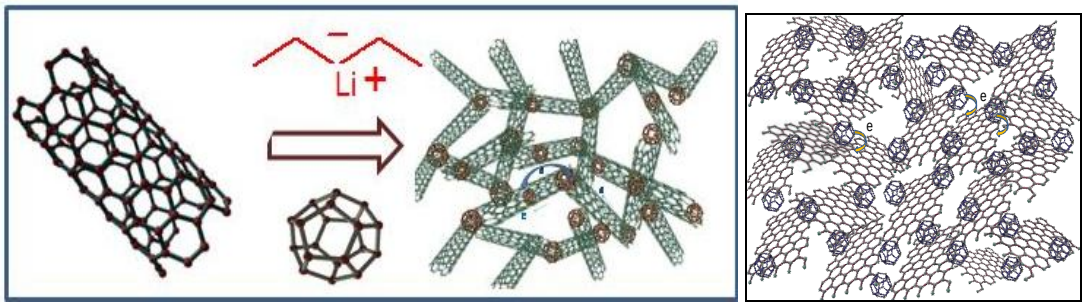

Figure 42 Schematics for synthesis of CNT-g-C_{60} and structure of CNT-g-C_{60}

Nomenclature of hybrid sensor	Fabrication process	Initial resistance of the sensors (kΩ)
CNT	2layers of CNT solution in chloroform sprayed	5±2
CNT-g-C_{60}	2layers of C_{60}-g-CNT solution in chloroform sprayed	8±3
CNT-l-C_{60}	1layer of CNT solution in chloroform sprayed followed by spray of 1layer of C_{60} solution in toluene	4±2
RGO	5layers of RGO solution in acetone sprayed	10±4
RGO-g-C_{60}	5 layers of C_{60}-g-RGO solution in acetone sprayed	10±5

Table 9 Structural characteristics of hybrid sensors

IV.2.3. Morphological study by atomic force microscopy (AFM)

The three dimensional AFM images of pristine CNT, GO and C_{60} are exhibited in Figure 43 (a), (b), (c) respectively. The diameter of C_{60} nanoparticle clusters, were calculated to be around 230 nm on an average.

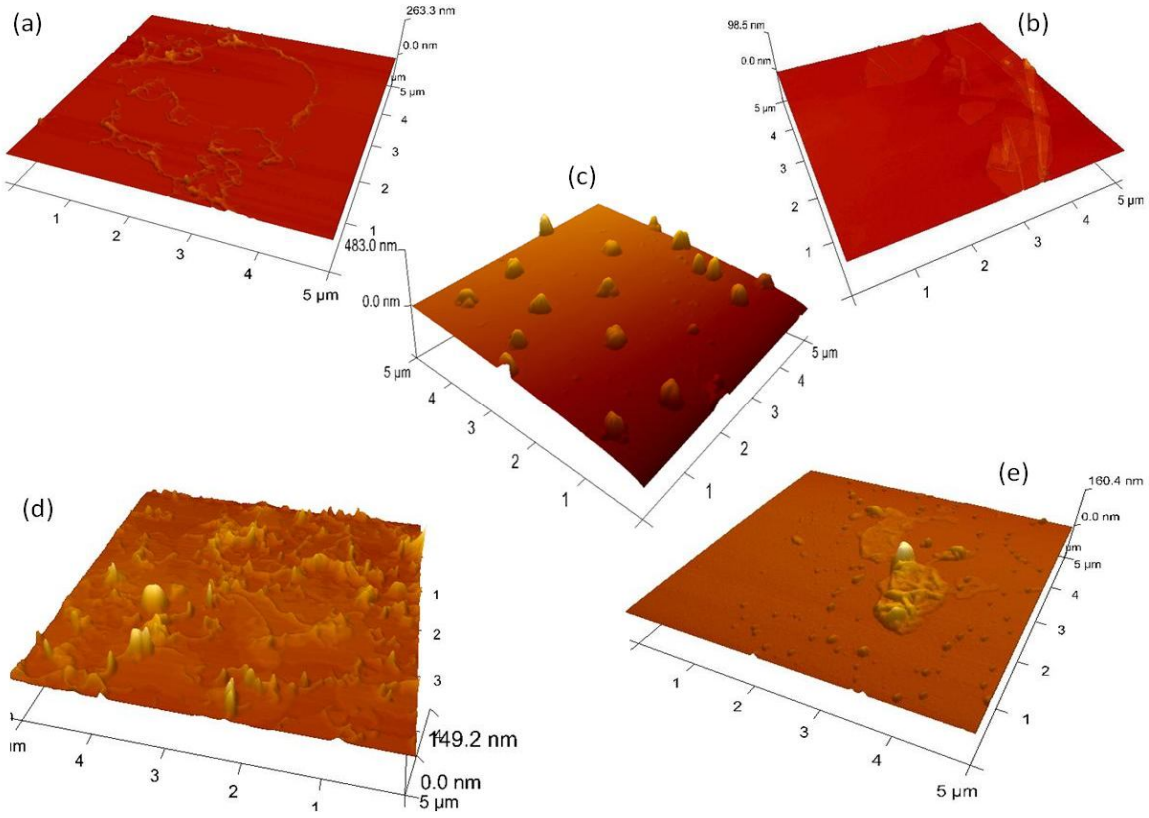

Figure 43 AFM images of (a) CNT (NC 7000) (b) GO (c) Buckminsterfullerene (C_{60}) (d) C_{60}-g-CNT and (e) C_{60}-g-RGO

The comparison of AFM images of pristine CNT and C_{60}-g-CNT shown respectively in Figure 43 (a) and (d), distinctly proves that a large number of C_{60} particles has been grafted on to CNT. Pristine CNT appears to have smooth cylindrical surface without any visible catalyst particles, whereas C_{60}-g-CNT consists of many protrusions from the surface of CNT mostly at the junctions which indicates that C_{60} nanoparticles are grafted mostly at the junctions of entangled CNT network. On the other hand the surface of pristine GO nanosheets appears to be quite smooth unlike that of C_{60}-g-RGO shown in Figure 43 (e), where dotted clusters are clearly visible on the surface of GO nanosheets due to the grafting of C_{60} nanoparticles.

IV.2.4. Morphological study by scanning electron microscopy (SEM)

Figure 44 (a) shows the SEM image of C_{60} nanoparticles when dropcasted on a silica substrate. Originally polyhedral pentagonal hexagonal shaped particles of some hundreds nanometer diameter are found to be observed. Whereas Figure 44 (b) and (c) exhibit SEM image of C_{60}, after dispersion in toluene and spraying onto silica substrate at high pressure at low and high resolution respectively. Surprisingly fullerene nanowhiskers (FNW) are formed in this case. It is reported by several researchers that C_{60} can be converted into FNW by the application of high temperature, pressure, or solvent atmosphere controlled self assembly approach [384], [385]. Interfacial polymerization of C_{60} nanoparticles may also produce FNW of diameters ranging from 300 nm to 1 µm with lengths of several micrometers [386], [387]. Therefore our case definitely provides an interesting finding where spray layer by layer technique could be used for the production of fullerene nanowhiskers. SEM image of C_{60} -g-RGO as depicted in Figure 44 (e) is full of dotted clusters of C_{60} nanoparticles on surface of graphene sheets. Comparison of this image with that of pristine RGO in Figure 44 (d) show the successful grafting of C_{60} on the surface of RGO.

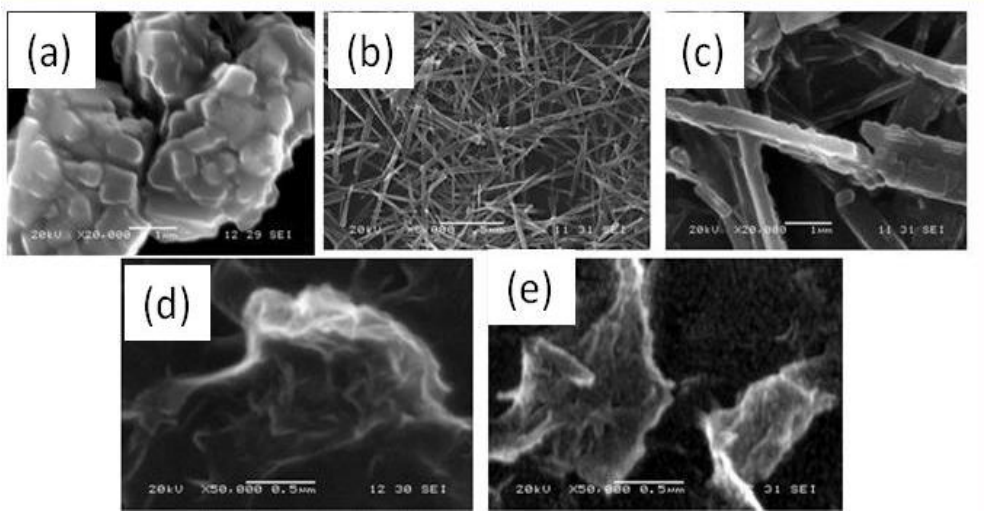

Figure 44 SEM images of (a) Buckminsterfullerene (C_{60}) spin coated on silica substrate (b, c) C_{60} sprayed on silica substrate (d) RGO (e) C_{60}-g-RGO

IV.2.5. Compositional analysis by thermo gravimetric analysis (TGA)

As shown in Figure 45, C_{60} undergoes only 3 wt. % of loss up to 650 °C whereas, around 9 wt. % of loss takes place between 650 and 800 °C. The slope of the decomposition curve changes clearly at around 650 °C. RGO undergoes around 12 wt. % of mass loss up to 800 °C with the TGA curve following a continuous slope. C_{60}-g-RGO on the other hand shows a combined

decomposition trend. It decomposes by 30 wt.% up to 800 °C may be due to the degradation of butyl group used as a linker between RGO and C_{60}. Beyond 600°C the slope of its decomposition curve is similar to that of C_{60} which proves successful grafting of C_{60} on to RGO. Similarly C_{60}-g-CNT undergoes around 20 wt. % of mass loss up to 800 °C although the component nanomaterials like CNT and C_{60} degrade of 4 wt. % and 12 wt. % respectively.

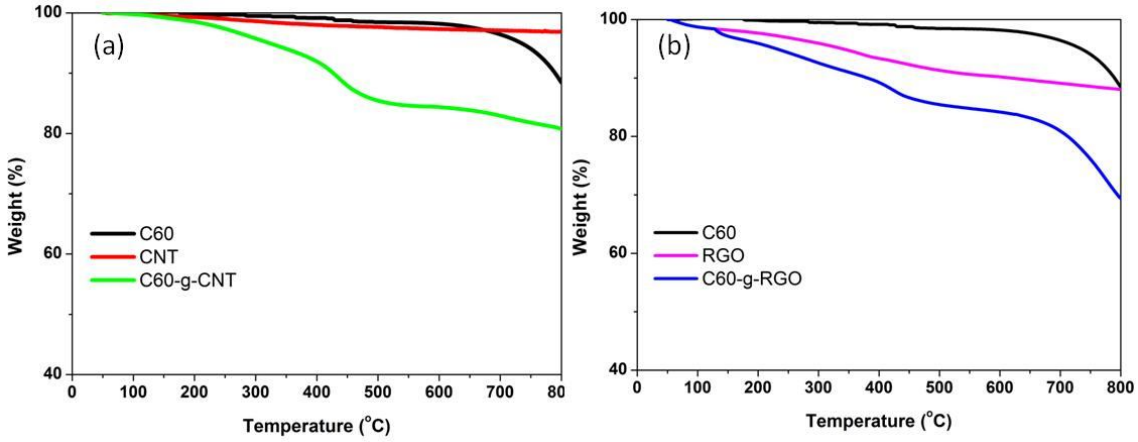

Figure 45 Compared thermogravimetric analysis curves of (a) C_{60}, RGO and C_{60}-g-RGO (b) C_{60}, CNT and C_{60}-g-CNT nanohybrids

IV.2.6. Dynamic vapour sensing characterizations

Figure 46 shows the normalized responses of a combination of three sensors CNT (NC 7000), C_{60}-l-CNT, C_{60}-g-CNT, when exposed to a set of eight VOC lung cancer biomarkers. As evident from Figure 46, the sensitivity of pristine CNT sensors underwent massive enhancement after hybridization with C_{60} either by layer after layer deposition of C_{60} and CNT in C_{60}-l-CNT or by covalent grafting in C_{60}-g-CNT. Moreover, it can be noted that the grafting of fullerene on CNT does not really change the selectivity of pristine CNT sensors, but it dramatically enhances its sensitivity, keeping the same ranking of selectivity. As already evident from the morphological images, C_{60} is grafted mostly at the junctions of CNT. The presence of spherical, strong electron acceptor C_{60} nanoparticles of exceptionally high surface to volume ratio at the CNT junctions may have a strong influence on the electronic mobility of CNT. Also for RGO, it is understandable that C_{60} causes separation of foils more easily, whereas for CNT it can also separate CNT junctions more easily. A strong influence on sensitivity naturally leads to an effect on selectivity of the sensors too. Thus, grafting of C_{60} onto CNT leads to a sensor, with a high inclination towards nonpolar VOC like cyclohexane, benzene, toluene etc. The effect of fullerene in the sensing performance of CNT is same for both C_{60}-l-CNT (deposited alternatively one layer after the other) and C_{60}-g-CNT (fullerene

being grafted on to CNT). But the enhancement of sensitivity reached in C_{60}-g-CNT is even much higher than that of C_{60}-l-CNT. In C_{60}-g-CNT, the morphology is expected to be better controlled, with C_{60} nanoparticles grafted at the junctions of CNT, unlike C_{60}-l-CNT where layers of C_{60} and CNT solutions are deposited one after the other onto the electrodes.

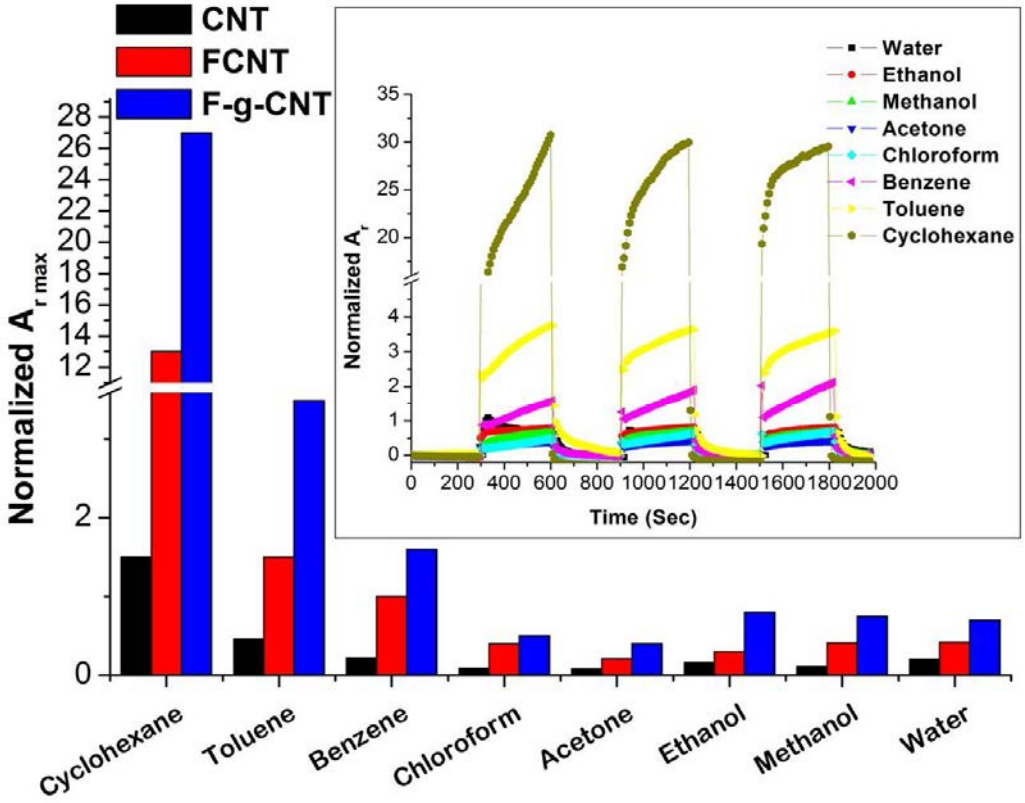

Figure 46 Normalized response of a 3 sensors array towards 8 VOC (equivalent to 1ppm) and chemo-resistive response of the C_{60}-g-CNT sensors towards 8 VOC (inset)

This finding is further supported by the fact that when chemo resistive signals of pristine RGO and C_{60}-g-RGO were compared in Figure 47 (a) and (b) respectively, the order of selectivity was found to be same for both. However the sensitivity i.e. the relative amplitudes were found to be much higher in the case of C_{60}-g-RGO sensors.

IV.2.7. Limit of detection at ppb level

The comparison of the chemo-resistive response pattern of RGO and C_{60}-g-RGO as depicted in Figure 47 (c) and (d) respectively, clearly shows that the signals have become more sensitive and smooth after the grafting of RGO with C_{60}. Table 10 also demonstrates that the noise density of the RGO based sensors has been considerably reduced after the grafting of C_{60}. The enhancement of sensitivity of RGO based sensors by around four times, due to the grafting of

C_{60} even at 400 ppb of VOC fully validates the reliability of our sensors even at extremely low levels of exposure to VOC.

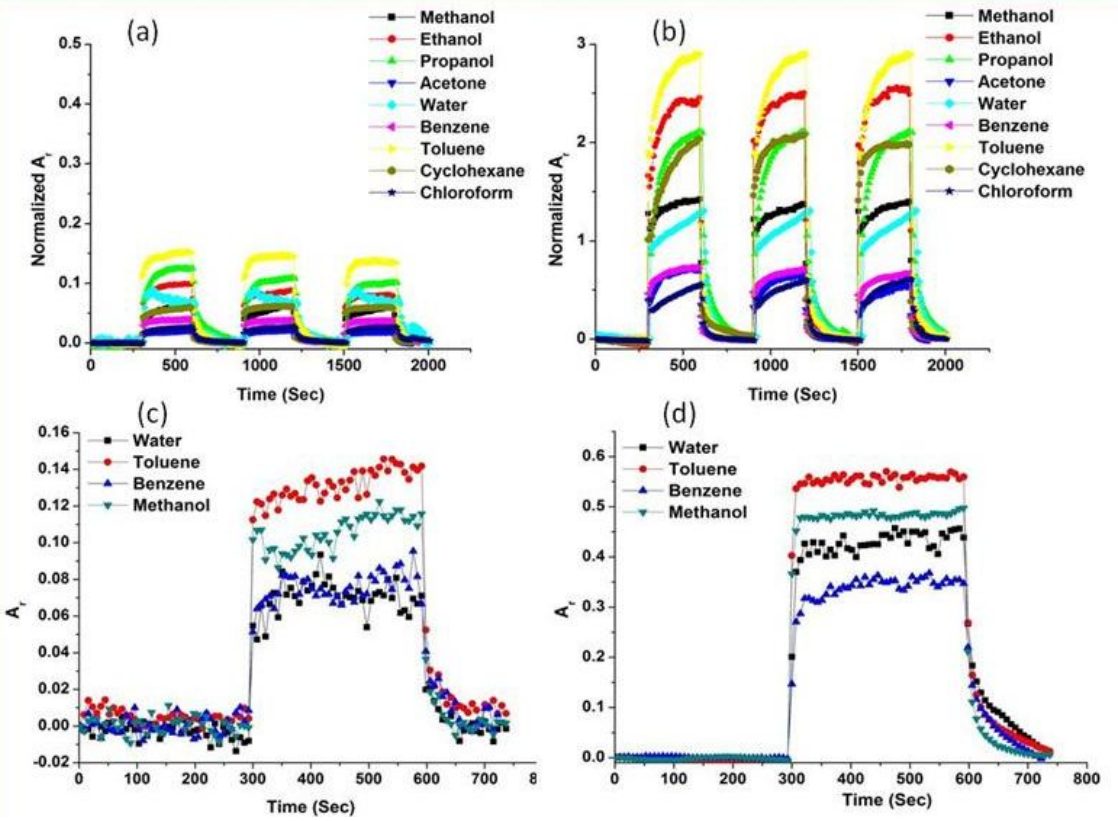

Figure 47 Normalized chemo-resistive response of (a) RGO and (b) C_{60}-g-RGO sensors towards 8 VOC under saturated vapour and chemo-resistive response of (c) RGO and (d) C_{60}-g-RGO sensors towards four selected VOC at 400 ppb

VOC	RGO	C_{60}-g-RGO
Toluene	61	109
Methanol	30	224
Benzene	18	231
Water	19	153

Table 10 Signal to noise (SNR) ratio of RGO and C60-g-RGO sensors towards four selected VOC at 400 ppb concentration

IV.2.8. Conclusion

It has been demonstrated in this section that grafting of Buckminsterfullerene at the junctions of CNT or graphene networks can strongly enhance both sensitivity and/or selectivity of CNT or graphene based vapour sensors. Controlled and amplified disconnection at junctions of CNT or graphene network, due to the grafting of spherical shaped zero dimensional

Buckminsterfullerene of high surface area, is the most probable reason of this improved sensing. Their low sensitivity and non adjustable selectivity to volatile organic compounds is a major limitation of pristine CNT or graphene sensors, which could be overcome by synthesizing their nanohybrids based on Buckminsterfullerene. The response's amplitude of pristine CNT or graphene sensors, which is designated by relative resistance amplitude, could be enhanced by more than ten times on grafting of Buckminsterfullerene. Although the ranking of selectivity to different selected VOC remained the same, but still due to an increase in sensitivity to a very high extent, the selectivity (designated by the difference in sensitivity to various VOC molecules) was improved automatically.

Thus the present study opens a new and novel approach for incrementing the sensitivity and tuning the selectivity of CNT or graphene sensors by improving the steric hindrance at their junctions through the grafting of Buckminster fullerene of high surface area instead of using a polymeric matrix.

Chapter V:
Vapour sensing properties conductive polymer nanocomposites (CPC)

Summary:

The vapour sensing performance of sulfonated poly (ether ether ketone) based nanocomposites is thoroughly studied in this chapter. The 3D architecture of nanoscale sensors were structured using a combination of two versatile techniques; adsorption of sulfonated poly (ether ether ketone) polymers of varying degree of sulfonation onto CNT along with its deposition onto electrodes by spray layer by layer process. The novelty of this part relies on the use of the degree of sulfonation as a tailoring parameter to control the sensitivity and selectivity of sulfonated PEEK/CNT based sensors. The ability of these sensors to construct an e-nose with an ability of discrimination of both single and binary mixture of VOC is elaborately studied. In the later part of this chapter the influence of hybrid nano-fillers on the vapour sensing performance of conductive polymer nanocomposite (CPC) sensors was studied keeping both the identity and the degree of sulfonation of the polymer matrix unaltered.

V.1. Introduction

Covalent/ non-covalent functionalization or coating of carbon nanomaterials [337] with selected macromolecules is a well appreciated strategy for the construction of performing vapour sensors. The selectivity of nanocomposite based chemoresistors is a function of several parameters such as size, shape and geometry of the nanofillers, control of tunnel junctions of the nano-fillers, structuration of 3D conductive architecture, dipolar, dispersive or hydrogen bonding interactions and overall solubility parameters [388]. Specifically in CPC, composed of an insulating polymer matrix in which a conductive network is structured from the percolation of nanofillers, the selectivity is brought about by the nature of the interactions between the chemical functions brought by the polymer matrix and the targeted VOC [389]. The selection of several polymer matrices of interest for CPC sensors has been investigated by researchers of our group already. Among them polymers such as poly (carbonate) [352], poly (methyl methacrylate) [207], poly(styrene) [196], poly (lactic acid) [390] and poly (ε-caprolactone) [202], were found highly selective towards acetone and chloroform [194]. Whereas, biopolymers like chitosan [206], [242], [391], starch, amylose, amylopectine [205] were showing a higher selectivity towards water vapour. Still there is a need for the fabrication of alcohol selective vapour sensors since some of the alcohols like methanol, ethanol, n-propanol etc are considered to be lung cancer biomarkers. With this target to fabricate alcohol selective vapour sensors and also keeping in mind, the potentiality of sulfonated poly (ether ether ketone) polymers for an application in methanol fuel cell [392], [393], the possibility of SPEEK /CNT nanocomposite to work as an alcohol selective VOC sensor could not be overruled. So far there is no report in literature on the vapour sensing application of poly (ether ether ketone). Poly (ether ether ketone) [PEEK] i.e., poly(oxy-1,4-phenylene-oxy-1,4-phenylene-carbonyl-1,4-phenylene) is a linear high performance thermostable engineering polymer with an aromatic, non-fluorinated backbone, in which 1,4-disubstituted phenyl groups are separated by ether (–O–) and carbonyl (–CO–) linkages [394]. Being highly crystalline, this polymer is insoluble in organic solvents, which is a serious disadvantage for several applications including sensing. However when subjected to sulfonation, PEEK loses its crystallinity and becomes soluble in a number of solvents depending on the degree of sulfonation (DS). PEEK can be easily sulfonated by concentrated sulfuric acid, chlorosulfonic acid pure or complexed sulfur trioxide or acetyl sulfate. SPEEK with varying degree of sulfonation can be obtained by varying the reaction time, acid concentration and reaction temperature. In case of sulfonated PEEK (SPEEK), having a degree of sulfonation (DS) ≥ 30%

is normally soluble in N,N-dimethyl formamide (DMF), dimethyl sulfoxide (DMSO), or N-methyl-2-pyrrolidinone (NMP); whereas SPEEK with DS ≥ 70% is soluble in methanol and hot water. On the other hand, NAFION is a sulfonated tetrafluoroethylene based fluoropolymer-copolymer discovered in the late 1960s by Walther GROT of DUPONT.Both NAFION and sulfonated poly (ether ether ketone) are consisting of hydrophobic polymer backbone along with hydrophilic sulfonate polar group clusters. The use of SPEEK and NAFION in methanol fuel cell application has been exhaustively explored by several researchers over the past few years [393].

In the present section the vapour sensing performance of sulfonated PEEK/ CNT nanocomposite sensors is studied thoroughly with a view to fabricate highly selective alcohol sensor that could be implemented as one of the components of an electronic nose for the detection and discrimination of cancer biomarker VOC. Since the breath extract is a complex mixture of several VOC, the ability of our sensor to identify and differentiate mixture of VOC is also studied.

V.2. Synthesis of sulfonated poly (ether ether ketone)/CNT nanocomposite vapour sensors

V.2.1. Sulfonation of Poly (ether ether ketone)

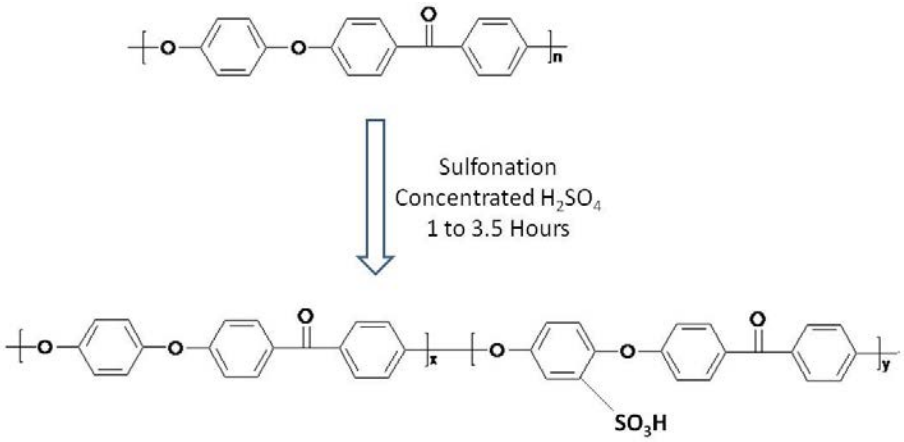

Figure 48 Synthesis of sulfonated PEEK

It is reported that the sulfonation reaction does not lead to chemical degradation and sulfone cross-linking, when the concentration of sulphuric acid is <100 wt. %. Sulfonation of PEEK (VICTREX 150 XF) was carried out in the laboratory as shown in Figure 48. 20 g of PEEK were

dissolved in 1L of conc. H_2SO_4 (95-98%) in a reaction kettle at room temperature with constant agitation to avoid heterogeneous sulfonation. Afterwards the temperature was increased to 50 °C and the reaction was continued for a desired time, ranging from 1 to 3.5 h to achieve the desired degree of sulfonation (DS). Then the polymer solution was gradually precipitated into a large excess of ice-cold water under continuous mechanical agitation. The agitation was continued one hour further and then the polymer suspension was left to settle overnight. The polymer precipitate was filtered and washed several times with distilled water until the pH was neutral. The polymer was then dried under vacuum for 8–10 h at 100 °C. The final product is the sulfonic acid form of PEEK (SPEEK) which is a copolymer comprising sulfonated PEEK and non-sulfonated PEEK structural units.

V.2.2. Fabrication of sensor

100 mg of SPEEK polymer of varying degree of sulfonation was dissolved in 20 mL DMF followed by the dispersion of 4 mg of carboxylated CNT into the solution by ultrasoication for several hours until the dispersion becomes homogeneous. Afterwards the fabrication of portable sensors was done by spray layer by layer technique as explained in appendix (page number 143). The SPEEK nanocomposite sensors based on hybrid fillers were also fabricated in a similar way, only replacing CNT by C_{60}-g-CNT. Carboxylated CNT and NAFION /CNT sensors were also prepared similarly for the purpose of comparison of their sensing performance.

V.3. Characterizations of sulfonated poly (ether ether ketone)

V.3.1. Determination of degree of sulfonation by nuclear magnetic resonance spectroscopy (NMR)

The ^{1}H-NMR spectra was recorded using DMSO-d6 as solvent and tetramethyl silane as internal standard. The ^{1}H-NMR spectrum of five SPEEK samples of varying DS is shown in Figure 49. The degree of sulfonation of SPEEK was also determined using ^{1}H-NMR. The introduction of SO_3H functional group resulted in a distinct signal for H_E proton at δ = 7.55 ppm. The intensity of H_E content is equivalent to SO_3H group content, therefore the degree of sulfonation can be calculated by taking the ratios between the peak area of H_E to the peak areas

for the rest of the aromatic hydrogens i.e. $H_{A,A',B,B',C,D}$. Degree of sulfonation was calculated from ^{1}H-NMR using equation 6,

$$\frac{n}{12-2n} = \frac{H_E}{\Sigma H_{A,A',B,B',C,D}} \quad \ldots\ldots\ldots\ldots (6)$$

Where 'n' is the number of H_E per repeat unit. Degree of sulfonation was calculated using equation 7.

$$DS\ (\%) = n*100 \quad \ldots\ldots\ldots\ldots\ldots\ldots (7)$$

The details of different reaction parameters and reaction conditions used for the preparation of SPEEK with varying degree of sulfonation are given in Table 11.

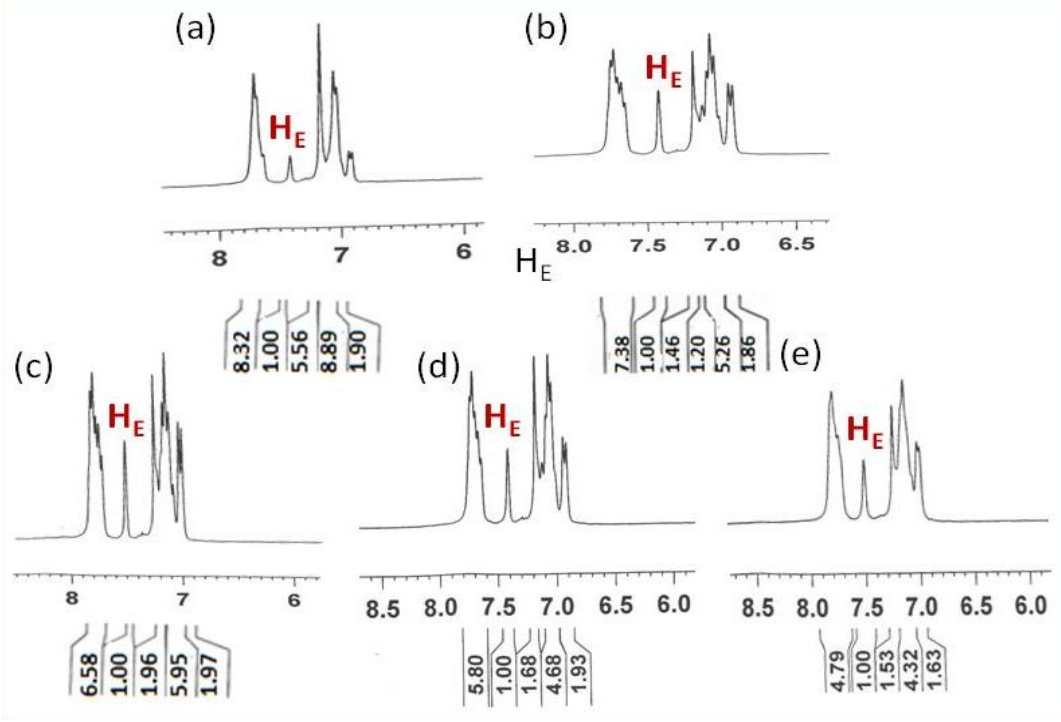

Figure 49 1H-NMR spectrum of (a) PEEK-S1, (b) PEEK-S2, (c) PEEK-S3, (d) PEEK-S4, (e) PEEK-S5

Nomenclature of the polymer	Reaction Temperature (°C)	Reaction time (Hours)	Degre of Sulfonation (DS) (%)	Nomenclature of the nanocomposite (SPEEK+3% nanofiller) sensor prepared by spray layer by layer process
PEEK-S1	50	1.5	45	PEEK-S1/CNT
PEEK-S2	50	2.0	55	PEEK-S2/CNT
PEEK-S3	50	2.5	65	PEEK-S3/CNT
PEEK-S4	50	3.0	75	PEEK-S4/CNT
PEEK-S5	50	3.5	85	PEEK-S5/CNT
PEEK-S5	50	3.5	85	PEEK-S5/ C_{60}-g-CNT

Table 11 Effect of reaction time on degree of sulfonation

V.3.2. Structural characterizations by FTIR spectroscopy

The comparison of FTIR spectra of PEEK-S5 and PEEK is shown in Figure 50 (a). The characteristic peaks associated with sulfonic acid groups in PEEK-S5 is a broad band at ~3440 cm^{-1} which is absent in PEEK. Peaks at 1085 cm^{-1} and 1022 cm^{-1} in PEEK-S5 are due to symmetric O=S=O stretching and S=O stretching respectively. A new absorption band, which appeared at 1222 cm^{-1} in the spectra of PEEK-S5 samples, was also assigned to the sulfonic functional group.

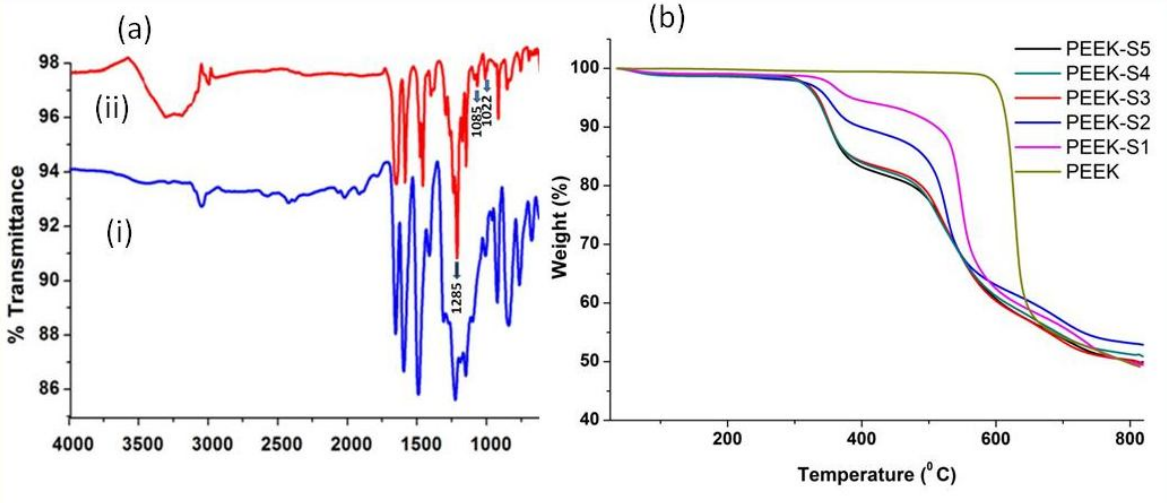

Figure 50 (A) FTIR spectrums of (i) PEEK (ii) PEEK-S5 (b) TGA curves of PEEK and sulfonated PEEK samples

V.4. Characterization of SPEEK/CNT nanocomposites

V.4.1. Study of degradation by thermo gravimetric analysis (TGA)

PEEK is a thermostable polymer in which the onset of degradation is found beyond 550 °C and up to 800 °C, 52 wt. % losses takes place in one step. Whereas the thermal stability of PEEK decreases progressively with increasing DS as visible in Figure 50 (b) due to the catalytic effect of sulfonic groups on degradation of the polymer chain, and the enhanced asymmetry in the PEEK structure due to the introduction of SO_3H groups. Normally three steps degradation occur in SPEEK samples. All the samples of SPEEK exhibited a minor mass loss below 200 °C i.e., in the range of 1-2 % due to loss of free or bound water. The next weight loss step in the 200-450 °C temperature range is due to the decomposition of the sulfonic acid groups and the final weight loss between 450-800 °C is due to the main chain degradation of polymers.

V.4.2. Morphological characterization by SEM and AFM

The morphology of SPEEK/CNT nanocomposites was studied by SEM and AFM. By comparing the SEM image of CNT and PEEK-S5/ CNT nanocomposite, as shown in Figure 51 (a) and (b) respectively, it is visible that the PEEK-S5 polymer has coated CNT everywhere in PEEK-S5/ CNT nanocomposite. AFM image of pristine CNT and PEEK-S5/CNT are shown in Figure 51 (c) and (d) respectively from which it is observed that spherical shaped sulfonated PEEK polymers are deposited over CNT in case of PEEK-S5/CNT nanocomposite.

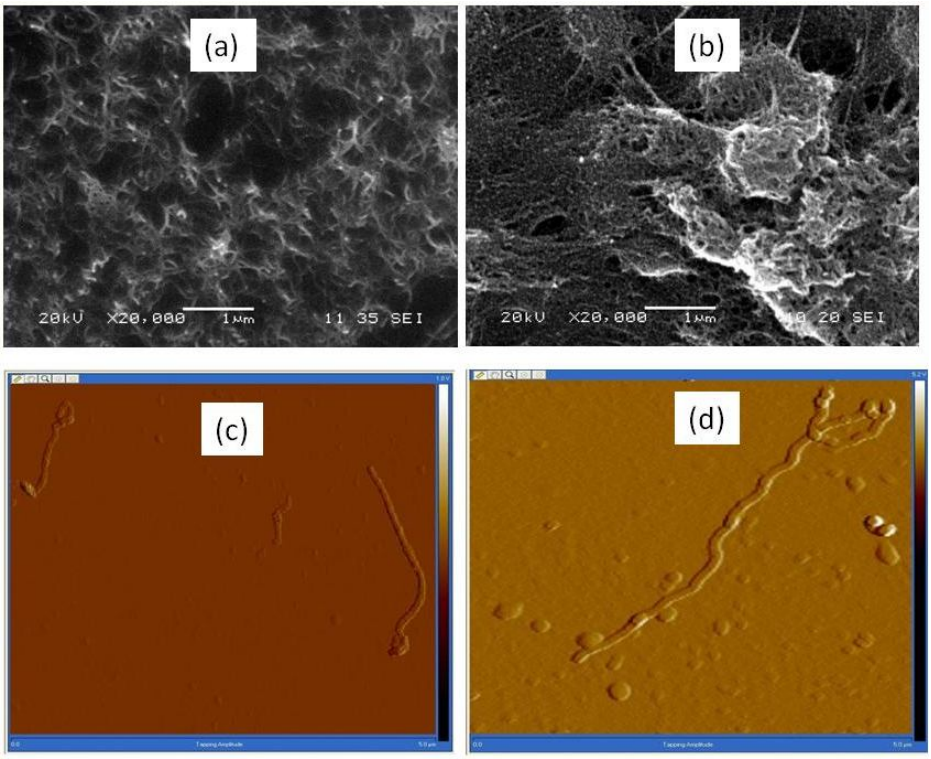

Figure 51 SEM image of (a) CNT and (b) PEEK-S5/CNT, AFM image of (c) CNT and (d) PEEK-S5/CNT

V.4.3. Vapour sensing performance of sulfonated poly (ether ether ketone)/CNT nanocomposites

V.4.3.1. Selection of targeted VOC

A single compound (pure VOC biomarker) is generally insufficient to monitor complex and heterogeneous situations in case of environmental exposures or chronic diseases. Consequently, exploring the total amount of exhaled VOC, called the volatome, may generate more suitable information regarding the complexity of processes underlying the pathophysiologies of interest. Certainly, analyzing the volatome implies a more sensitive and

specific discrimination between various conditions as it reflects changes in both exogenous and endogenous compounds [395]. Therefore it is important to verify the discriminating ability of array of sensors when exposed to mixture of VOC [396]–[400].

However it is quite tricky to sense lung cancer biomarkers in real conditions, considering that they are blended with many other VOC including water at high concentration (more than 80 %). Still, the detection of pure molecules must first be conducted before addressing a discriminating detection. Thus we restricted our study till now, mostly to the analysis of chemo-resistive properties of an array of sensors in the presence of synthetic biomarkers produced under controlled conditions in the laboratory, being aware of the remaining possible obstacles until the final validation with cancerous patients.

Nevertheless, since sulfonated PEEK nanocomposite based sensors were the last systems studied in this dissertation work, it was decided to check the ability of these sensors to discriminate both single and binary mixture of VOC. For a specific sensor array, discriminating a mixture from its components depends on the number of vapours in the mixture, their structural similarity (or more accurately, the similarity of their interactions with the interface layers of the array sensors), and vapour concentrations [401]. In this context, in order to constrain the mixture analysis problem, binary mixtures were selected, which are simplest VOC mixtures, judicially undertaken for initial experiments.

The response differences in binary mixture vapours were investigated already by *Jaisutti et al.*, using metal oxide based sensor arrays. The classification patterns of binary mixing vapours could be identified by a principal component analysis which demonstrated that the mixture points at various ratios are clearly separated [402].

V.4.3.2. Influence of DS of the polymer matrix on the performance of CPC sensors in pure and binary mixture of VOC

Figure 52 clearly displays the average maximum relative amplitudes ($A_{r\,max}$) of a set of five sulfonated PEEK sensors only varying in the DS of the polymer, and one additional sensor composed of carboxylated CNT upon exposure to a set of selected lung cancer biomarker pure and binary mixtures of VOC. The sensitivity, i.e., the response of all sulfonated PEEK based sensors, was found much higher than that of pristine carboxylated CNT in most of the VOC. However, the sulfonated PEEK based sensors were found to have a higher sensitivity for methanol, i.e., they are methanol selective. An increasing sensitivity to methanol with an increasing DS of sulfonated PEEK was also observed, as depicted in the inset curve of Figure

52. Among all the sulfonated PEEK based nanosensors of varying DS, the best performance is exhibited by PEEK-S5/CNT sensors in terms of sensitivity and selectivity. The ranking of selectivity of PEEK-S5/CNT sensor for the selected set of pure and binary VOC, as depicted in Figure 52, is as follows: [Methanol> methanol+ethanol> methanol+propanol> methanol+acetone> acetone> ethanol> methanol+benzene> propanol> benzene].

The $A_{r\ max}$ values of binary mixtures are located somewhere in between the $A_{r\ max}$ values of the two component VOC.

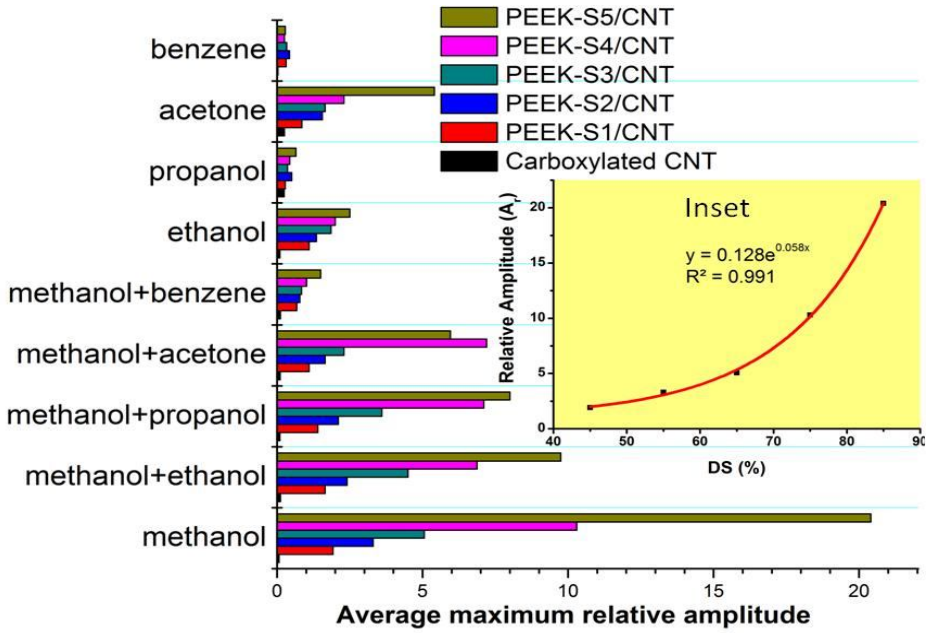

Figure 52 (a) Average maximum relative amplitude (A_r) of a set of pure and binary mixture to saturated VOC lung cancer biomarkers

V.4.3.3. Comparison of vapour sensing performance of CPC sensors based on sulfonated PEEK matrix with that of Nafion

Since both sulfonated (PEEK) and NAFION are sulfonated polymers with high methanol permeability, the sensing performance of NAFION-CNT sensors was compared to those of sulfonated PEEK based nanosensors. Figure 53 (a) and (b) exhibits the dynamic vapour sensing responses of PEEK-S5-CNT sensors to a set of lung cancer biomarker VOC before and after normalization respectively. The original responses (to saturated VOC) and the normalized responses (eliminating the effect of the varying number of molecules in different saturated VOC) of NAFION-CNT sensors are depicted in Figure 53 (c) and (d) respectively, for a set of eight selected pure VOC, which are known as lung cancer biomarkers. As expected, the

ranking of selectivity undergoes some changes after the responses have been normalized. But PEEK-S5/CNT sensors are still highly selective to methanol after the normalization of the sensing response. Unlike the sulfonated PEEK nanocomposite sensors, the sensitivity of NAFION-CNT sensor towards all saturated alcoholic VOC (methanol, ethanol, propanol) are very close to each other, hence it is difficult to discriminate them from one another. However, after the sensing response have been normalized, the sensitivity to 2-propanol and ethanol increases much more than to methanol. The sulfonated PEEK nanocomposite sensors are found more performing than NAFION-CNT sensors due to the following reasons: (1) a six times higher sensitivity to methanol, (2) a possible alteration of the DS, which allows to tailoring of sensitivity.

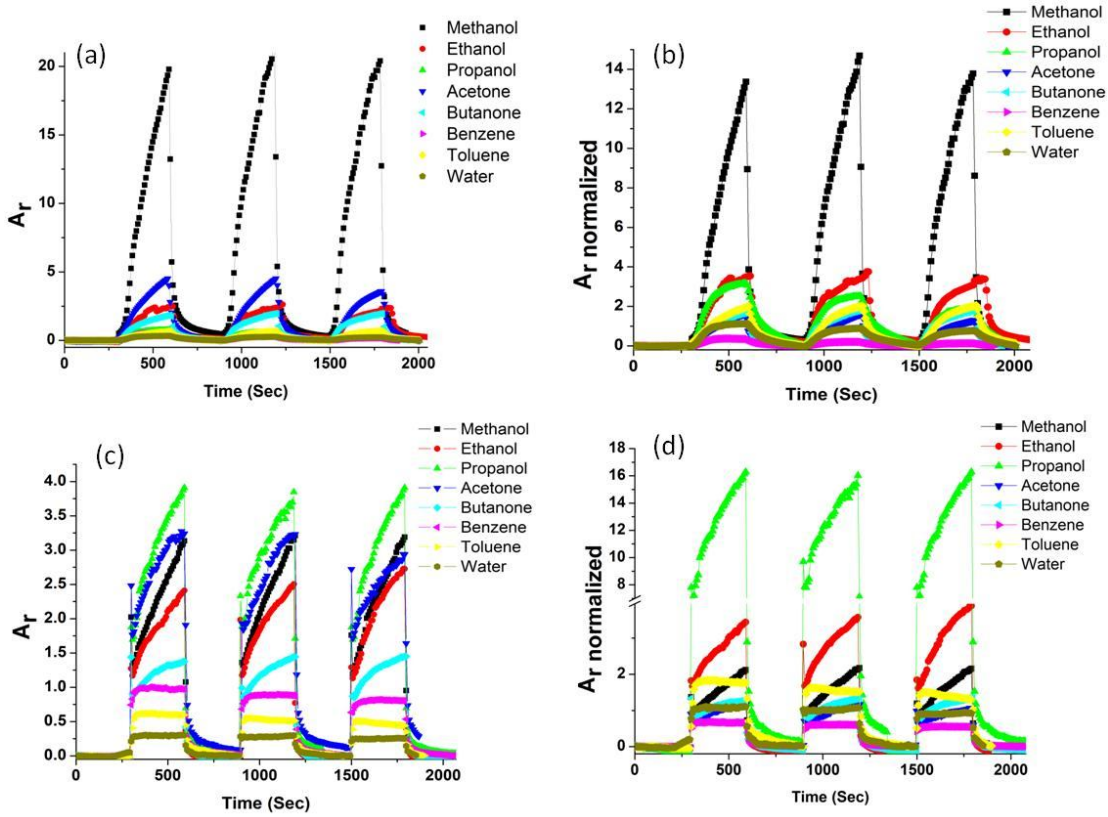

Figure 53 Chemo-resistive response of PEEK-S5/CNT (a, b) and Nafion/CNT sensors (c, d) to a set of lung cancer biomarker VOC before and after normalization of sensing response

V.4.3.4. Limit of detection

Figure 54 (a), (b) and (c) shows the chemo-resistive responses of carboxylated CNT, NAFION-CNT and PEEKS5-CNT sensors respectively exposed to pulses of 2 ppm to 340 ppb of methanol. At first glance it is clear that the signals of PEEKS5-CNT sensor are much

smoother, cleaner and larger, compared to the noisy and weaker signals of pristine CNT or NAFION-CNT. The determination of the signal to noise ratio (*SNR*) during sensing experiments with only trace levels of vapour molecules allows to quantify the noise density and ultimate sensitivity of sensors [359].

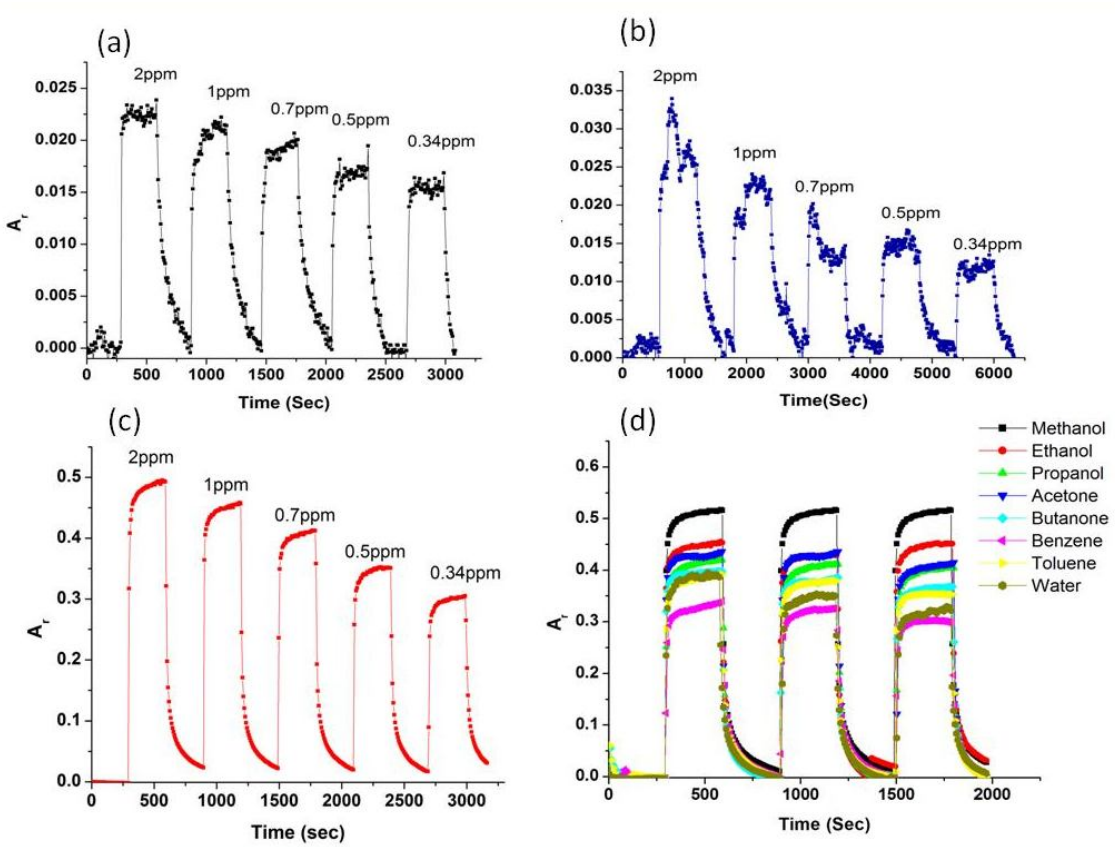

Figure 54 Chemo-resistive signals of (a) CNT (b) Nafion/CNT (c) PEEK-S5/CNT sensors under exposure to methanol in varying trace concentrations (d) chemo-resistive response of PEEK-S5/CNT sensor on exposure to a set of 8 VOC cancer biomarkers at 2 ppm

Methanol concentration (ppm)	SNR for carboxylated CNT	SNR for PEEK-S5/CNT
2	50	250
1	48	244
0.7	40	235
0.5	30	220
0.34	20	200

Table 12 SNR values of CNT and PEEK-S5/CNT sensors in methanol

Table 12 is collecting all the SNR values of pristine CNT and PEEK-S5/CNT sensors for pulses of 2, 1, 0.7, 0.5, 0.34 ppm of methanol. It can be noticed that the SNR values of CNT

based sensors are increased of five times after coating with sulfonated (PEEK), which confirms the better sensing performances of PEEK-S5/CNT sensors even at low VOC concentrations. As evident from Figure 54 (d), the ranking of selectivity for PEEKS5-CNT sensors at 2 ppm exposure is:[methanol> ethanol> n-propanol≈ acetone> butanone≈ toluene> water>benzene]. Therefore the SPEEK based sensors are methanol selective even for trace level concentrations.

V.4.4. Influence of hybrid fillers on performance of sulfonated PEEK based CPC sensors

It has been reported in chapter IV that the sensitivity of CNT based sensors could be significantly improved after the grafting of spherical Buckminsterfullerene at the junctions of CNT. To the light of this finding, the present study is carried out to check the influence of hybrid fillers on sensors based on conductive polymer nanocomposites sensing performances. As already shown in the previous sections, the SPEEK with a DS of 85 %, i.e., PEEKS5 based CPC are the most sensitive and selective, among all the other CPC sensors in which the DS has been varied. This is why it has been chosen to evaluate the effect of hybrid fillers on CPC sensors chemo-resistive properties.. The sensing performance of PEEKS5-CNT is compared with that of PEEKS5/C_{60}-g-CNT, where carbon nanotube are replaced by an equal amount of Buckminsterfullerene grafted CNT.

The chemo-resistive signals of the PEEK-S5/ C_{60}-g-CNT sensor to a set of VOC are shown in Figure 55 (a). By comparing its sensing responses with those of PEEK-S5/CNT in Figure 55 (b), it is clear that independently from the polymer matrix, which is the same in both sensors, the replacement of CNT with C_{60}-g-CNT results in a very high increase of sensitivity of the sensors. The sensitivity to methanol is increased of more than two times by the use of hybrid fillers, whereas the sensitivity to ethanol has is eight times larger. The ranking of selectivity of the CPC sensors is normally controlled by the chemical nature of the polymer matrix. Since in this experiment the polymer matrix is the same in both sensors, the selectivity ranking should be unchanged. However, the large increment of sensitivity brought by the use of hybrid fillers is found to somehow modify this ranking.

By comparing the AFM images of CNT with that of PEEK-S5/C_{60}-g-CNT as depicted in Figure 56 (a) and (b) respectively, it is clear that C_{60} particles are grafted all over the CNT network, particularly at the CNT junctions. Moreover, the C_{60}-g-CNT nanohybrid appears to be coated with the polymer matrix in PEEK-S5/C_{60}-g-CNT. A 3D AFM image of PEEK-S5/ C_{60}-g-CNT at higher resolution is also provided in Figure 56 (c) that better shows the details of the hybrid filler. The two dimensional AFM image of PEEK-S5/ C_{60}-g-CNT in Figure 56(d)

confirms the presence of bright spots of C_{60} aggregates at CNT junctions, and suggest that the nanofillers are well coated with a layer of polymer.

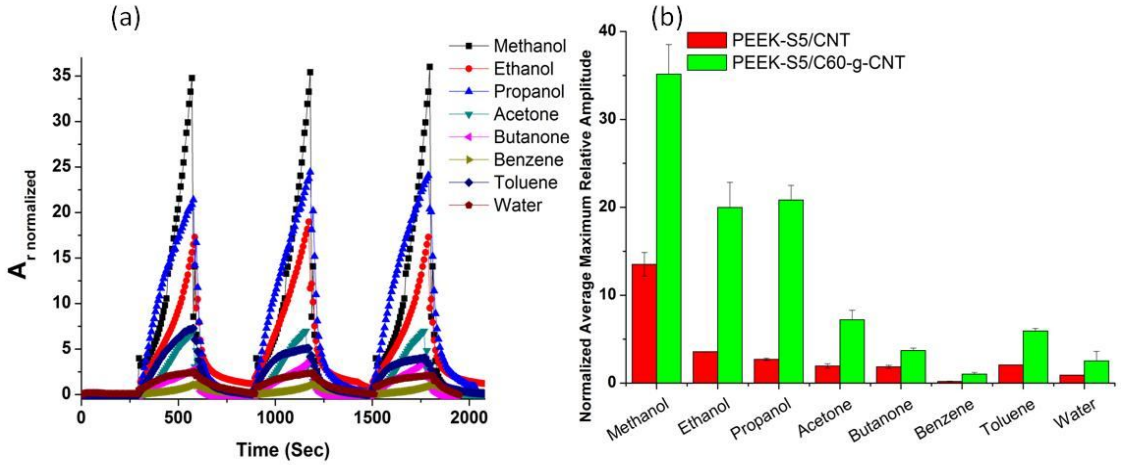

Figure 55 (a) Chemo-resistive response of PEEK-S5/C_{60}-g-CNT sensors to a set of lung cancer biomarker VOC (b) Normalized average maximum relative amplitude ($A_{r\ max}$) of a set of two sensors in eight VOC lung cancer biomarkers

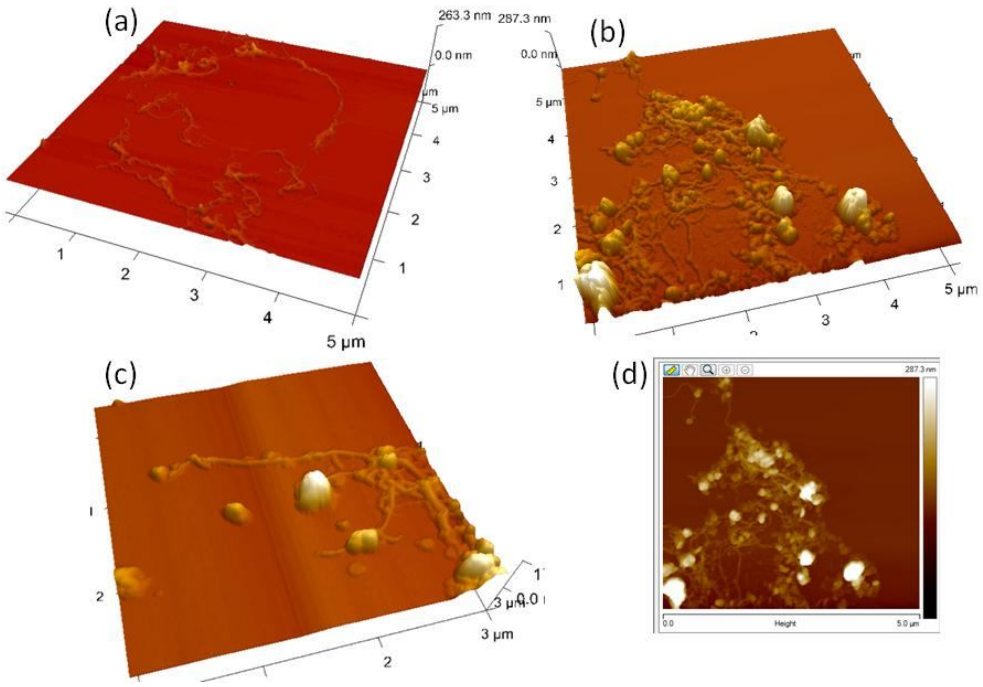

Figure 56 (a) 3D, AFM image of carboxylated CNT (b) (c) 3D, AFM image of PEEK-S5/C_{60}-g-CNT at different resolution, (d) 2D, AFM image of PEEK-S5/C_{60}-g-CNT

The tailoring of the carbon nanotubes nanojunctions by the grafting of C_{60} spherical nanofillers of very high surface area and electronic mobility, is expected to lead to a more effective

disconnection of the CNT conducting network that could explain the higher sensitivity of CPC sensors based on C_{60}-g-CNT hybrid filler.

V.5. Conclusion

A set of high performance chemo-resistive sensors were prepared based on sulfonated poly (ether ether ketone)/CNT nanocomposites, each sensor differing from the others in degree of sulfonation of PEEK. The degree of sulfonation of PEEK is found to impart a strong influence on the sensitivity and selectivity of the sensors. Among a set of 8 lung cancer biomarker VOC, the SPEEK nanocomposite sensors were found to possess highest selectivity for methanol. The degree of sulfonation of PEEK polymer was used for the first time as a tuning parameter to control the methanol sensitivity of the sensors. The vapour discrimination ability of the sensors was also studied for different binary mixtures of VOC where one of the two components was always methanol. The CPC sensors were found efficient to identify and discriminate a set of different single or binary mixtures of VOC biomarkers. The sensors were also found to be operative under exposure to very low concentration of VOC i.e., in sub-ppm level. Even the sub ppm level sensing performance of SPEEK/CNT sensors was far better than those of NAFION-CNT sensors in terms of sensitivity and signal to noise ratio. The influence of the hybrid filler on the sensing performance of CPC sensors was also thoroughly studied. Both degree of sulfonation of matrix polymer and the use of hybrid nanofillers were found to emerge as new generation sensitivity tuning parameters in chemoresistive sensors.

Chapter VI: Construction of electronic nose & conclusive remarks with future prospects

Summary:

In this last chapter of the thesis, the construction of an e-nose with different combination of sensor arrays was accomplished in combination with a principle component analysis (PCA mapping), which is a two or three dimensional mapping of multi-component data with a minimum loss of information. The efficiency of the e-nose, composed by assembling varying combination of sensors was compared. Finally several conclusive remarks are stated along with future prospects of this dissertation work.

VI.1. Library of sensors

The objective of this thesis was to fabricate different chemo-resistive sensors based on conductive nanocomposites with the ability to differentiate and discriminate a set of disease (such as lung cancer) biomarker VOC. Therefore in order to fabricate high performance sensors with high sensitivity and required selectivity towards targeted VOC, the adoption of different methodologies for the synthesis of conductive nanocomposite preparation was strongly emphasized. For this purpose different strategies were undertaken to synthesize conductive nanocomposites. The selectivity of as synthesized sensors was tuned by the variation of organic functionalization of smart carbon nanomaterials.

Below, the Table 13 summarizes all the different functionalized CNT/graphene based sensors fabricated in this dissertation work along with their selectivity.

Sensor Number	**Nomenclature**	**Best selectivity**	**Normalized maximum relative amplitude in VOC for which sensor shows best sensitivity ($A_{r\ normalized}$)**
1	Carboxylated CNT	-	-
2	RGO	-	-
3	RGO@PYAD	-	-
4	RGO@PYAD-MCD	Methanol	0.48
5	RGO@PYAD-NCD	Acetone	0.46
6	RGO@PBCD	Benzene	1.2
7	RGO@PYAD-PEGCD	Propanol	16
8	IO-POSS-g-CNT	Cyclohexane	5.3
9	TSPH-POSS/CNT	Acetone	4.9
10	C_{60}-g-CNT	Cyclohexane	27.3
11	C_{60}-g-RGO	Toluene	2.85
12	PEEK-S5/CNT	Methanol	21
13	PEEK-S5/ C_{60}-g-CNT	Methanol	55

Table 13 Library of fabricated sensors

Sensors 1, 2 and 3 are basic sensors without appreciable selectivity towards any particular analyte; whereas the rest of the sensors exhibit some particular ranking of selectivity depending mostly upon their surface functionality. Sensors 1 to 5 possess sensitivity (towards the VOC for which it is most selective) values ($A_{r\ normalized}$) <1; hence we may consider that these sensors possess lower range of sensitivity. Sensors 6, 8, 9, and 11 possess medium range of sensitivity values ($10 < A_{r\ normalized} < 1$), whereas sensors 7, 10, 12 and 13 possess a higher

range of sensitivity towards most selective VOC ($A_{r\ normalized}$ >10). Hence the library of fabricated sensors as shown in Table 13, possess sensors with different range of sensitivity and selectivity values.

VI.2. Principle component analysis (PCA mapping)

Sensor arrays can be used to generate a great deal of data in a very short time. A significant challenge exists in finding ways to extract the information useful in solving the problem at hand from the data. The graphical analysis of the raw data is often not possible since the number of samples and sensors is typically greater than three. Principal component analysis (PCA) provides one efficient approach for reducing the dimensionality of a data set with minimum loss of information. Often two or three principal components provide an adequate representation of the data, which is convenient for graphical output [403]–[408].

PCAis a simple and effective method to plot the set of data produced by an array of n-sensors exposed to m-vapours, and this method describes the simplifying of multi-dimensional data onto 2D or 3D axes. Basically PCA contributes new attributes (axis PC1, PC2, PC3) which are linear transformation of input attributes. The variance of these attributes is maximized, each attribute being orthogonal to other. More precisely, PCA is a powerful linear supervised learning pattern-recognition technique in which the response matrix is expressed in terms of linear combinations of the orthogonal response vectors (s_{ij}), so the r th principal component (X), is a summation of the *n* response vectors, for the vapours

$$\boldsymbol{Xr = \sum_{i=1}^{n} \alpha_{ir}\, s_{ij}} \quad \text{..... (8)}$$

where α_{ir} are the eigenvectors, sometimes referred to as the loadings. The variance of X, is maximized under the constraints that are defined by:

$$\boldsymbol{\sum_{i=1}^{n} \alpha_{ir} = 1} \quad \text{.....(9)}$$

Principal components are independent. The percentage of data variance contained in each principal component is determined by the eigen value [406]. The power of principal component analysis stems from the fact that the coefficient matrix, is chosen such that the principal components are mutually orthogonal, even though the original descriptors may have been heavily correlated [409].

The applications of PCA to data from chemical sensor arrays, is used for a variety of things, from a complete analysis of the data to a guide for other methods of data analysis. Oftentimes,

working with sensor arrays, especially electronic noses, requires only a differentiation of patterns. It is not necessary to identify components in a sample [403].

VI.3. E-Nose construction

Although the discrimination ability of chemo-resistive sensors can be intuitively assessed from their individual responses to analytes, this parameter becomes strongly difficult to quantify when they are assembled into an e-nose. In order to evaluate how sensors can discriminate the different vapours, an unsupervised classification analysis has been performed by using a principal component analysis. An electronic nose (e-nose) is an instrument that combines vapour sensor assembled in arrays and pattern analysis techniques for the detection, identification, or quantification of volatile compounds. The multivariate response of an array of chemical gas sensors with a broad and partially overlapping selectivity can be utilized as an "electronic fingerprint" to characterize a wide range of odours or volatile compounds by pattern-recognition means [410], [411]. The final objective of this research work is to construct a highly efficient electronic nose by suitable combination of, as fabricated sensors into arrays, suitable for the discrimination of a selected set of VOC lung cancer biomarkers. For this purpose we have considered different combinations of the fabricated sensors to be assembled in an e-nose and also compared their discriminating ability qualitatively by the aid of PCA mapping. The results of PCA, performed in a 3D space of responses, for different e-nose (consisting of varying combination of sensor's in the array) exposed to the selected set of vapours, are plotted in the following Figures 57.

The maximum and minimum values of x, y and z axis scales are kept identical for all e-nose for the ease of comparison. Three dimensional plots (PC1–PC2–PC3) are obtained by the collection of maximum relative amplitudes of each sensor exposed to the set of eight organic vapours recorded during 3 cycles and converted into an *m* by *n* matrix (*m* being the number of measurements and *n* the number of sensors).

- *E-Nose 1 (sensors 1, 2, 3 from Table 13)*

The e-nose 1 was constructed by the combination of the three most basic and simple sensors in an array (sensor 1, 2 and 3).This e-nose is composed of carboxylated CNT, reduced graphene oxide and pyrene adamantan linked graphene sensors. In 3D, the scores of PC1, PC2 and PC3 accounts for 100% of total variance. As depicted in Figure 57 (a), being composed of basic sensors with low sensitivity and selectivity, this e-nose appears not at all efficient for the discrimination of the set of VOC lung cancer biomarkers in 3D PCA mapping. The cluster

points corresponding to different VOC are close to each other all being localized in the central region of the PCA map. This e-nose 1 is to be used as a reference for evaluating the efficiency of other e-nose.

- *E-Nose 2 (sensors 1to 13 from Table 13)*

As evident from Figure 57 (b), the e-nose 2 is composed of 13 sensors in array, where all the sensors listed in Table 13 are integrated. Therefore it consists of 10 additional modified sensors along with three basic sensors. Finally 74.5% of the total variance within the data is contained in the three first principal components, which corresponds to better discrimination ability between clusters of vapours when compared to e-nose 1. The cluster points corresponding to most VOC (except water, toluene) appears to be quite well dispersed throughout the mapping zone unlike in Figure 57 (a).

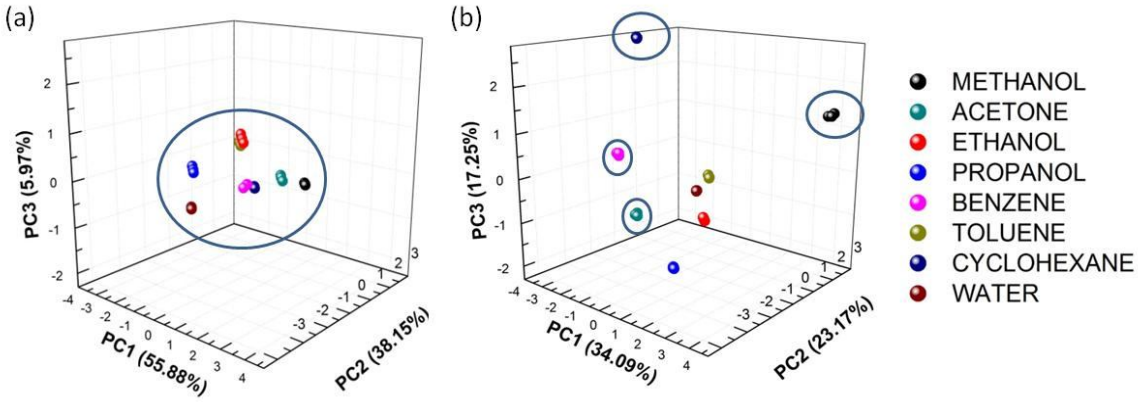

Figure 57 3D PCA mapping of (a) e-nose 1(sensor 1, 2, 3) (b) e-nose 2(sensor 1-13)

The quantitative demonstration of the improved efficiency of e-nose 2 compared to e-nose 1 is available from Table 14 and Table 15. For each VOC, one point corresponding to the average of three points (average maximum relative amplitude values of each of three cycles) is considered. The distance of each VOC point from all other VOC in the measured set is evaluated by equation 10.

The distance between two points is the length of the path connecting them. The shortest path distance is a straight line. In a 3 dimensional plane, the distance between points (x_1, y_1, z_1) and (x_2, y_2, z_2) is given by:

$$d = \sqrt{(x_2 - x_1)^2 + (y_2 - y)^2 + (z_2 - z)^2} \quad \text{..... (10)}$$

VOC	Methanol	Ethanol	Propanol	Acetone	Benzene	Toluene	Cyclohexane	Water
Methanol	0	2.62	3.73	2.675	2.94	2.81	2.307	3.78
Ethanol	2.62	0	1.92	2.05	1.469	2.47	1.199	2.139
Propanol	3.73	1.92	0	3.64	2.66	2.2	2.435	1.003
Acetone	2.67	2.05	3.64	0	1.13	4.17	1.28	3.31
Benzene	2.94	1.469	2.66	1.13	0	3.67	0.698	2.25
Toluene	2.81	2.47	2.2	4.17	3.67	0	3.1	2.92
Cyclohexane	2.307	1.199	2.435	1.28	0.698	3.1	0	2.144
Water	3.78	2.139	1.003	3.31	2.25	2.92	2.144	0

Table 14 3D distance between points corresponding to two VOC in e-nose 1

VOC	Methanol	Ethanol	Propanol	Acetone	Benzene	Toluene	Cyclohexane	Water
Methanol	0	4.97	6.529	6.01	6.707	6.4196	7.65	5.95
Ethanol	4.97	0	**1.617**	3.73	3.16	2.896	5.134	**1.795**
Propanol	6.529	**1.617**	0	4.166	3.41	3.19	5.66	2.177
Acetone	6.01	3.73	4.166	0	2.919	6.311	6.266	5.136
Benzene	6.707	3.16	3.41	2.919	0	4.469	3.58	3.47
Toluene	6.4196	2.896	3.19	6.311	4.469	0	4.297	**1.197**
Cyclohexane	7.65	5.134	5.66	6.266	3.58	4.297	0	4.186
Water	5.96	**1.795**	2.177	5.136	3.47	**1.197**	4.186	0

Table 15 3D distance between points corresponding to two VOC in e-nose 2

The shortest distance between points corresponding to methanol and benzene was 2.81 in e-nose1 whereas this same distance has been increased to 6.707 in e-nose 2. Therefore the efficiency of discrimination between methanol and benzene has increased by 138% in e-nose 2. Likewise the discrimination between any of two pairs of VOC has increased in e-nose 2 with only a few exceptions (ethanol/propanol, ethanol/water and toluene/water). Excepted for these three pair of VOC the discriminating efficiency of the e-nose 2 has undergone an overall improvement when compared to that of e-nose 1.

Therefore e-nose 2, constructed by the assembly of 13 sensors (fabricated during this research work), possess an appreciable ability of determination and discrimination of a set of lung cancer biomarker VOC unlike e-nose 1.

Moreover, there is sometimes a necessity to discriminate one particular VOC biomarker from a set of other VOC. In this case the use of complex e-nose 2 with a combination of 13 sensors may not be necessary. In fact, the integration of only one additional sensor with a high selectivity towards the targeted VOC into the sensor array comprising only the three basic

sensors (used as reference) can be quite efficient to discriminate the targeted VOC from the rest of others. An example of such e-nose prepared with this objective is provided in Figure 58.

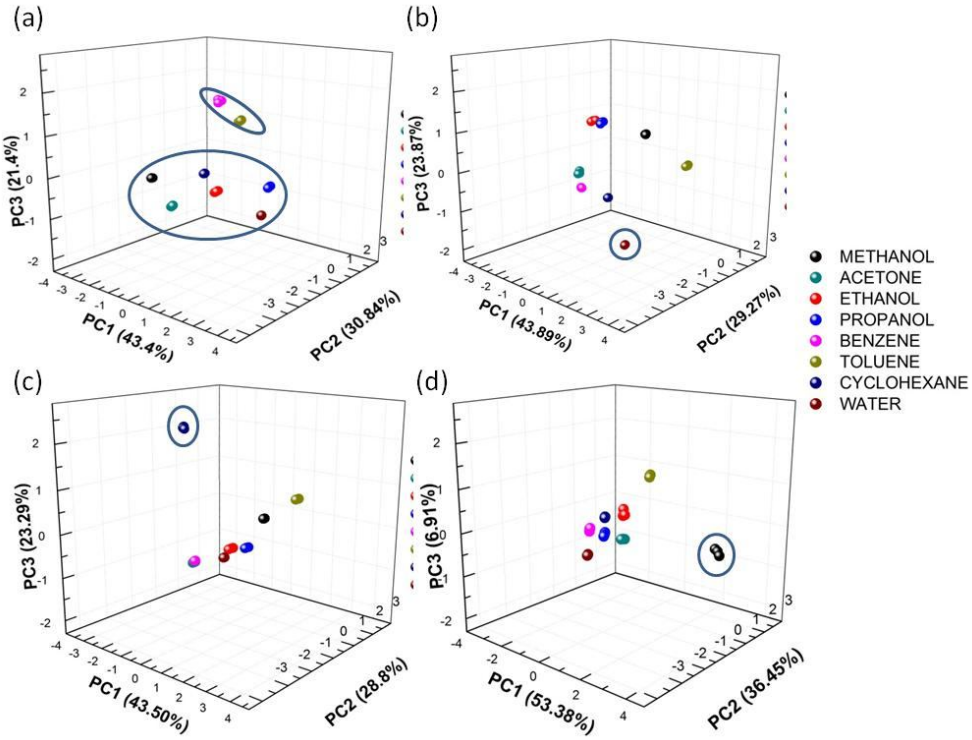

Figure 58 3D PCA mapping of (a) e-nose 3(sensor 1, 2, 3 and 6) (b) e-nose 4(sensor 1, 2, 3 and 7) (c) e-nose 5(sensor 1, 2, 3 and 10) (d) e-nose 6(sensor 1, 2, 3 and 13)

- *E-Nose 3 (sensors 1, 2, 3 and 6)*

The e-nose 3 is composed of a combination of four sensors. Keeping the same three sensors as in e-nose 1, one additional sensor i.e., sensor 6 (RGO@PBCD) is integrated in this e-nose 3. Comparing the 3D plot of PCA map for e-nose 1 (Figure 57 a) with that of e-nose 3 (Figure 58 a), it is clear that the insertion of sensor 6 has facilitated the benzene and toluene discrimination. Unlike e-nose 1 which shows a single cluster of all VOC, in e-nose 3, nonpolar aromatic hydrocarbons like benzene, toluene appears to be located in a separate cluster compared to all other VOC. The high selectivity of sensor 6 (RGO@PBCD) towards nonpolar aromatics (as shown in chapter 3) is responsible for this behaviour.

- *E-Nose 4 (sensors 1, 2, 3 and 7)*

Similarly, in e-nose 4 the fourth additional sensor is sensor 7 (RGO@PYAD-PEGCD). Comparing the 3D plot of PCA map for e-nose 1 (Figure 57 a) with that of e-nose 4 (Figure 58 b), it is evident that the insertion of sensor 7 has facilitated the discrimination of water vapour.

- *E-Nose 5 (sensors 1, 2, 3 and 10)*

Sensor 10 (C_{60}-g-CNT) is integrated in this e-nose 5 in addition to three basic sensors. The discrimination of the lung cancer biomarker cyclohexane is facilitated by the insertion of this cyclohexane selective sensor into the sensors array as observed in Figure 58 (c) unlike the reference e-nose 1 (Figure 57a).

- *E-Nose 6 (sensors 1,2,3 and 13)*

The additional fourth sensor in e-nose 6 is sensor 13 i.e., PEEK-S5/C_{60}-g-CNT, which possess a high affinity towards methanol. The insertion of sensor 13 has facilitated the discrimination of methanol from the rest of other VOC in the set as depicted in Figure 58 (d). Therefore this e-nose can act quite efficiently when methanol discrimination is required.

VI.4. Discrimination of pure and binary mixture of VOC by principle componenent analysis (PCA)

A multi component analysis has been carried out for the identification of individual VOC and their binary mixtures by the use of an e-nose (multi sensor array) and feature extraction of analytical information was done by PCA. PCA is regarded as a preprocessing algorithm that sometimes transforms the sensors output responses into a content of information more suitable for recognition [412], [413]. The set of methanol selective sensors elaborated in Table 11 of chapter V, were assembled in an array and integrated in an e-nose to evaluate their ability to discriminate both pure and binary mixtures of VOC. Since these sensors were mostly selective to methanol, experiments were carried out to check their ability to discriminate pure methanol from different binary mixtures each of which containing methanol as one of the two components. As pattern shown in Figure 59 (a) corresponds to the two first principal components (PC1, PC2) obtained by collection of maximum relative amplitudes of each sensor exposed to the set of vapours recorded during 3 cycles and converted into an *m* by *n* matrix accounting for 97.36 % of the total variance. The well discriminated nine clusters of points confirm that the e-nose system is efficient to discriminate both pure and binary mixtures of VOC.

Some studies based on principle component analysis of binary mixtures is already available from literature [414]. As studied by *Hsieh et al.,* Figure 59 (b) presents a principal components (PCA) plot derived from response data for three vapours obtained from the six polymer coated SAW sensor array. Individual vapour responses were generated experimentally and mixture

responses were synthesized by MONTE-CARLO simulation. The response vectors of vapour mixtures were synthesized from those of the component individual vapours under the assumption of additivity of responses, which has been verified for polymer-coated SAW sensors in several studies [401]. In this study by *Hsieh et al.*, the responses to individual vapours are linear and responses to mixtures of vapours are additive. The individual vapour response patterns appear unique enough to permit their recognition and discrimination relatively easily and the composite responses from the binary mixtures span the regions between those of the respective component vapours. *Severin et al.* also stated that, the swelling response of polymer coated SAW sensors to binary analyte mixtures is expected to be a weighted linear combination of the responses to the individual analytes in the vapour phase [415].

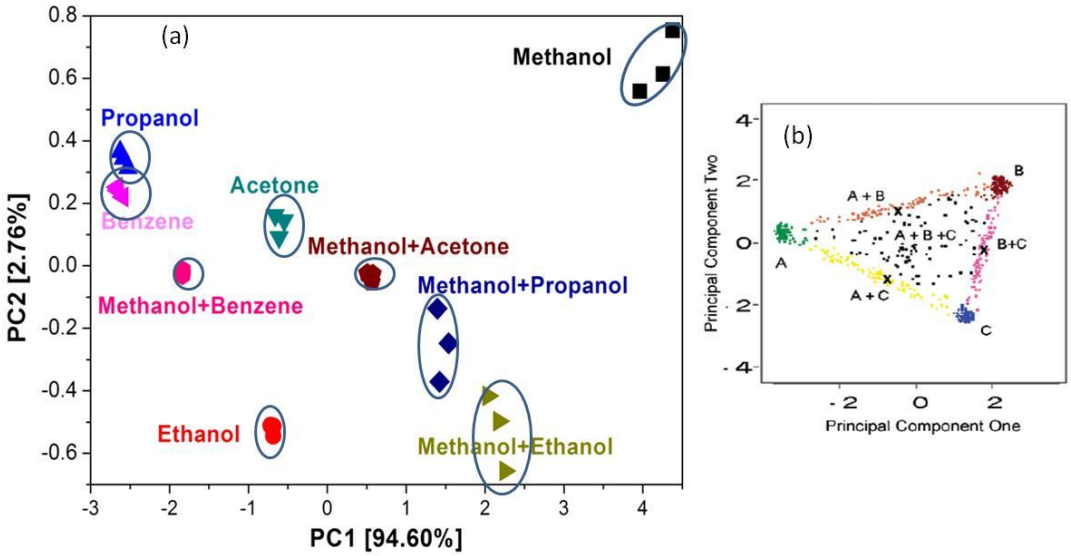

Figure 59 (a) 2D PCA curve for sulfonated PEEK nanocomposite based six sensors array (experimental) (b) Principal components plot of sensor array responses to three vapors A) toluene, B) hexane, C) 2-methoxyethanol and their binary and ternary mixtures where individual vapor responses were generated experimentally and mixture responses were synthesized by Monte Carlo simulation (from literature) [401]

However, the observation of our experimental results reveals that, the PCA clusters corresponding to any binary mixtures are situated in the space between that of the two components as depicted in Figure 59 (a), although not on a straight line like in the paper of *Hsieh et al.* [416]. Due to the limitations of our experimental device, it was not possible to change the mixing ratio of the two VOC of the mixture, to another value than that fixed by the division of the total vapour flow rate of $100cm^3.min^{-1}$ in two. Therefore, checking HSIEH's law would require adapting our device so that it will be possible to vary continuously the mixing ratio of each component. From this preliminary study on the sensing response of e-noses

towards binary mixtures, it was found that cluster points corresponding to binary mixtures are well discriminated from that of the pure VOC components. The position of binary mixtures appears to be intermediate to their pure components. Future perspective of the present work will concern the study of the evolution of the pattern of responses with changes of VOC mixture ratios, which will require more sophisticated equipment allowing to change the VOC ratio.

VI.5. Conclusion & future prospects

The development of conductive nanocomposite sensors for anticipated diagnosis of diseases like cancer was the objective of this thesis. Smart carbon nanomaterials, such as CNT or graphene were used as the basic material for chemo-resistive sensors' fabrication. Although pristine CNT/graphene is able to perform as chemo-resistive sensors, it possesses a low sensitivity and non-adjustable selectivity. Hence, covalent and non-covalent functionalizations of these carbon nanomaterials with various oligomeric, polymeric or inorganic molecules were done in order to tune the sensor's selectivity and sensitivity. Nanoswitching at the junctions of the percolated network formed by the carbon nanomaterials could be controlled by varying the organic functionality on the surface. Also the performance of smart chemo-resistive sensors could be controlled by various factors such as the architecture of the conductive network, the nature of interactions between polymer matrices and conductive nanofillers, solubility parameter, hydrogen bonding, hydrophilicity etc. Different strategies were undertaken for the functionalization of carbon nanomaterials in order to achieve a high sensitivity and adjustable selectivity to targeted VOC.

Functionalized cyclodextrin wrapped graphene sensors were designed successfully. In this novel work, tuneable organic functionality and host guest inclusion complex formation ability of cyclodextrin along with high surface area and electrical conductivity of graphene could be judicially exploited to fabricate a set of high performance sensors with tailorable selectivity. Perbenzylated cyclodextrin wrapped reduced graphene oxide sensors were found to show a higher affinity towards nonpolar aromatics whereas amino cyclodextrin wrapped reduced graphene oxide sensors could exhibit a higher affinity towards acetone due to potentially reversible imine bond formation between amino group and acetone. Thus, changing the organic functionality ofcyclodextrin made it possible to tune its selectivity towards the targeted VOC biomarkers. Additionally, the polymerized cyclodextrin wrapped reduced graphene oxide sensors were found to exhibit sensitivity several times larger towards polar

VOC than oligomeric cyclodextrin wrapped RGO sensors. However, short chain functionalized oligomeric cylodextrin wrapped RGO sensors were found effective to obtain different selectivity towards the targeted disease biomarker VOC.

The hybridization of more than one nanomaterial could also provide a path to alter the sensing performances of pristine carbon nanomaterials. Covalent or non-covalent functionalization of CNT by nanosized polyhedral oligomeric silsesquioxane was found to be a path to achieve an adjustable selectivity and enhanced sensitivity of chemo-resistors. Tuning the organic functionality of the POSS surface was found an effective factor to control the selectivity adjustment whereas the nanosized rigid cubic shaped POSS cage could positively influence the nanoswitching at junctions of CNT upon exposure to vapour molecules, resulting in a higher sensitivity. Iso octyl POSS grafted CNT was found to exhibit high selectivity towards nonpolar aliphatic hydrocarbons such as cyclohexane and n-pentane whereas trisilanol phenyl POSS/ CNT sensor showed a higher affinity towards acetone.

Moreover the grafting of spherical Buckminsterfullerene of high surface area and electronic mobility onto CNT/graphene was carried out in order to achieve a synergistic combination of properties in terms of sensing performances. An appreciable enhancement of the sensitivity of CNT/graphene based sensors was obtained from the grafting of Buckminsterfullerene at the junctions of the conductive network. Particularly it brought about a dramatic enhancement of their sensitivity to respectively cyclohexane and toluene keeping at the same time their ranking of selectivity unaltered.

A set of high performance methanol selective sensors based on sulfonated PEEK nanocomposites were fabricated and their degree of sulfonation was found to be a useful parameter controlling the sensitivity and selectivity of sensors. Either by increasing the degree of sulfonation of PEEK or by using hybrid nanofillers (Buckminsterfullerene grafted CNT), the sensitivity and selectivity to methanol of these conducting polymer nanocomposite (CPC) sensors could be tailored.

Finally it was possible to make a library with all the fabricated chemo-resistive sensors, made from functionalized CNT/graphene that were found highly selective towards the different targeted lung cancer biomarker VOC. These room temperature sensors were also found operative under ppm-ppb level of VOC, which is compulsory for the analysis of VOC biomarkers in human breath that are present at very low concentration.

By suitable combination of sensors from this library highly efficient e-noses were manufactured, which were able to discriminate a set of VOC lung cancer biomarkers from one

another. Moreover, some e-noses were found effective to discriminate one targeted VOC from a set of other VOC. It was also demonstrated that particular e-noses were suitable to discriminate pure and binary mixture of VOC. However due to limitations of the sensing device, only binary mixtures with identical proportions of two components could be compared to that of pure VOC components. In the PCA mapping the cluster of points corresponding to binary mixtures were found between those of the two pure components, although not exactly on a straight line and these points appeared to be well discriminated. More precise information about the sensing responses towards mixtures of VOC would possibly be extracted in future with a more sophisticated sensing equipment capable of creating binary, ternary or more complex mixture VOC with adjustable ratios of each component.

Thus, a more extensive study on sensory response towards different VOC mixtures comes under the future perspective of further research in this field. Additionally, the findings of this thesis are promising to switch to the next step, i.e., the confrontation of e-noses to real VOC biomarkers present in patients' breath in order to make an anticipated diagnosis of cancers. Real time monitoring of human breath extract by e-nose composed of chemo-resistive VOC sensors may emerge as a non-invasive and potentially inexpensive technique of early stage lung cancer detection in near future. This work also possesses a very high future prospect in other applications such as environmental monitoring and food degradation monitoring. Also comparison of the nature and concentration of VOC extract from healthy and diseased human skin may emerge as a non-invasive technique for detection of skin cancer melanoma in future.

LIST OF FIGURES

LIST OF TABLES

Reference

[1] C. L. Chaffer and R. A. Weinberg, “A perspective on cancer cell metastasis,” *Science.*, vol. 331, no. 6024, pp. 1559–1564, Mar. 2011.

[2] R. Siegel, D. Naishadham, and A. Jemal, “Cancer statistics,” *CA Cancer J Clin*, vol. 63, no. 1, pp. 11–30, 2013.

[3] J. Ferlay, E. Steliarova-Foucher, J. Lortet-Tieulent, S. Rosso, J. W. W. Coebergh, H. Comber, D. Forman, and F. Bray, “Cancer incidence and mortality patterns in Europe: estimates for 40 countries in 2012.,” *Eur. J. Cancer*, vol. 49, no. 6, pp. 1374–403, May 2013.

[4] G. Peng, M. Hakim, Y. Y. Broza, S. Billan, R. Abdah-Bortnyak, A. Kuten, U. Tisch, and H. Haick, “Detection of lung, breast, colorectal, and prostate cancers from exhaled breath using a single array of nanosensors.,” *Br. J. Cancer*, vol. 103, no. 4, pp. 542–551, Aug. 2010.

[5] M. Phillips, R. N. Cataneo, C. Saunders, P. Hope, P. Schmitt, and J. Wai, “Volatile biomarkers in the breath of women with breast cancer,” *J. Breath Res.*, vol. 4, no. 2, p. 026003, Jun. 2010.

[6] A. Jemal, F. Bray, and J. Ferlay, “Global cancer statistics,” *CA Cancer J Clin*, vol. 61, no. 2, pp. 69–90, 2011.

[7] Z. Altintas and I. Tothill, “Biomarkers and biosensors for the early diagnosis of lung cancer,” *Sensors Actuators B Chem.*, vol. 188, pp. 988–998, Nov. 2013.

[8] S. Sone, T. Nakayama, T. Honda, K. Tsushima, F. Li, M. Haniuda, Y. Takahashi, T. Suzuki, T. Yamanda, R. Kondo, T. Hanaoka, F. Takayama, K. Kubo, and H. Fushimi, “Long-term follow-up study of a population-based 1996-1998 mass screening programme for lung cancer using mobile low-dose spiral computed tomography,” *Lung cancer*, vol. 58, no. 3, pp. 329–41, Dec. 2007.

[9] D. Poli, P. Carbognani, M. Corradi, M. Goldoni, O. Acampa, B. Balbi, L. Bianchi, M. Rusca, and A. Mutti, “Exhaled volatile organic compounds in patients with non-small cell lung cancer: cross sectional and nested short-term follow-up study,” *Respir. Res.*, vol. 6, p. 71, Jan. 2005.

[10] H.-J. Sung and J.-Y. Cho, “Biomarkers for the lung cancer diagnosis and their advances in proteomics,” *BMB Rep.*, vol. 41, no. 9, pp. 615–25, Sep. 2008.

[11] Y.-E. Choi, J.-W. Kwak, and J. W. Park, “Nanotechnology for early cancer detection,” *Sensors*, vol. 10, no. 1, pp. 428–55, Jan. 2010.

[12] B. Bohunicky and S. A. Mousa, “Biosensors: the new wave in cancer diagnosis,” *Nanotechnol. Sci. Appl.*, vol. 4, pp. 1–10, Jan. 2010.

[13] G. Lollo, G. R. Rivera-Rodriguez, J. Bejaud, T. Montier, C. Passirani, J.-P. Benoit, M. García-Fuentes, M. J. Alonso, and D. Torres, “Polyglutamic acid-PEG nanocapsules as long circulating carriers for the delivery of docetaxel,” *Eur. J. Pharm. Biopharm.*, vol. 87, no. 1, pp. 47–54, May 2014.

[14] G. R. Rivera-Rodriguez, G. Lollo, T. Montier, J. P. Benoit, C. Passirani, M. J. Alonso, and D. Torres, “In vivo evaluation of poly-l-asparagine nanocapsules as carriers for anti-cancer drug delivery,” *Int. J. Pharm.*, vol. 458, no. 1, pp. 83–9, Dec. 2013.

[15] K. Hiroshi, H. Masaya, S. Nariyoshi, and M. Makoto, “Evaluation of volatile sulfur compounds in the expired alveolar gas in patients with liver cirrhosis,” *Clin. Chim. Acta*, vol. 85, no. 3, pp. 279–284, 1978.

[16] M. L. Simenhoff, J. F. Burke, J. J. Saukkonen, A. T. Ordinario, R. Doty, and S. Dunn, “Biochemical profile of uremic breath,” *N. Engl. J. Med.*, vol. 297, no. 3, pp. 132–135, 1977.

[17] S. Meinardi, K.-B. Jin, B. Barletta, D. R. Blake, and N. D. Vaziri, “Exhaled breath and fecal volatile organic biomarkers of chronic kidney disease.,” *Biochim. Biophys. Acta*, vol. 1830, no. 3, pp. 2531–7, Mar. 2013.

[18] C. Acevedo, E. Y. Sanchez, J. G. Reyes, and M. E. Young, “Volatile profiles of human skin cell cultures in different degrees of senescence,” *J. Chromatogr. B*, vol. 878, no. 3–4, pp. 449–455, Feb. 2010.

[19] C. Acevedo, E. Y. Sánchez, J. G. Reyes, and M. E. Young, “Volatile organic compounds produced by human skin cells,” *Biol. Res.*, vol. 40, no. 3, pp. 347–355, Jan. 2007.

[20] K. Nose, H. Ueda, T. Ohkuwa, T. Kondo, S. Araki, H. Ohtani, and T. Tsuda, “Identification and assessment of carbon monoxide in gas emanated from human skin,” *Chromatography*, vol. 27, no. 2, pp. 27–29, 2006.

[21] Y. Zilberman, U. Tisch, G. Shuster, W. Pisula, X. Feng, K. Müllen, and H. Haick, “Carbon nanotube/hexa-peri-hexabenzocoronene bilayers for discrimination between nonpolar volatile organic compounds of cancer and humid atmospheres,” *Adv. Mater.*, vol. 22, no. 38, pp. 4317–4320, 2010.

[22] B. Kumar, M. Castro, and J. F. Feller, “Quantum resistive vapour sensors made of polymer coated carbon nanotubes random networks for biomarkers detection,” *Chem. sensors*, vol. 3, no. 20, pp. 41–44, 2013.

[23] A. Mashir and R. A. Dweik, “Exhaled breath analysis: The new interface between medicine and engineering,” *Adv. Powder Technol.*, vol. 20, no. 5, pp. 420–425, Sep. 2009.

[24] R. Ionescu, Y. Broza, H. Shaltieli, D. Sadeh, Y. Zilberman, X. Feng, L. Glass-Marmor, I. Lejbkowicz, K. Müllen, A. Miller, and H. Haick, “Detection of multiple sclerosis from exhaled breath using bilayers of polycyclic aromatic hydrocarbons and single-wall carbon nanotubes,” *ACS Chem. Neurosci.*, vol. 2, no. 12, pp. 687–93, Dec. 2011.

[25] Z. . Xu, Y. Y. Broza, R. Ionsecu, U. Tisch, L. Ding, H. Liu, Q. Song, Y. Pan, F. . Xiong, K. . Gu, G. Sun, Z. . Chen, M. Leja, and H. Haick, “A nanomaterial-based breath test for distinguishing gastric cancer from benign gastric conditions,” *Br. J. Cancer*, vol. 108, no. 4, pp. 941–950, 2013.

[26] M. Santonico, G. Lucantoni, G. Pennazza, R. Capuano, G. Galluccio, C. Roscioni, G. La Delfa, D. Consoli, E. Martinelli, R. Paolesse, C. Di Natale, and A. D’Amico, “In situ detection of lung cancer volatile fingerprints using bronchoscopic air-sampling,” *Lung cancer*, vol. 77, no. 1, pp. 46–50, Jul. 2012.

[27] C. Turner, H. Knobloch, J. Richards, P. Richards, T. T. F. Mottram, D. Marlin, and M. A. Chambers, “Development of a device for sampling cattle breath,” *Biosyst. Eng.*, vol. 112, no. 2, pp. 75–81, Jun. 2012.

[28] M. Bruins, Z. Rahim, A. Bos, W. W. J. van de Sande, H. P. Endtz, and A. van Belkum, “Diagnosis of active tuberculosis by e-nose analysis of exhaled air,” *Tuberculosis*, vol. 93, no. 2, pp. 232–8, Mar. 2013.

[29] K. A. Wlodzimirow, A. Abu-Hanna, M. J. Schultz, M. A. W. Maas, L. D. J. Bos, P. J. Sterk, H. H. Knobel, R. J. T. Soers, and R. A. F. M. Chamuleau, “Exhaled breath analysis with electronic nose technology for detection of acute liver failure in rats,” *Biosens. Bioelectron.*, vol. 53, pp. 129–134, Sep. 2014.

[30] U. Tisch, I. Schlesinger, R. Ionescu, M. Nassar, N. Axelrod, D. Robertman, Y. Tessler, F. Azar, A. Marmur, J. Aharon-Peretz, and H. Haick, “Detection of Alzheimer’s and Parkinson's disease from exhaled breath using nanomaterial-based sensors,” *Nanomedicine*, vol. 8, no. 1, pp. 43–56, Jan. 2013.

[31] U. Tisch and H. Haick, “Chemical sensors for breath gas analysis: the latest developments at the Breath Analysis Summit 2013,” *J. Breath Res.*, vol. 8, no. 2, p. 27103, 2014.

[32] M. Strauch, A. Lüdke, D. Münch, T. Laudes, C. G. Galizia, E. Martinelli, L. Lavra, R. Paolesse, A. Ulivieri, A. Catini, R. Capuano, and C. Di Natale, “More than apples and oranges--detecting cancer with a fruit fly’s antenna,” *Sci. Rep.*, vol. 4, p. 3576, Jan. 2014.

[33] T. D. Gibson, O. Prosser, J. N. Hulbert, R. W. Marshall, P. Corcoran, P. Lowery, E. a. Ruck-Keene, and S. Heron, “Detection and simultaneous identification of microorganisms from headspace samples using an electronic nose.,” *Sensors Actuators B Chem.*, vol. 44, no. 1–3, pp. 413–422, Oct. 1997.

[34] M. E. Fleming-Jones and R. E. Smith, “Volatile organic compounds in foods: a five year study.,” *J. Agric. Food Chem.*, vol. 51, no. 27, pp. 8120–7, Dec. 2003.

[35] S. Ampuero and J. O. Bosset, “The electronic nose applied to dairy products: a review,” *Sensors Actuators B Chem.*, vol. 94, no. 1, pp. 1–12, Aug. 2003.

[36] M. Ghasemi-Varnamkhasti, S. S. Mohtasebi, M. Siadat, and S. Balasubramanian, “Meat quality assessment by electronic nose (machine olfaction technology).,” *Sensors*, vol. 9, no. 8, pp. 6058–83, Jan. 2009.

[37] J. A. Ragazzo-Sanchez, P. Chalier, D. Chevalier, and C. Ghommidh, “Electronic nose discrimination of aroma compounds in alcoholised solutions,” *Sensors Actuators B Chem.*, vol. 114, no. 2, pp. 665–673, Apr. 2006.

[38] T. Aguilera, J. Lozano, J. Paredes, F. J. Alvarez, and J. I. Suárez, “Electronic nose based on independent component analysis combined with partial least squares and artificial neural networks for wine prediction,” *Sensors*, vol. 12, no. 6, pp. 8055–72, Jan. 2012.

[39] C. K. Ho, A. Robinson, D. R. Miller, and M. J. Davis, “Overview of sensors and needs for environmental monitoring,” *Sensors*, vol. 5, no. 1, pp. 4–37, Feb. 2005.

[40] A. Lamagna, S. Reich, D. Rodríguez, A. Boselli, and D. Cicerone, “The use of an electronic nose to characterize emissions from a highly polluted river,” *Sensors Actuators B Chem.*, vol. 131, no. 1, pp. 121–124, Apr. 2008.

[41] S. Su, W. Wu, J. Gao, J. Lu, and C. Fan, “Nanomaterials-based sensors for applications in environmental monitoring,” *J. Mater. Chem.*, vol. 22, no. 35, pp. 18101–18110, 2012.

[42] E. H. M. Camara, P. Breuil, D. Briand, N. F. de Rooij, and C. Pijolat, “A micro gas preconcentrator with improved performance for pollution monitoring and explosives detection,” *Anal. Chim. Acta*, vol. 688, no. 2, pp. 175–82, Mar. 2011.

[43] C. Wongchoosuk, A. Wisitsoraat, A. Tuantranont, and T. Kerdcharoen, “Portable electronic nose based on carbon nanotube-SnO2 gas sensors and its application for detection of methanol contamination in whiskeys,” *Sensors Actuators B Chem.*, vol. 147, no. 2, pp. 392–399, Jun. 2010.

[44] Q. Liu, Q. Zhou, and G. Jiang, “Nanomaterials for analysis and monitoring of emerging chemical pollutants,” *Trends Anal. Chem.*, Apr. 2014.

[45] A. N. Mallya, R. Kottokkaran, and P. C. Ramamurthy, “Conducting polymer–carbon black nanocomposite sensor for volatile organic compounds and correlating sensor response by molecular dynamics,” *Sensors Actuators B Chem.*, vol. 201, pp. 308–320, Oct. 2014.

[46] P. K. Sekhar, E. L. Brosha, R. Mukundan, and F. H. Garzon, “Chemical sensors for environmental monitoring and homeland security,” *Electrochem. Soc. Interface*, vol. 19, no. 4, pp. 35–40, 2010.

[47] Z. Haddi, S. Mabrouk, M. Bougrini, K. Tahri, K. Sghaier, H. Barhoumi, N. El Bari, A. Maaref, N. Jaffrezic-Renault, and B. Bouchikhi, "E-Nose and e-Tongue combination for improved recognition of fruit juice samples," *Food Chem.*, vol. 150, pp. 246–253., Nov. 2013.

[48] T. Sobański, a. Szczurek, K. Nitsch, B. W. Licznerski, and W. Radwan, "Electronic nose applied to automotive fuel qualification," *Sensors Actuators B Chem.*, vol. 116, no. 1–2, pp. 207–212, Jul. 2006.

[49] A. R. V. Benvenho, R. W. C. Li, and J. Gruber, "Polymeric electronic gas sensor for determining alcohol content in automotive fuels," *Sensors Actuators B Chem.*, vol. 136, no. 1, pp. 173–176, Feb. 2009.

[50] B. Li, G. Sauvé, M. C. Iovu, M. Jeffries-El, R. Zhang, J. Cooper, S. Santhanam, L. Schultz, J. C. Revelli, A. G. Kusne, T. Kowalewski, J. L. Snyder, L. E. Weiss, G. K. Fedder, R. D. McCullough, and D. N. Lambeth, "Volatile organic compound detection using nanostructured copolymers.," *Nano Lett.*, vol. 6, no. 8, pp. 1598–602, Aug. 2006.

[51] R. Ermanok, O. Assad, K. Zigelboim, B. Wang, and H. Haick, "Discriminative power of chemically sensitive silicon nanowire field effect transistors to volatile organic compounds," *ACS Appl. Mater. Interfaces*, vol. 5, no. 21, pp. 11172–11183, Oct. 2013.

[52] S. J. Toal and W. C. Trogler, "Polymer sensors for nitroaromatic explosives detection," *J. Mater. Chem.*, vol. 16, no. 28, pp. 2871–2883, 2006.

[53] L. Pauling, a B. Robinson, R. Teranishi, and P. Cary, "Quantitative analysis of urine vapor and breath by gas-liquid partition chromatography.," *Proc. Natl. Acad. Sci. U. S. A.*, vol. 68, no. 10, pp. 2374–6, Oct. 1971.

[54] G. Pennazza, M. Santonico, and A. F. Agrò, "Narrowing the gap between breathprinting and disease diagnosis, a sensor perspective," *Sensors Actuators B Chem.*, vol. 179, pp. 270–275, Mar. 2013.

[55] A. Ulanowska, T. Ligor, M. Michel, N. Metody, and P. Lotnych, "Hyphenated and unconventional methods for searching volatile cancer biomarkers," *Ecol. Chem. Eng. S*, vol. 17, no. 1, pp. 87–100, 2010.

[56] A. Smolinska, A.-C. Hauschild, R. R. R. Fijten, J. W. Dallinga, J. Baumbach, and F. J. van Schooten, "Current breathomics—a review on data pre-processing techniques and machine learning in metabolomics breath analysis," *J. Breath Res.*, vol. 8, no. 2, p. 27105, 2014.

[57] Z.-M. Zhang, J.-J. Cai, G.-H. Ruan, and G.-K. Li, "The study of fingerprint characteristics of the emanations from human arm skin using the original sampling system by SPME-GC/MS," *J. Chromatogr. B,*, vol. 822, no. 1–2, pp. 244–52, Aug. 2005.

[58] J. Kwak, M. Gallagher, M. H. Ozdener, C. J. Wysocki, B. R. Goldsmith, A. Isamah, A. Faranda, S. S. Fakharzadeh, M. Herlyn, A. T. C. Johnson, and G. Preti, "Volatile biomarkers from human melanoma cells.," *J. Chromatogr. B. Analyt. Technol. Biomed. Life Sci.*, vol. 931, pp. 90–6, Jul. 2013.

[59] E. S. Greenberg, K. K. Chong, K. T. Huynh, R. Tanaka, and D. S. B. Hoon, "Epigenetic biomarkers in skin cancer," *Cancer Lett.*, vol. 342, pp. 170–177, Jan. 2012.

[60] Y. Y. Broza, R. Kremer, U. Tisch, A. Gevorkyan, A. Shiban, L. A. Best, and H. Haick, "A nanomaterial-based breath test for short-term follow-up after lung tumor resection," *Nanomedicine*, vol. 9, no. 1, pp. 15–21, Jan. 2013.

[61] J. Dummer, M. Storer, M. Swanney, M. McEwan, A. Scott-Thomas, S. Bhandari, S. Chambers, R. Dweik, and M. Epton, "Analysis of biogenic volatile organic compounds in human health and disease," *Trends Anal. Chem.*, vol. 30, no. 7, pp. 960–967, Jul. 2011.

[62] F. S. Cikach and R. A. Dweik, “Cardiovascular biomarkers in exhaled breath,” *Prog. Cardiovasc. Dis.*, vol. 55, no. 1, pp. 34–43, 2012.

[63] J. E. Szulejko, M. McCulloch, J. Jackson, D. L. McKee, J. C. Walker, and T. Solouki, “Evidence for cancer biomarkers in exhaled breath,” *IEEE Sens. J.*, vol. 10, no. 1, pp. 185–210, Jan. 2010.

[64] S. Rana, A. K. Singla, A. Bajaj, S. G. Elci, O. R. Miranda, R. Mout, and R. E. T. Al, “Array-based sensing of metastatic cells and tissues using,” *ACS Chem. Neurosci.*, no. 9, pp. 8233–8240, 2012.

[65] A. K. Pavlou, N. Magan, D. Sharp, J. Brown, H. Barr, and A. P. . Turner, “An intelligent rapid odour recognition model in discrimination of Helicobacter pylori and other gastroesophageal isolates in vitro.,” *Biosens. Bioelectron.*, vol. 15, no. 7–8, pp. 333–42, Oct. 2000.

[66] Y. Y. Broza, L. Zuri, and H. Haick, “Combined volatolomics for monitoring of human body chemistry,” *Sci. Rep.*, vol. 4, p. 4611, Jan. 2014.

[67] B. de Lacy Costello, A. Amann, H. Al-Kateb, C. Flynn, W. Filipiak, T. Khalid, D. Osborne, and N. M. Ratcliffe, “A review of the volatiles from the healthy human body,” *J. Breath Res.*, vol. 8, no. 1, p. 014001, Mar. 2014.

[68] W. Miekisch, J. K. Schubert, and G. F. E. Noeldge-Schomburg, “Diagnostic potential of breath analysis--focus on volatile organic compounds.,” *Clin. Chim. Acta.*, vol. 347, no. 1–2, pp. 25–39, Sep. 2004.

[69] W. Cheng and W. Lee, “Technology development in breath microanalysis for clinical diagnosis,” *J Lab Clin Med*, vol. 133, no. 3, pp. 218–228, 1999.

[70] C. Di Natale, A. Macagnano, E. Martinelli, R. Paolesse, G. D’Arcangelo, C. Roscioni, A. Finazzi-Agrò, and A. D’Amico, “Lung cancer identification by the analysis of breath by means of an array of non-selective gas sensors,” *Biosens. Bioelectron.*, vol. 18, no. 10, pp. 1209–1218, Sep. 2003.

[71] D. T. V Anh, W. Olthuis, P. Bergveld, and A. Van Den Berg, “A hydrogen peroxide sensor for exhaled breath measurement,” *Sensors Actuators B Chem.*, vol. 111–112, pp. 494–499, 2005.

[72] J. B. Yu, H. G. Byun, M. S. So, and J. S. Huh, “Analysis of diabetic patient’s breath with conducting polymer sensor array,” *Sensors Actuators B Chem.*, vol. 108, no. 1–2, pp. 305–308, Jul. 2005.

[73] X. Chen, Y. Wang, Y. Wang, Z. Hou, D. Xu, Z. Yang, and Y. Zhang, “A breath sensor using carbon nanotubes operated by field effects of polarization and ionization,” *Sensors Actuators A Phys.*, vol. 158, no. 2, pp. 328–334, Mar. 2010.

[74] M. D. Trotter, M. J. Sulway, and E. Trotter, “The rapid determination of acetone in breath and plasma,” *Clin. Chim. Acta*, vol. 35, no. 1, pp. 137–143, Nov. 1971.

[75] A. Manolls, “The diagnostic potential of breath analysis,” *Clin. Chem.*, vol. 29, no. 1, pp. 5–15, 1983.

[76] P. Mazzone, “Nanomedicine: Sniffing out lung cancer,” *Nat Nano*, vol. 4, no. 10, pp. 621–622, Oct. 2009.

[77] A. Damico, C. Dinatale, R. Paolesse, A. Macagnano, E. Martinelli, G. Pennazza, M. Santonico, M. Bernabei, C. Roscioni, and G. Galluccio, “Olfactory systems for medical applications,” *Sensors Actuators B Chem.*, vol. 130, no. 1, pp. 458–465, Mar. 2008.

[78] C. L. Silva, M. Passos, and J. S. Câmara, “Solid phase microextraction, mass spectrometry and metabolomic approaches for detection of potential urinary cancer biomarkers--a powerful strategy for breast cancer diagnosis,” *Talanta*, vol. 89, pp. 360–8, Jan. 2012.

[79] N. G. Hockstein, E. R. Thaler, D. Torigian, W. T. Miller, O. Deffenderfer, and C. W. Hanson, "Diagnosis of pneumonia with an electronic nose: correlation of vapor signature with chest computed tomography scan findings," *Laryngoscope*, vol. 114, no. 10, pp. 1701–1705, 2004.

[80] C. Deng, X. Zhang, and N. Li, "Investigation of volatile biomarkers in lung cancer blood using solid-phase microextraction and capillary gas chromatography-mass spectrometry," *J. Chromatogr. B,*, vol. 808, no. 2, pp. 269–77, Sep. 2004.

[81] F. L. Liu, P. Xiao, H. L. Fang, H. F. Dai, L. Qiao, and Y. H. Zhang, "Single-walled carbon nanotube-based biosensors for the detection of volatile organic compounds of lung cancer," *Phys. E Low-dimensional Syst. Nanostructures*, vol. 44, no. 2, pp. 367–372, Nov. 2011.

[82] H. J. O'Neill, S. N. Gordon, M. H. O'Neill, R. D. GIbbons, and J. P. Szldon, "A computerized in lung cancer technique for screening for the presence of breath biomarkers," *Clin. Chem.*, vol. 34, no. 8, pp. 1613–1618, 1988.

[83] S. M. Cho, Y. J. Kim, G. S. Heo, and S.-M. Shin, "Two-step preconcentration for analysis of exhaled gas of human breath with electronic nose," *Sensors Actuators B Chem.*, vol. 117, no. 1, pp. 50–57, Sep. 2006.

[84] H. Yu, L. Xu, and P. Wang, "Solid phase microextraction for analysis of alkanes and aromatic hydrocarbons in human breath," *J. Chromatogr. B*, vol. 826, no. 1–2, pp. 69–74, Nov. 2005.

[85] M. Hakim, Y. Y. Broza, O. Barash, N. Peled, M. Phillips, A. Amann, and H. Haick, "Volatile organic compounds of lung cancer and possible biochemical pathways," *Chem. Rev.*, vol. 112, no. 11, pp. 5949–66, Nov. 2012.

[86] S. M. Gordon, J. P. Szldon, B. K. Krotoszynski, R. D. Gibbons, and J. O. Neill, "Volatile organic compounds in exhaled air from patientswith lungcancer," *Clin. Chem*, vol. 1282, pp. 1278–1282, 1985.

[87] R. F. Machado, D. Laskowski, O. Deffenderfer, T. Burch, S. Zheng, P. J. Mazzone, T. Mekhail, C. Jennings, J. K. Stoller, J. Pyle, J. Duncan, R. A. Dweik, and S. C. Erzurum, "Detection of lung cancer by sensor array analyses of exhaled breath," *Am. J. Respir. Crit. Care Med.*, vol. 171, no. 11, pp. 1286–91, Jun. 2005.

[88] J. Luo, J. Luo, L. Wang, X. Shi, J. Yin, E. Crew, S. Lu, L. M. Lesperance, and C.-J. Zhong, "Nanoparticle-structured thin film sensor arrays for breath sensing," *Sensors Actuators B Chem.*, vol. 161, no. 1, pp. 845–854, Jan. 2012.

[89] N. Teshima, J. Li, K. Toda, and P. K. Dasgupta, "Determination of acetone in breath," *Anal. Chim. Acta*, vol. 535, no. 1–2, pp. 189–199, Apr. 2005.

[90] M. Phillips, K. Gleeson, J. M. B. Hughes, J. Greenberg, R. N. Cataneo, and L. Baker, "Volatile organic compounds in breath as markers of lung cancer : a cross-sectional study," *Lancet*, vol. 353, pp. 1930–1933, 1999.

[91] X. Chen, F. Xu, Y. Wang, Y. Pan, D. Lu, P. Wang, K. Ying, E. Chen, and W. Zhang, "A study of the volatile organic compounds exhaled by lung cancer cells in vitro for breath diagnosis," *Cancer*, vol. 110, no. 4, pp. 835–44, Aug. 2007.

[92] M. Phillips, R. N. Cataneo, B. A. Ditkoff, P. Fisher, J. Greenberg, R. Gunawardena, C. S. Kwon, F. Rahbari-Oskoui, and C. Wong, "Volatile markers of breast cancer in the breath," *Breast J.*, vol. 9, no. 3, pp. 184–91, 2003.

[93] P. Spanel, D. Smith, T. A. Holland, W. Al Singary, and J. B. Elder, "Analysis of formaldehyde in the headspace of urine from bladder and prostate cancer patients using selected ion flow tube mass spectrometry," *Rapid Commun. Mass Spectrom.*, vol. 13, no. 14, pp. 1354–9, Jan. 1999.

[94] M. Hakim, Y. Y. Broza, O. Barash, N. Peled, M. Phillips, A. Amann, and H. Haick, "volatile organic compounds of lung cancer and possible biochemical pathways," *Chem. Rev.*, vol. 112, no. 11, pp. 5949–5966, Sep. 2012.

[95] P. R. Galassetti, B. Novak, D. Nemet, C. Rose-Gottron, D. M. Cooper, S. Meinardi, R. Newcomb, F. Zaldivar, and D. R. Blake, "Breath ethanol and acetone as indicators of serum glucose levels: an initial report.," *Diabetes Technol. Ther.*, vol. 7, no. 1, pp. 115–23, Feb. 2005.

[96] M. Fleischer, E. Simon, E. Rumpel, H. Ulmer, M. Harbeck, M. Wandel, C. Fietzek, U. Weimar, and H. Meixner, "Detection of volatile compounds correlated to human diseases through breath analysis with chemical sensors," *Sensors Actuators B Chem.*, vol. 83, no. 1–3, pp. 245–249, Mar. 2002.

[97] S. Dragonieri, M. P. van der Schee, T. Massaro, N. Schiavulli, P. Brinkman, A. Pinca, P. Carratú, A. Spanevello, O. Resta, M. Musti, and P. J. Sterk, "An electronic nose distinguishes exhaled breath of patients with Malignant Pleural Mesothelioma from controls.," *Lung cancer*, vol. 75, no. 3, pp. 326–31, Mar. 2012.

[98] E. Hietanen, H. Bartsch, J. C. Bériziat, A. M. Camus, S. McClinton, O. Eremin, L. Davidson, and P. Boyle, "Diet and oxidative stress in breast, colon and prostate cancer patients: a case-control study.," *Eur. J. Clin. Nutr.*, vol. 48, no. 8, pp. 575–586, Aug. 1994.

[99] A. Baranska, E. Tigchelaar, A. Smolinska, J. W. Dallinga, E. J. C. Moonen, J. M. Dekens, C. Wijmenga, A. Zhernakova, and F. J. van Schooten, "Profile of volatile organic compounds in exhaled breath changes as a result of gluten-free diet," *J. Breath Res.*, vol. 7, no. 3, p. 037104, Sep. 2013.

[100] A. Bajtarevic, C. Ager, M. Pienz, M. Klieber, K. Schwarz, M. Ligor, T. Ligor, W. Filipiak, H. Denz, M. Fiegl, W. Hilbe, W. Weiss, P. Lukas, H. Jamnig, M. Hackl, A. Haidenberger, B. Buszewski, W. Miekisch, J. Schubert, and A. Amann, "Noninvasive detection of lung cancer by analysis of exhaled breath," *BMC Cancer*, vol. 9, p. 348, Jan. 2009.

[101] K.-H. Kim, S. A. Jahan, and E. Kabir, "A review of breath analysis for diagnosis of human health," *Trends Anal. Chem.*, vol. 33, pp. 1–8, Mar. 2012.

[102] N. S. Ramgir, "Electronic nose based on nanomaterials : issues , challenges , and prospects," *ISRN Nanomater.*, vol. 2013, pp. 1–22, 2013.

[103] L. Buck and R. Axel, "A novel multigene family may encode odorant receptors: a molecular basis for odor recognition," *Cell*, vol. 65, no. 1, pp. 175–87, Apr. 1991.

[104] K. Arshak, E. Moore, G. M. Lyons, J. Harris, and S. Clifford, "A review of gas sensors employed in electronic nose applications," *Sens. Rev.*, vol. 24, no. 2, pp. 181–198, 2004.

[105] A. D. Wilson and M. Baietto, "Applications and advances in electronic-nose technologies," *Sensors*, vol. 9, no. 7, pp. 5099–148, Jan. 2009.

[106] D. V Russo, M. J. Burek, R. M. Iutzi, J. A. Mracek, and T. Hesjedal, "Development of an electronic nose sensing platform for undergraduate education in nanotechnology," *Eur. J. Phys.*, vol. 32, no. 3, p. 675, 2011.

[107] M. C. Burl, B. J. Doleman, A. Schaffer, and N. S. Lewis, "Assessing the ability to predict human percepts of odor quality from the detector responses of a conducting polymer composite-based electronic nose," *Sensors Actuators B Chem.*, vol. 72, no. 2, pp. 149–159, Jan. 2001.

[108] H.T.Nagle, R.G.Osuna, and S.S.Schiffman, "The How and Why of Electronic Noses," *IEEE Spectr.*, vol. 35, no. 9, pp. 22–31., 1998.

[109] Z. Zheng and X. Lin, "Study on application of medical diagnosis by electronic nose," *World Sci. Technol.*, vol. 14, no. 6, pp. 2115–2119, Dec. 2012.

[110] T. C. Pearce, S. S. Schiffman, H. T. Nagle, and J. W. Gardner, *Handbook of Machine Olfaction: Electronic Nose Technology*. Wiley, 2006.

[111] H. V Shurmer and J. W. Gardner, "Odour discrimination with an electronic nose," *Sensors Actuators B Chem.*, vol. 8, no. 1, pp. 1–11, 1992.

[112] K. Persaud and G. Dodd, "Analysis of discrimination mechanisms in the mammalian olfactory system using a model nose," *Nature*, vol. 299, no. 5881, pp. 352–355, Sep. 1982.

[113] J. W. Gardner, H. W. Shin, and E. L. Hines, "An electronic nose system to diagnose illness," *Sensors Actuators B Chem.*, vol. 70, no. 1–3, pp. 19–24, Nov. 2000.

[114] J. W. Gardner and P. N. Bartlett, "Electronic noses. principles and applications," *Meas. Sci. Technol.*, vol. 11, no. 7, p. 1087, 2000.

[115] G. Harsanyi, "Tutorial polymer films in sensor applications : a review of present uses and future possibilities," *Sens. Rev.*, vol. 20, no. 2, pp. 98–105, 2000.

[116] A. Folinsky, "Lung cancer detection using an electronic nose," 2005.

[117] G. Konvalina and H. Haick, "Sensors for breath testing: from nanomaterials to comprehensive disease detection," *Acc. Chem. Res.*, vol. 47, no. 1, pp. 66–76, Jan. 2014.

[118] V. E. Bochenkov and G. B. Sergeev, "sensitivity , selectivity , and stability of gas-sensitive metal-oxide nanostructures," in *Metal Oxide Nanostructures and Their Applications*, vol. 3, 2010, pp. 31–52.

[119] R. D. S. Yadava and R. Chaudhary, "Solvation, transduction and independent component analysis for pattern recognition in SAW electronic nose," *Sensors Actuators B Chem.*, vol. 113, no. 1, pp. 1–21, Jan. 2006.

[120] W. a Groves, E. T. Zellers, and G. C. Frye, "Analyzing organic vapors in exhaled breath using a surface acoustic wave sensor array with preconcentration: Selection and characterization of the preconcentrator adsorbent," *Anal. Chim. Acta*, vol. 371, no. 2–3, pp. 131–143, Oct. 1998.

[121] A. D'Amico, C. Di Natale, A. Macagnano, F. Davide, A. Mantini, E. Tarizzo, R. Paolesse, and T. Boschi, "Technologies and tools for mimicking olfaction: status of the Rome 'Tor Vergata' electronic nose," *Biosens. Bioelectron.*, vol. 13, no. 6, pp. 711–21, Sep. 1998.

[122] K. J. Albert, N. S. Lewis, C. L. Schauer, G. A. Sotzing, S. E. Stitzel, T. P. Vaid, and D. R. Walt, "Cross-reactive chemical sensor arrays," *Chem. Rev.*, vol. 100, no. 7, pp. 2595–626, Jul. 2000.

[123] N. Bachar, L. Mintz, Y. Zilberman, R. Ionescu, X. Feng, K. Müllen, and H. Haick, "Polycyclic aromatic hydrocarbon for the detection of nonpolar analytes under counteracting humidity conditions," *ACS Appl. Mater. Interfaces*, vol. 4, no. 9, pp. 4960–5, Sep. 2012.

[124] C. Yao, L. Qu, and W. Fu, "Detection of fibrinogen and coagulation factor VIII in plasma by a quartz crystal microbalance biosensor," *Sensors*, vol. 13, no. 6, pp. 6946–56, Jan. 2013.

[125] M. M. Ayad, N. Salahuddin, and I. M. Minisy, "Detection of some volatile organic compounds with chitosan-coated quartz crystal microbalance," *Des. Monomers Polym.*, pp. 1–8, May 2014.

[126] B. Wang and H. Haick, "Effect of chain length on the sensing of volatile organic compounds by means of silicon nanowires," *ACS Appl. Mater. Interfaces*, vol. 5, no. 12, pp. 5748–56, Jun. 2013.

[127] A. T. C. Johnson, S. M. Khamis, G. Preti, J. Kwak, and A. Gelperin, "DNA-coated nanosensors for breath analysis," *IEEE Sens. J.*, vol. 10, no. 1, pp. 159–166, Jan. 2010.

[128] Y.-L. Zhao, L. Hu, J. F. Stoddart, and G. Grüner, "Pyrenecyclodextrin-decorated single-walled carbon nanotube field-effect transistors as chemical sensors," *Adv. Mater.*, vol. 20, no. 10, pp. 1910–1915, May 2008.

[129] M. S. Martínez-García, F. Simancas, A. J. Palma, A. M. Lallena, J. Banqueri, and M. A. Carvajal, "General purpose MOSFETs for the dosimetry of electron beams used in intra-operative radiotherapy," *Sensors Actuators A Phys.*, vol. 210, pp. 175–181, Apr. 2014.

[130] D. W. Chang, E. K. Lee, E. Y. Park, H. Yu, H. J. Choi, I. Y. Jeon, G. J. Sohn, D. Shin, N. Park, J. H. Oh, L. Dai, and J. B. Baek, "Nitrogen-doped graphene nanoplatelets from simple solution edge-functionalization for n-type field-effect transistors.," *J. Am. Chem. Soc.*, vol. 135, no. 24, pp. 8981–8, Jun. 2013.

[131] T. Alizadeh, "Chemiresistor sensors array optimization by using the method of coupled statistical techniques and its application as an electronic nose for some organic vapors recognition," *Sensors Actuators B Chem.*, vol. 143, no. 2, pp. 740–749, Jan. 2010.

[132] A. A. Khan, U. Baig, and M. Khalid, "Electrically conductive polyaniline-titanium(IV)molybdophosphate cation exchange nanocomposite: Synthesis, characterization and alcohol vapour sensing properties," *J. Ind. Eng. Chem.*, vol. 19, no. 4, pp. 1226–1233, Jul. 2013.

[133] T. T. Tung, M. Castro, I. Pillin, T. Y. Kim, K. S. Suh, and J. F. Feller, "Graphene - Fe3O4/PIL – PEDOT for the design of sensitive and stable quantum chemo-resistive VOC sensors," *Carbon N. Y.*, vol. 74, pp. 104–112, Mar. 2014.

[134] M. De Wit, E. Vanneste, H. J. Geise, and L. J. Nagels, "Chemiresistive sensors of electrically conducting poly(2,5-thienylene vinylene) and copolymers: their responses to nine organic vapours," *Sensors Actuators B Chem.*, vol. 50, no. 2, pp. 164–172, Jul. 1998.

[135] D. Huo, Y. Xu, C. Hou, M. Yang, and H. Fa, "A novel optical chemical sensor based aunr-mtpp and dyes for lung cancer biomarkers in exhaled breath identification," *Sensors Actuators B Chem.*, Apr. 2014.

[136] W. Miekisch, P. Fuchs, S. Kamysek, C. Neumann, and J. K. Schubert, "Assessment of propofol concentrations in human breath and blood by means of HS-SPME-GC-MS.," *Clin. Chim. Acta.*, vol. 395, no. 1–2, pp. 32–7, Sep. 2008.

[137] N. Peled, R. Ionescu, P. Nol, O. Barash, M. McCollum, K. VerCauteren, M. Koslow, R. Stahl, J. Rhyan, and H. Haick, "Detection of volatile organic compounds in cattle naturally infected with Mycobacterium bovis," *Sensors Actuators B Chem.*, vol. 171–172, pp. 588–594, Aug. 2012.

[138] D. Smith, T. Wang, J. Sulé-Suso, P. Spanel, and A. El Haj, "Quantification of acetaldehyde released by lung cancer cells in vitro using selected ion flow tube mass spectrometry," *Rapid Commun. Mass Spectrom.*, vol. 17, no. 8, pp. 845–50, Jan. 2003.

[139] R. Afrin, N. A. Shah, M. Abbas, M. Amin, and A. S. Bhatti, "Design and analysis of functional multiwalled carbon nanotubes for infrared sensors," *Sensors Actuators A Phys.*, vol. 203, pp. 142–148, Dec. 2013.

[140] J. Im, S. K. Sengupta, M. F. Baruch, C. D. Granz, S. Ammu, S. K. Manohar, and J. E. Whitten, "A hybrid chemiresistive sensor system for the detection of organic vapors," *Sensors Actuators B Chem.*, vol. 156, no. 2, pp. 715–722, Aug. 2011.

[141] O. Barash, N. Peled, U. Tisch, P. A. Bunn, F. R. Hirsch, and H. Haick, "Classification of lung cancer histology by gold nanoparticle sensors," *Nanomedicine*, vol. 8, no. 5, pp. 580–9, Jul. 2012.

[142] A. D. Wilson, "Review of electronic-nose technologies and algorithms to detect hazardous chemicals in the environment," *Procedia Technol.*, vol. 1, pp. 453–463, Jan. 2012.

[143] F. Röck, N. Barsan, and U. Weimar, "Electronic nose: current status and future trends," *Chem. Rev.*, vol. 108, no. 2, pp. 705–25, Feb. 2008.

[144] E. H. Oh, H. S. Song, and T. H. Park, "Recent advances in electronic and bioelectronic noses and their biomedical applications.," *Enzyme Microb. Technol.*, vol. 48, no. 6–7, pp. 427–37, May 2011.

[145] L. Pascual, I. Campos, R. Bataller, C. Olguín, E. García-Breijo, R. Martínez-Mañez, and J. Soto, "A 'humid electronic nose' for the detection of nerve agent mimics; a case of selective sensing of DCNP (a Tabun mimic)," *Sensors Actuators B Chem.*, Oct. 2013.

[146] C. Olguín, N. Laguarda-Miró, L. Pascual, E. García-Breijo, R. Martínez-Mañez, and J. Soto, "An Electronic Nose for the detection of Sarin, Soman and Tabun mimics and interfering agents," *Sensors Actuators B Chem.*, vol. 202, pp. 31–37, May 2014.

[147] C. Di Natale, R. Paolesse, E. Martinelli, and R. Capuano, "Solid-state gas sensors for breath analysis: A review," *Anal. Chim. Acta*, vol. 824, pp. 1–17, May 2014.

[148] M. L. Ebruna, C. B. Illotb, H. H. Arrakc, and G. S. Elfa, "The electronic nose : a fast and efficient tool for characterizing dates," *Fruits*, vol. 62, no. 6, pp. 377–382, 2007.

[149] R. Langer and D. A. Tirrell, "Designing materials for biology and medicine," *Nature*, vol. 428, no. 6982, pp. 487–492, Apr. 2004.

[150] M. Yoshida and J. Lahann, "Smart nanomaterials," *ACS Nano*, vol. 2, no. 6, pp. 1101–1107, Jun. 2008.

[151] A. Hulanicki, S. Geab, and F. Ingman, "Chemical sensors definitions and classification," *Pure App. Chem.*, vol. 63, no. 9, pp. 1247–1250, 1991.

[152] A. K. Wanekaya, M. Uematsu, M. Breimer, and O. A. Sadik, "Multicomponent analysis of alcohol vapors using integrated gas chromatography with sensor arrays," *Sensors Actuators B Chem.*, vol. 110, no. 1, pp. 41–48, Sep. 2005.

[153] G. S. Wilson, Y. Zhang, G. Reach, D. Moatti-Sirat, V. Poitout, D. R. Thévenot, F. Lemonnier, and J. C. Klein, "Progress toward the development of an implantable sensor for glucose," *Clin. Chem.*, vol. 38, no. 9, pp. 1613–7, Sep. 1992.

[154] J. Janata, "Chemical sensors," *Anal. Chem.*, vol. 64, no. 12, pp. 196–219, Jun. 1992.

[155] J. W. Grate, "Hydrogen-bond acidic polymers for chemical vapor sensing," *Chem. Rev.*, vol. 108, no. 2, pp. 726–45, Mar. 2008.

[156] S. K. Mishra, S. N. Tripathi, V. Choudhary, and B. D. Gupta, "SPR based fiber optic ammonia gas sensor utilizing nanocomposite film of pmma/reduced graphene oxide prepared by in situ polymerization," *Sensors Actuators B Chem.*, vol. 199, pp. 190–200, Apr. 2014.

[157] M. Batumalay, Z. Harith, H. Rafaie, F. Ahmad, M. Khasanah, S. W. Harun, R. M. Nor, and H. Ahmad, "Tapered plastic optical fiber coated with ZnO nanostructures for the measurement of uric acid concentrations and changes in relative humidity," *Sensors Actuators A Phys.*, vol. 210, pp. 190–196, Apr. 2014.

[158] N. a Rakow and K. S. Suslick, “A colorimetric sensor array for odour visualization,” *Nature*, vol. 406, no. 6797, pp. 710–3, Aug. 2000.

[159] E. Stussi, R. Stella, and D. De Rossi, “Chemoresistive conducting polymer-based odour sensors: influence of thickness changes on their sensing properties,” *Sensors Actuators B Chem.*, vol. 43, no. 1–3, pp. 180–185, Sep. 1997.

[160] J. F. Feller, B. Kumar, and M. Castro, “Conductive biopolymer nanocomposites for sensors,” in *Nanocomposites with Biodegradable Polymers Synthesis, Properties, and Future Perspectives*, 2010, pp. 368–399.

[161] J. F. Feller, M. Castro, and B. Kumar, “Polymer–carbon nanotube conductive nanocomposites for sensing,” in *Polymer carbon nanotube composites: Preparation, properties and applications*, 2011, pp. 760–803.

[162] N. Barsan and U. Weimar, “Fundamentals of metal oxide gas sensors,” in *IMCS 2012-The 14th International Meeting on Chemical Sensors*, 2012, pp. 618–621.

[163] M. E. Franke, T. J. Koplin, and U. Simon, “Metal and metal oxide nanoparticles in chemiresistors: does the nanoscale matter?,” *Small*, vol. 2, no. 1, pp. 36–50, Jan. 2006.

[164] J. Luo, S. Y. Ma, F. M. Li, X. B. Li, W. Q. Li, L. Cheng, Y. Z. Mao, and D. J. Gz, “The mesoscopic structure of flower-like ZnO nanorods for acetone detection,” *Mater. Lett.*, vol. 121, pp. 137–140, Apr. 2014.

[165] A. Berna, “Metal oxide sensors for electronic noses and their application to food analysis,” *Sensors*, vol. 10, no. 4, pp. 3882–910, Jan. 2010.

[166] V. S. Vaishanv, P. D. Patel, and N. G. Patel, “Indium tin oxide thin-film sensor for detection of volatile organic compounds (VOCs),” *Mater. Manuf. Process.*, vol. 21, no. 3, pp. 257–261, May 2006.

[167] Z. Wang and X. Hu, “Fabrication and electrochromic properties of spin-coated TiO 2 thin films from peroxo-polytitanic acid,” *Thin Solid Films*, vol. 352, pp. 62–65, 1999.

[168] B. Geng, C. Fang, F. Zhan, and N. Yu, “Synthesis of polyhedral znsno3 microcrystals with controlled exposed facets and their selective gas-sensing properties,” *small*, vol. 4, pp. 1337–1343, 2008.

[169] G. F. Fine, L. M. Cavanagh, A. Afonja, and R. Binions, “Metal oxide semi-conductor gas sensors in environmental monitoring.,” *Sensors*, vol. 10, no. 6, pp. 5469–502, Jan. 2010.

[170] M. M. Arafat, B. Dinan, S. A. Akbar, and A. S. M. A. Haseeb, “Gas sensors based on one dimensional nanostructured metal-oxides: a review,” *Sensors*, vol. 12, no. 6, pp. 7207–58, Jan. 2012.

[171] H. Bai and G. Shi, “Gas sensors based on conducting polymers,” *Sensors*, vol. 7, no. 3, pp. 267–307, Mar. 2007.

[172] A. Choudhury, “Chemical Polyaniline / silver nanocomposites : Dielectric properties and ethanol vapour sensitivity,” *Sensors Actuators B Chem.*, vol. 138, pp. 318–325, 2009.

[173] L. Dai, P. Soundarrajan, and T. Kim, “Sensors and sensor arrays based on conjugated polymers and carbon nanotubes,” *Pure Appl. Chem.*, vol. 74, no. 9, pp. 1753–1772, 2002.

[174] Y. Dan, Y. Cao, T. E. Mallouk, S. Evoy, and A. T. C. Johnson, “Gas sensing properties of single conducting polymer nanowires and the effect of temperature,” *Nanotechnology*, vol. 20, no. 43, p. 434014, Oct. 2009.

[175] M. Ates, “A review study of (bio)sensor systems based on conducting polymers,” *Mater. Sci. Eng. C*, vol. 33, no. 4, pp. 1853–9, May 2013.

[176] T. Hibbard, K. Crowley, and A. J. Killard, “Direct measurement of ammonia in simulated human breath using an inkjet-printed polyaniline nanoparticle sensor.,” *Anal. Chim. Acta*, vol. 779, pp. 56–63, May 2013.

[177] K. Potje-kamloth, “Chemical gas sensors based on organic semiconductor polypyrrole,” *Crit. Rev. Anal. Chem.*, vol. 32, no. 2, pp. 121–140, 2002.

[178] N. Strand, A. Bhushan, M. Schivo, N. J. Kenyon, and C. E. Davis, “Chemically polymerized polypyrrole for on-chip concentration of volatile breath metabolites,” *Sens. Actuators. B. Chem.*, vol. 143, no. 2, pp. 516–523, Jan. 2010.

[179] H. R. Hwang, J. G. Roh, D. D. Lee, J. O. Lim, and J. S. Huh, “Sensing behavior of the polypyrrole and polyaniline sensor for several volatile organic compounds,” *Met. Mater. Int.*, vol. 9, no. 3, pp. 287–291, Jun. 2003.

[180] S. Selvakumar, N. Somanathan, and K. A. Reddy, “Chemiresistor sensors based on conducting polymers for hypergolic propellants and acidic vapors of rocket exhaust plumes - a review,” *Propellants, Explos. Pyrotech.*, vol. 38, no. 2, pp. 176–189, Apr. 2013.

[181] S. E. Zohora and N. Hundewale, “Chemical sensors employed in electronic noses : A Review,” *Int. J. Soft Comput. Eng.*, vol. 3, no. 2, pp. 405–408, 2013.

[182] A. A. Athawale, S. V Bhagwat, and P. P. Katre, “Nanocomposite of Pd – polyaniline as a selective methanol sensor,” *Sensors And Actuators*, vol. 114, no. October 2004, pp. 263–267, 2006.

[183] J. Janata and M. Josowicz, “Conducting polymers in electronic chemical sensors,” *Nat. Mater.*, vol. 2, no. 1, pp. 19–24, Jan. 2003.

[184] B. K. Kuila and M. Stamm, “Transparent, versatile chemical vapor sensor using supramolecular assembly of block copolymer and carbon nanotubes.,” *Macromol. Rapid Commun.*, vol. 31, no. 21, pp. 1881–5, Nov. 2010.

[185] Y.-Z. Long, M.-M. Li, C. Gu, M. Wan, J.-L. Duvail, Z. Liu, and Z. Fan, “Recent advances in synthesis, physical properties and applications of conducting polymer nanotubes and nanofibers,” *Prog. Polym. Sci.*, vol. 36, no. 10, pp. 1415–1442, Oct. 2011.

[186] K. Hosono, I. Matsubara, N. Murayama, W. Shin, and N. Izu, “The sensitivity of 4-ethylbenzenesulfonic acid-doped plasma polymerized polypyrrole films to volatile organic compounds,” *Thin Solid Films*, vol. 484, no. 1–2, pp. 396–399, Jul. 2005.

[187] C.-B. Lim, J.-B. Yu, D.-Y. Kim, H.-G. Byun, D.-D. Lee, and J.-S. Huh, “Sensing characteristics of nano-network structure of polypyrrole for volatile organic compounds (VOCs) gases,” in *IEEE Sensors*, 2006, pp. 695–698.

[188] N. Hu, Y. Karube, C. Yan, Z. Masuda, and H. Fukunaga, “Tunneling effect in a polymer/carbon nanotube nanocomposite strain sensor,” *Acta Mater.*, vol. 56, no. 13, pp. 2929–2936, Aug. 2008.

[189] M. K. Njuguna, C. Yan, N. Hu, J. M. Bell, and P. K. D. V Yarlagadda, “Sandwiched carbon nanotube film as strain sensor,” *Compos. Part B J.*, vol. 43, pp. 2711–2717, 2012.

[190] S. Wen and D. D. L. Chung, “Carbon fiber-reinforced cement as a strain-sensing coating,” *Cem. Concr. Res.*, vol. 31, no. 4, pp. 665–667, Apr. 2001.

[191] J. Zhang, J. Liu, R. Zhuang, E. Mäder, G. Heinrich, and S. Gao, "Single MWNT-glass fiber as strain sensor and switch.," *Adv. Mater.*, vol. 23, no. 30, pp. 3392–7, Aug. 2011.

[192] A. Cusano, A. Cutolo, J. Nasser, M. Giordano, and A. Calabrò, "Dynamic strain measurements by fibre Bragg grating sensor," *Sensors Actuators A Phys.*, vol. 110, no. 1–3, pp. 276–281, Feb. 2004.

[193] C. Robert, J. F. Feller, and M. Castro, "Sensing skin for strain monitoring made of pc-cnt conductive polymer nanocomposite sprayed layer by layer.," *ACS Appl. Mater. Interfaces*, vol. 4, no. 7, pp. 3508–3516, Jun. 2012.

[194] M. Castro, B. Kumar, J. F. Feller, Z. Haddi, A. Amari, and B. Bouchikhi, "Novel e-nose for the discrimination of volatile organic biomarkers with an array of carbon nanotubes (CNT) conductive polymer nanocomposites (CPC) sensors," *Sensors Actuators B Chem.*, vol. 159, no. 1, pp. 213–219, Nov. 2011.

[195] T. T. Tung, J. F. Feller, T. Kim, H. Kim, W. S. Yang, and K. S. Suh, "Electromagnetic properties of Fe3O4-functionalized graphene and its composites with a conducting polymer," *J. Polym. Sci. Part A Polym. Chem.*, vol. 50, no. 5, pp. 927–935, Mar. 2012.

[196] S. Chatterjee, M. Castro, and J. F. Feller, "An e-nose made of carbon nanotube based quantum resistive sensors for the detection of eighteen polar/nonpolar VOC biomarkers of lung cancer," *J. Mater. Chem. B*, vol. 1, no. 36, p. 4563, 2013.

[197] T. T. Tung, M. Castro, J. F. Feller, T. Y. Kim, and K. S. Suh, "Hybrid film of chemically modified graphene and vapor-phase-polymerized PEDOT for electronic nose applications," *Org. Electron.*, vol. 14, no. 11, pp. 2789–2794, Nov. 2013.

[198] S. M. Briglin, M. S. Freund, P. Tokumaru, and N. S. Lewis, "Exploitation of spatiotemporal information and geometric optimization of signal/noise performance using arrays of carbon black-polymer composite vapor detectors," *Sensors Actuators B Chem.*, vol. 82, no. 1, pp. 54–74, Feb. 2002.

[199] Y. Zhou, Y. Jiang, G. Xie, X. Du, and H. Tai, "Gas sensors based on multiple-walled carbon nanotubes-polyethylene oxide films for toluene vapor detection," *Sensors Actuators B Chem.*, vol. 191, pp. 24–30, Feb. 2014.

[200] B. Adhikari and S. Majumdar, "Polymers in sensor applications," *Prog. Polym. Sci.*, vol. 29, no. 7, pp. 699–766, Jul. 2004.

[201] J. W. Grate, S. N. Kaganove, and D. A. Nelson, "Polymers for chemical sensors using hydrosilylation chemistry," no. June, 2001.

[202] M. Castro, J. Lu, S. Bruzaud, B. Kumar, and J. F. Feller, "Carbon nanotubes/poly(ε-caprolactone) composite vapour sensors," *Carbon N. Y.*, vol. 47, no. 8, pp. 1930–1942, Jul. 2009.

[203] M. Ding, Y. Tang, P. Gou, M. J. Reber, and A. Star, "Chemical sensing with polyaniline coated single-walled carbon nanotubes," *Adv. Mater.*, vol. 23, no. 4, pp. 536–40, Jan. 2011.

[204] C. Staii, A. T. Johnson, M. Chen, and A. Gelperin, "DNA-decorated carbon nanotubes for chemical sensing," *Nano Lett.*, vol. 5, no. 9, pp. 1774–8, Sep. 2005.

[205] B. Kumar, M. Castro, and J. F. Feller, "Tailoring the chemo-resistive response of self-assembled polysaccharide-CNT sensors by chain conformation at tunnel junctions," *Carbon N. Y.*, vol. 50, no. 10, pp. 3627–3634, Aug. 2012.

[206] B. Kumar, M. Castro, and J. F. Feller, "Controlled conductive junction gap for chitosan–carbon nanotube quantum resistive vapour sensors," *J. Mater. Chem.*, vol. 22, no. 21, p. 10656, 2012.

[207] J. F. Feller, J. Lu, K. Zhang, B. Kumar, M. Castro, N. Gatt, and H. J. Choi, "Novel architecture of carbon nanotube decorated poly(methyl methacrylate) microbead vapour sensors assembled by spray layer by layer," *J. Mater. Chem.*, vol. 21, no. 12, p. 4142, 2011.

[208] J. Lu, J. F. Feller, B. Kumar, M. Castro, Y. S. Kim, Y. T. Park, and J. C. Grunlan, "Chemo-sensitivity of latex-based films containing segregated networks of carbon nanotubes," *Sensors Actuators B Chem.*, vol. 155, no. 1, pp. 28–36, Jul. 2011.

[209] Y. Zhou, Y. Jiang, G. Xie, X. Du, and H. Tai, "Gas sensors based on multiple-walled carbon nanotubes-polyethylene oxide films for toluene vapor detection," *Sensors Actuators B Chem.*, vol. 191, pp. 24–30, Feb. 2014.

[210] G. Di Francia, A. I. Grimaldi, E. Massera, M. L. Miglietta, and T. Polichetti, "Real time investigation of swelling kinetics and electrical response in polymer nanocomposite based chemical sensor," *Procedia Chem.*, vol. 1, no. 1, pp. 939–942, Sep. 2009.

[211] C. Li, E. T. Thostenson, and T.-W. Chou, "Sensors and actuators based on carbon nanotubes and their composites: A review," *Compos. Sci. Technol.*, vol. 68, no. 6, pp. 1227–1249, May 2008.

[212] X. Zhang, Q. Guo, and D. Cui, "Recent advances in nanotechnology applied to biosensors," *Sensors*, vol. 9, no. 2, pp. 1033–53, Jan. 2009.

[213] J. Choi, E. J. Park, D. W. Park, and S. E. Shim, "MWCNT–OH adsorbed electrospun nylon 6,6 nanofibers chemiresistor and their application in low molecular weight alcohol vapours sensing," *Synth. Met.*, vol. 160, no. 23–24, pp. 2664–2669, Dec. 2010.

[214] Y. Yoon, K. Lee, S. Kwon, S. Seo, H. Yoo, S. Kim, Y. Shin, Y. Park, D. Kim, J.-Y. Choi, and H. Lee, "Vertical alignments of graphene sheets spatially and densely piled for fast ion diffusion in compact supercapacitors," *ACS Nano*, vol. 8, no. 5, pp. 4580–90, Apr. 2014.

[215] D. Jariwala, V. K. Sangwan, L. J. Lauhon, T. J. Marks, and M. C. Hersam, "Carbon nanomaterials for electronics, optoelectronics, photovoltaics, and sensing," *Chem. Soc. Rev.*, vol. 42, no. 7, pp. 2824–60, Apr. 2013.

[216] O. C. Compton, B. Jain, D. A. Dikin, A. Abouimrane, and K. Amine, "Chemically active reduced graphene oxide with tunable C / O ratios," *ACS Nano*, vol. 5, no. 6, pp. 4380–4391, 2011.

[217] E. Nyankson, E. Annan, D. S. Konadu, E. Sinayobye, E. A. Baryeh, and C. P. Ewels, "Layered nanomaterials-a review," *Glob. J. Eng. Des. Technol.*, vol. 1, no. 2, pp. 32–41, 2012.

[218] P. A. A. P. Marques, G. Gonçalves, S. Cruz, N. Almeida, M. K. Singh, J. Grácio, and A. C. M. Sousa, "Functionalized graphene nanocomposites," in *Advances in Nanocomposite Technology*, 2011.

[219] S. Sato and M. Ohfuchi, "Graphene — Novel material for nanoelectronics," *Fujitsu Sci. Tech. J*, vol. 46, no. 1, pp. 103–110, 2010.

[220] Y. Zhu, S. Murali, W. Cai, X. Li, J. W. Suk, J. R. Potts, and R. S. Ruoff, "Graphene and graphene oxide: synthesis, properties, and applications," *Adv. Mater.*, vol. 22, no. 35, pp. 3906–24, Sep. 2010.

[221] A. K. Geim, "Graphene: status and prospects," *Science.*, vol. 324, pp. 1530–1534, 2009.

[222] K. S. Novoselov, "Electric field effect in atomically thin carbon films," *Science.*, vol. 306, no. 5696, pp. 666–669, 2004.

[223] B. Mahar, C. Laslau, S. Member, R. Yip, and Y. Sun, "Development of carbon nanotube-based sensors — a review," *IEEE Sens. J.*, vol. 7, no. 2, pp. 266–284, 2007.

[224] H. Kim, A. Abdala, and C. W. Macosko, “Graphene/polymer nanocomposites,” *Macromolecules*, vol. 43, no. 16, pp. 6515–6530, Aug. 2010.

[225] Y. Shao, J. Wang, H. Wu, J. Liu, I. A. Aksay, and Y. Lin, “Graphene based electrochemical sensors and biosensors: a review,” *Electroanalysis*, vol. 22, no. 10, pp. 1027–1036, Mar. 2010.

[226] H. W. Kroto, “C_{60}-the third man,” *Nature*, vol. 318, pp. 162–163, 1985.

[227] L. V. Radushkevich and M. V. Lukyanovich, “About the structure of carbon formed by thermal decomposition of carbon monoxide on iron substrate,” *J. Phys. Chem.*, vol. 26, pp. 88–95, 1952.

[228] S. Iijima, “Helical microtubules of graphitic carbon,” *Nature*, vol. 354, pp. 56–58, 1991.

[229] E. Llobet, “Gas sensors using carbon nanomaterials: A review,” *Sensors Actuators B Chem.*, vol. 179, no. 2010, pp. 32–45, Mar. 2013.

[230] E. W. Hill, A. Vijayaragahvan, K. Novoselov, and A. M. Exfoliation, “Graphene sensors,” *IEEE Sensors*, vol. 11, no. 12, pp. 3161–3170, 2011.

[231] K. Chao-Yang, T. Jun, L. Zhong-Liang, L. Li-Min, Y. Wen-Sheng, W. Shi-Qiang, and X. Peng-Shou, “Growth of few-layer graphene on sapphire substrates by directly depositing carbon atoms,” *Chinese Phys. Lett.*, vol. 28, no. 11, p. 118101, 2011.

[232] A. K. Geim and K. S. Novoselov, “The rise of graphene,” *Nat Mater*, vol. 6, no. 3, pp. 183–191, Mar. 2007.

[233] P.Mukhopadhyay, R.K.Gupta, “Trends and frontiers in graphene-based polymer,” *Plast. Eng.*, no. January, pp. 32–43, 2011.

[234] S. Kochmann, T. Hirsch, and O. S. Wolfbeis, “Graphenes in chemical sensors and biosensors,” *Trends Anal. Chem.*, vol. 39, pp. 87–113, Oct. 2012.

[235] N. Camara, A. Tiberj, B. Jouault, A. Caboni, B. Jabakhanji, N. Mestres, P. Godignon, and J. Camassel, “Current status of self-organized epitaxial graphene ribbons on the C face of 6H–SiC substrates,” *J. Phys. D. Appl. Phys.*, vol. 43, no. 37, p. 374011, 2010.

[236] F. Ming and A. Zangwill, “Model and simulations of the epitaxial growth of graphene on non-planar 6H–SiC surfaces,” *J. Phys. D. Appl. Phys.*, vol. 45, no. 15, p. 154007, 2012.

[237] W. Choi, I. Lahiri, R. Seelaboyina, and Y. S. Kang, “Synthesis of graphene and its applications: a review,” *Crit. Rev. Solid State Mater. Sci.*, vol. 35, no. 1, pp. 52–71, Feb. 2010.

[238] D. R. Kauffman and A. Star, “Carbon nanotube gas and vapor sensors,” *Angew. Chemie*, vol. 47, no. 35, pp. 6550–6570, 2008.

[239] T. Zhang, S. Mubeen, N. V Myung, and M. A. Deshusses, “Recent progress in carbon nanotube-based gas sensors,” *Nanotechnology*, vol. 19, no. 33, p. 332001, Aug. 2008.

[240] J.-J. Adjizian, R. Leghrib, A. A. Koos, I. Suarez-Martinez, A. Crossley, P. Wagner, N. Grobert, E. Llobet, and C. P. Ewels, “Boron- and nitrogen-doped multi-wall carbon nanotubes for gas detection,” *Carbon N. Y.*, vol. 66, pp. 662–673, Jan. 2014.

[241] J. Huang and Q. Wan, “Gas sensors based on semiconducting metal oxide one-dimensional nanostructures,” *Sensors*, vol. 9, no. 12, pp. 9903–24, Jan. 2009.

[242] A. Bouvree, J. F. Feller, M. Castro, Y. Grohens, and M. Rinaudo, "Conductive polymer nano-biocomposites (cpc): chitosan-carbon nanoparticle a good candidate to design polar vapour sensors," *Sensors Actuators B Chem.*, vol. 138, no. 1, pp. 138–147, Apr. 2009.

[243] T. T. Tung, M. Castro, and J. F. Feller, "Electronic noses for vocs detection based on the nanoparticles hybridized graphene composites," in *12th IEEE International Conference on Nanotechnology (IEEE-NANO)*, 2012, p. 6322037.

[244] S. Basu and P. Bhattacharyya, "Recent developments on graphene and graphene oxide based solid state gas sensors," *Sensors Actuators B Chem.*, vol. 173, pp. 1–21, Oct. 2012.

[245] W.-D. Zhang and W.-H. Zhang, "Carbon nanotubes as active components for gas sensors," *J. Sensors*, vol. 2009, pp. 1–16, 2009.

[246] A. Goldoni, L. Petaccia, S. Lizzit, and R. Larciprete, "Sensing gases with carbon nanotubes: a review of the actual situation," *J. Phys. Condens. Matter*, vol. 22, no. 1, p. 13001, 2010.

[247] P. Bondavalli, P. Legagneux, and D. Pribat, "Carbon nanotubes based transistors as gas sensors: State of the art and critical review," *Sensors Actuators B Chem.*, vol. 140, no. 1, pp. 304–318, Jun. 2009.

[248] L. Hu, D. S. Hecht, and G. Gru, "Percolation in transparent and conducting carbon nanotube networks," *Nano Lett.*, vol. 4, no. 12, pp. 2513–2517, 2004.

[249] S. Kruss, A. J. Hilmer, J. Zhang, N. F. Reuel, B. Mu, and M. S. Strano, "Carbon nanotubes as optical biomedical sensors," *Adv. Drug Deliv. Rev.*, vol. 65, pp. 1933–1950, Jul. 2013.

[250] W. Yang, K. R. Ratinac, S. P. Ringer, P. Thordarson, J. J. Gooding, and F. Braet, "Carbon nanomaterials in biosensors: should you use nanotubes or graphene?," *Biosensors*, vol. 49, no. 12, pp. 2114–38, Mar. 2010.

[251] I. V. Anoshkin, A. G. Nasibulin, P. R. Mudimela, M. He, V. Ermolov, and E. I. Kauppinen, "Single-walled carbon nanotube networks for ethanol vapor sensing applications," *Nano Res.*, vol. 6, no. 2, pp. 77–86, Dec. 2013.

[252] S. K. Vashist, "Advances in graphene-based sensors and devices," *J. Nanomed. Nanotechnol.*, vol. 04, no. 01, pp. 1–2, 2012.

[253] C. Biswas and Y. H. Lee, "Graphene versus carbon nanotubes in electronic devices," *Adv. Funct. Mater.*, vol. 21, no. 20, pp. 3806–3826, Oct. 2011.

[254] W. Li, X. Geng, Y. Guo, J. Rong, Y. Gong, L. Wu, X. Zhang, and P. Li, "Reduced graphene oxide electrically contacted graphene sensor for highly sensitive nitric oxide detection," *ACS Nano*, vol. 5, no. 9, pp. 6955–6961, 2011.

[255] Y. Dan, Y. Lu, N. J. Kybert, Z. Luo, and A. T. C. Johnson, "Intrinsic response of graphene vapor sensors," *Nano Lett.*, vol. 9, no. 4, pp. 1472–5, Apr. 2009.

[256] Z.-M. Zhou, J. Zhou, J. Chen, R.-N. Yu, M.-Z. Zhang, J.-T. Song, and Y.-D. Zhao, "Carcino-embryonic antigen detection based on fluorescence resonance energy transfer between quantum dots and graphene oxide," *Biosens. Bioelectron.*, Apr. 2014.

[257] M. Li, Y. Wang, Y. Zhang, J. Yu, S. Ge, and M. Yan, "Graphene functionalized porous Au-paper based electrochemiluminescence device for detection of DNA using luminescent silver nanoparticles coated calcium carbonate/carboxymethyl chitosan hybrid microspheres as labels," *Biosens. Bioelectron.*, Apr. 2014.

[258] T. Kuila, S. Bose, P. Khanra, A. K. Mishra, N. H. Kim, and J. H. Lee, "Recent advances in graphene-based biosensors.," *Biosens. Bioelectron.*, vol. 26, no. 12, pp. 4637–48, Aug. 2011.

[259] X. Du, I. Skachko, A. Barker, and E. Y. Andrei, "Approaching ballistic transport in suspended graphene," *Nat. Nanotechnol.*, vol. 3, no. 8, pp. 491–495, Aug. 2008.

[260] P. T. Moseley, "Solid state gas sensors," *Meas. Sci. Technol.*, vol. 8, no. 3, pp. 223–237, 1997.

[261] M. S. Artiles, C. S. Rout, and T. S. Fisher, "Graphene-based hybrid materials and devices for biosensing," *Adv. Drug Deliv. Rev.*, vol. 63, no. 14–15, pp. 1352–60, Nov. 2011.

[262] F. Yavari and N. Koratkar, "Graphene-based chemical sensors," *J. Phys. Chem. Lett.*, vol. 3, no. 13, pp. 1746–1753, Jul. 2012.

[263] A. Salehi-Khojin, D. Estrada, K. Y. Lin, K. Ran, R. T. Haasch, J.-M. Zuo, E. Pop, and R. I. Masel, "Chemical sensors based on randomly stacked graphene flakes," *Appl. Phys. Lett.*, vol. 100, no. 3, p. 033111, 2012.

[264] F. Schedin, A. K. Geim, S. V Morozov, E. W. Hill, P. Blake, M. I. Katsnelson, and K. S. Novoselov, "Detection of individual gas molecules adsorbed on graphene," *Nat Mater*, vol. 6, no. 9, pp. 652–655, Sep. 2007.

[265] M. J. S. Spencer, "Gas sensing applications of 1D-nanostructured zinc oxide: insights from density functional theory calculations," *Prog. Mater. Sci.*, vol. 57, no. 3, pp. 437–486, Apr. 2012.

[266] N. Nakashima, S. Okuzono, H. Murakami, T. Nakai, and K. Yoshikawa, "DNA dissolves single-walled carbon nanotubes in water," *Chem. Lett.*, vol. 32, no. 5, pp. 456–457, 2003.

[267] J. T. Robinson, F. K. Perkins, E. Snow, M. Zalalutidinov, B. H. Houston, J. W. Baldwin, Z. Wei, and P. E. Sheehan, "Chemically modified graphene for sensing and nanomechanical applications," *NRL Rev.*, pp. 87–96, 2009.

[268] Rajesh, T. Ahuja, and D. Kumar, "Recent progress in the development of nano-structured conducting polymers/nanocomposites for sensor applications," *Sensors Actuators B Chem.*, vol. 136, no. 1, pp. 275–286, Feb. 2009.

[269] D. W. Boukhvalov, "Modeling of epitaxial graphene functionalization," *Nanotechnology*, vol. 22, no. 5, p. 55708, 2011.

[270] S. Hwang, Y. Park, and K. H. Yoon, "Smart materials and structures based on carbon nanotube composites," in *Carbon Nanotubes - Synthesis, Characterization, Applications*, 2003.

[271] E.-Y. Choi, T. H. Han, J. Hong, J. E. Kim, S. H. Lee, H. W. Kim, and S. O. Kim, "Noncovalent functionalization of graphene with end-functional polymers," *J. Mater. Chem.*, vol. 20, no. 10, p. 1907, 2010.

[272] H. J. Salavagione, G. Martínez, and G. Ellis, "Graphene-based polymer nanocomposites," in *Physics and Applications of Graphene - Experiments*, 2011, pp. 169–192.

[273] T. Kuila, S. Bose, A. K. Mishra, P. Khanra, N. H. Kim, and J. H. Lee, "Chemical functionalization of graphene and its applications," *Prog. Mater. Sci.*, vol. 57, no. 7, pp. 1061–1105, Sep. 2012.

[274] S. N. Tripathi, P. Saini, D. Gupta, and V. Choudhary, "Electrical and mechanical properties of PMMA/reduced graphene oxide nanocomposites prepared via in situ polymerization," *J. Mater. Sci.*, vol. 48, no. 18, pp. 6223–6232, May 2013.

[275] D. R. Dreyer, S. Park, C. W. Bielawski, and R. S. Ruoff, "The chemistry of graphene oxide," *Chem. Soc. Rev.*, vol. 39, no. 1, pp. 228–40, Jan. 2010.

[276] V. Georgakilas, M. Otyepka, A. B. Bourlinos, V. Chandra, N. Kim, K. C. Kemp, P. Hobza, R. Zboril, and K. S. Kim, "Functionalization of graphene: covalent and non-covalent approaches, derivatives and applications.," *Chem. Rev.*, vol. 112, no. 11, pp. 6156–214, Nov. 2012.

[277] H. Bai, Y. Xu, L. Zhao, C. Li, and G. Shi, "Non-covalent functionalization of graphene sheets by sulfonated polyaniline," *Chem. Commun.*, vol. 4, no. 13, pp. 1667–9, Apr. 2009.

[278] X. An, T. W. Butler, M. Washington, S. K. Nayak, and S. Kar, "Optical and sensing properties films laminated on polydimethylsiloxane membranes," *ACS Nano*, vol. 5, no. 2, pp. 1003–1011, 2011.

[279] N. G. Sahoo, S. Rana, J. W. Cho, L. Li, and S. H. Chan, "Polymer nanocomposites based on functionalized carbon nanotubes," *Prog. Polym. Sci.*, vol. 35, no. 7, pp. 837–867, Jul. 2010.

[280] K. Arshak, E. Moore, L. Cavanagh, J. Harris, B. McConigly, C. Cunniffe, G. Lyons, and S. Clifford, "Determination of the electrical behaviour of surfactant treated polymer/carbon black composite gas sensors," *Compos. Part A Appl. Sci. Manuf.*, vol. 36, no. 4, pp. 487–491, Apr. 2005.

[281] Y. Geng, M. Y. Liu, J. Li, X. M. Shi, and J. K. Kim, "Effects of surfactant treatment on mechanical and electrical properties of CNT/epoxy nanocomposites," *Compos. Part A Appl. Sci. Manuf.*, vol. 39, no. 12, pp. 1876–1883, Dec. 2008.

[282] M. Bystrzejewski, A. Huczko, H. Lange, T. Gemming, B. Büchner, and M. H. Rümmeli, "Dispersion and diameter separation of multi-wall carbon nanotubes in aqueous solutions," *J. Colloid Interface Sci.*, vol. 345, no. 2, pp. 138–42, May 2010.

[283] M. Trojanowicz, "Analytical applications of carbon nanotubes: a review," *Trends Anal. Chem.*, vol. 25, no. 5, pp. 480–489, May 2006.

[284] M. F. Islam, E. Rojas, D. M. Bergey, A. T. Johnson, and A. G. Yodh, "High weight fraction surfactant solubilization of single-wall carbon nanotubes in water," *Nano Lett.*, vol. 3, no. 2, pp. 269–273, Feb. 2003.

[285] M. Herrera-Alonso, A. Abdala, M. J. McAllister, I. Aksay, and R. K. Prud'homme, "Intercalation and stitching of graphite oxide with diaminoalkanes," *Langmuir*, vol. 23, no. 21, pp. 10644–9, Oct. 2007.

[286] M. J. Yoo, H. W. Kim, B. M. Yoo, and H. B. Park, "Highly soluble polyetheramine-functionalized graphene oxide and reduced graphene oxide both in aqueous and non-aqueous solvents," *Carbon N. Y.*, vol. 75, pp. 149–160, Apr. 2014.

[287] H. Y. Mao, Y. H. Lu, J. D. Lin, S. Zhong, A. T. S. Wee, and W. Chen, "Manipulating the electronic and chemical properties of graphene via molecular functionalization," *Prog. Surf. Sci.*, vol. 88, no. 2, pp. 132–159, May 2013.

[288] H. Yang, C. Shan, F. Li, D. Han, Q. Zhang, and L. Niu, "Covalent functionalization of polydisperse chemically-converted graphene sheets with amine-terminated ionic liquid," *Chem. Commun.*, no. 26, pp. 3880–2, Jul. 2009.

[289] C. Dong, A. S. Campell, R. Eldawud, G. Perhinschi, Y. Rojanasakul, and C. Z. Dinu, "Effects of acid treatment on structure, properties and biocompatibility of carbon nanotubes," *Appl. Surf. Sci.*, vol. 264, pp. 261–268, Jan. 2013.

[290] M. Sánchez and M. E. Rincón, “Effect of multiwalled carbon nanotube functionalization on the gas sensing properties of carbon nanotube–titanium dioxide hybrid materials,” *Diam. Relat. Mater.*, vol. 21, pp. 1–6, Jan. 2012.

[291] E. Espinosa, R. Ionescu, B. Chambon, G. Bedis, E. Sotter, C. Bittencourt, A. Felten, J. Pireaux, X. Correig, and E. Llobet, “Hybrid metal oxide and multiwall carbon nanotube films for low temperature gas sensing,” *Sensors Actuators B Chem.*, vol. 127, no. 1, pp. 137–142, Oct. 2007.

[292] K. R. Nemade and S. A. Waghuley, “In situ synthesis of graphene/SnO2 quantum dots composites for chemiresistive gas sensing,” *Mater. Sci. Semicond. Process.*, vol. 24, pp. 126–131, Aug. 2014.

[293] E. N. Kaya, S. Tuncel, T. V. Basova, H. Banimuslem, A. Hassan, A. G. Gürek, V. Ahsen, and M. Durmuş, “Effect of pyrene substitution on the formation and sensor properties of phthalocyanine-single walled carbon nanotube hybrids,” *Sensors Actuators B Chem.*, vol. 199, pp. 277–283, Apr. 2014.

[294] Z. Yan, Z. Peng, G. Casillas, J. Lin, C. Xiang, H. Zhou, Y. Yang, G. Ruan, A.-R. O. Raji, E. L. G. Samuel, R. H. Hauge, M. J. Yacaman, and J. M. Tour, “Rebar graphene,” *ACS Nano*, vol. 8, no. 5, pp. 5061–5068, Apr. 2014.

[295] T. Premkumar and K. E. Geckeler, “Graphene–DNA hybrid materials: Assembly, applications, and prospects,” *Prog. Polym. Sci.*, vol. 37, no. 4, pp. 515–529, Apr. 2012.

[296] X. Chen, J. Zhu, Q. Xi, and W. Yang, “A high performance electrochemical sensor for acetaminophen based on single-walled carbon nanotube−graphene nanosheet hybrid films,” *Sensors Actuators B Chem.*, vol. 161, no. 1, pp. 648–654, Nov. 2011.

[297] Z. Fan, J. Yan, L. Zhi, Q. Zhang, T. Wei, J. Feng, M. Zhang, W. Qian, and F. Wei, “A three-dimensional carbon nanotube/graphene sandwich and its application as electrode in supercapacitors.,” *Adv. Mater.*, vol. 22, no. 33, pp. 3723–8, Sep. 2010.

[298] J. Yan, T. Wei, Z. Fan, W. Qian, M. Zhang, X. Shen, and F. Wei, “Preparation of graphene nanosheet/carbon nanotube/polyaniline composite as electrode material for supercapacitors,” *J. Power Sources*, vol. 195, no. 9, pp. 3041–3045, 2010.

[299] Y.-K. Kim, H.-K. Na, S.-J. Kwack, S.-R. Ryoo, Y. Lee, S. Hong, S. Hong, Y. Jeong, and D.-H. Min, “Synergistic effect of graphene oxide/MWCNT films in laser desorption/ionization mass spectrometry of small molecules and tissue imaging,” *ACS Nano*, vol. 5, no. 6, pp. 4550–61, Jun. 2011.

[300] X. Li, Y. Chai, H. Zhang, G. Wang, and X. Feng, “Synthesis of polyaniline/tin oxide hybrid and its improved electrochemical capacitance performance,” *Electrochim. Acta*, vol. 85, pp. 9–15, Dec. 2012.

[301] Y-L.Liu, H-F.Yang, Z.-M. Liu, G.-L. Shen, and R-Q.Yu, “Gas sensing properties of tin dioxide coated onto multi-walled carbon nanotubes,” *Thin Solid Films*, vol. 497, pp. 355–360, 2006.

[302] Z. Wang, G. Chen, and D. Xia, “Coating of multi-walled carbon nanotube with SnO2 films of controlled thickness and its application for Li-ion battery,” *J. Power Sources*, vol. 184, no. 2, pp. 432–436, Oct. 2008.

[303] R. Leghrib, A. Felten, J. J. Pireaux, and E. Llobet, “Gas sensors based on doped-CNT/SnO2 composites for NO2 detection at room temperature,” *Thin Solid Films*, vol. 520, no. 3, pp. 966–970, Nov. 2011.

[304] Q. Yang, Q. Li, Z. Yan, X. Hu, L. Kang, Z. Lei, and Z.-H. Liu, “High performance graphene/manganese oxide hybrid electrode with flexible holey structure,” *Electrochim. Acta*, vol. 129, pp. 237–244, Mar. 2014.

[305] C. Zhang and T. Liu, "A review on hybridization modification of graphene and its polymer nanocomposites," *Chinese Sci. Bull.*, vol. 57, no. 23, pp. 3010–3021, Aug. 2012.

[306] X. Dong, Y. Ma, G. Zhu, Y. Huang, J. Wang, M. B. Chan-Park, L. Wang, W. Huang, and P. Chen, "Synthesis of graphene–carbon nanotube hybrid foam and its use as a novel three-dimensional electrode for electrochemical sensing," *J. Mater. Chem.*, vol. 22, no. 33, p. 17044, 2012.

[307] Z.-D. Huang, B. Zhang, S.-W. Oh, Q.-B. Zheng, X.-Y. Lin, N. Yousefi, and J.-K. Kim, "Self-assembled reduced graphene oxide/carbon nanotube thin films as electrodes for supercapacitors," *J. Mater. Chem.*, vol. 22, no. 8, p. 3591, 2012.

[308] X. Dong, B. Li, A. Wei, X. Cao, M. B. Chan-Park, H. Zhang, L.-J. Li, W. Huang, and P. Chen, "One-step growth of graphene–carbon nanotube hybrid materials by chemical vapor deposition," *Carbon N. Y.*, vol. 49, no. 9, pp. 2944–2949, Aug. 2011.

[309] D. Yu and L. Dai, "Self-assembled graphene/carbon nanotube hybrid films for supercapacitors," *J. Phys. Chem. Lett.*, vol. 1, no. 2, pp. 467–470, Jan. 2010.

[310] S. H. Lee, D. H. Lee, W. J. Lee, and S. O. Kim, "Tailored assembly of carbon nanotubes and graphene," *Adv. Funct. Mater.*, vol. 21, no. 8, pp. 1338–1354, Apr. 2011.

[311] D. H. Lee, J. E. Kim, T. H. Han, J. W. Hwang, S. Jeon, S.-Y. Choi, S. H. Hong, W. J. Lee, R. S. Ruoff, and S. O. Kim, "Versatile carbon hybrid films composed of vertical carbon nanotubes grown on mechanically compliant graphene films.," *Adv. Mater.*, vol. 22, no. 11, pp. 1247–52, Mar. 2010.

[312] H. Y. Jeong, D.-S. Lee, H. K. Choi, D. H. Lee, J.-E. Kim, J. Y. Lee, W. J. Lee, S. O. Kim, and S.-Y. Choi, "Flexible room-temperature NO_2 gas sensors based on carbon nanotubes/reduced graphene hybrid films," *Appl. Phys. Lett.*, vol. 96, no. 21, p. 213105, 2010.

[313] L. L. Zhang, Z. Xiong, and X. S. Zhao, "Pillaring chemically exfoliated graphene oxide with carbon nanotubes for photocatalytic degradation of dyes under visible light irradiation," *ACS Nano*, vol. 4, no. 11, pp. 7030–6, Nov. 2010.

[314] N. Li, C. Sioutas, A. Cho, D. Schmitz, C. Misra, J. Sempf, M. Wang, T. Oberley, J. Froines, and A. Nel, "Ultrafine particulate pollutants induce oxidative stress and mitochondrial damage," *Environ. Health Perspect.*, vol. 111, no. 4, pp. 455–460, Dec. 2002.

[315] M. Geiser, B. Rothen-Rutishauser, N. Kapp, S. Schürch, W. Kreyling, H. Schulz, M. Semmler, V. I. Hof, J. Heyder, and P. Gehr, "Ultrafine particles cross cellular membranes by nonphagocytic mechanisms in lungs and in cultured cells," *Environ. Health Perspect.*, vol. 113, no. 11, pp. 1555–1560, May 2005.

[316] K. Duarte, C. I. L. Justino, A. C. Freitas, A. C. Duarte, and T. A. P. Rocha-Santos, "Direct-reading methods for analysis of volatile organic compounds and nanoparticles in workplace air," *Trends Anal. Chem.*, vol. 53, pp. 21–32, Oct. 2013.

[317] L. Ma-Hock, V. Strauss, S. Treumann, K. Küttler, W. Wohlleben, T. Hofmann, S. Gröters, K. Wiench, B. van Ravenzwaay, and R. Landsiedel, "Comparative inhalation toxicity of multi-wall carbon nanotubes, graphene, graphite nanoplatelets and low surface carbon black.," *Part. Fibre Toxicol.*, vol. 10, no. 1, p. 23, Jun. 2013.

[318] N. L. Guo, Y. Wan, J. Denvir, D. W. Porter, M. Pacurari, M. G. Wolfarth, V. Castranova, Y. Qian, M. Babb, and R. Cancer, "Multi-walled carbon nanotube-induced gene signatures in the mouse lung: potential predictive value for human lung cancer risk and prognosis," *J Toxicol Env. Heal. A.*, vol. 75, no. 18, pp. 1129–1153, 2012.

[319] Y. Liu, Y. Zhao, B. Sun, and C. Chen, “Understanding the toxicity of carbon,” *Acc. Chem. Res.*, vol. 46, no. 3, pp. 702–713, 2013.

[320] C. Bussy, H. Ali-Boucetta, and K. Kostarelos, “Safety considerations for graphene: lessons learnt from carbon nanotubes,” *Acc. Chem. Res.*, vol. 46, no. 3, pp. 692–701, Mar. 2013.

[321] A. Bianco, “Graphene: safe or toxic? The two faces of the medal,” *Angew. Chemie*, vol. 52, no. 19, pp. 4986–97, May 2013.

[322] A. Schinwald, F. A. Murphy, A. Jones, W. MacNee, and K. Donaldson, “Graphene-based nanoplatelets : a new risk to the respiratory system as a consequence of their unusual aerodynamic properties,” *ACS Nano*, no. 1, pp. 736–746, 2012.

[323] E. Bergamaschi, “Occupational exposure to nanomaterials: Present knowledge and future development,” *Nanotoxicology*, vol. 3, no. 3, pp. 194–201, Jan. 2009.

[324] K. Donaldson, L. Tran, L. A. Jimenez, R. Duffin, D. E. Newby, N. Mills, W. MacNee, and V. Stone, “Combustion-derived nanoparticles: a review of their toxicology following inhalation exposure,” *Part. Fibre Toxicol.*, vol. 2, p. 10, Oct. 2005.

[325] T. A. Kuhlbusch, C. Asbach, H. Fissan, D. Göhler, and M. Stintz, “Nanoparticle exposure at nanotechnology workplaces: a review.,” *Part. Fibre Toxicol.*, vol. 8, no. 1, p. 22, Jan. 2011.

[326] P. A. Schulte, V. Murashov, R. Zumwalde, E. D. Kuempel, and C. L. Geraci, “Occupational exposure limits for nanomaterials : state of the art,” *J Nanopart Res*, vol. 12, pp. 1971–1987, 2010.

[327] K. S. Novoselov, A. K. Geim, S. V Morozov, D. Jiang, M. I. Katsnelson, I. V Grigorieva, S. V Dubonos, and A. A. Firsov, “Two-dimensional gas of massless Dirac fermions in graphene,” *Nature*, vol. 438, no. 7065, pp. 197–200, Nov. 2005.

[328] B. Zhang, Q. Li, and T. Cui, “Ultra-sensitive suspended graphene nanocomposite cancer sensors with strong suppression of electrical noise,” *Biosens. Bioelectron.*, vol. 31, no. 1, pp. 105–9, Jan. 2012.

[329] S. K. Yadav, S. S. Mahapatra, H. J. Yoo, and J. W. Cho, “Synthesis of multi-walled carbon nanotube/polyhedral oligomeric silsesquioxane nanohybrid by utilizing click chemistry,” *Nanoscale Res. Lett.*, vol. 6, no. 1, p. 122, Jan. 2011.

[330] R. F. Service, “Carbon sheets an atom thick give rise to graphene dreams,” *Science.*, vol. 324, no. May, pp. 875–877, 2009.

[331] A. A. Balandin, S. Ghosh, W. Bao, I. Calizo, D. Teweldebrhan, F. Miao, and C. N. Lau, “Superior thermal conductivity of single-layer graphene,” *Nano Lett.*, vol. 8, no. 3, pp. 902–7, Mar. 2008.

[332] C. Lee, X. Wei, J. W. Kysar, and J. Hone, “Measurement of the elastic properties and intrinsic strength of monolayer graphene.,” *Science.*, vol. 321, no. 5887, pp. 385–8, Jul. 2008.

[333] J. Hass, W. A. de Heer, and E. H. Conrad, “The growth and morphology of epitaxial multilayer graphene,” *J. Phys. Condens. Matter*, vol. 20, p. 323202, 2008.

[334] H. Chang, G. Wang, A. Yang, X. Tao, X. Liu, Y. Shen, and Z. Zheng, “A transparent, flexible, low-temperature, and solution-processible graphene composite electrode,” *Adv. Funct. Mater.*, vol. 20, no. 17, pp. 2893–2902, Sep. 2010.

[335] H. Chang and H. Wu, “Graphene-based nanomaterials: synthesis, properties, and optical and optoelectronic applications,” *Adv. Funct. Mater.*, vol. 23, no. 16, pp. 1984–1997, Apr. 2013.

[336] J. D. Fowler, M. J. Allen, V. C. Tung, Y. Yang, R. B. Kaner, B. H. Weiller, Ḱ. M. J. Allen, and Ḱ. V. C. Tung, "Practical Chemical Sensors from Chemically Derived Graphene," *ACS Nano*, vol. 3, no. January, pp. 301–306, 2009.

[337] T. T. Tung, M. Castro, T. Y. Kim, K. S. Suh, and J. F. Feller, "Graphene quantum resistive sensing skin for the detection of alteration biomarkers," *J. Mater. Chem.*, vol. 22, no. 40, p. 21754, 2012.

[338] K. Hu, D. D. Kulkarni, I. Choi, and V. V. Tsukruk, "Graphene–polymer nanocomposites for structural and functional applications," *Prog. Polym. Sci.*, Mar. 2014.

[339] P. Shahgaldian and U. Pieles, "Cyclodextrin derivatives as chiral supramolecular receptors for enantioselective sensing," *Sensors*, vol. 6, no. 6, pp. 593–615, Jun. 2006.

[340] M. V. Rekharsky and Y. Inoue, "Complexation thermodynamics of cyclodextrins," *Chem. Rev.*, vol. 98, no. 5, pp. 1875–1918, Jul. 1998.

[341] V. Monnaert, D. Betbeder, L. Fenart, H. Bricout, A. M. Lenfant, C. Landry, R. Cecchelli, E. Monflier, and S. Tilloy, "Effects of γ- and hydroxypropyl-γ-cyclodextrins on the transport of doxorubicin across an in vitro model of blood brain barrier," *J. Pharmacol. Exp. Ther.*, vol. 311, no. 3, pp. 1115–1120, 2004.

[342] N. Badi, P. Guégan, F.-X. Legrand, L. Leclercq, S. Tilloy, and E. Monflier, "β-Cyclodextrins modified by alkyl and poly(ethylene oxide) chains: A novel class of mass transfer additives for aqueous organometallic catalysis," *J. Mol. Catal. A Chem.*, vol. 318, no. 1–2, pp. 8–14, Mar. 2010.

[343] T. Ogoshi and A. Harada, "Chemical sensors based on cyclodextrin derivatives," *Sensors*, vol. 8, no. 8, pp. 4961–4982, Aug. 2008.

[344] I. Tabushi, Y. Kuroda, and K. Yokota, "A,B,D,F-tetrasubstituted β-cyclodextrin as artificial channel compound," *Tetrahedron Lett.*, vol. 23, no. 44, pp. 4601–4604, 1982.

[345] S. Lv, Y. Song, Y. Song, Z. Zhao, and C. Cheng, "Beta-cyclodextrins conjugated magnetic Fe3O4 colloidal nanoclusters for the loading and release of hydrophobic molecule," *Appl. Surf. Sci.*, vol. 305, pp. 747–752, Apr. 2014.

[346] Y. Guo, S. Guo, J. Ren, Y. Zhai, S. Dong, and E. Wang, "Nanosheets with high supramolecular recognition capability : synthesis and host guest inclusion for enhanced electrochemical performance," *ACS Nano*, vol. 4, no. 7, pp. 4001–4010, 2010.

[347] L. Kong, J. Wang, F. Meng, X. Chen, Z. Jin, M. Li, J. Liu, and X.-J. Huang, "Novel hybridized SWCNT–PCD: synthesis and host–guest inclusion for electrical sensing recognition of persistent organic pollutants," *J. Mater. Chem.*, vol. 21, no. 30, p. 11109, 2011.

[348] L. Li, W. Feng, and P. Ji, "Protein adsorption on functionalized multiwalled carbon nanotubes with," *Bioeng. Food, Nat. Prod. Protein*, vol. 57, no. 12, pp. 3507–3513, 2011.

[349] L. Yang, Y. Xu, X. Wang, J. Zhu, R. Zhang, P. He, and Y. Fang, "The application of β-cyclodextrin derivative functionalized aligned carbon nanotubes for electrochemically DNA sensing via host-guest recognition," *Anal. Chim. Acta*, vol. 689, no. 1, pp. 39–46, Mar. 2011.

[350] Z. Guo, Y. Feng, D. Zhu, S. He, H. Liu, X. Shi, J. Sun, and M. Qu, "Light-switchable single-walled carbon nanotubes based on host-guest chemistry," *Adv. Funct. Mater.*, vol. 23, no. 40, pp. 5010–5018, Apr. 2013.

[351] J. F. Feller, B. Kumar, and M. Castro, "Conductive biopolymer nanocomposites for sensors," in *Nanocomposites with biodegradable polymers: Synthesis, Properties & Future Perspectives*, 1st ed., V. Mital, Ed. Oxford (UK): Oxford University Press, 2011, pp. 368–399.

[352] J. Lu, B. Kumar, M. Castro, and J. F. Feller, "Vapour sensing with conductive polymer nanocomposites (CPC): Polycarbonate-carbon nanotubes transducers with hierarchical structure processed by spray layer by layer," *Sensors Actuators B Chem.*, vol. 140, no. 2, pp. 451–460, Jul. 2009.

[353] William S. Hummers and R. E. Offeman, "Preparation of Graphitic Oxide," *J. Am. Chem. Soc.*, vol. 80, no. 6, pp. 1339–1339, 1958.

[354] R. Haddad, M. Holzinger, R. Villalonga, A. Neumann, J. Roots, a. Maaref, and S. Cosnier, "Pyrene-adamantane-β-cyclodextrin: An efficient host–guest system for the biofunctionalization of SWCNT electrodes," *Carbon N. Y.*, vol. 49, no. 7, pp. 2571–2578, Jun. 2011.

[355] Y. El Ghoul, R. Renia, I. Faye, S. Rassou, N. Badi, V. Bennevault-Celton, C. Huin, and P. Guégan, "Biomimetic artificial ion channels based on beta-cyclodextrin," *Chem. Commun.*, vol. 49, no. 99, pp. 11647–9, Dec. 2013.

[356] J. F. Feller and Y. Grohens, "Evolution of electrical properties of some conductive polymer composite textiles with organic solvent vapours diffusion," *Sensors Actuators B Chem.*, vol. 97, no. 2–3, pp. 231–242, Feb. 2004.

[357] B. Kumar, J. F. Feller, M. Castro, and J. Lu, "Conductive bio-Polymer nano-Composites (CPC): chitosan-carbon nanotube transducers assembled via spray layer-by-layer for volatile organic compound sensing," *Talanta*, vol. 81, no. 3, pp. 908–15, May 2010.

[358] Fedors, "A method of estimating both the solubility parameters and molar volumes of liquids," *Polym Eng Sci.*, vol. 14, pp. 147–154, 1974.

[359] T. Gao, M. D. Woodka, B. S. Brunschwig, and N. S. Lewis, "Chemiresistors for array-based vapor sensing Using composites of carbon black with low volatility organic molecules," *Chem. Mater.*, vol. 18, no. 22, pp. 5193–5202, 2006.

[360] Y. Yang, L. Qu, L. Dai, T.-S. Kang, and M. Durstock, "Electrophoresis coating of titanium dioxide on aligned carbon nanotubes for controlled syntheses of photoelectronic nanomaterials," *Adv. Mater.*, vol. 19, no. 9, pp. 1239–1243, May 2007.

[361] E. Shi, L. Zhang, Z. Li, P. Li, Y. Shang, Y. Jia, J. Wei, K. Wang, H. Zhu, D. Wu, S. Zhang, and A. Cao, "TiO2-coated carbon nanotube-silicon solar cells with efficiency of 15%," *Sci. Rep.*, vol. 2, p. 884, Jan. 2012.

[362] Y.-S. Kim, K. Kumar, F. T. Fisher, and E.-H. Yang, "Out-of-plane growth of CNTs on graphene for supercapacitor applications," *Nanotechnology*, vol. 23, no. 1, p. 015301, Jan. 2012.

[363] B. Zhang, Y. Chen, J. Wang, W. J. Blau, X. Zhuang, and N. He, "Multi-walled carbon nanotubes covalently functionalized with polyhedral oligomeric silsesquioxanes for optical limiting," *Carbon N. Y.*, vol. 48, no. 6, pp. 1738–1742, May 2010.

[364] Q.-F. Li, Y. Xu, J.-S. Yoon, and G.-X. Chen, "Dispersions of carbon nanotubes/polyhedral oligomeric silsesquioxanes hybrids in polymer: the mechanical, electrical and EMI shielding properties," *J. Mater. Sci.*, vol. 46, no. 7, pp. 2324–2330, Nov. 2010.

[365] G. Li, L. Wang, H. Ni, and C. U. P. Jr, "Polyhedral oligomeric silsesquioxane (POSS) polymers and copolymers : A Review," *J. Inorg. Organomet. Polym.*, vol. 11, no. 3, 2002.

[366] P. Iyer, J. A. Mapkar, and M. R. Coleman, "A hybrid functional nanomaterial: POSS functionalized carbon nanofiber," *Nanotechnology*, vol. 20, no. 32, p. 325603, Aug. 2009.

[367] A. Castaldo, E. Massera, L. Quercia, and G. Di Francia, “Filled polysilsesquioxanes: a new approach to chemical sensing,” *Macromol. Symp.*, vol. 247, no. 1, pp. 350–356, Feb. 2007.

[368] E. Massera, a. Castaldo, L. Quercia, and G. Di Francia, “Fabrication and characterization of polysilsesquioxanes nanocomposites based chemical sensor,” *Sensors Actuators B Chem.*, vol. 129, no. 1, pp. 487–490, Jan. 2008.

[369] N. T. Dintcheva, E. Morici, R. Arrigo, and F. P. La Mantia, “The role of POSS on the structure-properties relationships in polystyrene based nanocomposites,” 2011.

[370] M. Hakim, Y. Y. Broza, O. Barash, N. Peled, M. Phillips, A. Amann, and H. Haick, “Volatile organic compounds of lung cancer and possible biochemical pathways,” *Chem. Rev.*, vol. 112, pp. 5949–5966, 2012.

[371] F. Wudl, “Fullerene materials,” *J. Mater. Chem.*, vol. 12, no. 7, pp. 1959–1963, Jun. 2002.

[372] W. Kratschmer, L. D. Lamb, K. Fostiropoulos, and D. R. Huffman, “Solid C60: a new form of carbon,” *Nature*, vol. 347, no. 6291, pp. 354–358, Sep. 1990.

[373] Y. Jin, R. J. Curry, J. Sloan, R. A. Hatton, L. C. Chong, N. Blanchard, V. Stolojan, H. W. Kroto, and S. R. P. Silva, “Structural and optoelectronic properties of C60 rods obtained via a rapid synthesis route,” *J. Mater. Chem.*, vol. 16, no. 37, p. 3715, 2006.

[374] P. J. Krusic, E. Wasserman, P. N. Keizer, J. R. Morton, and K. F. Preston, “Radical Reactions of C60,” *Science.*, vol. 254, no. 5035, pp. 1183–1185, Nov. 1991.

[375] P. R. Somani, S. P. Somani, and M. Umeno, “Carbon – Science and Technology,” *Carbon – Sci. Tech*, vol. 1, pp. 1–3, 2008.

[376] X. Zhang, Y. Qu, G. Piao, J. Zhao, and K. Jiao, “Reduced working electrode based on fullerene C60 nanotubes@DNA: Characterization and application,” *Mater. Sci. Eng. B*, vol. 175, no. 2, pp. 159–163, Nov. 2010.

[377] Y. Zhao, Y.-H. Kim, A. C. Dillon, M. J. Heben, and S. B. Zhang, “Hydrogen storage in novel organometallic buckyballs,” *Phys. Rev. Lett.*, vol. 94, no. 15, p. 155504, Apr. 2005.

[378] D. Yu, K. Park, M. Durstock, and L. Dai, “Fullerene-grafted graphene for efficient bulk heterojunction polymer photovoltaic devices,” *J. Phys. Chem. Lett.*, vol. 26, pp. 1113–1118, 2011.

[379] C. Li, Y. Chen, Y. Wang, Z. Iqbal, and S. Mitra, “A fullerene – single wall carbon nanotube complex for polymer bulk heterojunction photovoltaic cells,” *J. Mater. Chem.*, vol. 17, pp. 2406–2411, 2007.

[380] Z. Liu, Y. Xu, X. Zhang, X. Zhang, Y. Chen, and J. Tian, “Porphyrin and fullerene covalently functionalized graphene hybrid materials with large nonlinear optical properties,” *J. Phys. Chem. B*, vol. 113, no. 29, pp. 9681–9686, 2009.

[381] X. Zhang, Y. Huang, Y. Wang, Y. Ma, Z. Liu, and Y. Chen, “Synthesis and characterization of a graphene–C60 hybrid material,” *Carbon N. Y.*, vol. 47, no. 1, pp. 334–337, Jan. 2009.

[382] P. Song, Y. Shen, B. Du, Z. Guo, and Z. Fang, “Fabrication of fullerene-decorated carbon nanotubes and their application in flame-retarding polypropylene,” *Nanoscale*, vol. 1, no. 1, pp. 118–21, Oct. 2009.

[383] T. T. Tung, M. Castro, T. Y. Kim, K. S. Suh, and J. F. Feller, “High stability silver nanoparticles – graphene / poly (ionic liquid) - based chemoresistive sensors for volatile organic compounds detection,” *Anal. Bioanal. Chem.*, vol. 406, no. 16, pp. 3995–4004, 2014.

[384] G. Li, P. Liu, Z. Han, G. Piao, J. Zhao, S. Li, and G. Liu, "A novel approach to fabrication of fullerene C60 nanotubes: Using C60–pyridine colloid as a precursor," *Mater. Lett.*, vol. 64, no. 3, pp. 483–485, Feb. 2010.

[385] X. Zhang and X.-D. Li, "Solvent atmosphere controlled self-assembly of unmodified C60: A facile approach for constructing various architectures," *Chinese Chem. Lett.*, Apr. 2014.

[386] G. Li, Z. Han, G. Piao, J. Zhao, S. Li, and G. Liu, "To distinguish fullerene C60 nanotubes and C60 nanowhiskers using Raman spectroscopy," *Mater. Sci. Eng. B*, vol. 163, no. 3, pp. 161–164, Jul. 2009.

[387] M. Sathish and K. Miyazawa, "Synthesis and characterization of fullerene nanowhiskers by liquid-liquid interfacial precipitation: influence of C60 solubility," *Molecules*, vol. 17, no. 4, pp. 3858–65, Jan. 2012.

[388] H. C. Wang, Y. Li, and M. J. Yang, "Sensors for organic vapor detection based on composites of carbon nonotubes functionalized with polymers," *Sensors Actuators B Chem.*, vol. 124, no. 2, pp. 360–367, Jun. 2007.

[389] J. Lu, B. J. Park, B. Kumar, M. Castro, H. J. Choi, and J. F. Feller, "Polyaniline nanoparticle-carbon nanotube hybrid network vapour sensors with switchable chemo-electrical polarity.," *Nanotechnology*, vol. 21, no. 25, p. 255501, Jun. 2010.

[390] B. Kumar, M. Castro, and J. F. Feller, "Poly(lactic acid)–multi-wall carbon nanotube conductive biopolymer nanocomposite vapour sensors," *Sensors Actuators B Chem.*, vol. 161, no. 1, pp. 621–628, Jan. 2012.

[391] B. Kumar, J. F. Feller, M. Castro, and J. Lu, "Conductive bio-polymer nano-composites (CPC): chitosan-carbon nanotube transducers assembled via spray layer-by-layer for volatile organic compound sensing.," *Talanta*, vol. 81, no. 3, pp. 908–15, May 2010.

[392] D. Gupta, A. Madhukar, and V. Choudhary, "Effect of functionality of polyhedral oligomeric silsesquioxane [POSS] on the properties of sulfonated poly(ether ether ketone) [SPEEK] based hybrid nanocomposite proton exchange membranes for fuel cell applications," *Int. J. Hydrogen Energy*, vol. 38, no. 29, pp. 12817–12829, Sep. 2013.

[393] D. Gupta and V. Choudhary, "Studies on novel heat treated sulfonated poly(ether ether ketone) [SPEEK]/diol membranes for fuel cell applications," *Int. J. Hydrogen Energy*, vol. 36, no. 14, pp. 8525–8535, Jul. 2011.

[394] M. H. D. Othman, A. F. Ismail, and A. Mustafa, "Physico-chemical study of sulfonated poly (ether ether ketone) membranes for direct methanol fuel cell application," *Malaysian Polym. J.*, vol. 2, no. 1, pp. 10–28, 2007.

[395] A. W. Boots, J. J. B. N. van Berkel, J. W. Dallinga, A. Smolinska, E. F. Wouters, and F. J. van Schooten, "The versatile use of exhaled volatile organic compounds in human health and disease," *J. Breath Res.*, vol. 6, no. 2, p. 027108, Jun. 2012.

[396] C. Wang, F. Chen, and X.-W. He, "Kinetic detection of benzene/chloroform and toluene/chloroform vapors using a single quartz piezoelectric crystal coated with calix[6]arene," *Anal. Chim. Acta*, vol. 464, no. 1, pp. 57–64, Jul. 2002.

[397] S. Patel, M. W. Jenkins, R. C. Hughes, W. G. Yelton, and A. J. Ricco, "Differentiation of chemical components in a binary solvent vapor mixture using carbon/polymer composite-based chemiresistors," *Anal. Chem.*, vol. 72, no. 7, pp. 1532–42, Apr. 2000.

[398] K. Brudzewski and J. Ulaczyk, "An effective method for analysis of dynamic electronic nose responses," *Sensors Actuators B Chem.*, vol. 140, no. 1, pp. 43–50, Jun. 2009.

[399] A. Gulbag and F. Temurtas, “A study on quantitative classification of binary gas mixture using neural networks and adaptive neuro-fuzzy inference systems,” *Sensors Actuators B Chem.*, vol. 115, no. 1, pp. 252–262, May 2006.

[400] A. J. Ricco, R. M. Crooks, and G. C. Osbourn, “Surface acoustic wave chemical sensor arrays : new chemically sensitive interfaces combined with novel cluster analysis to detect volatile organic compounds and mixtures,” *Acc. Chem. Res.*, vol. 31, no. 5, pp. 289–296, 1998.

[401] M. Hsieh and E. T. Zellers, “Limits of recognition for simple vapor mixtures determined with a microsensor array,” *Anal. Chem.*, vol. 76, no. 7, pp. 1885–1895, 2004.

[402] R. Jaisutti, T. Hongkachern, and T. Osotchan, “Response differences of binary vapors from mixtures in liquid and gas phases,” in *First International Conference on Sensor Device Technologies and Applications*, 2010, pp. 249–252.

[403] P. C. Jurs, G. a Bakken, and H. E. McClelland, “Computational methods for the analysis of chemical sensor array data from volatile analytes.,” *Chem. Rev.*, vol. 100, no. 7, pp. 2649–78, Jul. 2000.

[404] Y. Wang and J.-S. Shih, “Multi-Channel Piezoelectric Crystal Gas Sensor with Principal Component Analysis for Organic Solvent Pollutants from Polymer Plants,” *J. Chinese Chem. Soc.*, vol. 53, pp. 1427–1437, 2006.

[405] K. Witt, S. Reulecke, and A. Voss, “Discrimination and characterization of breath from smokers and non-smokers via electronic nose and GC/MS analysis,” in *33rd Annual International Conference of the IEEE Engineering in Medicine and Biology Society.*, 2011, vol. 2011, pp. 3664–3667.

[406] J. W. Gardner, “Detection of vapours and odours from a multisensor array using pattern recognition Part 1. Principal component and cluster analysis,” *Sensors Actuators B Chem.*, vol. 4, no. 1–2, pp. 109–115, May 1991.

[407] J. W. Gardner, E. L. Hines, and H. C. Tang, “Detection of vapours and odours from a multisensor array using pattern-recognition techniques Part 2. Artificial neural networks,” *Sensors Actuators B Chem.*, vol. 9, no. 1, pp. 9–15, Jul. 1992.

[408] E. Llobet, J. Brezmes, X. Vilanova, J. E. Sueiras, and X. Correig, “Qualitative and quantitative analysis of volatile organic compounds using transient and steady-state responses of a thick-film tin oxide gas sensor array,” *Sensors Actuators B Chem.*, vol. 41, no. 1–3, pp. 13–21, Jun. 1997.

[409] M. C. Lonergan, E. J. Severin, B. J. Doleman, S. A. Beaber, R. H. Grubbs, and N. S. Lewis, “Array-based vapor sensing using chemically sensitive , carbon black - polymer resistors,” *Chem. Mater.*, vol. 4756, no. 14, pp. 2298–2312, 1996.

[410] R. Gutierrez-Osuna, “Pattern analysis for machine olfaction: a review,” *IEEE Sens. J.*, vol. 2, no. 3, pp. 189–202, Jun. 2002.

[411] M. S. Freund and N. S. Lewis, “A chemically diverse conducting polymer-based ‘electronic nose,’” in *Proceedings of the National Academy of Sciences of the United States of America*, 1995, vol. 92, no. 7, pp. 2652–2656.

[412] Z. Haddi, M. Bougrini, K. Tahri, Y. Braham, M. Souiri, N. El Bari, A. Maaref, A. Othmane, N. Jaffrezic-Renault, and B. Bouchikhi, “A hybrid system based on an electronic nose coupled with an electronic tongue for the characterization of moroccan waters,” *Sensors & Transducers*, vol. 27, pp. 190–197, 2014.

[413] M. Penza and G. Cassano, “Application of principal component analysis and artificial neural networks to recognize the individual VOCs of methanol/2-propanol in a binary mixture by SAW multi-sensor array,” *Sensors Actuators B Chem.*, vol. 89, no. 3, pp. 269–284, Apr. 2003.

[414] M. Stankova, P. Ivanov, E. Llobet, J. Brezmes, X. Vilanova, I. Gràcia, C. Cané, J. Hubalek, K. Malysz, and X. Correig, "Sputtered and screen-printed metal oxide-based integrated micro-sensor arrays for the quantitative analysis of gas mixtures," *Sensors Actuators B Chem.*, vol. 103, no. 1–2, pp. 23–30, Sep. 2004.

[415] E. J. Severin, B. J. Doleman, and N. S. Lewis, "An investigation of the concentration dependence and response to analyte mixtures of carbon black/insulating organic polymer composite vapor detectors," *Anal. Chem.*, vol. 72, no. 4, pp. 658–68, Feb. 2000.

[416] M. K. Baller, H. P. Lang, J. Fritz, C. Gerber, J. K. Gimzewski, U. Drechsler, H. Rothuizen, M. Despont, P. Vettiger, F. M. Battiston, J. P. Ramseyer, P. Fornaro, E. Meyer, and H. Guntherodt, "A cantilever array-based artificial nose," *Ultramicroscopy*, vol. 82, pp. 1–9, 2000.

Appendix

1. Smart carbon nanomaterials used in this study

Size, shape and geometry of the nanofillers may influence the sensing performance of chemoresistive sensors due to their influence on conductive architecture. Different varieties of carbon nanomaterials such as two dimentional carbon nanotubes, one dimensional graphene, zero dimensional Buckminsterfullerenes were used as sensing materials in this thesis.

1.1. Carbon Nanotubes (CNT)

All the MWNTs used in this thesis were kindly provided by nanocyl S.A., Belgium. They were produced via the catalytic carbon vapor deposition (CVD) process. The physical properties of three different varieties of MWNT used in this thesis are listed below in tabular form (Table 1A).

Property	NC 7000	NC 3100	NC 3101	Method
Average Diameter (nm)	9.5	9.5	9.5	TEM
Average Length (µm)	1.5	1.5	1.5	TEM
Carbon Purity (%)	90	>95	>95	TGA
Metal Oxide (%)	10	<5	<5	TGA
-COOH functionalization (%)	0	0	<4	XPS

Table 1A Physicochemical properties of MWNT s of different grades

1.2. Buckminsterfullerene (C_{60})

Zero dimensional Buckminsterfullerenes (C_{60}) have polyhydral pentagonal-hexagonal carbon rings in which each carbon atom is bonded to three other neighbours. Fullerene-C_{60} of 99.5% purity was purchased from Sigma Aldrich. They appeared as black crystalline powders.

2. Steps for the fabrication of the sensors

Vapour sensors were fabricated from conductive nanocomposites by following several steps elaborated below.

2.1. Solution mixing

For the fabrication of portable sensors, solution mixing was found to be more convenient and practical than melt mixing. Requirement of less quantity of raw materials, low power

consumption, easy preparation method are the advantages of this versatile technique. Synthesized nanocomposites or nanohybrids, were subjected to dispersion in a suitable solvent followed by ultrasonication for 1 h at 50 ˚C with a Branson 3510 device (100W, 40 kHz) in order to obtain an appreciable level of homogeneity as shown in Figure 1A.

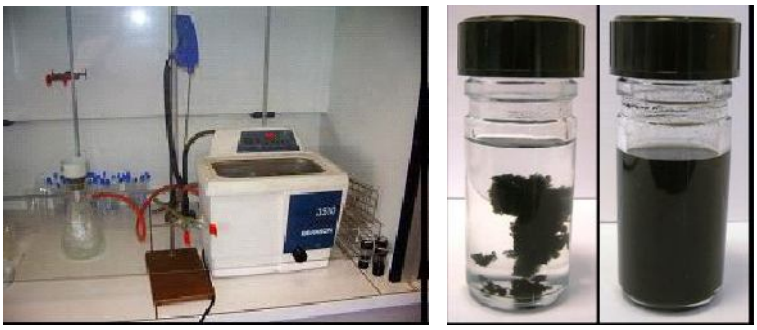

Figure 1A Ultrasonic bath (left) and solution of nanocomposite before and after sonication (right)

2.2. Preparation of the electrode

The electrodes were prepared by mechanical cross-sectional cutting of commercial 22 nF ceramic capacitors, which consist of a series of interdigitated metal lines (25 wt.% Ag/75 wt.% Pd). Prior to deposition of those materials, these electrodes were polished and washed with ethanol to remove any existed dust particles.

2.3. Deposition of synthesized nanocomposite onto electrode

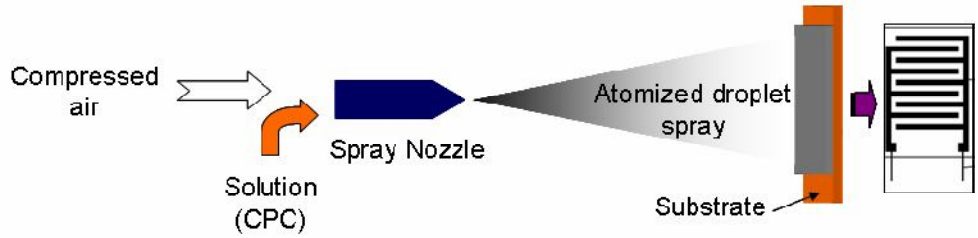

Figure 2A Schematic drawing for solution spray deposition process

The final step of sensors fabrication is the deposition of conductive nanocomposite dispersion on to the interdigitated electrodes followed by evaporation of the solvent. Spray layer by layer technique (sLbL) was employed for this purpose using a homemade device (Figure 2A), equipped with a spray valve controller (Valve Mate 8040) allowing a precise control of the nozzle scanning speed (Vs = 50mm/sec), solution flow rate (index 2), air pressure (0.1 MPa), and target to nozzle distance (8 cm). After fabrication, vapour sensors were conditioned at 30^{o} C in a controlled atmosphere for one night. The initial resistances of sensors are well controlled

by changing spray number of layers which acts as a well controlled tool for structuring thin film of nanometer to micron level thickness.

3. Characterization of the nanocomposites

In order to support successful synthesis of different nanohybrids or nanocomposites, various morphological, thermal and structural characterization techniques were employed.

3.1. Morphological characterization

In order to understand the structure of conductive architecture in different conductive nanocomposites or nanohybrids, various types of microscopy was carried out.

3.1.1. Atomic Force Microscopy (AFM)

Atomic force microscopy (AFM) is a powerful surface analytical technique used in air, liquid or vacuum to generate very high-resolution images of a surface and can provide some topographic, chemical, mechanical and electrical information. An AFM consists of a sharp micro-fabricated tip attached to a cantilever, which is scanned across a sample. The nano-scale characterization of nanomaterials based sensors was done using atomic force microscopy (AFM) under ambient conditions using light tapping mode (TM-AFM) on a calibre multimode scanning probe microscope from Bruker-Veeco (France). The ratio of the set point amplitude to the free amplitude was maintained approximately at 0.9. AFM tips Veeco (France) had typical resonance frequency between 300 and 400 kHz and tip radius between 5 and 15 nm. The set point amplitude of antimony doped silicon tapping mode cantilever (LTESP model, Veeco, USA) was about 4.5 V.

For AFM observation, samples were prepared by depositing the dispersion onto a freshly cleaved silicon substrate by spin coating at 2500 rpm for 30 s using SPIN150-NPP (SPS-Europe), followed by vacuum drying at 60^{o}C for 3 h. Silicon wafer substrates were cleaned with de-mineralized water and were dried in UV chamber prior to solution deposition. The diameters of CNT/ Buckminsterfullerene or quantum dots and thickness of graphene sheets were measured using the section analysis software of the microscope (SPM lab software). As shown in the Figure 3A, The diameter of MWNT was found to be around 10 nm where as the thickness of graphene oxide sheets was calculated as 1.2 nm and the diameter of C_{60} nanoparticle clusters, were calculated to be around 230 nm on an average.

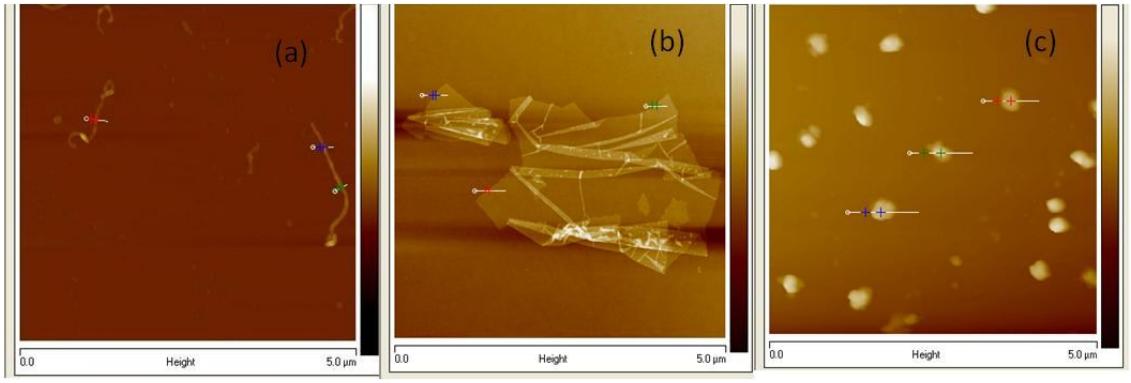

Figure 3A The AFM images of MWNT, graphene oxide and Buckminsterfullerene respectively (from left)

3.1.2. Scanning Electron Microscipy (SEM)

A scanning electron microscope (SEM) is a type of electron microscope that produces images of a sample by scanning it with a focused beam of electrons. The electrons interact with atoms in the sample, producing various signals that can be detected and that contain information about the sample's surface topography and composition. The morphology of nanocomposites or nanohybrids was observed under the ZEISS EVO Series Scanning Electron Microscope Model (EVO 50). Figure 4A, shows the SEM images of MWNT, graphene and Buckminsterfullerene. The elemental profile of the membrane was recorded to investigate the presence of various elements by in a Bruker-AXS Energy Dispersive X-ray (EDX) System (Model QuanTax 200).

3.1.3. Transmission Electron Microscopy (TEM)

Transmission Electron Microscope JEOL 2010F- type-high contrast (HC) was used to observe the conductive architecture of CNT or graphene as in Figure 5A. The microscope had accelerating voltage from 80 to 200 kV and standard magnification from 1000 to 800000 times. Illuminating system consisted of cool beam electron gun with pre-centered LaB_6 filaments. There were three-stage condenser lens (1st, 2nd, 3rd) and five apertures. A beam total angle was 2˚in all directions.

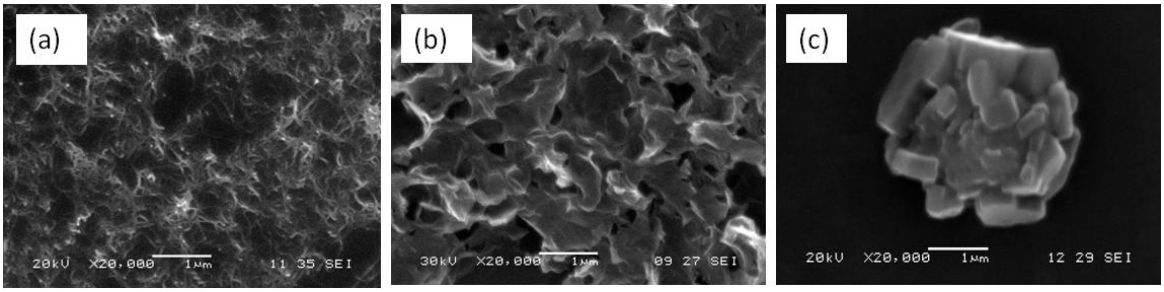

Figure 4A The SEM images of (a) MWNT, (b) graphene oxide and (c) Buckminsterfullerene respectively

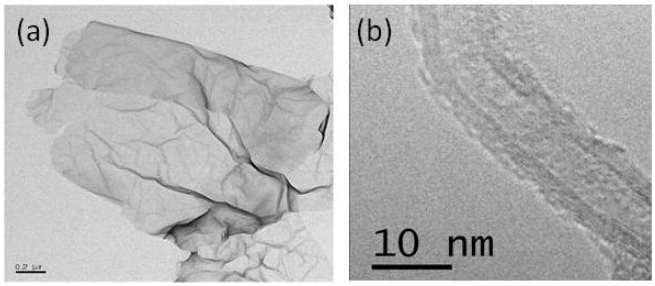

Figure 5A The TEM images of graphene oxide and MWNT respectively (from left)

3.2. Thermal characterization

3.2.1. Thermogravimetric Analysis (TGA)

Thermo gravimetric analysis or thermal gravimetric analysis (TGA) is a method of thermal analysis in which changes in physical and chemical properties of materials are measured as a function of increasing temperature (with constant heating rate), or as a function of time (with constant temperature and/or constant mass loss). TGA is commonly used to determine selected characteristics of materials that exhibit either mass loss or gain due to decomposition, oxidation, or loss of volatiles (such as moisture). Common applications of TGA are (1) materials characterization through analysis of characteristic decomposition patterns, (2) studies of degradation mechanisms and reaction kinetics, (3) determination of organic content in a sample, and (4) determination of inorganic (e.g. ash) content in a sample, which may be useful for corroborating predicted material structures or simply used as a chemical analysis. Thermo gravimetric analysis of all samples was carried out on Pyris 6 TGA instrument of Perkin Eimer in nitrogen atmosphere at a heating rate 20°C/min in the temperature range 50°C to 750°C.

3.2.2. Differential Scanning Calorimetry (DSC)

The thermal properties were studied by differential scanning calorimetry (DSC). The glass transition temperature of the membranes was calculated using TA DSC Q 200 instrument in the temperature range of 40-300 °C in nitrogen atmosphere with sample size 5±2 mg at a heating rate of 10 °C/min

3.3. Structural characterization

3.3.1. Wide Angle X-Ray Diffraction

X-ray crystallography is a tool used for determining the atomic and molecular structure of a crystal, in which the crystalline atoms cause a beam of X-rays to diffract into many specific directions.The X-ray diffraction (XRD) patterns of all the samples were obtained with an X-ray diffractometer model no PW3040-60 X'pert PRO (Netherland) with 40kV voltage, 30mA current and CuKα = 1.54Å, at a scanning rate 0.02° per second in a 2θ range from 2°-40°.

3.3.2. Fourier Transform Infrared Spectroscopy

Fourier transform infrared spectroscopy (FTIR) is a technique which is used to obtain an infrared spectrum of absorption, emission, photoconductivity or Raman scattering of a solid, liquid or gas. An FTIR spectrometer simultaneously collects spectral data in a wide spectral range. This confers a significant advantage over a dispersive spectrometer which measures intensity over a narrow range of wavelengths at a time. The FT-IR spectra of samples were obtained using Thermo Nicolet IR 200 spectrometer.

3.3.3. UV-Visible Spectroscopy

Ultraviolet/visible spectroscopy is useful as an analytical technique for two reasons. First it can be used to identify some functional groups within molecules and secondly, it can be used for more quantitative analysis. Ultraviolet/visible spectroscopy is used extensively in chemical and biochemical research, for a variety of tasks. For most spectra the solution obeys Beer's Law. This states that the light absorbed is proportional to the number of absorbing molecules, i.e., to the concentration of absorbing molecules. Nevertheless this is only true for dilute solutions. A second law, Lamberts's law, tells us that the fraction of radiation absorbed is independent of the intensity of the radiation. Combining these two laws gives the Lambert Beers' law:

$$log \frac{I}{I_0} = \frac{\in}{c}$$

I_O = the intensity of the incident radiation

I = the intensity of the transmitted radiation

ε = the molar absorption coefficient

l = the path length of the absorbing solution (cm)

c = the concentration of the absorbing species in mol dm^{-3}

UV-visible spectroscopy was done using CARY WIN UV BIO-50 within 250-750 nm range. Rectangular cubic cell ($1cm^2$ cross sectional area and 2.5cm length) was used for UV spectroscopy experiments.

3.3.4. Nuclear Magnetic Resonance Spectroscopy

NMR is a powerful tool which is used to identify functional groups in particular chemical bonding. The NMR spectra were recorded on a Bruker AV300 spectrometer, operating at 300 MHz. Electrospray-ionization mass spectra (ESIMS) was recorded with an API 2000 spectrometer.

4. Other materials and synthesis

4.1.Materials

1-pyrenebutyric acid N-hydroxysuccinimide ester (Aldrich, 95%), 1-adamantanemethylamine (Aldrich, 98%) triphenylphosphine (Aldrich, 99%), sodium azide (Aldrich, 99.5%), 2-propynyl-tetra-O-acetyl-β-D-glucopyranoside (Aldrich, 97%), ascorbic acid sodium salt (Fluka, 99%), sodium methoxide (Fluka, 97%), cupric sulfate pentahydrate (Fluka, 99%), iodine (Alfa Aesar, 99%), anhydrous pyridine (Aldrich, 99.8%), acetic anhydride (Aldrich, 99%) were used as received without further purification. CH_2Cl_2 (VWR, 100%) was dried over CaH_2 and distilled just before use. The deuterated solvents (D_2O, DMSO-d6) were purchased from Eurisotop. The β-CD (Roquette, 98%) was purified before use. A saturated solution of β-CD was prepared at 80°C, then slowly cooled to room temperature and left at 0°C for one night. The crystallized β-CD was then filtered and dried under vacuum at 80°C over one night. All solvents ethanol, methanol, DMF, formaldehyde, acetone, toluene, benzene, propanol, isopropanol, o-xylene, from Acros Organics (Belgium) was used as received. Aminopropyl Iso Ocyl POSS and trisilanol phenyl POSS were purchased from Hybrid Plastics, USA.

4.2.Synthesis of functionalized cyclodextrins

4.2.1. Synthesis of heptakis(6-deoxy-6-(1,2,3-triazolyl) methylene β-D-glucopyranoside) β-CD or mannose functionalized CD (MCD)

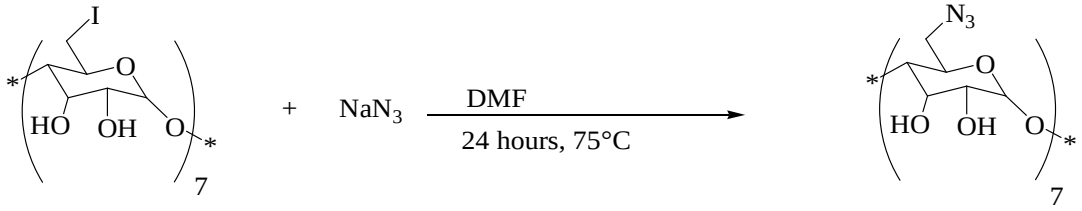

Step 1 Synthesis of heptakis(6-deoxy-6-azido)β-CD

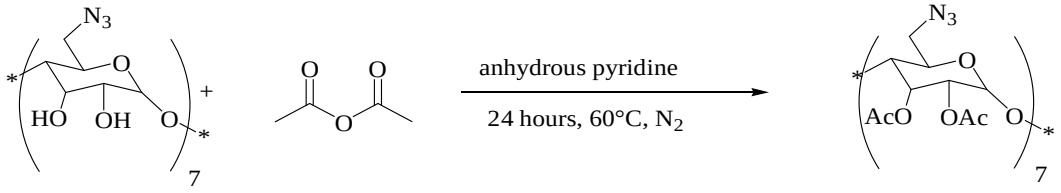

Step 2 Synthesis of heptakis(6-deoxy-6-azido-2,3-di-O-acetyl)β-CD

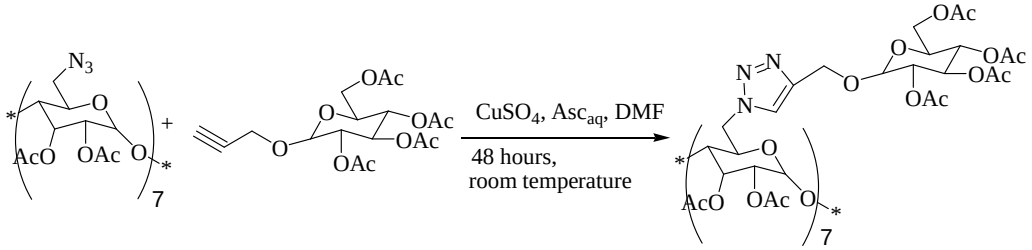

Step 3 Synthesis of heptakis(6-deoxy-6-(1,2,3-triazolyl)methylene-tetra-O-acetyl-β-D glucopyranoside - 2,3-di-O-acetyl) β-CD

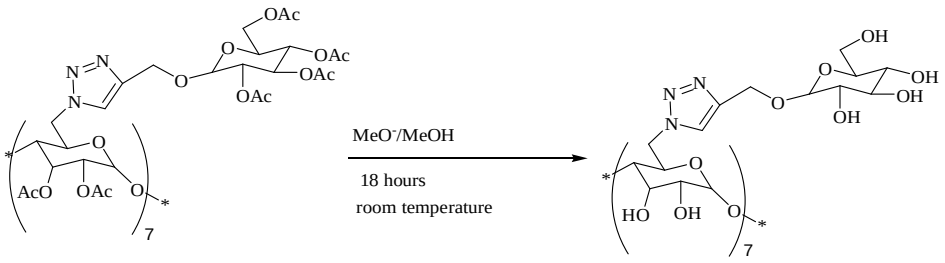

Step 4 Synthesis of heptakis(6-deoxy-6-(1,2,3-triazolyl)methylene-β- glucopyranoside) β-CD

Figure 6A Four step synthsis of heptakis(6-deoxy-6-(1,2,3-triazolyl)methylene-β- glucopyranoside) β-CD

A solution of β-cyclodextrin in anhydrous DMF (4.4 mmol in 90 mL), I_2 (92.5 mmol) and Ph_3P (92.5 mmol) were added followed by stirring at 80 °C for 18 hours. A freshly prepared solution of NaOMe in MeOH (45 mL) was carefully introduced in the reaction vessel after the reaction mixture was cooled to room temperature and concentrated. The reaction mixture was

precipitated in methanol. The resulting brown solid was dried under high vacuum. 6.095 g of compound was recovered (yield of 72.6%).

In the next step, NaN_3 (31.3 mmol,) was added to a solution of heptakis (6-deoxy-6-iodo) β-CD in DMF (3.2 mmol) and the resulting suspension was stirred at 75 °C for 24 hours. The suspension was concentrated followed by treatment with a large excess of water. The precipitated compound was filtered, washed with water, and dried under high vacuum to yield a stable white powder (3.71 g, 88%).

Then to a solution of heptakis (6-deoxy-6-azido)β-CD (2.7 mmol) in anhydrous pyridine (65.2 mL), acetic anhydride (215 mmol) was added. The mixture was stirred for 24 hours at 60°C under nitrogen. The solution was then concentrated and the residue was dissolved in dichloromethane and washed with 10% HCl in water followed by water. The organic layer was dried over sodium sulfate and concentrated to yield white product (0.96 g, 66.8%).

2-propynyl-tetra-O-acetyl-β-D-glucopyranoside (0.54 mmol) was added to a solution of heptakis(6-deoxy-6-azido-2,3-di-O-acetyl)β-CD (0.07 mmol) in DMF (2.4 mL). Cupric sulfate pentahydrate (0.54 mmol) and a freshly prepared solution of sodium ascorbate (1.08 mmol) in water (0.6 ml) were successively added to the mixture. The solution was stirred for 48hours at room temperature. After evaporation of solvents, the crude product was dissolved in CH_2Cl_2. The product was extracted three times with an ammonia solution (5N) and three times with water. The organic layer was retained, the solvent was removed and the product was dried under vacuum when the yield was 88.5% (290 mg).

Resulting, Heptakis (6-deoxy-6-(1,2,3-triazolyl) methylene-tetra-O-acetyl-β-D-glucopyranoside-2,3-di-O-acetyl) β-CD ($6.3.10^{-2}$ mmol) was added to the solution of NaOMe in MeOH (1M). The heterogeneous solution was stirred for 18 hours at room temperature. The mixture was filtered and the precipitate was dried under vacuum. A white powder was recovered which was purified by silica chromatography with the mixture H_2O/ethanol as eluant (95/5 until 75/25). The expected product (as in Figure 6A) was collected with a yield of 40%.

4.2.2. Synthesis of heptakis(6-deoxy-6-amino)β-CD (NCD)

As shown in Figure 7A, heptakis (6-deoxy-6-azido)β-CD (153 mmol) was dissolved in DMF (40 mL) and PPh_3 (24.2 mmol) was added. The solution was stirred under N_2 for 2h. Concentrated aqueous NH_3 (6 mL, ≈ 35%) was then added dropwise to the solution followed by stirring. The suspension was then concentrated under reduced pressure to approximately 10

mL and 150 mL of ethanol was added in order to precipitate the product. The precipitate was washed with ethanol and dried under high vacuum to yield a white solid.

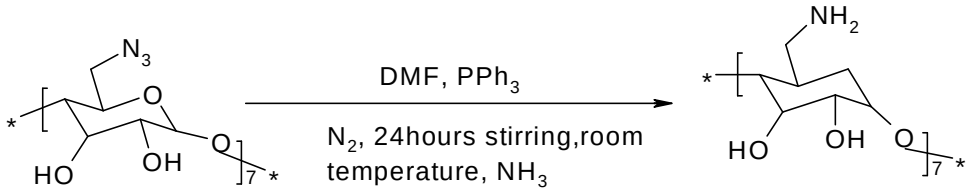

Figure 7A Synthsis of heptakis(6-deoxy-6-amino)β-CD(NCD)

4.2.3. Synthesis of perbenzylated β–cyclodextrin (PBCD)

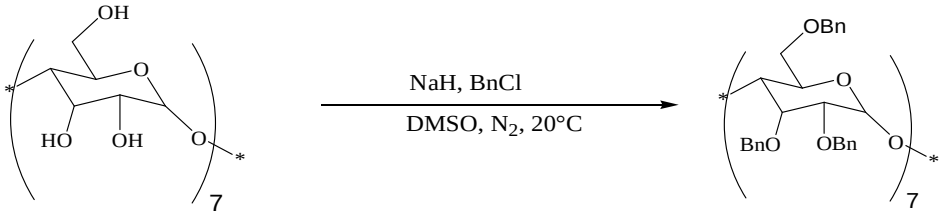

Figure 8A Synthesis of perbenzylated cyclodextrin

β–cyclodextrin (7.1g) were added at room temperature under nitrogen to a solution of NaH (259 mmol) and benzyl chloride (259 mmol) was carefully added dropwise to the solution. The mixture was stirred vigorously at room temperature in anhydrous DMSO for 24 hours. The reaction mixture was then neutralized with water followed by the extraction of the aqueous layer with Et_2O. The combined organic layers were dried, filtered and concentrated. Silica gel choromatography of the residue gave 17.9 g of perbenzylated β–cyclodextrin (yield: 94%) as depicted in Figure 8A.

4.3. Characterization of synthesized products

4.3.1. Characterization of the synthesis of pyrene adamantan

^{1}H NMR ($CDCl_3$) shows the characteristic peaks as below

ppm, δ: 8.33-7.86 (9H, Py), 5.39 (broad peak, 1H, NH), 3.43, 3.41, 3.38 (t, 2H, H_a), 2.97,2.95 (d, 2H, H1), 2.34-2.16 (m, 4H, Hc, Hb), 1.95 (broad peak, 3H, H5), 1.71, 1.67, 1.61,1.58 (q, 6H, H3), 1.46, 1.45 (d, 6H, H2)

^{13}C NMR ($CDCl_3$) shows the following peaks

ppm, δ: 172.83 (C=O), 136.08-123.57 (Py), 51.10 (C1), 40.40 (C2), 37.07 (C3), 36.42 (Cc), 33.76 (C4), 32.99 (Ca), 28.35 (C5), 27.71 (Cb)

For $C_{31}H_{33}NO$, ESIMS: 436.40 uma $[M+H]^+$, 458.40 uma $[M+Na]^+$, 474.40 uma $[M+K]^+$

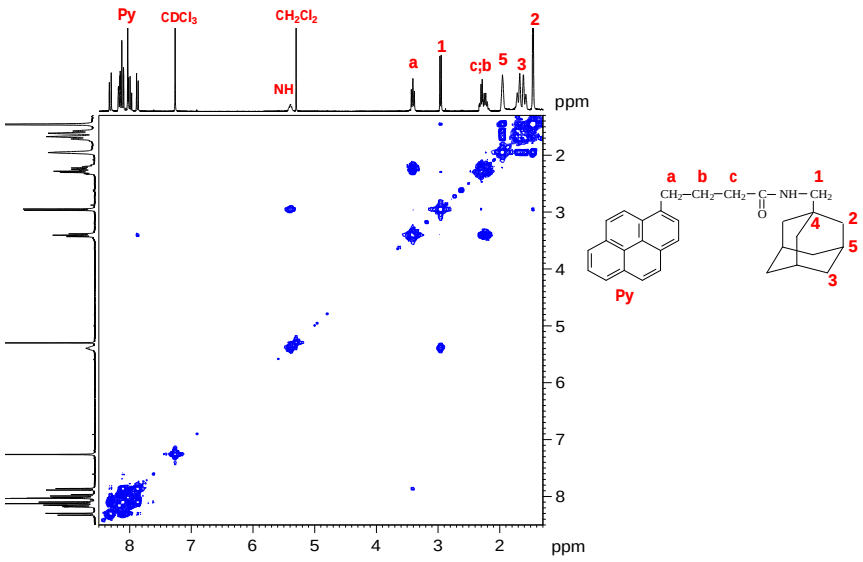

Figure 9ACOSY NMR spectrum of pyrene butyric acid adamantanemethyl amide in $CDCl_3$

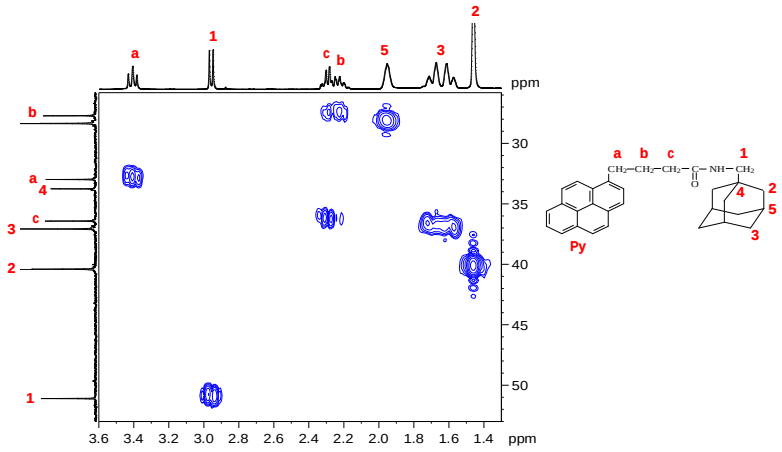

Figure 10A HMQC NMR spectrum of pyrene butyric acid adamantanemethyl amide in $CDCl_3$

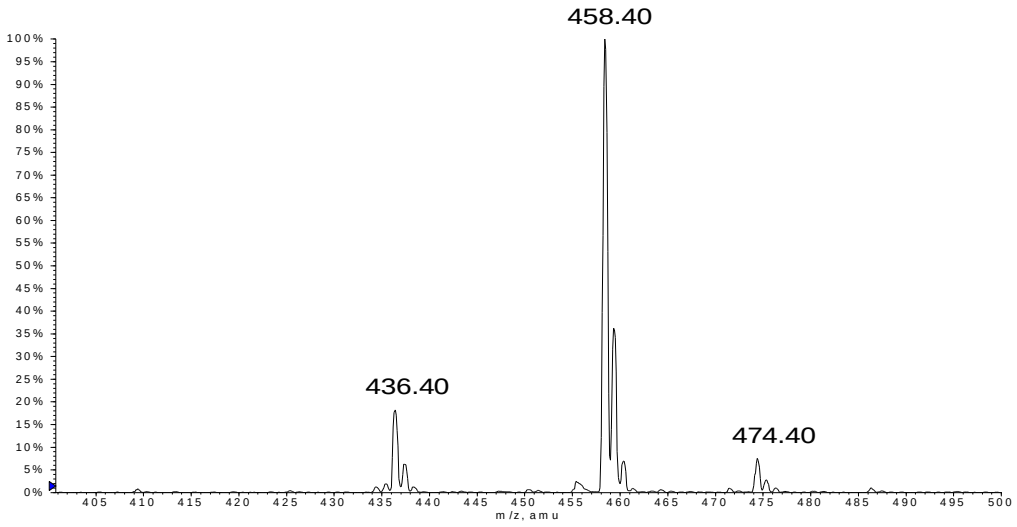

Figure 11A ESIMS of pyrene butyric acid adamantanemethyl amide

4.3.2. Characterization of the synthesis of heptakis(6-deoxy-6-(1,2,3-triazolyl)methylene-β-D-glucopyranoside)β-CD (MCD)

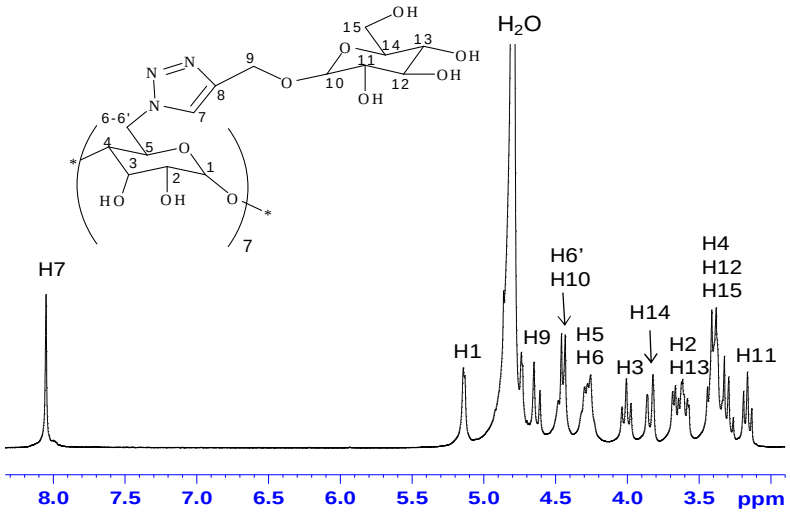

Figure 12A ^{1}H NMR spectrum of heptakis(6-deoxy-6-(1,2,3-triazolyl)methylene-β-D-glucopyranoside)β-CD (EB12-31c) in D_2O at 25°C

^{1}H NMR (D_2O) ppm, δ: 8.04 (s, 7H, H7) 5.12 (d, 7H, H1), 4.68 (dd, 14H, H9), 4.44 (d,14H, H6, H10), 4.27 (d, 14H, H5, H6), 4.00 (t, 7H, H3), 3.84 (d, 7H, H14), 3.74-3.52 (m, 14H, H2, H13), 3.48-3.23 (m, 28H, H4,H12, H15), 3.15 (t, 7H, H11)

^{13}C NMR (D_2O) ppm, δ: 143.88 (7C, C8), 127.39 (7C, C7), 101.93 (14C, C1, C10), 83.27-60.52 (70C, C2 to C5, C9, C11 to C15), 50.55 (7C, C6) .

For $C_{105}H_{161}N_{21}O_{70}$, ESIMS: 968.5 uma $[M+3Na]^{3+}$, 1440.6 uma $[M+2Na]^{2+}$

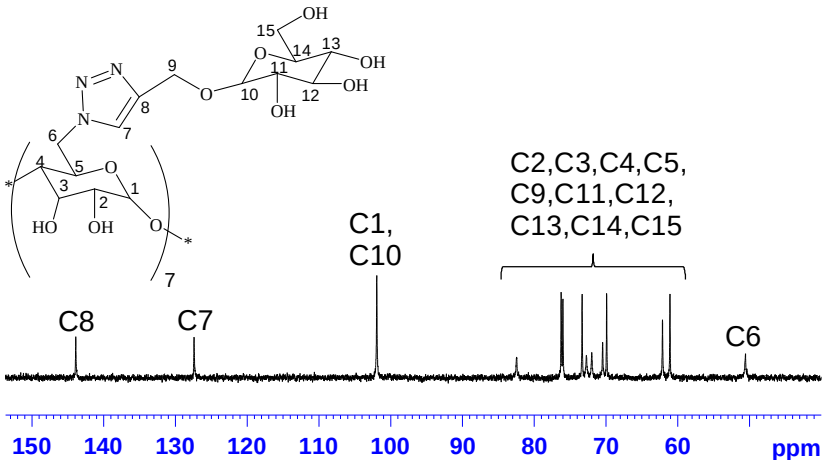

Figure 13A ^{13}C NMR spectrum of heptakis(6-deoxy-6-(1,2,3-triazolyl)methylene-β-D glucopyranoside)β-CD (EB12-46a) in D_2O at 25°C

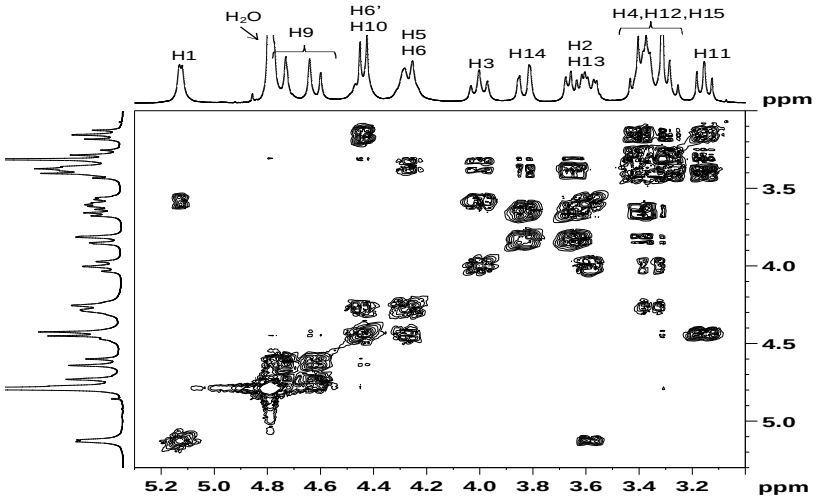

Figure 14A COSY NMR spectrum of heptakis (6-deoxy-6-(1,2,3-triazolyl)methylene-β-D-glucopyranoside)β-CD (EB12-31c) in D_2O at 25°C

4.3.3. Characterization of the synthesis of heptakis(6-deoxy-6-amino)β-CD (NCD)

^1H NMR (D_2O) ppm, δ: 5.17 (d, 7H, H1), 4.21 (m, 7H, H5), 3.98 (dd, 7H, H3), 3.68 (dd, 7H, H2), 3.59 (t, 7H, H4), 3.46 (dd, 7H, H6), 3.26 (dd, 7H, H6') ^{13}C NMR (D_2O) ppm, δ: 104.1 (7C, C1), 84.9 (7C, C4), 74.9, 74.3 (14C, C2, C3), 70.5 (7C, C5), 42.9 (7C, C6)

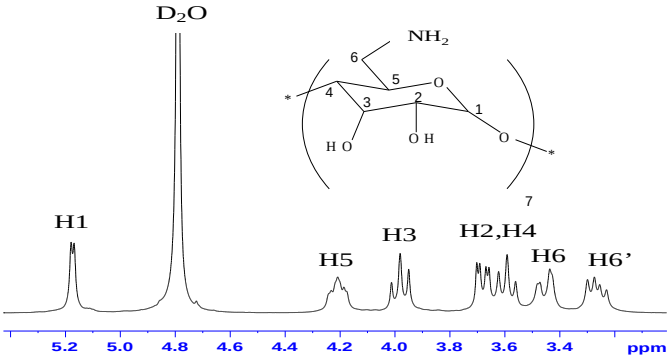

Figure 15A1H NMR spectrum of heptakis(6-deoxy-6-amino) β-CD (NCD) in D2O at 25°C

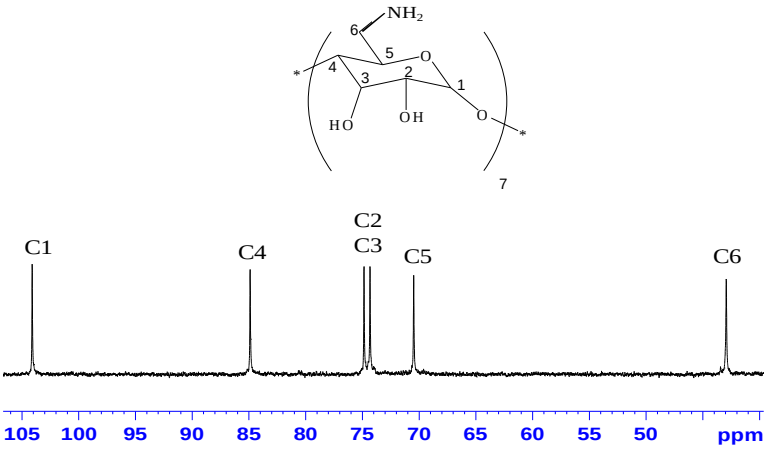

Figure 16A13C NMR spectrum of heptakis(6-deoxy-6-amino) β-CD (NCD) in D2O at 25°C

4.3.4. Characterization of the synthesis of perbenzylated β–cyclodextrin (PBCD)

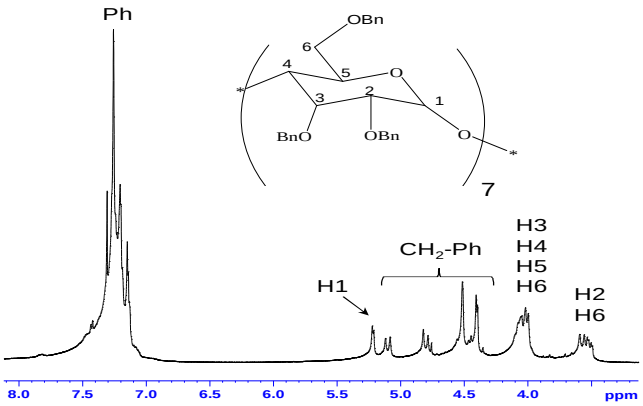

Figure 17A 1H NMR of perbenzylated β–cyclodextrin in CDCl3

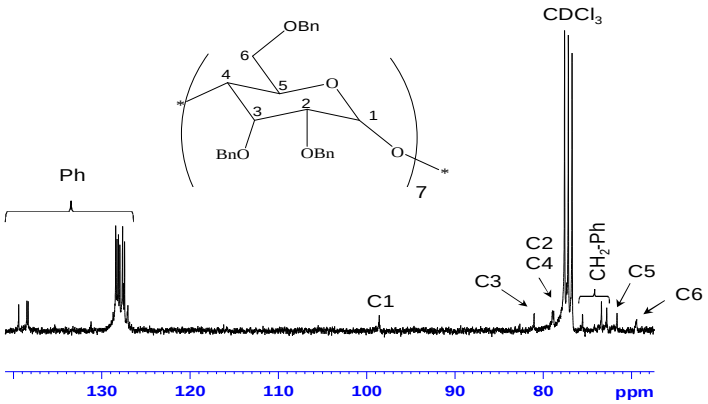

Figure 18A13C NMR of perbenzylated β–cyclodextrin in CDCl3.

^{1}H NMR ($CDCl_3$) ppm, δ: 8.40-6.84 (m, 105H, aromatic H), 5.22 (d, 7H, H1), 5.18-4.34 (m, 42H, CH_2-Ph), 4.24-3.92 (m, 28H, H3, H4, H5, H6), 3.69-3.45 (m, 14H, H2, H6)

^{13}C NMR ($CDCl_3$) ppm, δ: 139.41, 138.48, 138.34 (3 × C aromatic quaternary), 130.0-126.2 (CH aromatic), 98.57 (C1), 81.04 (C3), 78.95 (C2), 78.82 (C4), 75.55, 73.41, 72.81 (3 × CH_2-Ph), 71.64 (C5), 69.44 (C6)

Oral Presentations in international conferences

1. **Sananda Nag**, Emilie Bertrand, Veronique Celton, Lisday Duarte, Mickaël Castro, Veena Choudhary, Philippe Guegan, Jean-François Feller /Detection of Some Lung Cancer Biomarkers with Quantum Resistive Vapour Sensors Made of Functionalized β Cyclodextrin - Reduced Graphene Oxide, **POLYTECH- 2012**, December 15-17, Pune, India

2. **Sananda Nag**, Mickaël Castro, Jean-François Feller, Veena Choudhary/ Functionalized Carbon Nanotube Based Hybrid Chemical Vapour Sensor for the Anticipated Diagnosis of Disease, **ICMAST-2013**, September 13-17, Prague, Czech Republic

3. **Sananda Nag**, Mickaël Castro, Jean-François Feller, Veena Choudhary/ Functionalized Carbon Nanotube Based Hybrid Chemical Sensor for the Anticipated Diagnosis of Disease, **ICFM-2014**, February 5-7, IIT-KGP, India

4. **Sananda Nag**, Lisday Duarte, Emilie Bertrand, Veronique Celton, Mickaël Castro, Veena Choudhary, Philippe Guegan, Jean-François Feller/ Reduced Graphene Oxide Based Hybrid Functional Vapour Sensors for Human Health Monitoring, **Graphene-2014**, May 6-9, Toulouse, France

5. **Sananda Nag**, Lisday Duarte, Veronique Celton, Mickaël Castro, Veena Choudhary, Philippe Guegan, Jean-François Feller/Reduced Graphene Oxide Based Functional Nanocomposite Vapour Sensors for Human Health Monitoring, **Nanostruc-2014**, May 20-21, Madrid,Spain

6. CASTRO M , **Nag S** , Nag Chowdhury S , Feller JF/ Development of Chemo and Piezo-Resistive sensors based on Conductive Polymer Composites, **ICMAST 2013**, September 13-17, Prague, Czech Republic

7. Mickael CASTRO, **Sananda NAG**, Suvam Nag CHOWDHURY, Jean-François FELLER/ Conductive Polymer Composites as active layer for vapor and strain sensing applications, **ISIEM 2013**, October 27-31, Rennes-France

8. Philippe Guégan, Lisday Duarte, **Sananda Nag**, Mickaël Castro,Véronique Bennevault Celton, Jean François Feller, / Synthesis of Bio based Polyesters and Polyamides for the design of transducers sensitive to Some Lung Cancer VOC Biomarkers, **IUPAC Macro2014**, July 6-11, Chiang Mai, Thailand

Poster Presentations

1. **Sananda Nag**, Mickaël Castro, Jean-François Feller, Veena Choudhary/ Quantum Resistive Sensors for Anticipated diagnosis of Cancer, **GFP-2012**, Lorient, France

2. **Sananda Nag**, Mickaël Castro, Veena Choudhary, Philippe Guegan, Jean-François Feller/ Quantum Resistive Vapour Sensors Made of Reduced Graphene Oxide Based Functional Hybrid Materials for Detection of Some Lung Cancer Biomarkers, **GFP- 2013**, Nantes, France

Research Publications

1. Sananda Nag, Lisday Duarte, Emilie Bertrand,Véronique Celton, Mickaël Castro, Veena Choudhary, Philippe Guegan, Jean-François Feller, Ultrasensitive QRS made by supramolecular assembly of functionalized cyclodextrins and graphene for the detection of lung cancer VOC biomarkers (communicated)

2. Sananda Nag, Mickaël Castro, Veena Choudhary, Jean-François Feller, Influence of polyhedral oligomeric silsesquioxane on the molecular selectivity of CNT based hybrid chemical vapour sensors for disease diagnosis (to be submitted)

3. Sananda Nag, Mickaël Castro, Veena Choudhary, Jean-François Feller, Tailoring of selectivity & sensitivity of CNT / graphene based vapour sensors by grafting with fullerene (to be submitted)

4. Sananda Nag, Deeksha Gupta, Mickaël Castro, Veena Choudhary, Jean-François Feller, Influence of degree of sulfonation on the selectivity and sensitivity of Poly (ether ether ketone)/CNT nanocomposite volatile organic compound sensors (to be submitted)

5. Suvam Nag Chowdhury, Sananda Nag, Mickaël Castro, Veena Choudhary, Jean-François Feller, A Review on Quantum Resistive Sensors for Humans and Materials Health Monitoring(under preparation)

6. Sananda Nag, Mickaël Castro, Veena Choudhary, Jean-François Feller, CPC Vapor Sensors Based on Hybrid Fillers for the Detection of Cancer Biomarkers (under preparation)

Abstract

The analysis of specific VOC in exhaled breath (identified as biomarkers of specific disease like cancer) give an idea of metabolic and physiological activities of an individual and can provide non-invasive and potentially inexpensive anticipated diagnosis of several diseases including cancer. The invention of a fast, reliable, economic and portable technique is highly required before breath testing become a clinical reality. Nanomaterial based sensor arrays can fulfill all these requirements and can form a solid foundation for identification of disease related VOC patterns in exhaled breath. The objective of this thesis was to fabricate different chemo-resistive sensors based on conductive nanocomposites with ability to differentiate and discriminate a set of disease (such as lung cancer) biomarker VOC. Therefore in order to fabricate high performance sensors with high sensitivity and required selectivity towards targeted VOC, adoption of different methodologies for the synthesis of conductive nanocomposite, was strongly emphasized. Covalent and noncovalent functionalizations of these carbon nanomaterials with various oligomeric, polymeric or inorganic molecules were done in order to tune the sensor's selectivity and sensitivity. Nanoswitching at the junctions of percolated network formed by the carbon nanomaterials could be controlled by varying the organic functionality on the surface. Finally a set of high performance chemoresistive vapour sensors, with different selectivity towards targeted lung cancer VOC could be fabricated and successfully integrated in an e-nose with high efficiency towards detection and discrimination of a set of disease specific VOC biomarkers.

RESUME DE LA THESE EN FRANÇAIS

L'analyse de COV spécifiques dans l'halèine (identifié comme biomarqueurs de maladies telles que le cancer) donne une idée de l'activité métabolique et physiologique d'un individu et peut fournir un diagnostic anticipé non-invasif et potentiellement peu coûteux de plusieurs maladies dont le cancer. Mais avant que des tests médicaux ne puissent devenir une réalité clinique, il est nécessaire de développer une technique d'analyse rapide, fiable, économique et portable. Les réseaux de senseurs (nez électroniques) à base de nanomatériaux qui peuvent satisfaire toutes ces exigences, constituent l'élément clef de l'identification des maladies par leur empreinte de COV dans l'haleine. L'objectif de cette thèse est de fabriquer différents senseurs chemo-résistifs à base de nanocomposites conducteurs ayant la capacité de discriminer un ensemble de maladies (comme le cancer du poumon) par l'analyse de leur biomarqueur (COV). Par conséquent, afin de fabriquer des senseurs de haute performance avec une grande sensibilité (ppb) et une sélectivité adaptée aux COV ciblés, différentes méthodologies d'élaboration de nanocomposites conducteur, ont été implémentées. Des fonctionnalisations covalentes et non-covalentes de ces nanomatériaux de carbone ont été réalisées avec différents types de molécules, i.e., oligomères, polymères ou minérales afin d'ajuster la sélectivité et la sensibilité des capteurs. La nanodéconnection des jonctions du réseau percolé formé par les nanocharges de carbone a ainsi pu être contrôlée en faisant varier la fonctionnalité chimique de leur surface. Finalement un ensemble de senseurs de vapeur chemorésistifs de hautes performances, ayant une sélectivité pour les biomarqueurs du cancer du poumon ont pu être fabriqués et intégrés avec succès dans un nez électroniques.